Channel succession and sediment transport in the Black Vermillion River

by

Michael E. McNair

B.L.A., Mississippi State University, 1998

M.C.R.P., Clemson University, 2018

AN ABSTRACT OF A DISSERTATION

Submitted in partial fulfillment of the requirements for the degree

DOCTOR OF PHILOSOPHY

Department of Environmental Design and Planning

College of Architecture, Planning, and Design

Kansas State University

Manhattan, Kansas

2023

Abstract

Tuttle Creek Reservoir in northeaster Kansas has lost approximately 47% of its capacity due to excessive sediment being supplied from upstream since completion in 1961. The Black Vermillion River (BVR) is a tributary of the Big Blue River which flows into Tuttle Creek Reservoir. This research utilizes three unique data sets within three separate but related studies to better understand sediment being produced by bank erosion along the BVR. The first study sought to understand how the channel evolution of the upper BVR could be influencing streambank erosion and sediment production. Seven study reaches in the upper BVR watershed, each with two cross sections, that were first monitored between 2007 and 2010 were resurveyed in 2021. The cross-sectional data suggest that channel incision is waning or has ceased, and that the channel has entered a phase of rapid widening with minor aggradation, as 12 of 14 cross section experienced widening over the 14-year study period. Analysis of sequential LiDAR data from 2010 (12) and 2018 of the entire upper BVR riverbank indicated that the widening observed at the cross sections was indicative of most of the riverbank in the study area, with 76 of 78 1-km river segments experiencing net erosion (widening) in the Irish Creek, Main Stem, and Weyer Creek subwatersheds. In the North Fork subwatershed, the same pattern of net erosion was observed upstream of the Weyer Creek confluence; however, downstream all ten 1-km river segments experienced net deposition, which was supported by cross sectional data in the same area.

The second study expanded the use of the 2010, 2012, and 2018 lidar data to include the BVR main channel in the lower BVR watershed, which identified an area of severe erosion in the lower BVR watershed with area of heavy deposition downstream near the confluence of the BVR and the Big Blue River. The second study utilized the lidar data to evaluate the effect of the presence, amount, and density of woody vegetation on erosion and deposition rates. Banks with no, little, and ample woody vegetation were isolated. Rates of erosion were

calculated for each category with banks void of woody vegetation experiencing between 57% and 288% more erosion when compared to banks with at least some woody vegetation. In contrast, no correlation was found between LiDAR-derived vegetation density metrics and erosion in any of the study reaches. No correlation was found between the LiDAR metrics and deposition except in the North Fork-Lower Main Stem channel in Marshall County, where a modest correlation (R^2 0.35) was found.

The third study evaluated the use of Structure-from-Motion (SfM) Photogrammetry to monitor erosion "hotspots" over a 1.5-year period at both a seasonal and annual temporal scale. The data suggest SfM is better suited for the monitoring of erosion than deposition, as vegetation establishment where deposition occurs interferes with the SfM image collection. Three study banks experienced large amounts of erosion up to 1.34m^3 per square meter of bank face, while other banks became vegetated and experienced little change or minor net deposition. In addition, the average erosion per meter of the bank face of the three study banks in the upper watershed was greater than that of the six in the lower watershed.

` The three data sets and methodologies provided information that could be employed in other areas of the Tuttle Creek Reservoir watershed and guide BVR restoration efforts. Traditional cross-sectional and other data provided insight into the evolutional phase of the BVR. Lidar derived DEMs and subsequent DoDs provide estimates of erosion and deposition along the entire channel of the BVR and three of its tributaries, and may provide more accurate locations erosional "hotspots" than the methods previously used by the KWO. Erosion hotspots identified with repeat lidar surveys could then be monitored using more exact surveying methods, such as traditional surveying and SfM. The process of creating DoDs along riverbanks could easily be applied to all the Tuttle Creek watershed within Marshall and Nemaha Counties. It is also believed that SfM could be an effective tool in monitoring most of the erosion hotspots within the BVR, as most of them are well suited for the use of SfM.

Channel succession and sediment transport in the Black Vermillion River

by

Michael E. McNair

B.L.A., Mississippi State University, 1998
M.C.R.P., Clemson University, 2018

A DISSERTATION

Submitted in partial fulfillment of the requirements for the degree

DOCTOR OF PHILOSOPHY

Department of Environmental Design and Planning
College of Architecture, Planning, and Design

Kansas State University
Manhattan, Kansas

2023

Approved by:

Co-Major Professor
Dr. Trisha Moore

Approved by:

Co-Major Professor
Dr. Timothy Keane

Abstract

Tuttle Creek Reservoir in northeaster Kansas has lost approximately 47% of its capacity due to excessive sediment being supplied from upstream since completion in 1961. The Black Vermillion River (BVR) is a tributary of the Big Blue River which flows into Tuttle Creek Reservoir. This research utilizes three unique data sets within three separate but related studies to better understand sediment being produced by bank erosion along the BVR. The first study sought to understand how the channel evolution of the upper BVR could be influencing streambank erosion and sediment production. Seven study reaches in the upper BVR watershed, each with two cross sections, that were first monitored between 2007 and 2010 were resurveyed in 2021. The cross-sectional data suggest that channel incision is waning or has ceased, and that the channel has entered a phase of rapid widening with minor aggradation, as 12 of 14 cross section experienced widening over the 14-year study period. Analysis of sequential LiDAR data from 2010 (12) and 2018 of the entire upper BVR riverbank indicated that the widening observed at the cross sections was indicative of most of the riverbank in the study area, with 76 of 78 1-km river segments experiencing net erosion (widening) in the Irish Creek, Main Stem, and Weyer Creek subwatersheds. In the North Fork subwatershed, the same pattern of net erosion was observed upstream of the Weyer Creek confluence; however, downstream all ten 1-km river segments experienced net deposition, which was supported by cross sectional data in the same area.

The second study expanded the use of the 2010, 2012, and 2018 lidar data to include the BVR main channel in the lower BVR watershed, which identified an area of severe erosion in the lower BVR watershed with area of heavy deposition downstream near the confluence of the BVR and the Big Blue River. The second study utilized the lidar data to evaluate the effect of the presence, amount, and density of woody vegetation on erosion and deposition rates. Banks with no, little, and ample woody vegetation were isolated. Rates of erosion were

calculated for each category with banks void of woody vegetation experiencing between 57% and 288% more erosion when compared to banks with at least some woody vegetation. In contrast, no correlation was found between LiDAR-derived vegetation density metrics and erosion in any of the study reaches. No correlation was found between the LiDAR metrics and deposition except in the North Fork-Lower Main Stem channel in Marshall County, where a modest correlation (R^2 0.35) was found.

The third study evaluated the use of Structure-from-Motion (SfM) Photogrammetry to monitor erosion "hotspots" over a 1.5-year period at both a seasonal and annual temporal scale. The data suggest SfM is better suited for the monitoring of erosion than deposition, as vegetation establishment where deposition occurs interferes with the SfM image collection. Three study banks experienced large amounts of erosion up to 1.34m^3 per square meter of bank face, while other banks became vegetated and experienced little change or minor net deposition. In addition, the average erosion per meter of the bank face of the three study banks in the upper watershed was greater than that of the six in the lower watershed.

` The three data sets and methodologies provided information that could be employed in other areas of the Tuttle Creek Reservoir watershed and guide BVR restoration efforts. Traditional cross-sectional and other data provided insight into the evolutional phase of the BVR. Lidar derived DEMs and subsequent DoDs provide estimates of erosion and deposition along the entire channel of the BVR and three of its tributaries, and may provide more accurate locations erosional "hotspots" than the methods previously used by the KWO. Erosion hotspots identified with repeat lidar surveys could then be monitored using more exact surveying methods, such as traditional surveying and SfM. The process of creating DoDs along riverbanks could easily be applied to all the Tuttle Creek watershed within Marshall and Nemaha Counties. It is also believed that SfM could be an effective tool in monitoring most of the erosion hotspots within the BVR, as most of them are well suited for the use of SfM.

Copyright

© Michael McNair 2023.

Table of Contents

List of Figures xv

List of Tables xxiii

Acknowledgments xxv

Chapter I – Introduction 1

European Settlement and Channel Change 1

Sedimentation of Tuttle Creek Reservoir 3

General Methodology 4

Research Goals and Questions 7

Significance 9

Study Area and Site Selection 12

Sass & Keane (2012) Study Reaches 13

Irish Creek 14

BVR Main Stem 15

North Fork 16

Structure-from-Motion Study Bank Sites 17

Chapter II – Study Background and Literature Review 20

Ecoregions 20

Western Corn Belt Plains (Ecoregion 47) 21

The Flint Hills (Ecoregion 28) 22

Geology and Physiographic Regions 22

Soils 24

Climate 25

Historical Vegetation Communities..... 26

Dynamic Equilibrium..... 27

Stream Energy and Stream Power..... 28

Overland Erosional Processes..... 30

Rainsplash..... 30

Sheetwash..... 30

Rill..... 31

Gully..... 31

In-Channel Erosional Processes..... 32

Fluvial Entrainment..... 32

Pore Pressure..... 34

Dry Ravel..... 36

Soil Piping/Seepage..... 36

Freeze=Thaw..... 37

Ice Scour/Ice Jams..... 38

Mass Wasting..... 38

Anthropogenic Alterations to the Black Vermillion River Watershed..... 39

Agricultural Development..... 39

Loss of Riparian Vegetation..... 43

BVR Channelization..... 45

Channel Evolution Models..... 47

Schumm Harvey and Watson (1984)..... 47

Simon and Hupp (1986)..... 49

Cluer and Thorne (2013) 52
Rosgen Successional Scenarios (2006 53
Use of Structure-from-Motion (SfM) Photogrammetry in Fluvial Geomorphology . 60
Basics of Photogrammetry and Structure-from-Motion 61
SfM vs. Traditional Photogrammetry 63
Use of SfM in Riverbank Monitoring and Comparison to Other Techniques ... 65
Use of Repeat LiDAR Datasets to Monitor Riverbank Change 69
Chapter III – Channel Succession of the Black Vermillion River 71
Introduction 71
Study Area Description 73
BVR Watershed Change in Land Use 76
BVR Channelization 78
BVR Impoundments 80
Channel Evolution Models 81
Rosgen Successional Scenarios (1996, 2006, 2014) 86
BVR Stream Type in 2009 89
Availability of Data 89
Methods 90
Geomorphic Changes in Dimension, Pattern, and Profile at the Sass & Keane (2012) Study Reaches 91
Dimension 91
Profile and Pattern 93
Channel Material 93

Summary of Variables and Ratios Collected at the Seven Sass & Keane (2012 Study Reaches 94

Geomorphic Change along the Entire BVR River Channel Using 2010-12 and 2018 DEMs 94

Patterns and Amounts of Erosion and Deposition along the BVR Channel 100

Results and Discussion 101

Irish Creek 101

Irish Creek 1 102

Irish Creek 2 104

Irish Creek 3 106

Irish Creek System Wide 108

BVR Main Stem 113

BVR Main Stem 2 115

BVR Main Stem 3 117

BVR Main Stem System Wide 119

North Fork 121

North Fork 1 123

North Fork 2 126

North Fork System Wide 127

Chapter III Summary and Conclusions 133

Chapter IV – Quantification of the Effects of Woody Riparian Vegetation on Black Vermillion River Streambank Erosion and Deposition Utilizing Repeat LiDAR-Derived Elevation Data 139

Introduction 139

Sedimentation of Tuttle Creek Reservoir 142

Study Area 146

Methods and Methodological Results 149

LiDAR Data 149

Horizontal Correction 154

Geoid Correction 157

Accuracy Assessment 158

Flight Line Co-Registration Error 161

DoD Error Propagation, Probabilistic Thresholding & Riverbank Volume Change 164

Volume Change within Woody Vegetation Classes 167

Effects of Understory and Overstory Density on Erosion and Deposition Rates 170

Results and Discussion 175

Volume Change 175

Volume Change by Amount of Woody Vegetation 182

Effects of Understory and Overstory Vegetation Density 190

Conclusion 191

Chapter V – Evaluating the Use of Structure-from-Motion Photogrammetry to Seasonally and Annually Monitor Black Vermillion River Erosion “Hotspots” 194

Introduction 194

Tuttle Creek Reservoir Watershed Erosion “Hotspots” 195

Use of SfM to Monitor Riverbank Geomorphic Change..... 199
Study Area..... 200
Methods 202
Site Selection 202
SfM Photogrammetry Process..... 205
Volume Change & Evaluating the Use of SfM to Monitor Erosion Hotspots.. 210
Combined Error Estimation 211
Volume Change Calculations Using Cloud Compare 212
Results and Discussion 216
Evaluation of Checkpoint XY Errors over the Study Period..... 218
Percentage of Matching Cells when Calculating Volume Change with Empty Voids in CC 220
Volume Change..... 224
Sensitivity of Deposition to Interpolation..... 224
Volume Change Calculations for Entire Study Period and Leaf-off to Leaf-off Conditions..... 227
Use of SfM to Monitor BVR Erosional Hotspots at a Fine Temporal Scale.... 230
Erosional Processes and River Flows 241
Conclusion 247
Chapter VI – Summary and Conclusions 249
Comparison of Data Set Spatial and Temporal Resolution 250
Cross Section Summaries..... 251

Future Research 254

Contributions 255

References 257

Appendix A: Study Reach Cross Sections 276

Appendix B: Study Bank Point Clouds and DoDs 280

Appendix C: CloudCompare Volume Change for All Periods 290

Appendix D: SfM Study Banks: BVR Discharge Overlain with Erosion 292

List of Figures

Figure 1 Black Vermillion Watershed 1

Figure 2 Sedimentation of Tuttle Creek: 2007 to 2022 4

Figure 3 BVR Subwatersheds Upstream of Frankfort and Expanded Study Area..... 12

Figure 4 Irish Creek Subwatershed and Study Reach Locations 15

Figure 5 BVR Mainstem Subwatershed and Study Reach Locations 16

Figure 6 North Fork Subwatershed and Study Reach Locations..... 17

Figure 7 Typical SfM Study Bank 18

Figure 8 SfM Study Bank Sites 19

Figure 9 Ecoregions of Eastern Kansas 21

Figure 10 Physiographic Regions of Kansas..... 23

Figure 11 Illustration of Lane's Balance 28

Figure 12 Hjulstrom Diagram 33

Figure 13 Illustration of Bank Failure and Pore Water Pressure 35

Figure 14 Urbanization Storm Hydrograph..... 40

Figure 15 Land Use, Sediment Yield and Channel Response to Urbanization 42

Figure 16 Timing of Channelization in the BVR..... 46

Figure 17 Cluer & Thorne (2014) Stream Evolution Model (SEM) 53

Figure 18 Rosgen Classification System Level I Stream Types 54

Figure 19 Rosgen Classification Metrics Illustration 55

Figure 20 Key to Rosgen Classification System 56

Figure 21 Rosgen Stream Succession Scenarios 58

Figure 22 Photogrammetry Diagram 62

Figure 23 Typical GCP Layout on 120-acre Site 65

Figure 24 Lane's Balance 71

Figure 25 Location of the BVR Watershed in NE Kansas 73

Figure 26 Subwatersheds and Study Reaches of Sass & Keane (2012) 74

Figure 27 Annual Precipitation at Frankfort, KS 2007-2021 76

Figure 28 Rosgen Successional Scenarios 85

Figure 29 Key to Rosgen Classification System 87

Figure 30 Rosgen Level II Classification Dimensions and Ratios of Irish Creek 2021 Riffle Cross Section 87

Figure 31 Illustration of Bank Profile 92

Figure 32 Irish Creek 3 Pool Cross Section 97

Figure 33 Flightline Correction for 2010-2018 DoD 99

Figure 34 IC1 Riffle Cross Section, 2007, 2009, 2021 103

Figure 35 Irish Creek 2 Pool Cross Section 106

Figure 36 Irish Creek Erosion and Deposition 2010 - 2018 110

Figure 37 Irish Creek Streambank Erosion by Drainage Area 112

Figure 38 Irish Creek Area of Severe Erosion 112

Figure 39 Eroding Bank within Irish Creek Segment 18 113

Figure 40 Western Main Stem Channelization 1967-2021 114

Figure 41 BVR Main Stem 2 Riffle Cross Section 2007, 2009, 2021 117

Figure 42 BVR Main Stem 3 Riffle Cross Section 2007, 2009, 2021 118

Figure 43 BVR Main Stem Erosion and Deposition 2010 (12) - 2018 119

Figure 44 North Fork 1 Riffle Cross Section Looking Upstream 124

Figure 45 North Fork 1 Riffle Cross Section 2007, 2009, 2021 124

Figure 46 North Fork 1 Pool Cross Section 2007, 2009, 2021 125

Figure 47 North Fork 1 Pool Cross Section Downstream Meander Migration 126

Figure 48 North Fork 2 Riffle Cross Section 2007, 2009, 2021 127

Figure 49 North Fork 2 Erosion and Deposition 2010 (12) – 2018 128

Figure 50 Weyer Creek Reach Channelization between 2012 and 2014 129

Figure 51 Weyer Creek Erosion and Deposition 2012 – 2018 130

Figure 52 Hjulström-Sundborg diagram with NF1 and NF2 Competence 132

Figure 53 North Fork 2 Increase in Woody Vegetation 2008 – 2019 133

Figure 54 Black Vermillion Watershed in Northeast Kansas 143

Figure 55 Tuttle Creek Reservoir Watershed and Sedimentation 145

Figure 56 BVR Subwatersheds with Sass & Keane (2012) Study Reaches..... 147

Figure 57 Process for Creation of BVR Riverbank DoDs 151

Figure 58 DoD Legend 154

Figure 59 DoD Correction at Sass & Keane (2012) Study Reach North Fork 2 156

Figure 60 Horizontal Offset Points 156

Figure 61 Marshall Co. Study Area Geoid 03-12B Difference Surface with Random Points 158

Figure 62 Comparison of 2007, 2021Traditional Surveyed Cross Sections to 2010 and 2018 DEM Generated Cross Sections 161

Figure 63 2010 – 2018 DoD Flight Line Coregistration Error Correction 163

Figure 64 Examples of Change in Slope in BVR Agricultural Fields 163

Figure 65 Process for Assessing the Presence of Woody Vegetation on Erosion and Deposition 167

Figure 66 Vegetation Categories Adopted from Sass & Keane (2012) 168

Figure 67 Woody Vegetation Classification Assisted by Individual Tree Top Point Analysis..... 170

Figure 68 Understory NRD and Pool Cross Sections at Irish Creek 1 and 2..... 173

Figure 69 Volume Change for Marshall and Nemaha Co. DoDs at the 95%CI 177

Figure 70 NF-LMS Erosion and Deposition Upstream of Frankfort (2010 (12) – 2018) 178

Figure 71 Examples of Human Induced Erosion and Deposition 179

Figure 72 NF-LMS Erosion and Deposition Downstream of Frankfort (2010-2018) .. 180

Figure 73 NF-LMS Area of High Erosion due to Downstream Meander Migration 180

Figure 74 Channelized Reach of Weyer Creek 181

Figure 75 Marshall Co. Erosion and Deposition by Amount of Vegetation (CI 95%). 184

Figure 76 Nemaha Co. Erosion and Deposition by Amount of Vegetation (CI 95%). 186

Figure 77 Sass & Keane (2012) Main Stem 2 Study Reach with 2012-2018 DoD 187

Figure 78 Sass & Keane (2012) Main Stem 2 Cross Sections with 2012-2018 DoD 187

Figure 79 Small Area of Channelization in Weyer Creek 188

Figure 80 Area of Weyer Creek with Riparian Vegetation Removed and High Erosion 188

Figure 81 Area along Irish Creek NRD Map Overlain with 2010-2018 DoD 191

Figure 82 Sedimentation of Tuttle Creek 2007 to 2022 195

Figure 83 Tuttle Creek Reservoir and Big Blue River Watershed 196

Figure 84 Missed Erosion Hotspot in KWO Assessment..... 197

Figure 85 Black Vermillion Watershed Location in NE Kansas 201

Figure 86 BVR USGS Station #688500 Flow Data: 11/20 to 07/22 202

Figure 87 Typical BVR Riverbank with no Overhanging Riparian Vegetation 203

Figure 88 Structure-from-Motion Study Banks and Study Area 203

Figure 89 Area of High Erosion in Lower BVR 204

Figure 90 Typical Arrangement of Ground Control Points and Checkpoints 205

Figure 91 Ground Control Point 12” x 12” Marker 206

Figure 92 Automated Flight Planning using DJI Flight Planner 207

Figure 93 Process of Removing Bank Vegetation 209

Figure 94 Projection Directions and Planes 211

Figure 95 Rotation of SfM Study Bank along the Z-Axis to Due North 214

Figure 96 XY-Plane DoD Legend 218

Figure 97 XZ-Plane DoD Legend 218

Figure 98 Ground Control Points in Summer 219

Figure 99 UAV Survey XY RMSE by Date 219

Figure 100 Study Bank 09 Point Clouds from 12/20 and 07/22 223

Figure 101 Study Bank 19 Point Clouds from 11/20 and 07/22 223

Figure 102 Study Bank 23 Point Clouds from 11/20 and 07/22 223

Figure 103 Percentage Increase of Erosion and Deposition from Empty to Interpolated Voids by Percentage Matching Cells 224

Figure 104 Cross Section of a Concave Portion of SB16 225

Figure 105 Three Example of Interpolated Voids Resulting in Deposition 226

Figure 106 Study Bank Erosion and Deposition per Study Period 229

Figure 107 Chapter II 2010-2018 DoD with SfM Study Banks 230

Figure 108 Three Examples of Accumulation of Winter Deposition 232

Figure 109 Study Bank 30's Second (Winter) Period 233

Figure 110 Study Bank 19's Second (Winter) Period 233

Figure 111 March 2021 High Flow Water Line on Study Bank 19 234

Figure 112 Two Examples of Vegetation Concentrated at One End of Study Bank .. 235

Figure 113 Example of Vegetation of Entire Study Bank 236

Figure 114 Two Examples of Erosion Concentrated at Toe of Bank in 4th Period 239

Figure 115 Increase in Bank Vegetation on SB23: Summer 2022 240

Figure 116 Scour at Toe of Study Bank 16: Summer 2022 240

Figure 117 Selected Study Bank 30 Point Clouds and DoDs Illustrating Rotational Slump 242

Figure 118 BVR Discharge Over Erosion per Period: Study Bank 30 243

Figure 119 Selected Study Bank 31 Point Clouds and DoDs Illustrating Fall 244

Figure 120 BVR Discharge Over Erosion per Period: Study Bank 31 244

Figure 121 Selected Study Bank 19 Point Clouds and DoDs..... 245

Figure 122 BVR Discharge Over Erosion per Period: Study Bank 19..... 246

List of Tables

Table 1 BVR Sass & Keane (2012) Study Reaches 13

Table 2 Soil Name and Properties Adjacent to Sass & Keane (2012) Reaches 25

Table 3 Runoff Coefficients for the Rational Method 41

Table 4 Sediment Removal Effectiveness of Riparian Buffer Zones 44

Table 5 Schumm et al. (1984) Channel Evolution Model Type Descriptions 49

Table 6 Stage Descriptions Adapted from Simon and Hupp (1986) 50

Table 7 Study Reach Soil Properties Adapted from Sass & Keane (2012) 75

Table 8 Change in Subwatershed Centerline Length 79

Table 9 Change in Study Reach Watershed Controlled Area 81

Table 10 CEMs with Stage/Type Descriptions 84

Table 11 BVR Study Reach Characteristics and Rosgen Classification 89

Table 12 Irish Creek Rosgen Classification Metrics 101

Table 13 Irish Creek Cross Sectional Data 102

Table 14 Irish Creek Sass & Keane (2012) Pool Study Bank Data 102

Table 15 Streambank Erosion and Deposition by Subwatershed 109

Table 16 BVR Mainstem Rosgen Classification Metrics 114

Table 17 BVR Mainstem Cross Section Data 115

Table 18 BVR Mainstem Sass & Keane (2012) Pool Study Bank Data 115

Table 19 North Fork Rosgen Classification Metrics 122

Table 20 North Fork Cross Section Data..... 122

Table 21 North Fork Sass & Keane (2012) Pool Study Bank Data 122

Table 22 NRD and Tree Top Density Independent Variables 174

Table 23 Erosion and Deposition by Subwatershed and County 176

Table 24 Marshall County Erosion and Deposition by Amount of Woody Veg. 183

Table 25 Nemaha County Erosion and Deposition by Amount of Woody Veg. 186

Table 26 BVR SfM Study Bank Soil Properties 205

Table 27 SfM Image Collection Dates 210

Table 28 SfM Evaluation Periods 210

Table 29 SfM Study Bank Characteristics 217

Table 30 Volume Change Entire Study Period 221

Table 31 Volume Change Leaf-off to Leaf-off Conditions..... 222

Acknowledgments

First and foremost, I would like to thank Dr. Tim Keane for his mentorship within the realms of rivers, academics, and teaching over the last five years. I am especially grateful for his patience, as my time at KSU has extended two years into his retirement. I would also like to thank the other members of my committee and the Director of the PhD program, Dr. Trisha Moore, Dr. Abigail Langston, Professor Howard Hahn, and Dr. Anne Beamish for their time, flexibility, and continued support throughout this process. A special thank you to Dr. Moore, who graciously agreed to act as Co-major Professor in the 11th hour of my doctoral journey.

I would also like to thank the landowners for allowing me access to their property over a three-year period. Their contribution to the better understanding and management of the Black Vermillion River is greatly appreciated.

I am eternally thankful and grateful for my mom, Dr. Frances McNair, whose support on every level has made this endeavor possible. I would like to thank my siblings and niece, Mary, William and Virgie, and my friends for their support and encouragement over the last five years, as it was both needed and appreciated on many occasions.

Finally, I would like to thank the late Billy Klingensmith, whose love, encouragement, and support gave me the courage to begin this journey, and his family. We began this journey together, and I can only hope that he would be happy with the outcome.

CHAPTER I – Introduction

Anthropogenic alterations to watersheds and their corresponding stream and riparian corridors often result in negative effects on stream ecosystem functions (Hellmund & Smith, 2006). This research focuses upon the effects of human development on erosion, deposition, and sediment. More specifically, this research attempts to evaluate sediment transport due to channel evolution (geomorphic channel adjustment) of the Black Vermillion River (BVR) caused by the conversion of its watershed from native tallgrass prairie and gallery forest to agricultural land uses (Reichman, 1987). The BVR is located primarily in Marshall and Nemaha Counties in NE Kansas (Figure 1).



Figure 1: Black Vermillion Watershed location in KS, (Sass & Keane, 2012)

European Settlement and Channel Change

On a global level, sediment is one of the most ubiquitous nonpoint pollutants of freshwater, with streambank erosion accounting for up to 80% of the total sediment load in many streams and rivers, and the Midwestern U.S. is no exception (Darby & Simon,

1999; Sekely, Mulla, & Bauer, 2002; Sass & Keane, 2012). A “stable” stream in equilibrium, as most in the Midwest were prior to European settlement, does not aggrade or degrade and maintains a consistent dimension, pattern, and profile as it transports water and sediment supplied by its watershed (Mackin, 1948; Leopold & Maddock, 1963; Rosgen, 1996). European settlement of the Midwest began around the time of the Civil War (1860s) resulting in alterations to fluvial systems, primarily by two practices: 1) land use change to agriculture and 2) channelization (Meade, 2009; Simon & Rinaldi, 2000). These alterations resulted in disequilibrium within rivers and streams, which set in motion geomorphological changes that are still ongoing as rivers and streams attempt to adjust their dimension, pattern, and profile to the new hydrologic and sediment regimes (Mackin, 1948; Lane, 1954; Rosgen, 1996; Simon & Rinaldi, 2000). The concepts of stream equilibrium and stream adjustment resulting from anthropogenic watershed alterations are discussed in detail in *Chapter II: Study Background and Literature Review*.

River and stream adjustment due to disturbance, both anthropogenic and natural, generally follow a pattern of down cutting (incision), incision and widening, rapid widening, widening and aggradation, and ending with the establishment of a “quasi-equilibrium” at a new, often lower, elevation (Schumm, 1977; Schumm, Harvey, & Watson, 1984; Simon & Hupp, 1986; Rosgen, 1994; Cluer & Thorne, 2014). This pattern of river adjustment following disturbance is described in a number of “channel evolution models” (CEMs) that have been developed over the last four decades (e.g., Schumm et al., 1984; Simon and Hupp, 1986; Cluer and Thorne, 2014; Rosgen 1996,

2006, 2014). CEMs are also discussed in detail in *Chapter II: Study Background and Literature Review*.

Sedimentation of Tuttle Creek Reservoir

Streambank erosion occurs predominantly during the widening phases of the various CEMs (Bull, 1997; Darby & Simon, 1999; Sekely et al., 2002; Sass & Keane, 2012), and is known to cause excessive sediment production, which, as noted by Sass & Keane (2012), may lead to the loss of reservoir storage capacity (sedimentation) downstream (Beach, 1994; Hargrove, Johnson, Snethen, & Middendorf, 2010). A prime example of reservoir sedimentation is Tuttle Creek Reservoir in NE Kansas (Figure 2). Tuttle Creek Reservoir covers an area of approximately 49.4 km^2 during normal conditions and 214.8 km^2 at full flood capacity (Sass & Keane, 2012; US-COE, 2011), and is a multi-use reservoir managed by the United States Army Corps of Engineers (US-COE, 2011).

Tuttle Creek Reservoir was originally designed to facilitate flood control and flow management of the lower Missouri River by impounding up to 524,613,846 m^3 of water (US-COE, 1998); however, since it became operational in 1962, sediment delivered by the Big Blue River and its tributaries has led to an estimated 47.9% decrease in storage capacity according to the Kansas Water Office (KWO) (Rattanavong, 2019). The BVR flows into the Big Blue River, which empties into the Tuttle Creek Reservoir. While the BVR only accounts for approximately 6% of the Tuttle Creek Reservoir watershed, it is physiographically similar to much of the Big Blue River's watershed. Therefore, evaluation of streambank erosion and channel evolution of the BVR may add to the

overall understanding of sediment being delivered to Tuttle Creek Reservoir in order to better guide restoration efforts aimed at reducing sedimentation of the reservoir.

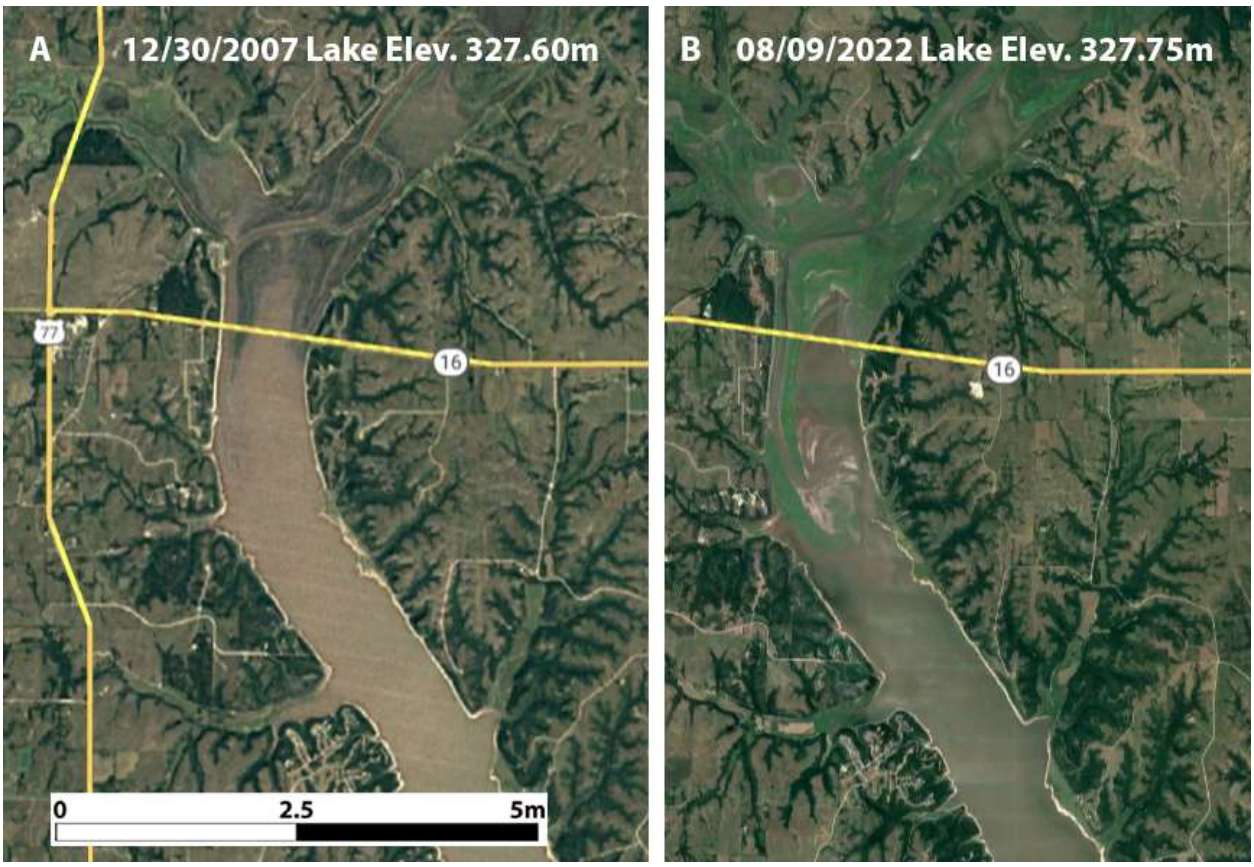


Figure 2: Sedimentation of Tuttle Creek Reservoir: North end of reservoir at the same lake elevation (A) 2007 and (B) 2022: Source: Google Earth

General Methodology

Three unique data sets and methodologies were used to develop three related studies (Chapters III, IV, and V in this dissertation) aimed at evaluating erosion and deposition along the BVR channel over the past 15 years. The following is a brief synopsis of the datasets and methodologies used in each of the three studies.

Chapter III utilized a portion of a dataset created by Sass & Keane (2012) between 2007 and 2010, which was resurveyed for this study in 2021, to evaluate channel evolution of the BVR. Seven of the original nine Sass & Keane (2012) study

reaches located in three subwatersheds upstream of Frankfort, KS were included in this study. Each study reach contained one longitudinal profile, two cross sections (pool and riffle), two study bank profiles and channel material data. Channel evolution was evaluated by comparing the current (2021) channel dimension, pattern, profile, and channel material to that observed and manually surveyed between 2007 and 2010.

A second dataset of repeat digital elevation models (DEMs) derived from LiDAR (light detection and ranging) data was also used in Chapter III to evaluate BVR channel evolution but at a system-wide scale. The DEMs and LiDAR data were publicly available through the State of Kansas GIS Data Access & Support Center and funded by the USGS 3D Elevation Program (3DEP), FEMA, NRCS, and the Kansas GIS Policy Board. A digital elevation model (DEM) is a depiction of the bare ground (bare earth) topographic surface that excludes all vegetation, buildings, and other surface objects (USGS, 2021). The DEMs used for this research are gridded images (rasters) where each cell represents a 1m x 1m area, with the value of each cell being the average elevation within the cell. LiDAR data was available for Marshall County in 2010 and 2018 and for Nemaha County in 2012 and 2018. The BVR riverbanks were delineated and the portions of each year's DEM within the banks extracted. The earlier DEMs (2010 and 2012) were subtracted from the more current DEMs (2018) to create digital elevation models of difference (DoDs), which are grid surfaces where each cell represents the change in elevation. The DoDs were then used to estimate amounts and locations of erosion and deposition along all BVR riverbanks included in this study between 2010-12 and 2018. Comparison of the BVR channel bank DEMs aided in

determining if the changes observed at the Sass & Keane (2012) study reaches were indicative of each subwatershed overall.

Chapter IV further utilized the DEM and LiDAR datasets introduced in Chapter III along with historical aerial photographs to investigate amounts and patterns of erosion and deposition along the BVR riverbanks as well as the effects of woody riparian vegetation on riverbank erosion and deposition rates. First, systematic errors common when using legacy LiDAR datasets were identified and corrected and amounts of erosion and deposition estimated. Next, the effects of the presence, amount, and density of riparian woody vegetation on bank erosion and deposition were evaluated. Automated tree top detection analysis using the LiDAR data along with aerial photographs was used to determine areas along both right and left banks of the BVR with no woody vegetation, little woody vegetation, and ample woody vegetation. Portions of the riverbank for each vegetation category were isolated, and the erosion and deposition within each category estimated by comparing DEMs from 2010-12 and 2018. In addition, the effects of understory and overstory vegetation density on bank erosion and deposition were assessed using vegetation density metrics derived from the 2010, 2012, and 2018 LiDAR point clouds. Each left and right bank was divided into 100-m segments. For each segment, erosion and deposition was extracted using the repeat DEMs, which was then compared to the over and understory vegetation density metrics for each segment.

Chapter V assess the feasibility of using Structure from Motion (SfM) Photogrammetry to accurately monitor BVR riverbank erosional “hotspots” void of woody vegetation, which were shown by the results of Sass & Keane (2012) and

Chapter IV to have higher erosion rates than banks where at least some woody vegetation is present. Generally, SfM utilizes highly overlapping images collected with a drone and specialized software to create 3-dimensional point clouds, in this case, of riverbanks. This process was repeated 5-6 times on nine study banks over a 1.5-year period, and the resulting models then compared in order to estimate amounts and patterns of erosion and deposition along the banks. This process of comparing sequential topographic data is similar to that employed in Chapter IV using LiDAR data but for a smaller area and at a much higher spatial and temporal resolution.

Research Goals and Questions

The overarching goal for this research was to better understand the sources, processes, and patterns of erosion and deposition in the Black Vermillion River system that result in excess sediment being delivered to the Big Blue River and Tuttle Creek Reservoir. The primary research question:

> With the aim of guiding river restoration efforts, how do a variety of methods such as traditional river surveying methods, LiDAR-derived DEMs, and SfM Photogrammetry compare when utilized to estimate amounts and patterns of streambank erosion and deposition over time at both the reach and system-wide scales?

Each of the three studies (Chapters III, IV, and V) outlined above had specific objectives and research questions aimed at achieving the overarching goal while answering various facets of the primary research question.

The two objectives of Chapter III were: 1) to use traditional surveying methods to resurvey, cross sections, longitudinal profiles, and bed materials of seven of nine Sass & Keane (2012) study reaches, and then use that data to better understand how the

BVR channel evolution is influencing sediment production, and 2) to use repeat LiDAR-derived DEMs from 2010 (12) and 2018 to determine if changes at the Sass & Keane (2012) study reaches are representative of all BVR riverbanks. The questions associated with these objectives were:

1. How has the dimension, pattern, profile, and channel material changed at the seven Sass & Keane (2012) study reaches included in this study over the last 14 years (2007 to 2021)?
2. How do the changes in dimension, pattern, profile, and channel material reflect the channel evolution of the BVR, and how might this evolution influence sediment production?
3. Do the DoDs created by comparing DEMs from 2010-12 and 2018 indicate the changes at the seven study reaches are representative of the entire river channel within each subwatershed?

The two objectives of Chapter IV were: 1) use DoDs created by comparing DEMs from 2010 (12) and 2018 to determine amounts and patterns of erosion and deposition along 151 km of the BVR and three of its tributaries and 2) use the DoD and LiDAR point cloud data to assess how the presence, amount, and density of woody vegetation affects riverbank erosion and deposition. The questions associated with these objectives were:

1. How much streambank erosion/deposition occurred from 2010 (2012 for portions of the BVR in Nemaha County) to 2018 in each subwatershed included in this study?
2. Where has erosion/deposition occurred within each subwatershed?
3. Do the rates of erosion and deposition along banks void of woody vegetation differ from the rates along banks that have little and/or ample woody vegetation?

4. How does understory and overstory vegetation density affect erosion and deposition along the BVR riverbanks?

The objective for Chapter V was to evaluate the use of SfM photogrammetry to monitor BVR riverbank erosion "hotspots," which are typically void of woody vegetation, at both an annual as well as a fine (seasonal) temporal scale. The questions associated with this objective were:

1. Is drone-based photogrammetry a feasible method for monitoring riverbank erosion at a fine temporal scale along channels with high banks and variable vegetation cover as found in the BVR?
2. Is there any relation between river flow events and erosional processes common in the BVR system?

Significance

All three studies included in this research will contribute to the understanding of sediment being delivered to Tuttle Creek Reservoir, especially due to riverbank erosion. According to the 2018 *Tuttle Creek Watershed Restoration Protection Strategies (WRAPS) Plan,* the sediment load being delivered to Tuttle Creek Reservoir needs to be reduced from 5.83 to 2.83 million tons annually to meet the suggested total maximum daily load (TMDL). The BVR physiography and land use is similar to much of the Tuttle Creek Reservoir watershed, and understanding sediment production in the BVR system could be used to better understand sediment production in other areas of the watershed with similar land uses and drainage areas.

Chapter III documents BVR channel change since 2009 by adding to the dataset created by Sass & Keane (2012) at seven study reaches located throughout the BVR watershed and thus contributes to the understanding of the evolution of the channel at

those locations. This chapter also continues the monitoring of channel changes in the BVR Basin, which may be “informative regarding mechanisms and rates of adjustment in moving toward quasi-equilibrium channel conditions” (Keane & Sass, 2017). The system-wide DoD analysis introduced in Chapter III helps determine if changes at the Sass & Keane (2012) study reaches are reflective of the entire channel.

Perhaps the most important contribution of Chapter IV was implementing and building upon the process of creating DoDs that provide a record of geomorphic change over the entire earth surface within each (Marshall Co. and Nemaha Co.) study area. LiDAR analysis is only limited by the coverage of the LiDAR datasets and may be used to study upland as well as fluvial geomorphology. Repeat LiDAR surveys of large areas are just now becoming more common, as the 2018 LiDAR data used in this study just became publically available in 2022. When isolating the DoDs to portions of the BVR riverbanks, they may provide more accurate estimates of locations and amounts of riverbank erosion and deposition than methods previously used by the KWO. In addition, the methods detailed in Chapter IV could be applied to other areas of the Big Blue River’s watershed included in the 2010, 2012, and 2018 LiDAR surveys.

Chapter IV also adds to the understanding of the influence of woody riparian vegetation on rates of streambank erosion along the entire BVR channel over an 8-year period in Marshall County and 6-year period in Nemaha County. Sass & Keane (2012) found the bank erosion rate of banks void of woody vegetation at 7 of 18 study banks) and those with at least some woody vegetation to be 0.45 m/yr and 0.12 m/yr, respectively, and this study attempts to corroborate the Sass & Keane (2012) findings.

Chapter V provides detail and accurate amounts of riverbank erosion over a 1.5-year period at specific locations (erosion “hotspots”) void of overhanging woody vegetation, which were determined to have higher erosion rates than riverbanks with at least some woody vegetation in Chapter IV. Previously, SfM has been primarily used to study gravel and cobble dominated rivers in montane environments (e.g., Dietrich, 2014; Mirijovsky & Langhammer, 2015; Tamminga, Eaton, and Hugenhlotz, 2015; Hamshaw, Bryce, Rizzo, and O’Neil-Dunne, 2017; Marteau, Vericat, Gibbins, Batalla, and Green, 2017; Langhammer & Vacková, 2018), which are quite different from the BVR. Duro, Crosato, Kleinhans, & Uijttewaal (2018) monitored banks of the straight, mid-sized Meuse River typified by complex vertical scarps of cohesive bank material more similar to the BVR riverbanks; however, the maximum bank height was 3.5m while the maximum bank height in the lower BVR is approximately 8m.

Chapter V evaluates the feasibility of using SfM to monitor BVR riverbanks typified by high, often-vertical banks with varying amounts of herbaceous riparian vegetation. Chapter V also builds on the body of research using SfM to monitor river geomorphology in eastern Kansas, where Lazell et al. (2022) utilized UAV surveys in conjunction with traditional surveying methods to monitor the effectiveness of erosion control structures along the Cottonwood River. To my knowledge, SfM has not yet been used to monitor streambank erosion in such a small agricultural river as the BVR with a narrow channel and steep, high banks in the glaciated region of NE KS.

Study Area and Site Selection

The study area of Sass & Keane (2012) also serves as the study area for Chapter III and consists of three BVR subwatersheds upstream of the USGS gauging station, located approximately 3.7 km downstream of Frankfort KS. However, the study area was expanded for Chapters IV and V to include the portion of the BVR Main Stem between the USGS gauging station and the confluence of the BVR and the Big Blue River approximately 19 km downstream of Frankfort (Figure 3).

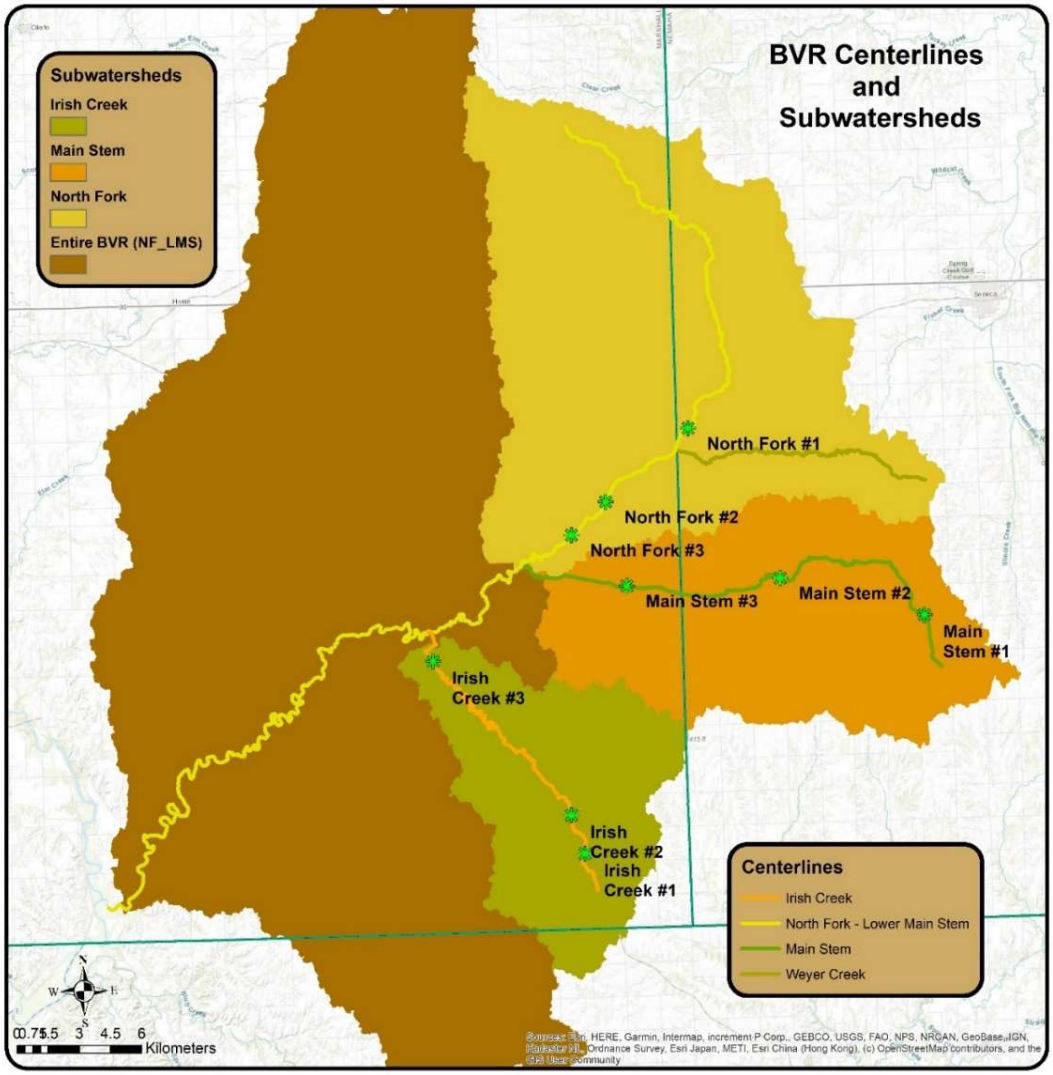


Figure 3: BVR Subwatersheds Upstream of Frankfort, KS, and Expanded Study Area: Green asterisks indicate Sass & Keane (2012) Study Reaches

The bulk of the BVR watershed is located in Marshall and Nemaha Counties with a small portion located in Pottawattamie County in NE Kansas (Sass & Keane, 2012). The drainage area of the BVR upstream from the USGS gauging station in Frankfort is 1062 km^2. (USDA -SCS, 1966; Sass, 2011). The primary land use in the entire study area, the BVR watershed, is tillage agriculture interspersed with small amounts of pasture.

Sass & Keane (2012) Study Reaches

Sass & Keane (2012) monitored nine study reaches; however, only seven study reaches were included in this study, due to landowners' access permission. Sass & Keane (2012) chose three representative reaches within each of the three subwatersheds upstream of Frankfort: 1) Irish Creek (IC), 2) BVR Main Stem (MS) and 3) BVR North Fork (NF) (Figure 3). Within each study reach, two representative cross sections were chosen, one at a riffle characterized by shallow fast-moving water in a relatively straight portion of the river, and one at a pool, characterized by deep slow-moving water usually located in a curve of the river known as a meander bend. Table 1 indicates the study reach lengths and placement of cross sections included in this study.

Reach (ft.)	Length (ft.)	Pool X-Sec Station (ft.)	Riffle X-Sec Station (ft.)
IC 1	12+35	5+72	1+56
IC 2	16+74	16+46	11+34
IC 3	17+22	5+51	0+00
MS 2	15+51	1+90	3+82
MS 3	13+60	5+38	3+90
NF 1	16+76	3+12	12+53
NF 2	22+86	5+86	0+33

Table 1: BVR Sass & Keane (2012 Study Reach Length and Cross Section Stations: Note lengths and station locations are in feet and in survey notation where stations are every 100' (first number) with the second number being the distance from the station (e.g., station 5+72 is 572 ft. from the beginning of the reach). Survey Notation was used for because of its use in the original Sass & Keane (2012) table.

Irish Creek

The Irish Creek's watershed is in Marshall County except for a small portion in Pottawattamie County and drains approximately 120.5 km^2. The headwaters of Irish Creek lie to the southeast of Frankfort and are strongly influenced by the Flint Hills Uplands physiographic region that lies to the south (Sass, 2012) (Figure 3). As Irish Creek flows north towards Frankfort, the physiography of the watershed becomes more typical of the Glaciated Region of KS with its glacial till soils (USDA -SCS, 1966). Characteristics of the Glaciated Region of KS are discussed in more detail in *Chapter II: Background and Literature Review*. The Irish Creek watershed is also located within the tallgrass prairie region of Kansas. This region was originally composed of a mix of prairie grasses, such as big bluestem (*Andropogon gerardii*), little bluestem (*Schizachyrium scoparum*), Indian grass (*Sorghastrum nutans*), sideoata grama (*Bouteloua curtipendula*), and switchgrass (*Panicum virgatum*).

Numerous flow-through water impoundments have been constructed in the Irish Creek watershed, and these impoundments alter the flow characteristics of the creek creating irregularities when calculating runoff and flow rates (US-COE, 1998; Sass & Keane, 2012). A flow-through impoundment is an artificial water body that collects runoff from a portion of the subwatershed then releases the water in a controlled manner over a longer period of time than would naturally occur. The Irish Creek watershed consist of rolling topography with an elevation change of 88 m over a distance of 27.4 km (USDA - SCS, 1966; Sass & Keane, 2012). The three representative reaches monitored in the Irish Creek Watershed are shown below in Figure 4.

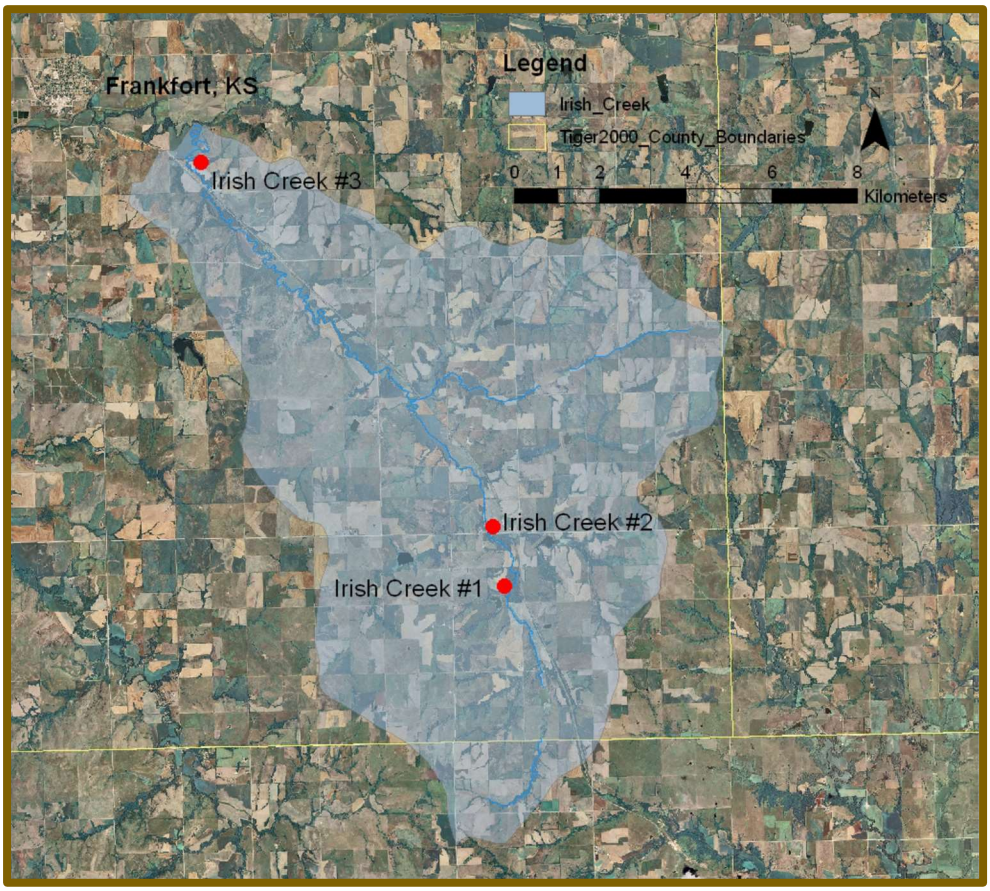


Figure 4: Irish Creek Subwatershed and Study Reach Locations (Sass, 2011):

BVR Main Stem

The BVR Main Stem originates in Nemaha County to the east of Marshall County and flows from east to west draining approximately 217 km 2. The BVR Main Stem watershed contains many small flow-through impoundments as well as the largest impoundment in the entire BVR watershed, Centralia Lake. Centralia Lake was finished in 1991, covers approximately 1.6 km^2, and controls 32.4 km^2 (approx. 20%) of the Main Stem's watershed (USDA -SCS, 1966; Sass & Keane, 2012). The Main Stem watershed is also located in the tallgrass region of KS and therefore historically had similar plant communities as the Irish Creek watershed (Sass, 2012). The elevation change over the course of the BVR Main Stem is 79.25 m over a distance of 43.5 km,

which is the flattest of the three subwatersheds. The three reaches monitored by Sass & Keane (2012) in the Main Stem subwatershed are shown in Figure 5.

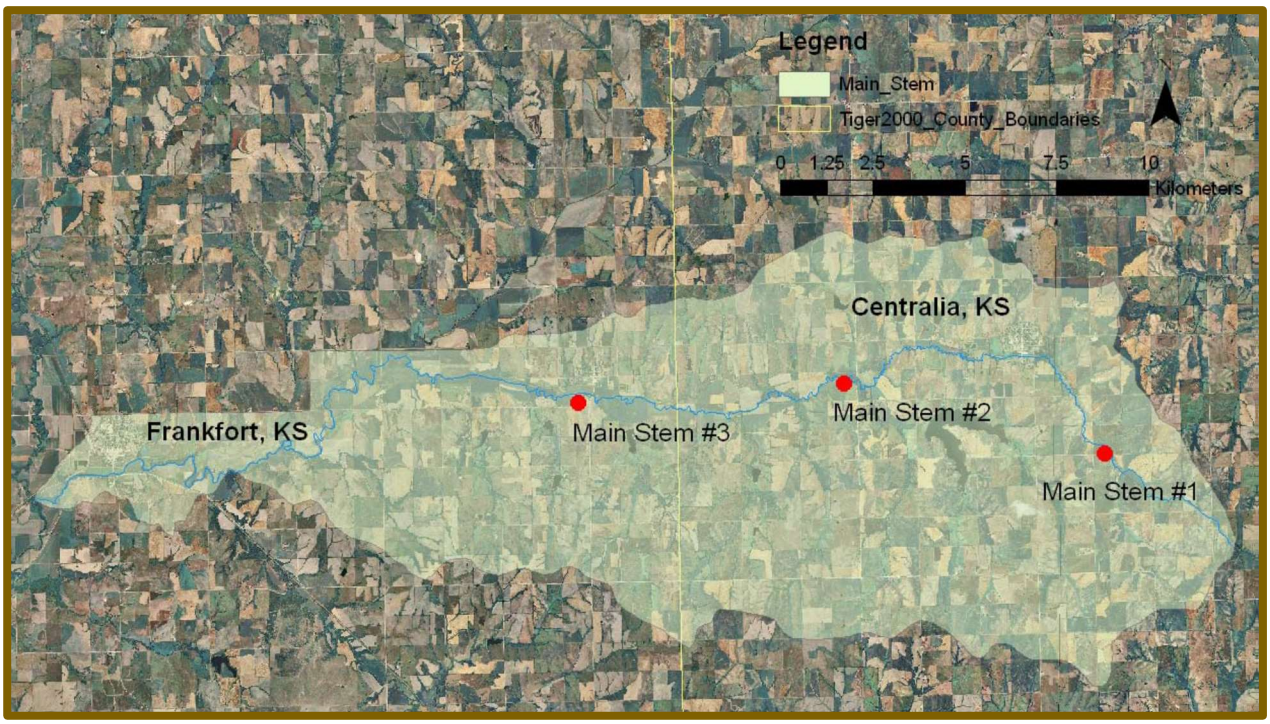


Figure 5: BVR Main Stem Subwatershed and Study Reach Locations (Sass, 2011)

North Fork

The North Fork of the BVR is the largest of the three subwatersheds included in Sass & Keane (2012) and covers approximately 313.4 km^2. The confluence of the BVR Main Stem and North Fork is located approximately 14 km upstream of Frankfort, KS. At the point of confluence, the North Fork is the main channel, as it is associated with higher drainage area and discharge than the BVR Main Stem upstream of that point. Therefore, the BVR Main Stem upstream of the confluence point is a tributary of the North Fork and Main Stem downstream of that point. The BVR North Fork is also in the tallgrass region of KS and consists of rolling topography with entrenched streams (Sass & Keane, 2012). The elevation change over the course of the BVR North Fork is

100.25 m over a distance of 37 km. The North Fork subwatershed and study reaches are shown in Figure 6.

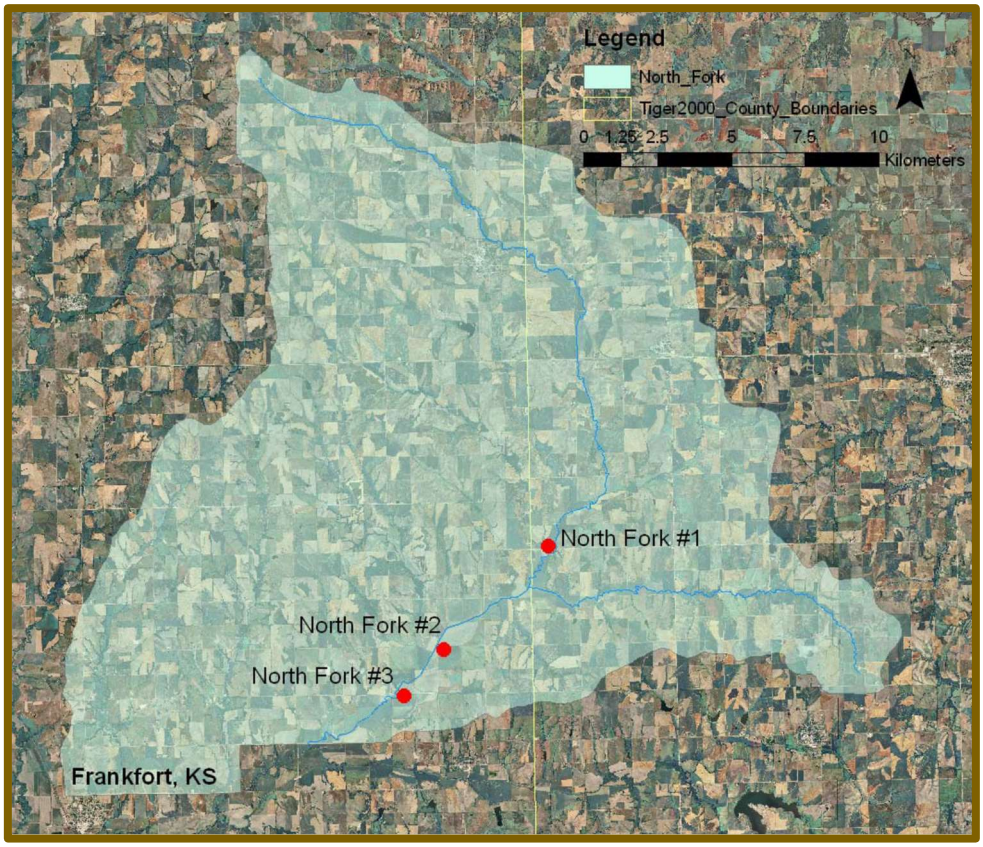


Figure 6: North Fork Subwatershed and Study Reach Locations (Sass, 2011)

Structure-from-Motion Study Bank Sites

Sass & Keane (2012) used traditional differential level surveying technique, and this research also used traditional survey methods when resurveying the Sass & Keane (2012) study reaches. In the spirit of seeking new, less costly, and less time-consuming methods for monitoring streambank erosion, this research also employed structure-from-motion (SfM) photogrammetry to monitor a number of erosion "hotspots" throughout the BVR system. As noted, SfM utilizes overlapping images collected with a

drone and specialized SfM software to create three-dimensional models of stream banks that can be compared to each other over time. This process is explained in more detail in *Chapter II: Study Background and Literature Review.* Nine SfM study bank sites were selected for periodic streambank monitoring using SfM photogrammetry. These sites were selected based upon their suitability for such monitoring, characterized by actively eroding banks that have little vegetation on or overhanging the bank (Figure 7). Three SfM sites were located in the Sass & Keane (2012) study area with two sites located along the BVR North Fork and one along the BVR Main Stem. The remaining six additional sites were located along the BVR Main Stem downstream of the USGS gauging station at Frankfort, KS (Figure 8).



Figure 7: Typical SfM Study Bank

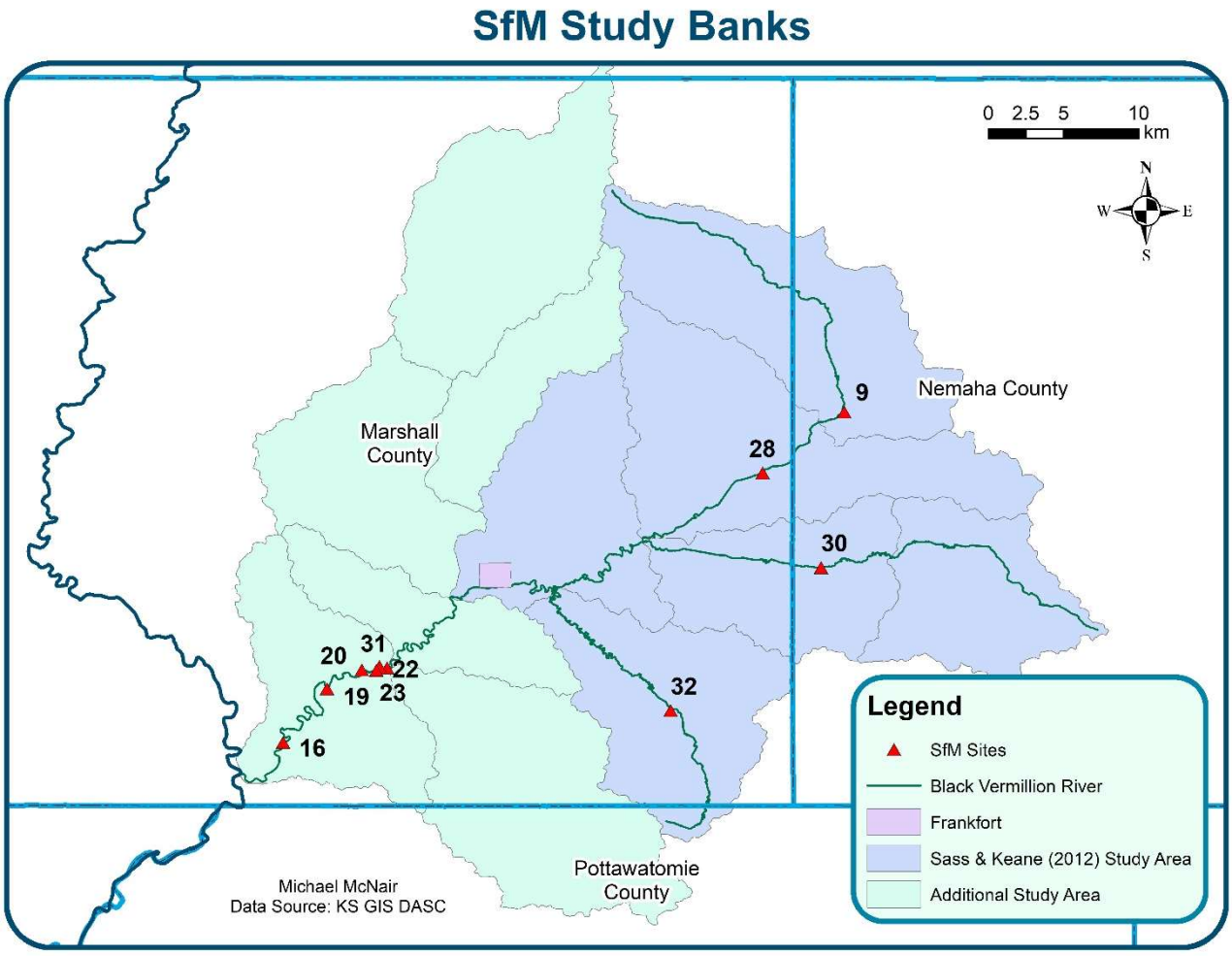


Figure 8: SfM Study Bank Sites: Numbers are Study Bank ID#s

CHAPTER II – Study Background and Literature Review

This section serves to define topics, concepts, and themes central to Chapters III, IV and V. First, the regional background of the study area is presented including the ecoregions, physiographic regions, climate, geology, soils, and historic vegetation communities. The concept of stream dynamic equilibrium will be explained including Stream Energy and Lane's (1954) balance. Erosional processes are then discussed with an emphasis on in-channel processes, as streambank erosion is the primary focus of this research. Next, a brief history is given highlighting the effects of agricultural development and channelization on the BVR and its watershed, followed by a discussion of channel evolution models that reflect channel adjustments initiated by the disturbances related to agricultural development. Finally, two remote sensing technologies utilized in this study to monitor streambank erosion, LiDAR-derived digital elevation models, and structure-from-motion (SfM) photogrammetry, are discussed.

Ecoregions

Ecoregions are areas where the type, quality, and quantity of environmental resources related to the overall ecosystem are generally similar (US-EPA, 2018). Ecoregions are delineated based on the analyzation of patterns and composition of both biotic and abiotic phenomena, such as geology, landforms, soils, vegetation, climate, land use, wildlife, and hydrology (Omernik, 1987). Ecoregions are organized in a nested hierarchal system of four levels (I-IV), with each higher level being finer, more detailed, and more homogeneous (US-EPA, 2018). At the Level III ecoregion, the BVR lies mostly within the Western Cornbelt Plains with a small portion lying in the Flint Hills: therefore, these two ecoregions are briefly discussed (Figure 9).

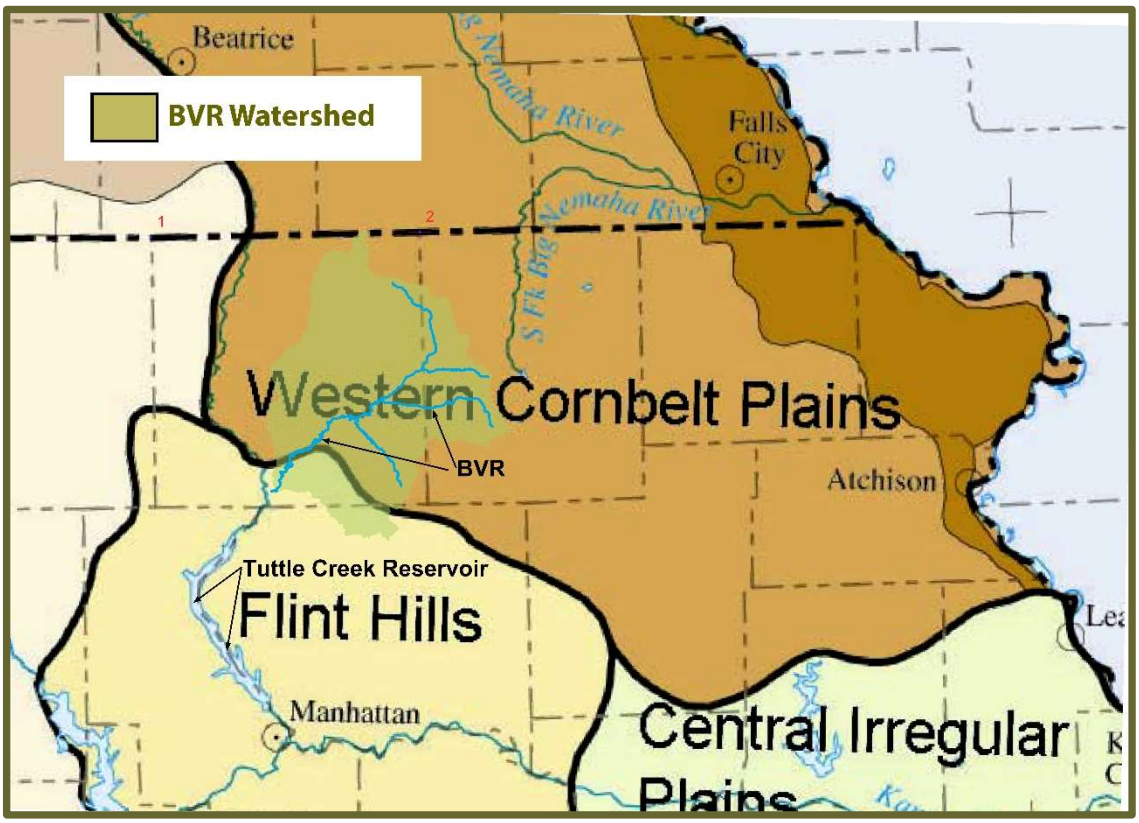


Figure 9: Ecoregions of Eastern Kansas

Western Corn Belt Plains (Ecoregion 47)

While tallgrass prairie once covered most of the Western Corn Belt Plains (WCBP), 75 percent of the landcover is now used for cropland agriculture (Chapman, Omernik, Freeouf, Huggins, & McCauley, 2001). The area is typified by gently rolling glaciated till plains and hilly loess plains, with an average precipitation of 63-89 cm, falling primarily in the growing season (Chapman et al., 2001). The warm, moist soils of the WCBP result in one of most productive areas of corn and soybeans in the world. Contamination of groundwater from fertilizers, pesticides, and concentrated livestock production are environmental concerns of the WCBP (Chapman et al., 2001).

The Flint Hills (Ecoregion 28)

"The Flint Hills is a region of rolling hills with relatively narrow steep valleys and is composed of shale and cherty limestone with rocky soils. In contrast to surrounding ecological regions that are mostly in cropland, most of the Flint Hills region is grazed by beef cattle. The Flint Hills mark the western edge of the tallgrass prairie and contain the largest remaining intact tallgrass prairie in the Great Plains." (Chapman et al., 2001).

Geology and Physiographic Regions

Kansas can be divided into 11 physiographic regions based on the physical geography or physiography (Figure 10) (KGS, 2007), with the bulk of the BVR watershed located in the Glaciated Physiographic Region of Kansas and a small portion of the Irish Creek Watershed lying in the Flint Hills Physiographic region. These two physiographic regions have similar underlying bedrock consisting of alternating layers of shale and limestone created by cycles of rise and fall in an inland sea some 270 million years ago (Aber, 2007; Walters, 1954). The limestone layers were formed when the sea was deep and full of crustaceans whose shells provided the necessary calcium carbonate (Reichman, 1987). The shale layers were formed from the mud present during low sea levels. Approximately 70 to 80 million years ago, a time of mountain building known as the Laramide Orogeny occurred in North America that resulted in the tilt we see in these layers today which is approximately 4% to the north/northwest (National Park Service, 2020).

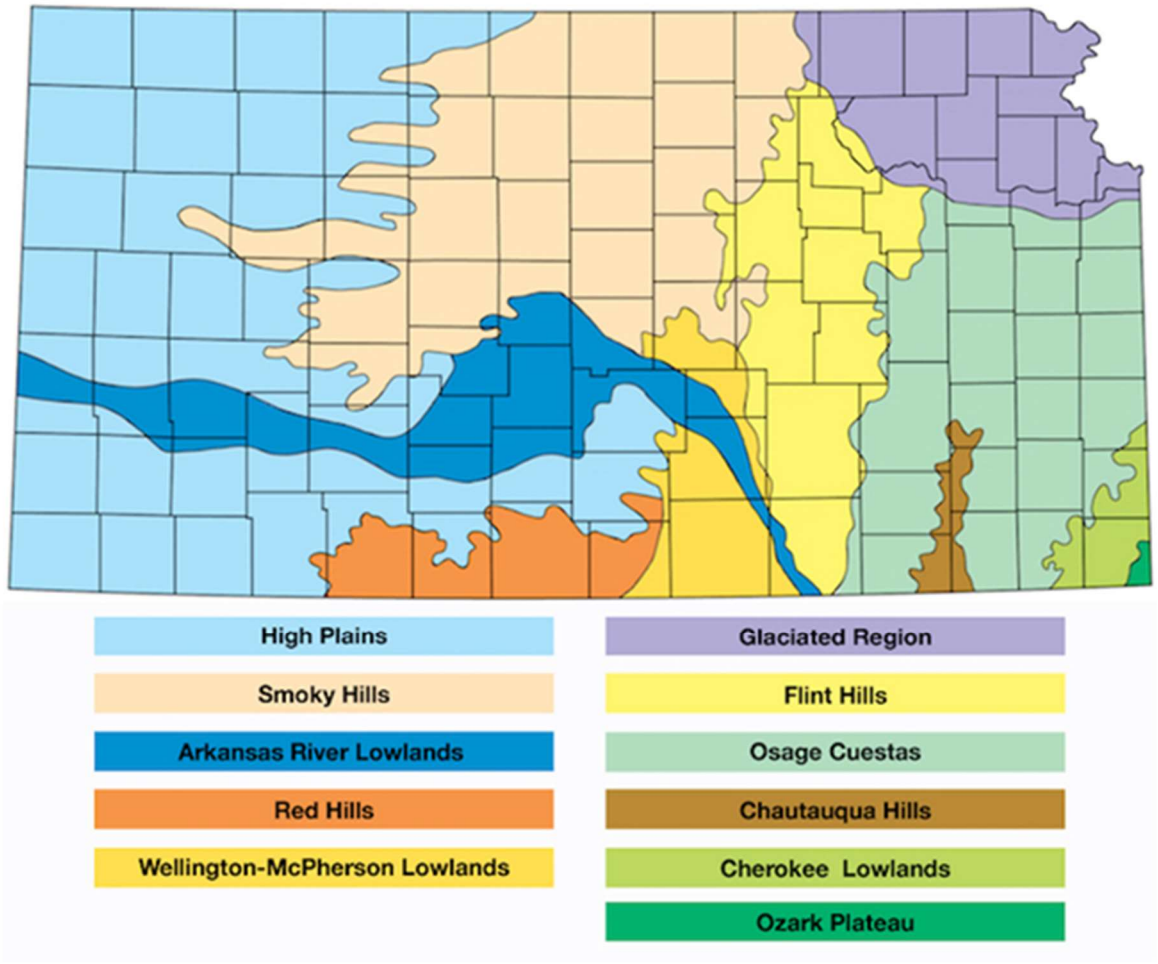


Figure 10: Physiographic Regions of Kansas

In the Glaciated Region of Kansas, the bedrock is overlain with a layer of glacial till that is not present in the Flint Hills Region, as the Pre-Illinoian Glacier only covered the Glaciated Region some 600,000 years ago (KGS, 2007). This glacial till consists of boulders, cobbles, gravel, sand, silt, and clay, and glacial erratics composed primarily of Sioux quartzite (KGS, 2007). Glacial till deposits have been known to exceed 12 m in depth in some locations within the BVR watershed (KGS, 2007). In the Flint Hills Region, this glacial till is not present; however, chert, or flint, is common in the topsoil, which is deeper in the valleys than along ridges. Chert is the result of precipitation of silica within voids in the limestone and is therefore embedded in the limestone. Chert is

more resistant to erosion than limestone and is left behind as residual lag when the more easily eroded limestone is removed by weathering (Aber, 2007). The Flint Hills have steep valleys, up to 30.5 m relief in some cases, due to stream erosion, and flash flooding is common with most of the surface runoff occurring during spring and early summer (Aber, 2007).

Peorian eolian loess, fine-grain sediment carried by wind, were deposited throughout the BVR watershed near the end of more recent Wisconsinan glaciation approximately 25,000 – 30,000 and 12,000 years ago (Rousseau, Antoine, Kunesch, Hatté, Rossignol, Packman, and Gauthier, 2007; Meade, 2009). These loesses were deposited to a greater extent along the ridges of the BVR watershed and the thicknesses of these deposits decreases from north to south within the BVR watershed (Luttenegger, 1987; Meade, 2009).

Soils

The formation of soil and its subsequent characteristics is affected by five factors: 1) parent material, 2) biota, 3) climate, 4) relief, and 5) time. These factors influence one another as well as the formation of soil (Smith & Smith, 2000; Harpstead, Sauer, Bennett, & Bratz, 2001; NRCS, 2008). The soils found in the BVR watershed are of the Mollisol order, which are indicative of grassland areas. Mollisol soils have distinctive horizons containing high amounts of organic matter contributed by grasses over hundreds to thousands of years (Reichman, 1987; Smith & Smith, 2000).

The native tallgrass prairie with its humus rich soils, have been replaced primarily with cultivated fields of row crops. The removal of vegetation and subsequent tillage exposed the soil to the full force of raindrop impacts that decompose the soil aggregates

allowing soil particles to be more easily entrained (Knox, 2001). Therefore, much of the native soil in the BVM watershed has been moved from the fields to the river and subsequently deposited downstream (Sass, 2011). When soil particles are moved by water in this manner, they are known as alluvium. Alluvium is deposited on floodplains repeatedly during flood events and is common in riparian corridors (Sass, 2011). The soils adjacent to the BVR have a high clay content ranging between 23% and 47% and were formed from the alluvium parent material noted above

. Table 2 below shows the major soil properties of the stream reaches monitored in Sass & Keane (2012) as reported by the NRCS Soil Survey.

Table 2: Soil Names and Properties Adjacent to Study Sites of Sass & Keane (2012): As reported by the NRCS Soil Survey (NRCS, 2010): MS=Main Stem, NF

Location	Soil Name	Parent Material	Percent Clay	Liquid Limit	Bulk Density	Minor Association
MS1	Kennebec Silt Loam	Fine-silty alluvium	25.4%	40.5%	1.37 g/cm^3	Wabash
MS2	Kennebec Silt Loam	Fine-silty alluvium	25.4%	40.5%	1.37 g/cm^3	Wabash
MS3	Nodaway Silt Loam	Calcareous fine-silty alluvium	23%	35.3%	1.30 g/cm^3	Wabash, Aquolls
NF1	Kennebec Silt Loam	Fine-silty alluvium	25.4%	40.5%	1.37 g/cm^3	Wabash
NF2	Wabash silty clay loam	Clayey alluvium	47.1%	62.6%	1.35 g/cm^3	none
NF3	Nodaway silt loam	Calcareous fine-silty alluvium	23%	35.3%	1.30 g/cm^3	Wabash, Aquolls
IC1	Kennebec Silt Loam	Fine-silty alluvium	25.4%	40.5%	1.37 g/cm^3	Wabash
IC2	Kennebec Silt Loam	Fine-silty alluvium	25.4%	40.5%	1.37 g/cm^3	Wabash
IC3	Wabash silty clay loam	Clayey alluvium	47.1%	62.6%	1.35 g/cm^3	none

Climate

For any given region, climate is defined as the prevailing weather conditions over a long period of time (Smith & Smith, 2000). The study area averages between 81 and

89 cm of precipitation per year and is considered continental (Aber, 2007). Northeast Kansas receives a surplus of water after evapotranspiration and plant uptake, which supplies water to the fluvial systems in the area (Aber, 2007). Average humidity is between 45 and 50%, and most of the precipitation falls during the growing season between April and September (Oznet, 2008). On average, January is the coldest month with an average daily high of 5.5° C (42° F); however, for an average of 8 to 10 days a year, the temperature may reach a low of -17.8° C (0° F) (Oznet, 2008). On average, July is the hottest month with an average daily high of 34.4° C (94° F); however, for approximately 10 days each summer, the temperature reaches a high of 37.8° C (100° F) (Oznet, 2008). There are approximately 220 cloudy or partly cloudy days and 145 sunny days in northeast Kansas (Oznet, 2008)

Historical Vegetation Communities

Subsequent to human occupation, it is estimated that approximately 42% of the earth's terrestrial surface was grassland (Reichman, 1987; Smith & Smith, 2000). The average precipitation for a grassland or prairie is between 25.4 cm and 81.3 cm, and NE Kansas overlaps the upper portion of this range (Aber, 2007). Periodic fire and grazing are required to maintain a prairie by suppressing the growth of woody species (Smith & Smith, 2000; Briggs, Knapp, Blair, & Heisler, 2005). Historically, the BVR watershed in northeast Kansas was home to a tallgrass prairie consisting of species such as big bluestem (*Andropogon gerardii*), Indian grass (*Sorghastrum nutans*), and switchgrass (*Panicum virgatum*) (Reichman, 1987; Haddock, 2005). While northeast Kansas did historically receive enough precipitation to support deciduous forest, woody species were confined to riparian areas due to fire and grazing (KSLS, 2005). The tallgrass

prairie of northeast Kansas was dotted with bur oak (*Quercus macrocarpa)* in somewhat of a savanna configuration; however, most large woody species were confined to riparian corridors that included black walnut *(Juglans nigra)*, sycamore *(Platanus occidentalis),* and cottonwood *(Populus deltoids)* (KSLS, 2005; Sass, 2011).

Dynamic Equilibrium

The primary founders of the science of geomorphology were G.K. Gilbert and W. M. Davis who practiced in the late 19th and early 20th centuries (Lane, 1954). Gilbert (1877) and Davis (1902) developed the concept that in streams transporting sediment, grade was a condition of their equilibrium and Gilbert conducted extensive quantitative research in the area of sediment transport. The connection between engineering and fluvial geomorphology goes back much further to 1697 when Dominique Gugliemini was perhaps the very first writer on the subject (Lane, 1954). In an attempt to integrate the two originating disciplines by revising the concepts of Gilbert and Davis, Mackin (1948) further developed the concept of equilibrium with the concept of the "graded" stream (a stream in equilibrium). Building on the work of Gilbert, Davis and Mackin, Lane (1954) developed a qualitative proportionality equation of stream equilibrium, which has since evolved into "dynamic equilibrium" and is perhaps the most cited such equation in the literature today (Riley, 1998 p. 128). Lane's equation is as follows (Figure 11).

$$\boldsymbol{Q_s d \propto Q_w S}$$

- Q_s = sediment load (bed material load since it is predominantly responsible for the geomorphology of the stream)
- d = particle diameter or size of the sediment particles
- Q_w = water discharge
- S= slope (Lane, 1954)

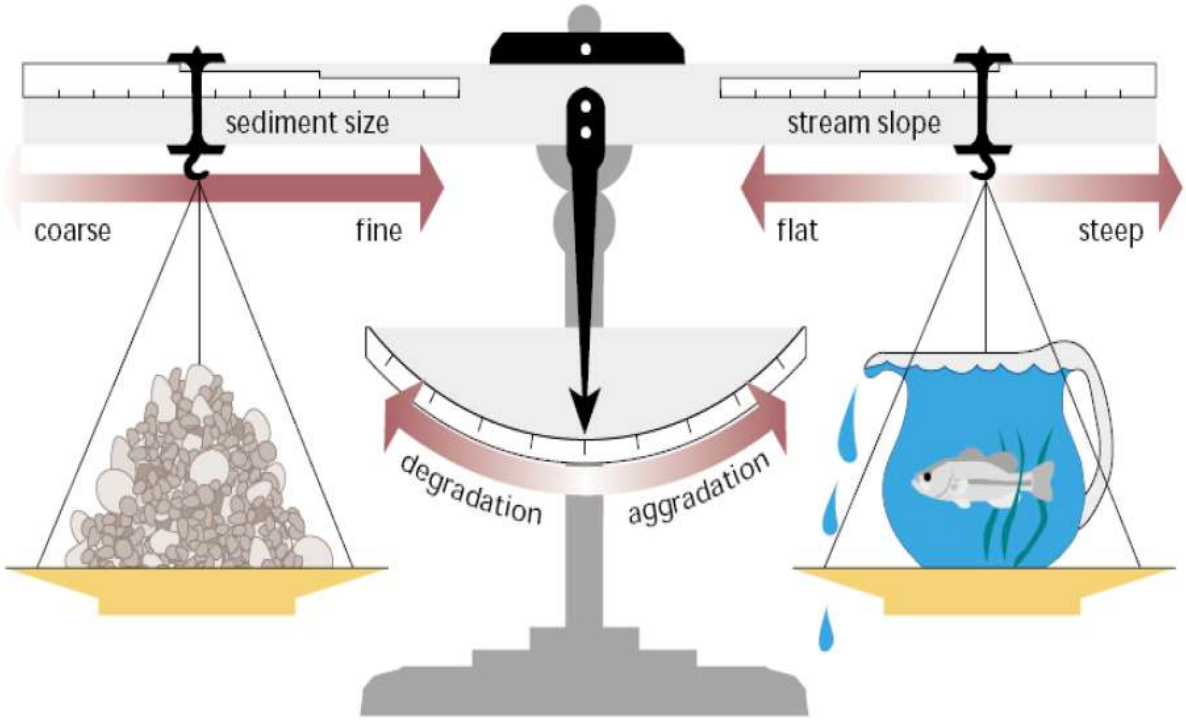


Figure 11: Illustration of Lane's Balance showing the effects of the four variables on stream equilibrium, (Rosgen, 1996)

Stream Energy and Stream Power

Stream energy expressed as stream power provides the quantitative physics behind Lane's qualitative equation. Generally, there are three types of energy in a fluvial system. One, potential energy in a fluvial system is the energy possessed by water as related to gravity; therefore, water in the headwaters of a fluvial system contains more potential energy than water in the lower reaches of the system. Two, kinetic energy is the energy an object possesses when in motion, when work is being performed. As the mass of water flows downstream, most of its potential energy is converted to kinetic energy. Three, thermal energy is the flow of heat energy and as the mass of water moves downstream, potential energy is converted to thermal energy as a result of friction and thermal loss (Knighton, 2014).

Generally, there are four types of work performed by water moving downslope in a fluvial system: 1) work against viscous shear and turbulence, 2) work against friction at the channel's wetted perimeter, 3) work done in the entrainment of particles, and 4) work done transporting the sediment load (Knighton, 2014). Channels that are narrow and deep tend to have higher energy and thus have the ability to do the types of work noted above more so than channels that are shallow and wide. The kinetic energy of a fluvial system may be dissipated in a number of ways, such as spill resistance in drops and steps, channel roughness or sinuosity, bed undulations such as ripples and dunes, cross sectional shape, and particle transport (Rosgen, 1996; Knighton, 2014).

Stream energy is expressed as stream power in the following equation:

$$\Omega = \gamma Q S$$

Where Ω is stream power, γ is the specific weight of water, a constant, Q is the discharge of water and S is the slope (Knighton, 2014). If the discharge or slope of a fluvial system is increased, as when the slope is increased via channelization or the discharge because of a change in landcover, the stream power is increased and therefore the amount of energy dissipation must also increase. Some of the ways energy dissipation may be increased include an increase in the amount of sediment being transported, an increase in the size of sediment being transported, a change in the meander pattern, a change in roughness, or any combination of these variables (Sass & Keane, 2012; Knighton, 2014). The relationship between changes in stream power and stream energy dissipation can be seen in Lane's equation. Referring to Figure 11 above, as stream slope is increased (increase in stream power) either the

sediment size or sediment load must also be increased (increase in energy dissipation) in order to maintain equilibrium.

Overland Erosional Processes

Rainsplash

The force of a raindrop impact on soil is a function of the drop size and velocity and can have a number of effects on the soil surface such as consolidation, fracturing chemical and physical bonds, or transport of soil particles via splash (Knighton, 2014). As soil particles are mobilized by splash, the particles splashed in the downhill direction travel farther than those splashed uphill resulting in a net downhill transport of soil overall (Dunne & Leopold, 1998). Rainsplash is important on steep slopes with little or no vegetation, where soil particles are detached then subsequently transported downhill by other processes such as overland and rill flow (Dunne & Leopold, 1998; Knighton, 2014).

Sheetwash

Once water has filled the surface depression storage, it becomes overland flow, also known as sheetwash (Knighton, 2014). Sheetwash does not have a uniform depth, but rather consists of a thin film of water that contains tiny, irregular threads of slightly deeper and faster water. On gentle slopes, sheetwash along with detachment caused by rainsplash may remove a uniform depth of soil from the hillslope (Dunne & Leopold, 1998; Knighton, 2014). Where detachment is generally more attributable to rainsplash, transport plays a major role of overland flow or sheetwash; however, detachment and

transport due to sheetwash alone does increase as slope gradient and length increases (Knighton, 2014).

Rill

Once flow becomes concentrated in separate channels, rills are formed that are small channels typically 50-300 mm wide and up to 300 mm deep (Knighton, 2014). This concentration of runoff results in a substantial increase in both detachment and transport of soil particles. Rills are usually ephemeral, discontinuous, and often obliterated between storms resulting in their significance being underestimated (Dunne & Leopold, 1998; Knighton, 2014).

Gully

Once rills incise to approximately 0.30 m deep and become relatively permanent watercourses, they are then classified as gullies. Gullies are not stable stream channels and are characterized by steep sides, a low width/depth ratio, and a headcut at the upslope end creating a stepped longitudinal profile (Knighton, 2014). Gullies range in size from a few feet wide and deep to tens of feet deep and miles long, often develop rapidly, and are indicative of accelerated erosion that often does great damage to individual pieces of property (Dunne & Leopold, 1998). Common causes of gullies are deforestation, excessive burning of vegetation, and overgrazing. In addition, these conditions are often exacerbated by climate change (Knighton, 2014)

In-Channel Erosional Processes

Fluvial Entrainment

Erosion of individual particles from river and stream banks and bed is known as fluvial entrainment (Knighton, 2014). The initial entrainment or mobilization of streambed and streambank particles is the first component of in-channel sediment transport processes (Thorne, 2006). This initial entrainment depends partially on the physical properties of the sediment or bedload particle, such as the grain size and particle shape characteristics (roundness, sphericity, cohesiveness, and embeddedness) (Gordon, Finlayson, & McMahon, 1992). Lift, drag, and shear forces produced by turbulent streamflow are constantly acting on particles along the bed and banks, and when these forces become greater than shear strength forces, the *threshold* for entrainment has been reached and the particle is mobilized (Gordon et al., 1992). When the streambed is dominated by sand and silt, the threshold is lower than when the bed has high degree of embeddedness or cohesion (Knighton, 2014).

The force required for initial particle entrainment can be described by 1) critical velocity and 2) critical shear stress. Looking first at critical velocity, Hjulstrom (1939) developed “curves showing the limiting velocities required for erosion, transportation and deposition of uniform material” (Figure 12) (Gordon et al., 1992). The velocity required for erosion of very small particles is similar to that of very large particles due to small particles of silt and clay having electromagnetic bonds that increase cohesiveness resulting in this type of fine-grained material eroding as aggregates rather than individual particles (Thorne, 2006). The Hjulstrom curves also illustrate that for very

small particles, there is a large difference in the velocity needed to erode the particle and the velocity needed to keep the particle in suspension; conversely, with very large particles, the difference in the velocity needed to erode and deposit the particle is very small (Gordon et al., 1992). The shortcoming of the Hjulstrom curves is that they are for uniform particles, and in the real world, a much wider range of particle sizes will move at a specific velocity depending on the particle characteristics described at the beginning of this section (Gordon et al., 1992).

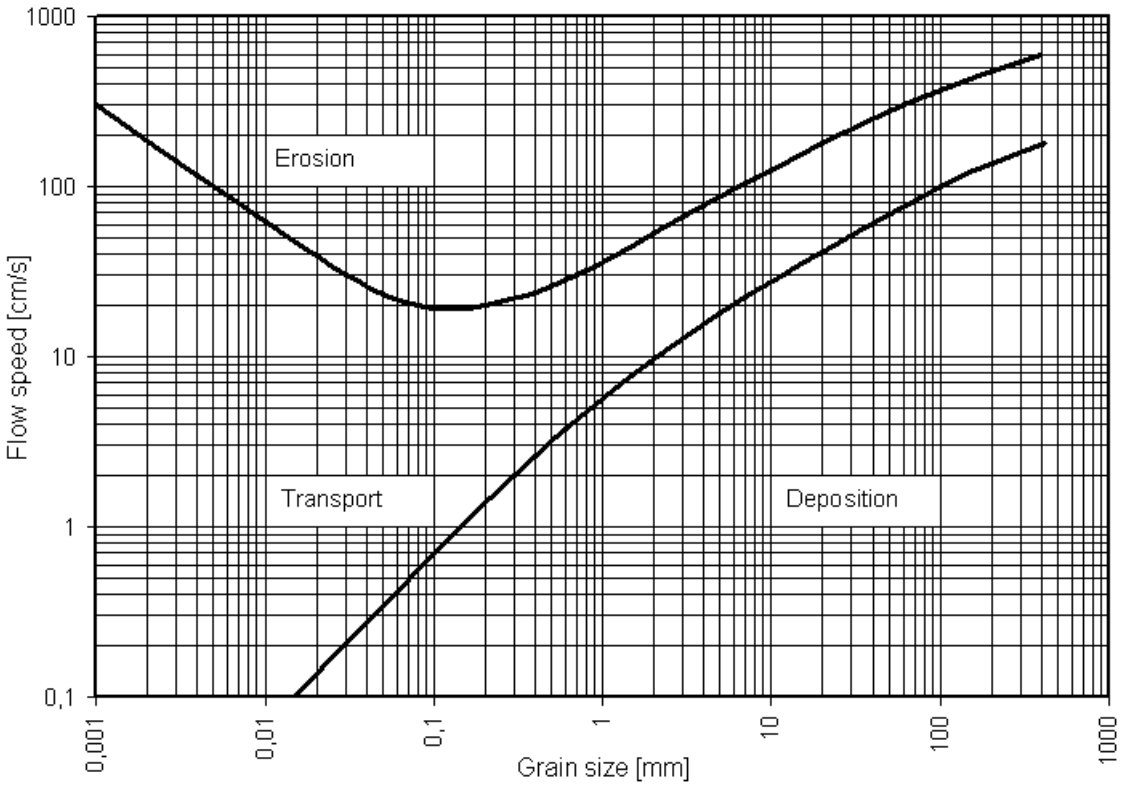


Figure 12: Hjulstrom Diagram (Hjulstrom, 1935)

An “alternative” to considering the critical velocity necessary to entrain a particle is considering the critical shear stress, which, very much like velocity, increases with an increase in discharge and is unevenly distributed throughout the cross section (Gordon

et al., 1992). Shields (1936) was the first to introduce an equation for critical shear stress containing a “dimensionless critical shear stress” constant “that is a function of particle shape, fluid properties, and arrangement of the surface particles” as well as a value reflecting a hydraulically rough or smooth environment (Gordon et al., 1992). In sand and silt bed streams where hydraulically smooth conditions exist, the particles on the bed surface are completely covered by the laminar sublayer resulting in the particles being “dragged together as a ‘grain carpet” (Gordon et al., 1992, p.333). When hydraulically rough conditions are present, as is the case in most rivers and streams, individual grains and particles are exposed to turbulence and can mobilize individually and randomly (Gordon et al., 1992). As with shear velocity, the shear stress needed to mobilize any given particle depends on the “grain size, grain shape, the degree of packing, and lift and drag forces” (Knighton, 2014 p. 109).

Pore Pressure

Pore pressure can be defined as the amount of saturation pressure experienced by soil. Soil may have negative pore pressure, which is characterized by ample free water absent of hydrogen bonding within the soil (Sass, 2011). Positive pore pressure occurs in dryer conditions when there is less free water available. Loosely structured soils tend to contract when pore pressure is high, and this contraction leads to an increase in pore water pressure and decrease in frictional, shear strength. In contrast, tight soils such as those high in clay content tend to expand (Iverson et al., 2000). As the water content of soil increases due to infiltration of precipitation, a rise in the groundwater table, or rising streams, soil water content increases leading to the pore pressure approaching and eventually becoming negative. Rising water in a stream

provides pressure toward the bank negating pore pressure pushing bank material towards the stream channel. However, with a rapid decline in stage following a flood event, which is common in flashy systems such as the BVR, the hydrostatic force of the water helping maintain the bank profile is lost sometimes leading to mass planar or rotational failures (Rinaldi, Casagli, Dapporto, & Gargini, 2004; Sass, 2011) (Figure 13). Simon and Collison (2001) note “negative pore water pressures increase the shear strength of unsaturated, cohesive materials by providing tension between particles (p. 1422).”

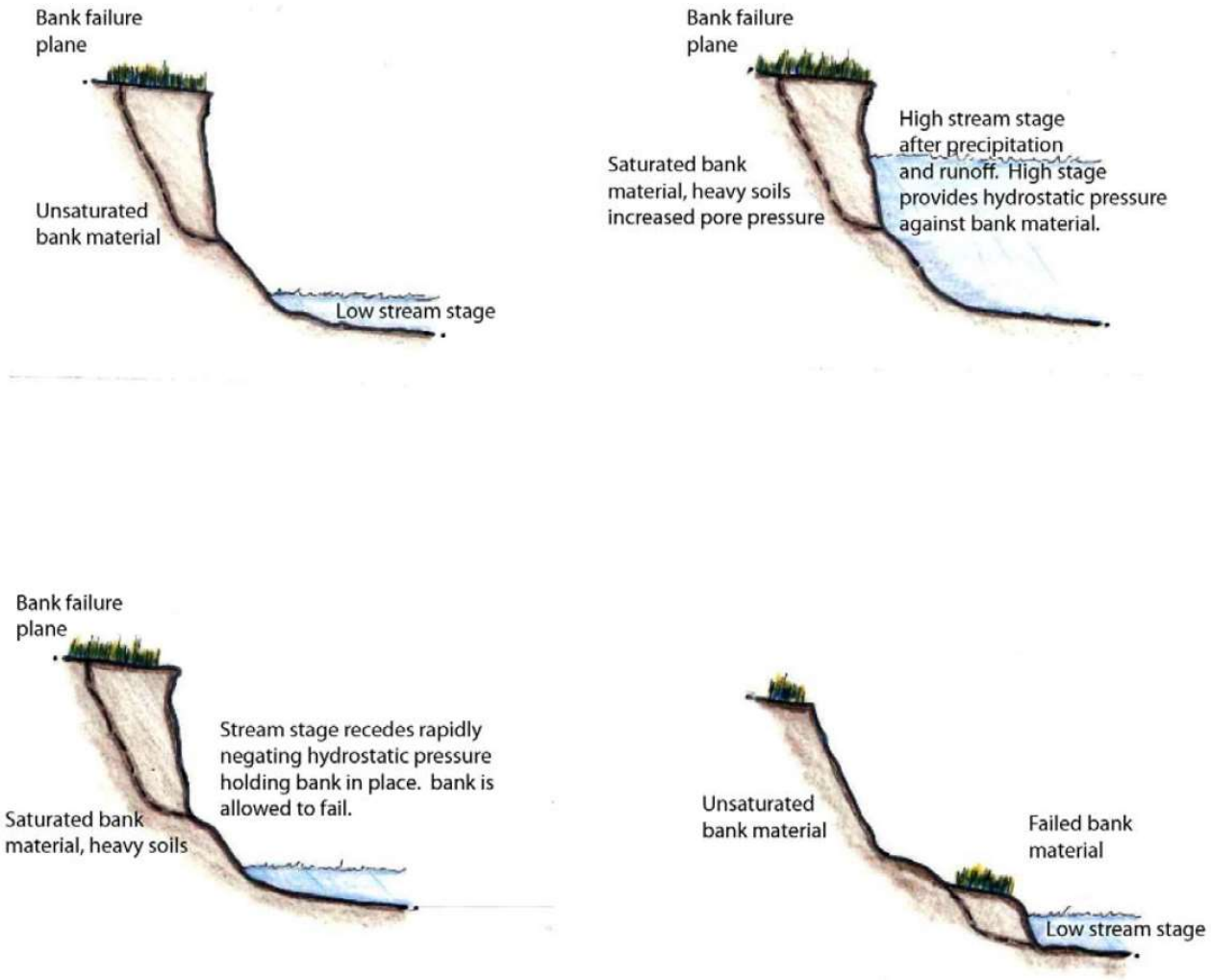


Figure 13: Illustration of Bank Failure and Pore Water Pressure (Sass, 2011)

Dry Ravel

The movement of soil particles or aggregates downslope by way of rolling, bouncing, or sliding is known as *dry ravel* (Gabet, 2003). Dry ravel tends to be greater on steep slopes where the shear strength of soil particles connected to the bank is more likely to be exceeded. Causes of dry ravel include animal movement on unstable slopes, wind, freeze-thaw, and the movement of vegetation (Rice, 1982). Gabet (2003) states that dry ravel may be "...the primary creep-like transport process on the planet…" (p. 22.2). Dry Ravel tends to be more prevalent in arid environments prone to wildfires than in humid or semi-humid regions such as northeast Kansas (Gabet, 2003).

Soil Piping/Seepage

After precipitation has infiltrated into the ground, it then moves by one of two methods: 1) *Piping* occurs when water moves through well-defined, underground channels and 2) *Seepage* occurs when water moves through interstitial spaces within the soil matrix. The velocity of water tends to increase as it moves through pipes leading to erosion within the pipes. Pipes empty into receiving streams as groundwater and generally have a lag time 30-40% longer than seepage (Jones, 1997). Soil pipes may be ephemeral, transporting water only during rain events, or perennial, transporting water continuously. Ephemeral pipes within the top 150-mm layer of soil tend to collect and transmit water efficiently and have the highest rate of discharge in proportion to drainage area (Jones, 1997). Open channels may be formed by pipes near the surface when the top of the pipe collapses (Knighton, 2014).

Mass streambank failure may be initiated by seepage and soil piping (Wilson, Periketi, Fox, Dabney, Shields, & Cullum, 2007). Soil piping may cause bank failure when pipes emptying along the lower bank entrain soil particles leading to undercut banks and eventually bank failure. Seepage may allow the flow of water over the bank surface resulting in erosion of soil particles from the bank similar to that caused by soil piping. Seepage also has the potential to erode clay particles from the soil, thus reducing soil cohesion and increasing bank susceptibility to mass wasting (Knighton, 2014; Sass, 2011). "In situ studies by Wilson et al. (2007) found that sediment concentrations increase during high flow discharges to as much as 660g/L, and in laboratory settings to as high as 4500 g/L, illustrating high erosion rates due to piping and seepage" (Sass, 2011 p, 47).

Freeze-Thaw

Streambank soils in humid-temperate and sub-arctic regions experience the influence of frost and ice crystals during winter months (Lawler, 1995). When water enters cracks and crevices in the top layer of soil and then freezes, it expands detaching small particles or peds of soil. Upon thawing and contracting, water then moves further into the soil horizon before refreezing, expanding, and detaching or loosening more soil particles. Once detached or loosened, soil particles then become more susceptible to dry ravel and subsequent fluvial entrainment once at the toe of bank (Lawler, 1995). Freeze-thaw tends to be more significant in downstream reaches and has been found to be responsible for the majority of bank erosion during winter months in areas where temperatures fluctuate above and below freezing (Wolman, 1959; Lawler, 1986; Stott, 1997; Wynn & Mostaghimi, 2006).

Ice Scour/Ice Jams

It does get cold enough in the BVR watershed to freeze running water; therefore, ice scours may contribute to streambank and bed erosion. Mechanical action is applied to the bank surface as ice floating on the water surface comes into contact with the bank at whatever stage may be present at the time (Collinson, 1971; Smith & Pearce, 2002). Large amounts of ice may scour the streambed creating depressions and undulating bed topography. In addition, localized streambank and bed scour can occur, as water is forced to flow around ice jams similar to the effects of large woody debris or logjams along streambanks (Collinson, 1971; Smith & Pearce, 2002).

Mass Wasting

Mass wasting, also known as mass failure, occurs when erosional processes, such as soil piping, pore pressure changes, entrainment of bank toe material, excess shear stress, or general loss of soil cohesiveness, along with gravitational forces cause the downslope movement of large masses of soil (Dunne & Leopold, 1998; Fox et al., 2007; Harpstead et al., 2001). Incision of the BVR initiated by land use change and channelization has steepened streambanks resulting in weaker banks being more prone to mass failure than prior to incision (Thorne, 1999). Steeper banks result in more gravitational forces acting on the soil along the failure plane, eventually overcoming the threshold of frictional forces exerted by individual soil particles. “Steep banks tend to fail through planar slab failures, while shallow banks tend to fail rotationally” (Thorne, 1999; Sass, 2011 p. 49).

The two types of mass wasting common in northeast Kansas are fall and rotational slump; however rotational slump seems to be more common. The Rosgen “F” and “G” stream types common throughout the BVR maintain steep bank slopes and tend to be more vulnerable to mass failure due to undercutting of the upper banks; however, woody riparian vegetation may reduce bank failure by increasing soil cohesion (Rosgen, 1996; Sass, 2011). Mass wasting of bank material deposits colluvium in the stream channel, where it may then be entrained and transported downstream resulting in widening of the stream channel and increased sediment yields (Sass, 2011).

Anthropogenic Alterations to the Black Vermillion River Watershed

Agricultural Development

As noted, anthropogenic changes to land use result in alterations to the hydrology of watersheds. The BVR watershed was historically dominated by tallgrass prairie with gallery forest along streams and rivers (KSLS, 2005; Sass & Keane, 2016); however, beginning in the late 1800s with European settlement, the dominant land use has become agricultural with approximately 60% of BVR watershed currently being used for row crops (Meade, 2009). The transition from tallgrass prairie and natural gallery forest in the BVR watershed to agricultural uses has reduced the amount of foliar interception and infiltration of rainwater resulting in an increase in the volume and velocity of stormwater being delivered to streams, thus increasing stream discharge and peak stream power, and reducing centroid lag time of the storm hydrograph (Leopold, 1968). This reduction in lag time can be seen in a narrower and more peaked

hydrograph (Figure 14) (Gordon et al., 1992). The narrower and more peaked the hydrograph, the faster stormwater runoff is entering and leaving the stream system and this type of hydrograph is termed flashy (Perkins & Solo-Gabriele, 1997). The increase in the speed at which water enters the stream is due primarily to the lack of hydraulic friction on overland flow over bare soil compared to vegetated surfaces (Knox, 2001). In addition, as seen in the lower hydrograph in figure 14, the peak discharge is increased resulting in an increase in peak stream power. Due to the increase in the shear stress exerted on the bed and banks during high flows, accelerated bank and bed erosion occurs leadings to stream incision and widening.

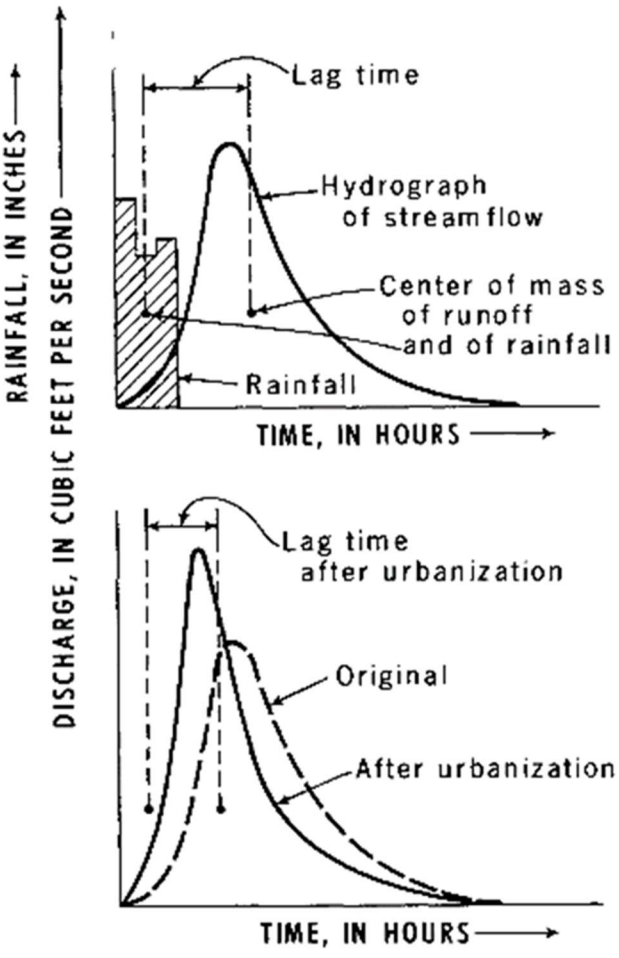


Figure 14: Storm Hydrograph indicating change in flow characteristics before and after "urbanization", which includes agricultural land uses (Leopold, 1968)

The percentage of a rain event that runs off a given land cover is known as the runoff coefficient. As seen in Table 3 below, natural woodland and forest for rolling topography is 0.15, and this rate is increased to 0.30 for pasture (grazing) land and 0.55 for cultivated land with clay and loam, which is the dominant soil type in the Black Vermillion Watershed. Native tallgrass prairie is not listed in this more general table; however, Qiao (2017) monitored a portion of Range Research Station of

Oklahoma State University that is dominated by native tallgrass prairie species and found the runoff coefficient to be 0.044 for the four water years over which the study was conducted. The increase in the runoff coefficient from 0.044 to 0.30-0.55 is partially responsible for the peaked hydrograph and channel degradation discussed earlier. Overall, it is estimated that discharges in the BVR have increased by 40% compared to predevelopment discharges (Sass, 2011; US-COE, 1998). This increase in discharge results in an increase in flooding of agricultural fields from the stream channel that in turn increases channelization and the building of flood berms by farmers in order to protect their crops (Meade, 2009; Peterson, 1991).

Table 3: Runoff Coefficients for the Rational Method (Chow, Maidment, & Mays, 1988)

	FLAT	ROLLING	HILLY
Pavement & Roofs	**0.90**	**0.90**	**0.90**
Earth Shoulders	0.50	0.50	0.50
Drives & Walks	0.75	0.80	**0.85**
Gravel Pavement	**0.85**	**0.85**	**0.85**
City Business Areas	0.80	**0.85**	**0.85**
Apartment Dwelling Areas	0.50	0.60	0.70
Light Residential: 1 to 3 units/acre	0.35	0.40	0.45
Normal Residential: 3 to 6 units/acre	0.50	0.55	0.60
Dense Residential: 6 to 15 units/acre	0.70	0.75	0.80
Lawns	0.17	0.22	0.35
Grass Shoulders	0.25	0.25	0.25
Side Slopes, Earth	0.60	0.60	0.60
Side Slopes, Turf	0.30	0.30	0.30
Median Areas, Turf	0.25	0.30	0.30
Cultivated Land, Clay & Loam	0.50	0.55	0.60
Cultivated Land, Sand & Gravel	0.25	0.30	0.35
Industrial Areas, Light	0.50	0.70	0.80
Industrial Areas, Heavy	0.60	0.80	**0.90**
Parks & Cemeteries	0.10	0.15	0.25
Playgrounds	0.20	0.25	0.30
Woodland & Forests	0.10	0.15	0.20
Meadows & Pasture Land	0.25	0.30	0.35
Unimproved Areas	0.10	0.20	0.30

The conversion of natural landscapes to agricultural uses also alters the sediment regime of the watershed. The removal of vegetation and subsequent tillage expose the soil to the full force of raindrop impacts that decompose the soil aggregates allowing soil particles to be more easily entrained (Knox, 2001). The effects of urbanization on the sediment yield of watersheds, which for this study is defined as beginning with agriculture, has been well documented beginning in the 1960s. As seen in Figure 15 below, Wolman (1967) developed a sediment yield curve for a Maryland watershed; however, this pattern is also applicable to northeast Kansas. Sediment yield in Wolman (1967) increased from an average 25 tons/square mile/year (t/sqmi/yr) to 600 t/sqmi/yr, approximately 25 times greater, during the cropping phase of urbanization. A decline to an estimated 300 t/sqmi/yr (0.47 t/ac/yr) for the decade or so immediately preceding due to a reduction in small-field farming and areas near expanding urban centers were allowed to return to brush with the speculation of

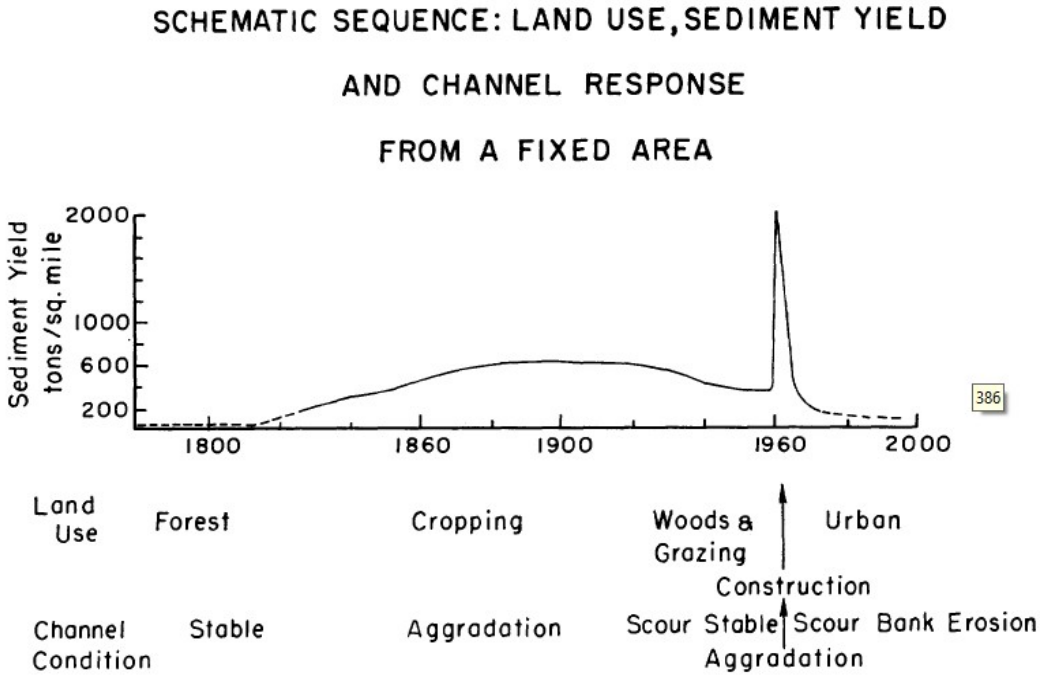


Figure 15: Land use, Sediment yield and Channel Response to Urbanization (Wolman, 1967)

development. The spike in sediment yield comes during the construction phase of denser residential and commercial development; however, the Black Vermillion watershed never experienced this phase of urbanization. It is possible that if the graph were for a watershed that remained agricultural, the sediment yield curve would not curve downward as it does just before the construction phase but would rather remain at a constant level or perhaps increase as incision and degradation of the receiving stream increases. Over a long period of time in watersheds such as the BVR, the curve could slowly trend downward due to farming practices such as terracing and cover crops increasing infiltration and reducing runoff (Rittenburg et al., 2015; Basche & DeLonge, 2019).

Loss of Riparian Vegetation

In natural environments, the amount of sediment entering a stream and the velocity of floodwaters are regulated by the riparian vegetation. Riparian vegetation acts as a filter of sediment being transported from uplands via stormwater runoff, and a well-vegetated riparian zone can filter out a large amount of sediment. For example, the riparian forest along the Little River in Georgia traps nearly 100% of the sediment from its watershed, which is agriculture in nature, and other studies have reported sediment removal of riparian areas as high as 80% and 90% (Table 4) (Hellmund & Smith, 2006). Riparian vegetation also increases the roughness of the channel along the banks and floodplains, which may lead to increased deposition due to a decrease in velocity and energy during a major flooding event (Thorne, 1999).

Table 4: Sediment Removal Effectiveness of Riparian Buffer Zones (Hellmund & Smith, 2006)

Sediment removal effectiveness of riparian buffer zones.

LOCATION	BUFFER VEGETATION	BUFFER WIDTH (M)	SLOPE (%)	PERCENT REDUCTION[1]	REFERENCE
Pennsylvania	Oats	6	14	76 (by mass)	Hall et al. (1983)
Nebraska	Grass and grass + woody plants	7.5–15.0	6–7	12–82 (by mass) 40–81 (by concentration)	Schmitt et al. (1999)
Connecticut	Grass + woody plants Orchardgrass Grass	30 4.6–9.1 4.6–9.1	5 11–16 3.5	92 11–16 } (by concentration) 66–82	Clausen et al. (2000) Dillaha et al. (1988, 1989) Magette et al. (1989)
Oregon	Not specified	30	Not specified		Moring (1982)
Rocky Mountains	Primary coniferous forest	9	35-55	Nearly all	Haupt (1965)
Maryland	Mixed hardwood forest	265 ft (81m)	2-5	"most"	Lowrance (1988)
North Carolina	Not specified	330 ft (101m)	up to 20	50	Cooper (1987)

[1] Pollutant reduction attributable to buffers is expressed as percent of the pollutant leaving cultivated fields.

Adapted from Wenger, S. (1999). "A review of the scientific literature on riparian buffer width, extent and vegetation." Athens, Office of Public Service and Outreach, Institute of Ecology, University of Georgia; and from Dosskey, M. G. (2001). "Toward quantifying water pollution abatement in response to installing buffers on crop land." *Environmental Management* 28: 577–598, with additions (Moring 1982, Haupt 1965).

Before European settlement, approximately 2% of North America was covered with riparian vegetation, however, approximately 89% of native riparian vegetation has been lost over the past 200 years (Popotnik & Giuliano, 2000; Sass, 2011). The bulk of native riparian vegetation of North America has been lost to logging, transition of these areas to agriculture, and urban development (Popotnik & Giuliano, 2000). Historically, riparian gallery forests in the tallgrass prairie were limited to the floodplain of the rivers and did not become established in the open prairie. This containment of the forest to riparian corridors was primarily due to natural grazing and burning regimes (Reichman, 1987; Sass & Keane, 2012). The BVR watershed has lost an average of 80-85% of the woody vegetation within its riparian corridor resulting in an increase sediment entering the river, a decrease in streambank stability, and a loss of regulation of floodwater velocity (Sass & Keane, 2016).

BVR Channelization

Channelization, the physical realignment of a stream channel in order to shorten the channel and increase channel capacity, is perhaps the most widespread and harmful anthropogenic alteration to rivers and streams (Davis, 2007; Meade, 2009). Channelization in the BVR watershed was done primarily to prevent flooding of nearby agricultural fields. While channelization of the BVR was done in a piecemeal fashion by farmers and private land owners since the early 1900s, the vast majority of channelization occurred between the 1950's and 1980's in conjunction with state and federal agencies such as the Soil Conservation Service (now NRCS) (Meade, 2009). Main Stem, North Fork and Weyer Creek all have numerous reaches that were channelized in the 1970s and 1980s (Figure 16). While channelization does alleviate flooding near the location of the altered channel, it often results in negative effects such as downstream aggradation and upstream degradation (incision), evidenced by dramatically increased bank erosion due to an increase in gradient and channel depth coupled with a decrease in channel roughness (Schumm et al., 1984).

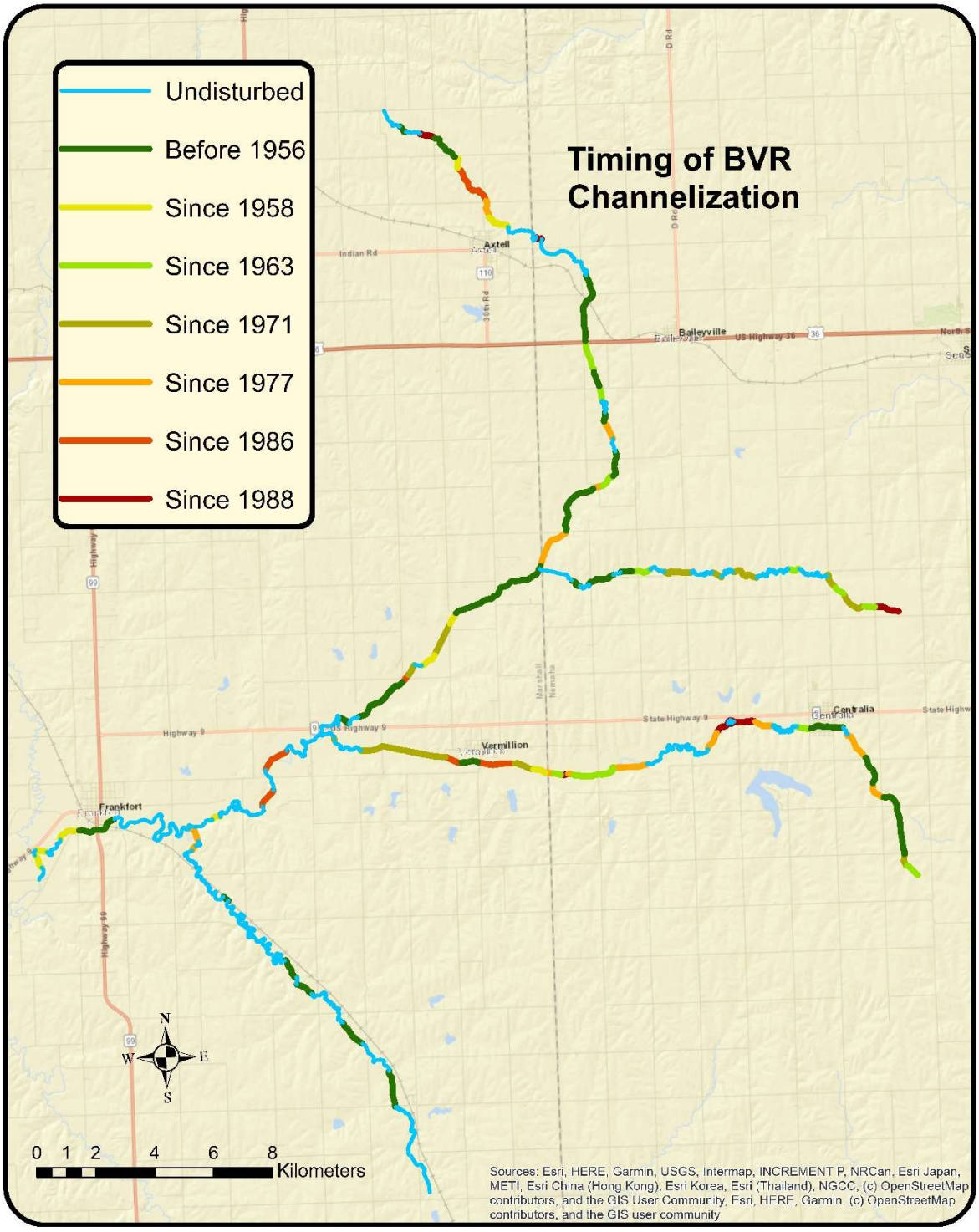


Figure 16: Timing of Channelization in the BVR (Adapted from Mead, 2008)

Channel Evolution Models

After inputs of water and sediment to the BVR were altered by land use changes and channelization, the river was thrown into disequilibrium and has proceeded to evolve through a sequence of geomorphological changes in an attempt to regain equilibrium. Over the past several decades, there have been a number of models developed that seek to explain the process of stream adjustment or evolution resulting from changes in flow and sediment regimes (Schumm et al., 1984; Simon & Hupp, 1986; Sass & Keane, 2012; Rosgen, 2006; Cluer & Thorne, 2014). These models are known as channel evolution models (CEM's), and one of the goals of this study is to understand how the evolution of the BVR fits into these models. Following are four CEMs that attempt to describe this channel adjustment resulting from changes in watersheds. The synopsis of these four models is taken from Keane & Sass (2017).

1. Schumm, Harvey, and Watson (1984)
2. Simon and Hupp (1986)
3. Cluer and Thorne (2014)
4. Rosgen Successional Scenarios (2006)

Schumm, Harvey, and Watson (1984)

The CEM described in Schumm et al. (1984) was developed based on the observation and measurement of three streams of variable size in the upper Yazoo River Subbasin in north central Mississippi (Schumm et al., 1984):

1. Tippah River (1,036 km^2 drainage area (DA))
2. Pigeon Roost Creek (518 km^2 DA)
3. Oaklimiter Creek (109 km^2 DA)

There had been significant land use change and channelization in all three watersheds and the authors described the watersheds as ". . . representative of watersheds in those areas upstream of the flood control reservoirs in northern Mississippi in which streams are not transporting gravels. . ." (Schumm et al., 1984, p. 121). It was also noted by the authors that the size and range of conditions in the Oaklimiter Creek led to it being chosen for the bulk of the detailed fieldwork and CEM development (Schumm et al., 1984).

Schumm et al. (1984) introduced a CEM that consists of five channel types representing five distinct phases of the transition of a channel from instability caused by changes in the watershed to a state of stability or quasi-equilibrium. The CEM described in Schumm et al. (1984) consists of five sequential phases represented by channel Types I through V (Table 5). This CEM begins with a state of quasi-equilibrium in the Type I channel. Channel Types II through IV represent a series of unstable and/or transitional channel forms, and channel Type V represents the re-establishment of a quasi-equilibrium channel at a lower elevation. See Table 5 for the specific descriptions of these Channel Types or phases of transition. These Channel Types are primarily described with cross-sectional dimensions. In Oaklimiter Creek, the authors indicate a state approaching quasi-equilibrium when:

1. The ratio (F) of the channel top width to channel depth equaled six.
2. This F ratio was achieved when the average sediment depth was three feet, the channel slope was reduced and when the development of alternating bars led to a meandering thalweg (Schumm et al., 1984).

Table5: Schumm et al. (1984) Channel Evolution Model Stream Type Descriptions, (Keane & Sass, 2017)

Stream Type	Dominant Process	Width/Depth Ratio Range	Description
I	Transport of sediment	4-7	Very little or no sediment storage in the bed and a "U" shaped cross section
II	Degradation	3-4	Highly variable sediment accumulation; steep nearly vertical banks; increasing channel depth
III	Rapid widening	4.5-5.6	Accumulation of sediment/deposition on the streambed; accelerated bank erosion nearly vertical banks
IV	Aggradation and development of berms and bars	5.7-6.4	Channel widening continues but a reduced rate; sediment accumulation on bed; reduced bank angles; meandering thalweg at low stage w/alternate bars
V	Aggradation and development of berms and bars	7-12	"Dynamic equilibrium" attained; alternate bars stabilized with vegetation; bank angles below geotechnical threshold

Simon and Hupp (1986)

The CEM presented in Simon & Hupp (1986) is similar to Schumm et al. (1984). The streams observed in the study were located in the Obion, Forked Deer, and Hatchie River Basins in eastern Tennessee that all flow into the Mississippi River (Simon & Hupp, 1986). The Simon & Hupp (1986) study area's surficial geology is dominated by alluvial unconsolidated Wisconsin glacial loess with minimal bedrock control allowing stream channels to easily adjust their dimension, pattern, and profile following a disturbance (Simon & Hupp, 1986). The rivers in the study area experienced dredging and straightening between 1959 and 1978.

"Channel-morphology data collected from 1982 to 1984 were compared to previous surveys to determine channel changes with time" (Simon & Hupp, 1986 p. 13). The study resulted in a six "Stage" model described in Table 6.

Table 6: Stage Descriptions Adapted from Simon and Hupp (1986) (Keane & Sass, 2017)

Stage	Bed-Level Adjustment Type	Network Location	Channel Bed Process	Active Widening	Failure Types	Bank Surface	Approx. Bank Angles
I. Pre-modified	Pre-modified	Upstream-most reaches	Transport of sediment or mild aggradation	No	N/A	N/A	20-30°
II. Constructed	N/A	Where applicable	Dredging	By man	N/A	N/A	18-34°
III. Degradation	Migrating degradation	Upstream from AMD	Degradation	No	N/A	N/A	20-30°
IV. Threshold	Migrating degradation	Close to AMD	Degradation	Yes	Slab- rotational, pop-out	Vertical face upper bank	70-90° 25-50°
V. Aggradation	Secondary aggradation	Upstream of AMD	Aggradation	Yes	Slab-rotational, pop-out, low angle slides	Vertical face upper bank and slough-line	70-90° 25-40° 20-25°
VI. Restabilization	Downstream imposed aggradation	Downstream of AMD	Aggradation	No	Low angle slides, pop-out	Vertical face upper bank slough-line	70-90° 25-35° 15-20°

Note: AMD, area of maximum disturbance.

An obvious difference between the Simon & Hupp model and the Schumm et al. (1984) model is the addition of a constructed channel form (Stage II) immediately following the pre-modified channel form due to the channel dredging and straightening (channelization) (Keane & Sass, 2017; Simon & Hupp, 1986; Thorne, 1999). Other differences and similarities in the models described in (Thorne, 1999) are:

- Stage IV of Simon & Hupp (1986) is equivalent to stream Type III stage in Schumm et al. (1984); however, during this stage Simon and Hupp indicated continued bed degradation while Schumm et al. indicate the beginning of bed aggradation.
- Bank morphology and the indication of bank stability by the presence of vegetation are emphasized to a greater extent in the Simon and Hupp model compared to the Schumm, Harvey and Watson model.
- Critical bank height is considered in both models and “requires application of bank stability analyses capable of predicting critical bank height and

slope angles with respect to slab-type and rotational slip failures. . .” (Thorne, 1999, p. 105).

- Another difference in the models noted in Keane & Sass (2017) is that in the Schumm et al. model, width to depth ratio is the primary characteristic for channel “type” classification, while in the Simon and Hupp model bank angle and vegetation were the primary considerations for “stage” identification.
- Simon (1989) indicates that Stage I and Stage VI are considered stable and therefore reflect conditions where bank stability and sediment transport rates are “natural” (Keane & Sass, 2017).

One shortcoming of the Schumm et al. and Simon & Hupp models is a focus only on streambank dimensions and bank morphology, without addressing the importance of pattern or sinuosity in channel evolution (Keane & Sass, 2017). Thorne (1999) recognizes this shortcoming by stating:

> “On the basis of the observations made at the Long Creek study site, it is proposed here that an additional stage be added to the existing CEMs to account for late-stage incised-channel evolution involving the development of cross-sectional asymmetry, planform adjustments from straight or braided to meandering, and the formation of a new floodplain at a lower elevation than the pre-incision floodplain.” As quoted in (Darby and Simon, 1999, p. 118).

Cluer and Thorne (2014)

Just as Simon and Hupp expanded the Schumm et al. CEM with an additional "stage", Cluer and Thorne (2014) added two more "stages" to previously developed CEMs and proposed an expanded Stream Evolution Model (SEM) (Figure 17):

1. A multi-channel precursor stage
2. An additional Stage VII suggested by Thorne (1999)

As noted by Keane and Sass (2017), Cluer and Thorne (2014) provided an advancement to models of channel reaction to change by including a detailed set of physical, vegetative, habitat, and ecosystem benefits associated with each stage of their SEM.

Perhaps the most important advancement of such models by Cluer and Thorne (2014) was the cyclical nature of their model as compared to the linear structure of previous models (Keane & Sass, 2017). Cluer and Thorne (2014) describes "stream evolution as a cyclical, rather that linear, phenomenon, recognizing an *evolutionary cycle* within which streams advance through a common sequence, skip some stages entirely, recover to a previous stage, or even repeat parts of the evolutionary cycle". These concepts of "short circuits" and stage retrogressions rather than progressions are supported by Hawley, Bledsoe, Stein, & Haines, (2012), as they explain the concepts of "complex, discontinuous response sequences" and "resets" (Hawley et al., 2012 p. 724).

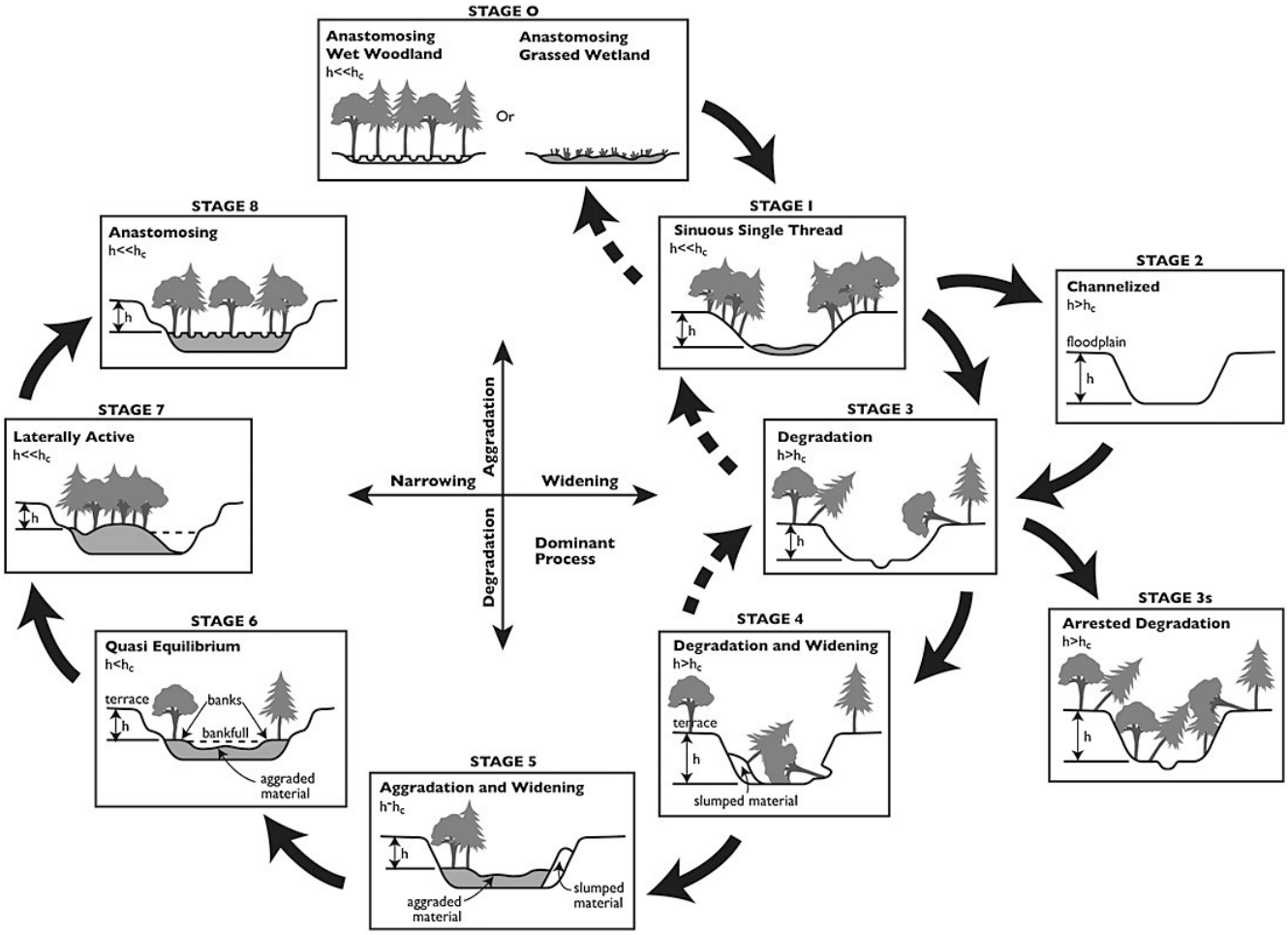


Figure 17: Cluer & Thorne (2014) Stream Evolution Model (SEM)

Rosgen Successional Scenarios (2006)

Before discussing the successional scenarios of Rosgen (2006) it will be helpful to briefly discuss the stream classification system presented in Rosgen (1994, 1996). In the mid-1990s David L. Rosgen, building on the work of Mackin, Leopold and Wolman, Schumm, Brice and Blodgett, Smith, and many others, developed his river and stream classification system (Rosgen, 1994). This classification system organizes stream feature data into specific combinations and groups rivers and streams “by similar slope, entrenchment of the channel in the stream valley, sinuosity (degree of meandering),

bankfull width-depth ratio, and type of soils and geology influencing the channel" (Riley, 1998 p. 150).

Rosgen's classification system is a 4-level hierarchical system and the assessment for classification is conducted at a reach scale equal to approximately 20-30 times the bankfull width that includes at least one representative riffle cross section (Rosgen, 1994; Sass, 2011). Level I "geomorphic characterization" provides a broad characterization by integrating "the landform and fluvial features of valley morphology with channel relief, pattern, shape, and dimension," while also considering the "influences of climate, depositional history, and life zones (desert shrub, alpine, etc.) on channel morphology" (Rosgen, 1994 p. 174). Level I assessment consists of nine stream types denoted by the letters A through G and two additional types Aa+ and DA as seen in Figure 18 below. This lettering system is the "signature" of the Rosgen Classification System (Sass, 2011).

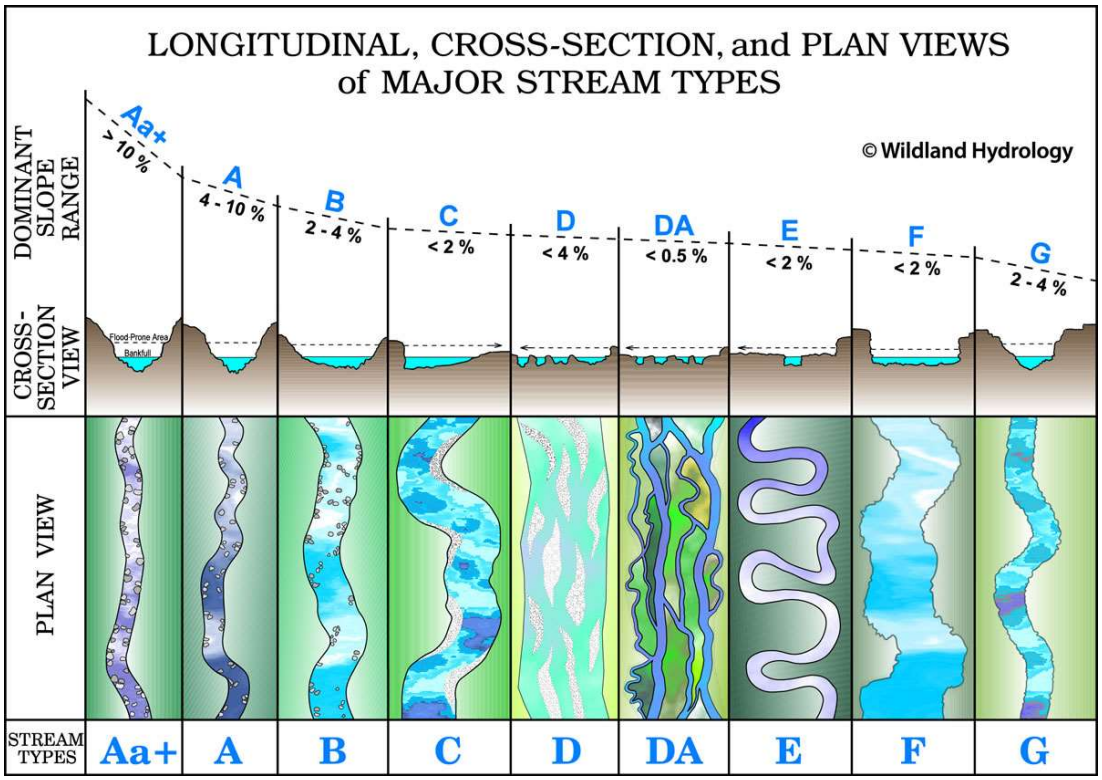


Figure 18: Rosgen Classification System Level I Stream Types (Rosgen, 1994)

Rosgen Level II assessment further delineates the stream types of Level I based on a number of field-measured criteria of representative “reference reaches” resulting in the identification of a stream type that can then be extrapolated to other reaches of similar valley type and lithology where field data may not be available (Rosgen, 1994). The criteria measured in Level II are entrenchment ratio (flood-prone width/bankfull width), width/depth ratio, sinuosity, channel material, and water surface slope at bankfull discharge (Figure 19) (Rosgen, 1994). Figure 20 illustrates all of the possible stream types at the Level II assessment.

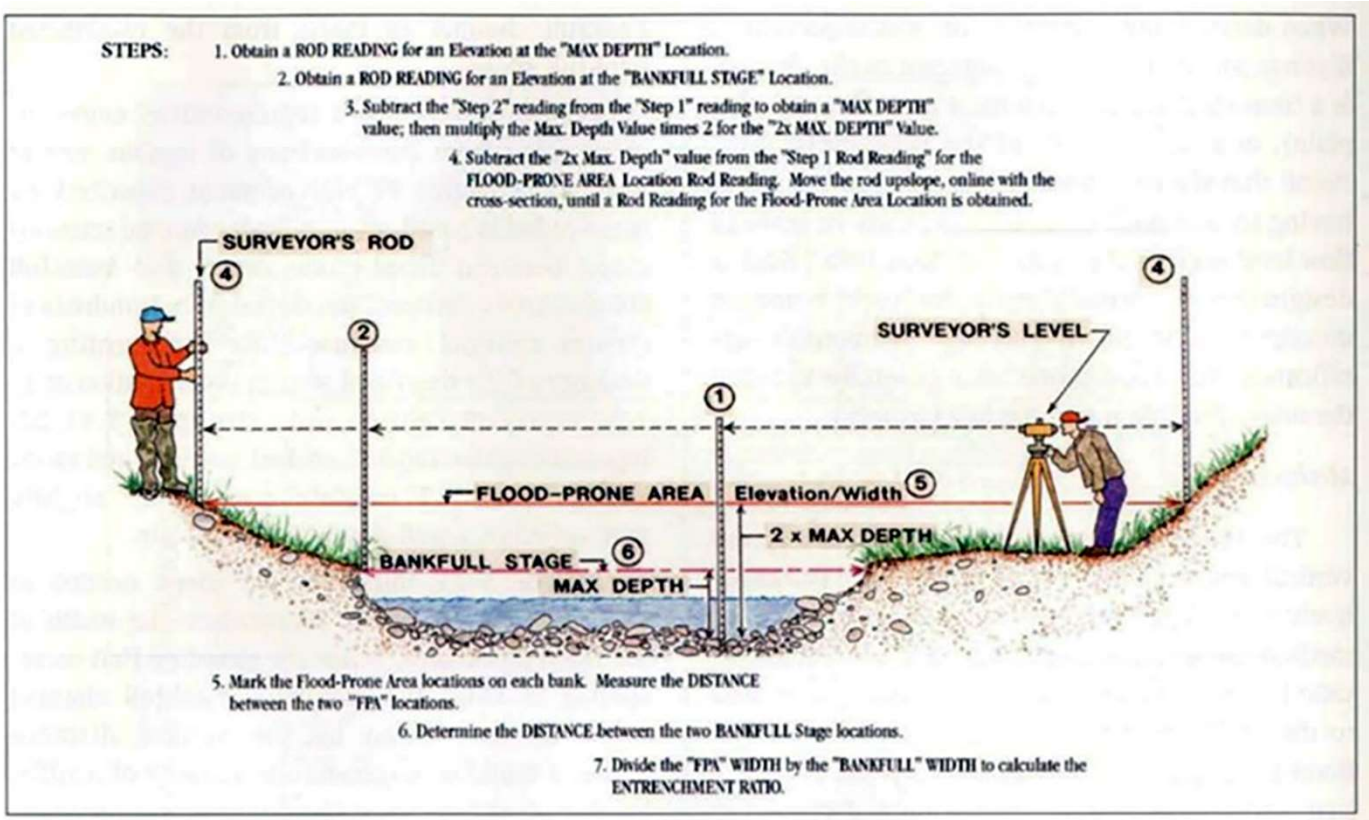


Figure 19: Rosgen Classification System Metrics: Illustration showing bankfull width, flood prone width and max depth (Rosgen, 1994)

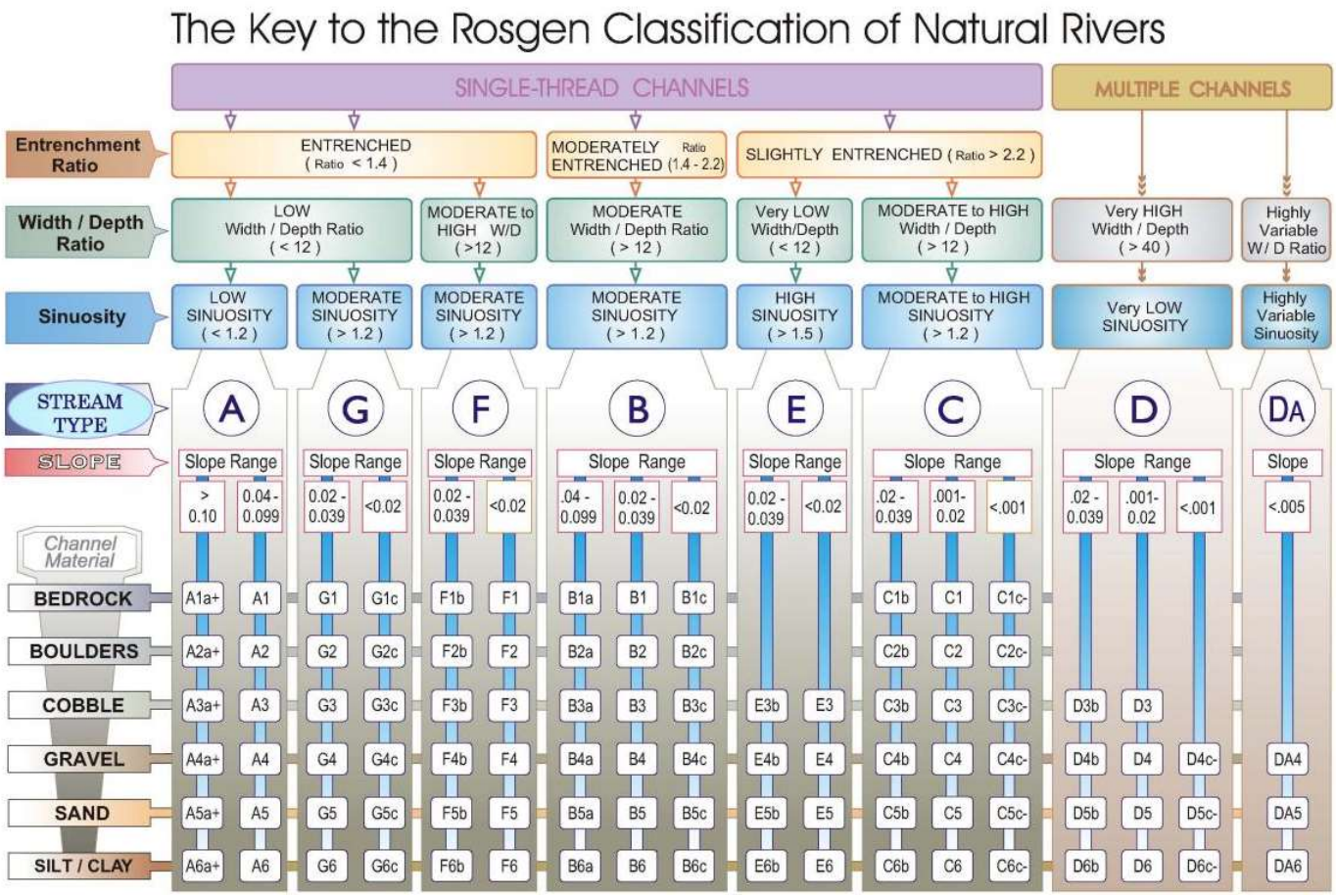


Figure 20: Key to Rosgen Classification System (Rosgen, 1994)

Level III assessment requires additional field collected data including riparian vegetation, the pattern of depositional features, sediment supply, stream size and order, meander patterns, bank material, and flow regime (Rosgen, 1996; Sass, 2011). Level III is a characterization of the current state of the stream as related to stability, response potential and function, and is useful for other related studies such as the assessment of biological systems (Rosgen, 1996; Sass, 2011).

Level IV assessment is intended “to verify process-based assessments of stream condition, potential, and stability as predicted from preceding analyses” and is “achieved through reach-specific observation and analyses of sediment condition, stream flow and

stability measurements" (Rosgen, 1996 p. 7-1). Level IV assessment is "reach specific" and should only be extrapolated to streams with very similar type and condition (Rosgen, 1996; Sass, 2011).

Based on the classification system outlined above, Rosgen (1996, 2006, 2014) have presented a number of documented sequences of channel adjustment as streams attempt to regain stability following significant disturbances that are known as "channel succession scenarios" (Keane & Sass, 2017). "Stream channel succession is the result of adverse consequences of accelerated sediment supply, accelerated bank erosion rates, degradation, aggradation from channel disturbance, streamflow changes, and sediment budget changes that lead to channel change (Rosgen, 1996 p. 2-44). These changes result in stability shifts and adjustments leading to stream channel morphological changes and eventual stream type changes over time" (Rosgen, 2008). As described in Simon et al. (2008), these succession scenarios are guided by the process of widening and filling, "as well as lengthening, flattening, and increasing curvature that represent the various forms possible as channels attempt to regain stable function" (Keane & Sass, 2017 p. 1517). Figure 21 below illustrates seventeen succession scenarios documented by Rosgen (1996, 2006, and 2014).

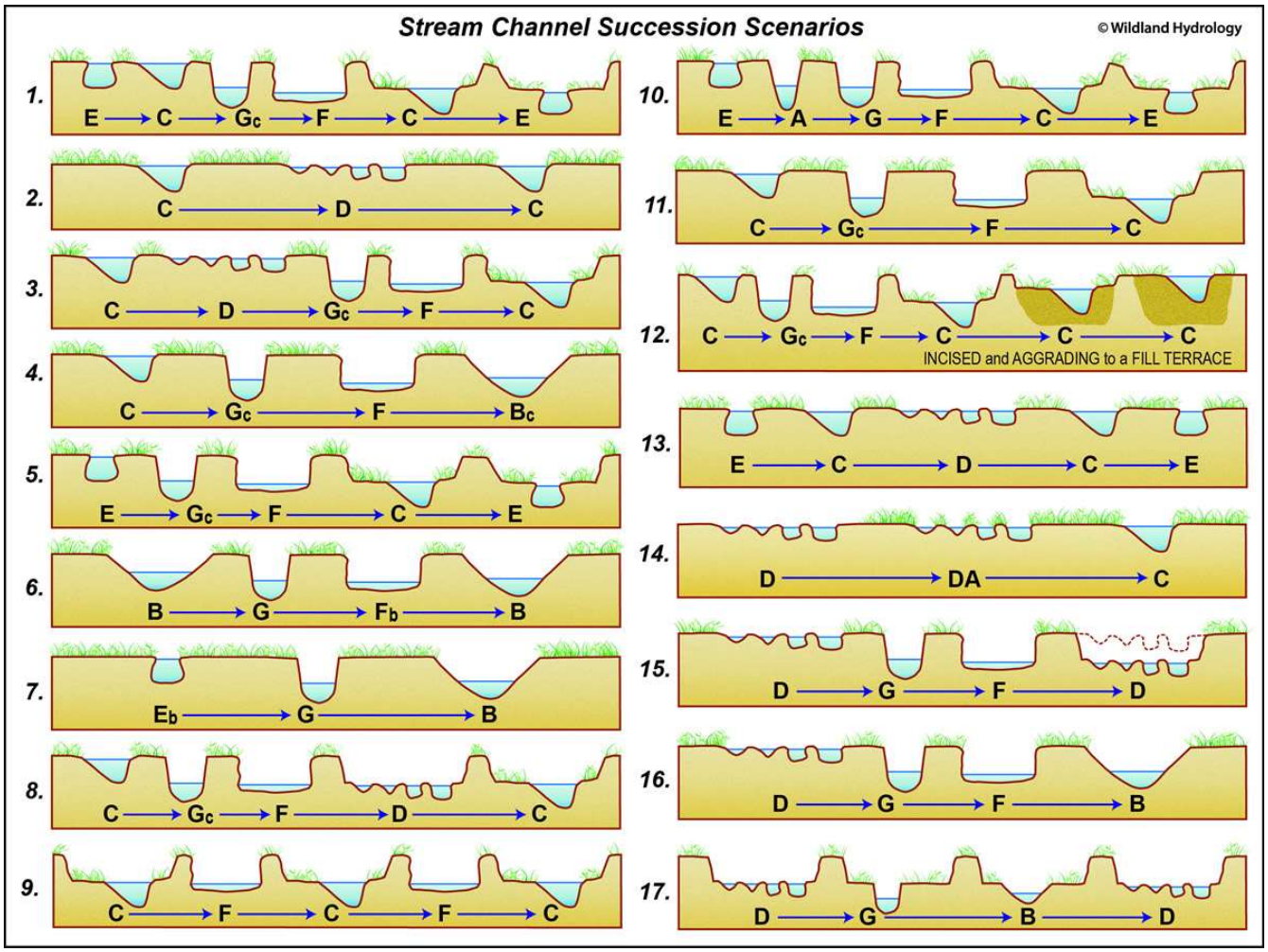


Figure 21: Rosgen Stream Succession Scenarios (Wildland Hydrology, 2021)

The Rosgen succession scenarios have characteristics similar to the CEM's presented by Schumm et al. (1984), Simon and Hupp (1986) as well as the modifications to these CEM's presented in Hawley et al. (2012) and Cluer and Thorne (2014); however, there are some notable distinctions: (Keane & Sass, 2017 p. 1517).

- Rosgen's classification system is based on measurable criteria related to channel dimension, pattern, and profile, which allow a more exact parameterization of channel change than previous CEMs (Keane & Sass, 2017 p. 1517).

- Rosgen's succession scenarios, documented from multiple real-world river systems, reflect a broader range of conditions, such as hydrology, boundary conditions, and vegetation, making them more in line with the SEM presented by Cluer and Thorne (2013) (Keane & Sass, 2017 p. 1517).

All of the CEMs discussed do have general similarities:

- Begin with a state of equilibrium
- Changes in the watershed conditions result in imbalance, usually increasing the volume and velocity of water entering the stream system
- Streams incise as they attempt to adjust to the new flow regime
- "Bed degradation usually precedes and predisposes channel widening..." (Harvey & Watson, 1986)
- Changes in bank height and/or boundary conditions results in mass bank failures resulting in widening of the stream channel (Keane & Sass, 2017).
- When sufficient widening has occurred to allow for an increase in sinuosity sufficient to create depositional features and floodplains, the stream may reach a new state of quasi-equilibrium often at a lower elevation (Keane & Sass, 2017).

Since the Rosgen's classification system and successional scenarios are based on measurable criteria related to channel dimension, pattern, and profile, which allows a more exact parameterization, it was used as the primary CEM when assessing the evolution of the BVR in this study. All of the CEMs discussed above rely on cross-sectional change to evaluate channel evolution; however, new remote sensing technologies allow for the collection of three-dimensional data at large spatial extents and higher temporal resolutions that may facilitate new ways of evaluating channel evolution.

Use of Structure from Motion (SfM) Photogrammetry in Fluvial Geomorphology

Methods for measuring river and stream bank erosion vary in spatial resolution, temporal resolution, and accuracy. In addition, methods that determine changes in bank profiles over time also detect and quantify the different stages of channel evolution or succession (Duro et al., 2018; Rosgen, 1996). Traditional riverbank surveying methods include erosion pins, recurrent cross-section, bank profile, and longitudinal profile surveying. However, these methods provide only two-dimensional data with the resolution dependent on the number of pins installed or the number of points collected at each cross section and/or the total number of cross sections, and "their accuracies may be affected by several factors, such as subaerial processes, which are land-based processes above the waterline such as mass wasting" (Couper, Stott, & Maddock, 2002; Duro et al., 2018). When surveying cross sections, the accuracy of most high-accuracy GPS systems and total stations ranges from millimeters to a few centimeters; however, the spatial and temporal resolution of cross section surveying may be sensitive to episodic, intermittent, or localized erosion (e.g., Brasington et al, 2000) (Duro et al., 2018).

Fluvial systems are "continuous systems that vary across multiple space and time scales..." (Marcus & Fonstad, 2010), and therefore, require continuous data in order to understand the full range of river functions and structure (Lane, Richards, & Chandler, 1994). Prior to the last decade, the vast majority of data used in fluvial geomorphology was collected via the traditional field surveying methods, such as surveying with differential laser level, total stations, and GPS systems; however, new remote sensing technologies can provide researchers with data that is of higher spatial

accuracy and resolution as well as higher temporal resolution (Mirijovsky & Vavra, 2012). The three-dimensional complexity of large areas of riverbank can currently be surveyed by a number of remote sensing techniques (Duro et al., 2018). This research focuses on the remote sensing technique of Structure from Motion (SfM) photogrammetry that offers a low-cost, low data collection times, and comparable accuracies to other 3-D remote sensing bank monitoring techniques such as, airborne laser scanner (ALS), terrestrial laser scanner (TLS), and light detection and ranging (LiDAR) (Hamshaw, Engel, Rizzo, O'Neil-Dunne, & Dewoolkar, 2019). SfM requires only a mid-grade single lens reflex (SLR) camera ($1,000) for terrestrial surveying or a high-end recreational grade drone ($2,000) for aerial surveying. In contrast, a TLS can be upwards of $10,000 and a LiDAR-capable drone upwards of $20,000.

Basics of Photogrammetry and Structure from Motion

"The core concept of SfM is the science of photogrammetry, using photographs to make quantitative measurements of the scene they represent" (Dietrich, 2014 p.1). Photos used in the photogrammetric processes are considered to be a perspective projection, which is simply when a three-dimensional object is projected onto a picture plane (Brock, 1975; Slama, 1980; Lane, Richards, & Chandler, 1993). A straight line passes from a single point in object space, through the perspective center of the camera lens, and then to a single point in image space on the image plane (Figure 22) (Lane, 1993). The relationship between object space and image and the collinearity equations describing "the relationship between two such mutually associated coordinate systems" is shown in Figure 22 below (Lane, 1993).

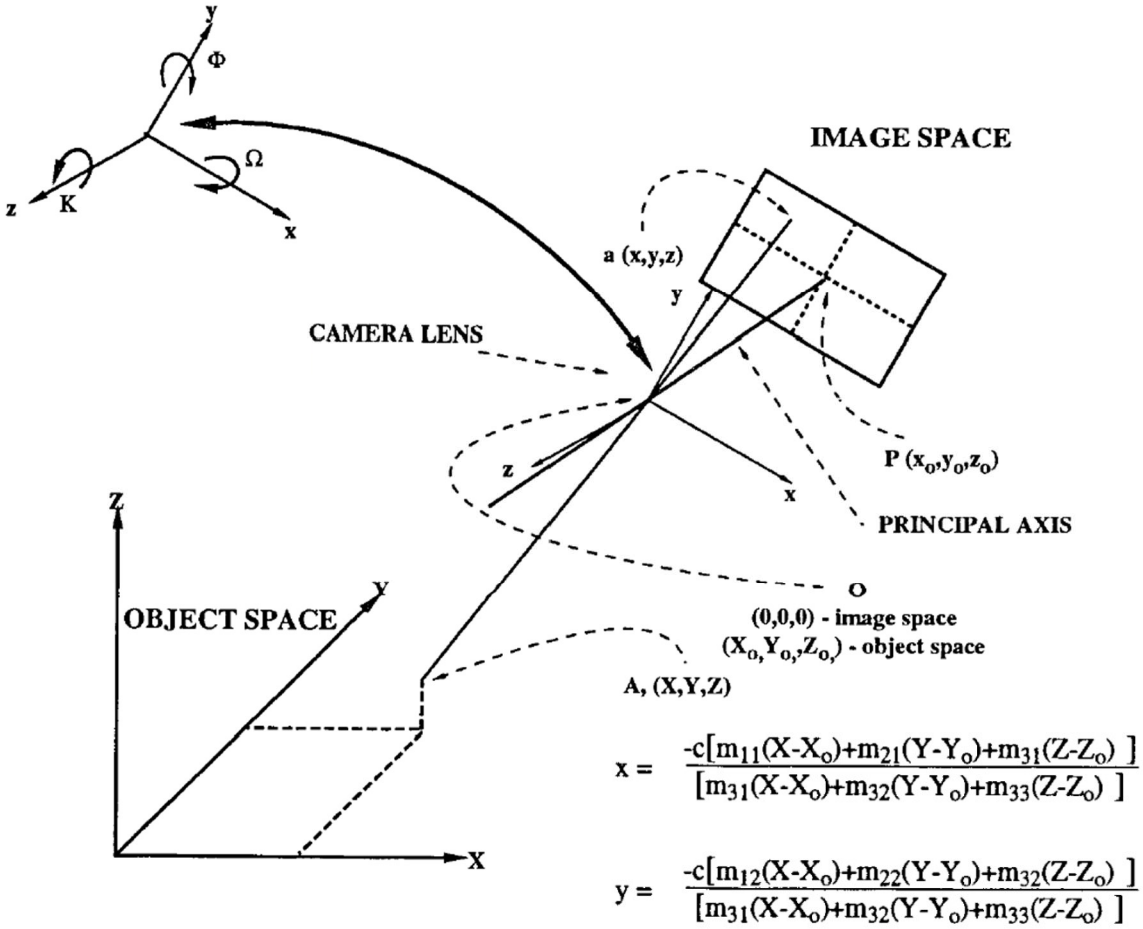


Figure 22: Photogrammetry Diagram: "The relationship between the object space and image space and the collinearity equations that describe the relationship between two such mutually associated coordinate systems" (Lane, 1993)

Where:	x, y, z	=	Co-ordinates of point a in the image space
	X, Y, Z	=	Co-ordinates of point A in the object space
	X_0, Y_0, Z_0	=	Co-ordinates of perspective center of the lens I in the object space
	K	=	Scale Factor
	$m_{11} – m_{33}$	=	Elements of the rotational matrix which are functions of Ω, Φ, and K on
	c	=	the focal length of the camera

A minimum of two photographs as well as the parameters of the collinearity equation are needed to determine the co-ordinates of points in the object space (Lane et al., 1993). The camera position in object space, the camera orientation (in the

instance of a drone, the roll, pitch, and yaw), and the scale factor must be considered (Figure 22). The stereo perspective facilitates the calculation of the distance from the camera to objects in the photograph using trigonometry when the internal camera geometry, lens distortions, and distance between images (parallax) is known; however, this traditional photogrammetric approach requires *a priori* determination of the exact camera positions (Dietrich, 2014). Shadowing is another downside of this type of stereo photogrammetry, which results in areas of missing data (Dietrich, 2014).

This type of early, classic photogrammetry was used by a number of authors to quantify landform change. For example, Rapp (1960) calculated the mean deposition rate on the scree cones of Mount Templet using a series of photographs dating back to 1,882 (Lane, 1993). Lo & Wong (1973) “used an aerial analogue to calculate the magnitude of gully erosion during a single storm event using two 35 mm cameras located vertically above the gully” (Lane et al., 1993).

SfM vs. Traditional Photogrammetry

SfM photogrammetric software and algorithms allow for the creation of very accurate point clouds and subsequent Digital Elevation Models (DEMs) from optical imagery collected with an unmanned aerial vehicle (UAV). Similar to traditional photogrammetry, SfM also uses images captured from different viewpoints to recreate the three-dimensional geometry of a surface (Fonstad, Dietrich, Courville, Jensen, & Carbonneau, 2013). The primary difference between the two is SfM software utilizes vision-based image-matching algorithms developed beginning in the 1970s, with iterations still being developed today. SfM software allows for unstructured image acquisition with no *a priori* knowledge of camera positions, as SfM is capable of

accurately calibrating and back-calculating relative non-metric camera positions in a reliable automated digital photogrammetric process (Dietrich, 2014). This new image matching approach has the ability to recognize conjugate features, which is when a single point or feature is present in multiple images (Fonstad et al., 2013). In addition, with classic digital photogrammetry, the collinearity equations that describe the relationship between a 3-d object and its projection are solved after the input of ground control points (GCPs); however, in the SfM workflow the collinearity equation are solved before the input of real-world coordinates.

Although individual point clouds and DEMs created using SfM can be highly precise, accurate registration of repeat models to a coordinate system and specific location is accomplished using GCPs with real-world coordinates. Although most SfM software can register models using only 3 GCPs, “best practice is to use a minimum of 5 GCPs for a single flight area” (Civil Tracker, 2023). All of the sites monitored in this research are within a single flight area, with the largest site being approximately two acres. Laying out GCPs is similar to “holding down a tarp in the wind” (Civil Tracker, 2023). GCPs are placed near the corners of a given site with the fifth GCP near the middle of the site (Figure 23), which prevents “doming” of the SfM point cloud during processing (Civil Tracker, 2023). GCPs should also be placed at varying elevations within the site. For each repeat SfM model, the five GCPs are used to register the point cloud using a 7-parameter transformation that includes three rotation parameters (roll, pitch, and yaw), three translation parameters (X, Y, and Z), and one scale parameter (Fonstad et al., 2013). SfM requires a smaller number of GCPs for the final model

reconstruction than traditional photogrammetry resulting in a minimization of the GCP x, y, and z errors (Dietrich, 2016).



Figure 23: Typical Layout of GCPs on a 120-acre Site (Civil Tracker, 2023)

Use of SfM in Riverbank Monitoring and Comparison to Other 3-D Techniques

Current methods for measuring streambank erosion and deposition range from photo-electric erosion pins to terrestrial laser scanning; however, compared to SfM, they only have high resolution in either time or space, but not both (Couper et al., 2002; Rinaldi & Darby, 2008). SfM Photogrammetry is a remote sensing technique for the three-dimensional monitoring of riverbank erosion that offers comparable accuracies to ALS, TLS, and LiDAR. Many early uses of SfM to monitor fluvial geomorphology were terrestrial based (Bird, Hogan, & Schwab, 2010; Dietrich, 2014; Micheletti, Chandler, & Lane, 2015). For example, Bird et al. (2010) collected images along a small (15 m) reach of Carnation Creek in British Columbia under a mature riparian forest canopy using a 35 mm SLR camera mounted on a 10 m-long pole achieving a ground

resolution of 0.03 m and mean vertical accuracy of 0.024 m when compared to the elevations of 10 RTK-GPS surveyed ground control points (GCPs).

Terrestrial laser scanners (TLS) provide the highest spatial accuracy for reconstructing 3-D surfaces when coupled with Real Time Kinematic Global Navigation Systems (RTK-GNSS) and are often used as the benchmark for accuracy assessments of other data collection methods (Prosdocimi, Calligaro, Sofia, Fontana, & Tarolli, 2015; Eltner & Schneider, 2015; Meinen & Robinson, 2020). With millimeter resolution and accuracies often < 0.02 m, sequential TLS surveys have successfully detailed patterns of erosion and deposition along river and stream banks (Resop & Hession, 2010; Leyland, Darby, Teruggi, Rinaldi, & Ostuni, 2015; Duro et al., 2018). The advantages of TLS over traditional cross-sectional surveying in capturing erosion patterns, especially overhanging blocks, is illustrated in O'Neal and Pizzuto (2011). TLS is relatively labor intensive, as scanning is typically done approximately every 200'. TLS equipment may also be mounted on a boat when surveying the banks of navigable rivers dramatically reducing collection times compared to terrestrial set up but introduces other field logistic and post processing issues (Alho, Kukko, Hyyppä, Kaartinen, & Jaakkola, 2009; Leyland et al., 2017; Duro et al., 2018).

Dietrich (2014) created SfM 3-D point clouds of two horizontal features (a lawn and a depositional river bar) and two vertical features (building face and river cut bank utilizing images collected with a 35 mm camera mounted on a 4.5 m pole and held by hand. When compared to TLS, the horizontal surfaces performed much better than the vertical surfaces. Dietrich (2014) also conducted repeatability analysis of SfM and found good agreement (average R2 0.99905) between three sets of SfM models

created from 3 unique photosets of the same study area, and tested uncertainty within the same datasets and study area using 250 RTK-GPS-surveyed checkpoints, resulting vertical RMSE of 1.88 cm and range of 0.4 cm. Micheletti et al. (2015) used a TLS benchmark to assess the accuracy of a digital terrain model (DTM) of a 10-m long 1.2-m high riverbank in Switzerland resulting in a vertical RMES of 0.07 m.

Before UAVs were affordable and practical for SfM image collection, other aerial vehicles of low-altitude image collection were utilized to monitor of fluvial environments at a larger scale, such as a helikite (helium blimp) (Fonstad et al., 2013) and helicopters (Dietrich, 2014; Javernick, Brasington, & Caruso, 2014). Recent, rapid development of UAV technology allowing the low-altitude collection of photographs has markedly expanded the application of SfM photogrammetry to fluvial geomorphology (Eltner & Schneider, 2015). The low flying altitude enables the acquisition of images with a high level of detail resulting in higher spatial accuracy than that of traditional aerial imagery (Mirijovsky & Vavra, 2012).

Early use of SfM in conjunction with UAVs such as Hugenholtz et al. (2013) produced a DEM for a 1.92 km^2 (192 ha) area of Bigstick Sand Hills in southwest Saskatchewan, Canada at an altitude of 200 m, and accuracy was assessed using 99 checkpoints surveyed with RTK-GPS. Hugenhlotz et al. (2013) found the horizontal and vertical RMSE errors of the checkpoints to be 0.18 m and 0.29 m, respectively, with the vertical RMSE equivalent to a LiDAR dataset of the same area collected in 2005. Mirijovsky & Langhammer (2015) utilized a multi-rotor UAV to collect images in the spring and fall of 2013 and 2014 of a 0.08-ha study area containing Javori Brook, a mid-mountain stream in the Czech Republic. The resulting SfM DEMs of Mirijovsky &

Langhammer (2015) had an average vertical RMSE of 0.031 m and were found to be highly accurate and precise when compared with LiDAR data. While evaluating the effects of an extreme flood event in 2013 on a braided gravel-bed river in Alberta, Canada (Elbow River), Tamminga et al. (2015) used UAV-based SfM to create DEMs of the study site before and after the flood (2012 and 2013). The 2012 and 2013 DEMs had vertical RMSE of 0.088 m and 0.047 m, respectively, for exposed areas and 0.098 m and 0.007 m, respectively, for submerged areas. Hamshaw et al. (2017) collected images for SfM processing of approximately 20 km of river corridor in central Vermont during four UAV campaigns in 2015 and 2016. The accuracy of the SfM DEMs was compared to TLS scans at seven locations using RTK-GPS cross-sectional data resulting in an overall RMSE of 0.289 m for the SfM DEMs and 0.089 m for the TLS data.

As noted in the *Significance* section of Chapter I, all of the studies discussed above were conducted on montane, gravel-bed, and often braided rivers/streams, which are very different from the cohesive, often vertical banks of the BVR that can reach a height of 7.5 m in the lower watershed. Duro et al. (2018) utilized SfM to evaluate bank retreat on a 1.2 km restored bank of the Meuse River in the Netherlands achieving high accuracy when compared to ALS and RTK GPS. Although the cohesive, vertical banks of the Meuse River are more similar to banks of the BVR, the maximum height was only 3.5 m, which is half the height of the maximum BVR bank height of approximately 8 m. A recent study, (Layzell, Peterson, Moore, & Bigham, 2022), utilized SfM in the assessment of streambank stabilization along the Cottonwood River in Eastern Kansas, which is in an area physiographically similar with similar bank heights as the BVR.

Use of Repeat LiDAR Datasets to Monitor Riverbank Change

The active remote sensing technology LiDAR (Light Detection and Ranging) has also become popular in the field of fluvial geomorphology due to its ability to provide detailed, accurate images of terrestrial elements in riverine landscapes that lie above, and in some cases below, the water surface (Marcus & Fonstad, 2010; Szafarczyk & Toś, 2022). LiDAR scans are collected from an airborne platform by emitting thousands of laser pulses directed towards the target of interest, which in this case, is a riverine landscape. In vegetated areas, each pulse will have multiple returns with the last return representing the ground. The round-trip travel time is then recorded for each return within each pulse. Simultaneously, the aircraft's position and attitude (roll, pitch, and yaw) are recorded using a global positioning system (GPS) and inertial measurement unit (IMU) (Kessler, Gupta, Dolliver, & Thoma, 2012). Return times combined with position and attitude of the aircraft allow for accurate estimation of horizontal and vertical positions of points and objects on the ground (Kessler et al., 2012). The LiDAR data is processed into a point cloud, from which ground points can be filtered and used to construct raster digital elevation models (DEMs) that represent the "bare earth" surface. LiDAR-derived DEMs collected at different times can be compared by subtracting the earlier DEM from the latter DEM to create a digital elevation model of difference (DoD) that provides continuous estimates of volume change within a given geographical area. Areas of erosion and deposition along riverbanks can be identified when applying this technique to river channels. While not numerous, a number of studies have used repeat LiDAR surveys to estimate geomorphic change along riverbanks at both the reach (Moretto, Delai, Rigon, Picco, Mao, & Lenzi, 2012;

Anderson & Pitlick, 2014) and catchment (Kessler et al., 2012; Schaffrath, Belmont, & Wheaton, 2015; DeLong et al., 2022) scales.

Kessler et al. (2012) quantified bank erosion along 446 km of river and streams in Blue Earth County, MN using repeat LiDAR surveys from 2005 and 2009, and independently assessed accuracy using 78 MnDOT hard surface points collected with an RTK GPS unit. When compared to the 78 hard surface points, Kessler et al. (2012) found the RMSE at the 95% confidence interval of the 2005 and 2009 DEMs too be ±0.20 m and ±0.14 m, respectively. Schaffrath et al. (2015) speculated that Kessler et al. (2012) had overpredicted riverbank erosion because systematic errors associate with the use of different GEOID models were not addressed. Schaffrath et al. (2015) outlines methodology for correcting systematic errors in DEM and subsequent DoDs used in the research presented here, such as correction for different GEOID models, horizontal offset, and poor co-registration of flight lines. These corrections are discussed in detail in Chapter IV.

CHAPTER III - Channel Succession of the Black Vermillion River

Introduction

The concept of river and stream geomorphic adjustment following disturbances that exceed a given geomorphic threshold has been discussed since the 1800s (Gilbert, 1877; Davis, 1902; Mackin, 1948; Leopold, Miller, & Wolman, 1964; Keane & Sass, 2017). Building on the work of Gilbert, Davis, and Mackin, Lane (1954) developed a qualitative, proportional equation of stream equilibrium (Lane's Balance), which has since evolved into "dynamic equilibrium" and is perhaps the most cited qualitative stream equilibrium equation in the literature today (Riley, 1998) (Figure 24):

$$Q_s d \propto Q_w S$$

- Q_s = sediment load (bed material load since it is predominantly responsible for the geomorphology of the stream)
- d = particle diameter or size of the sediment particles
- Q_w = water discharge
- S = slope (Lane, 1954)

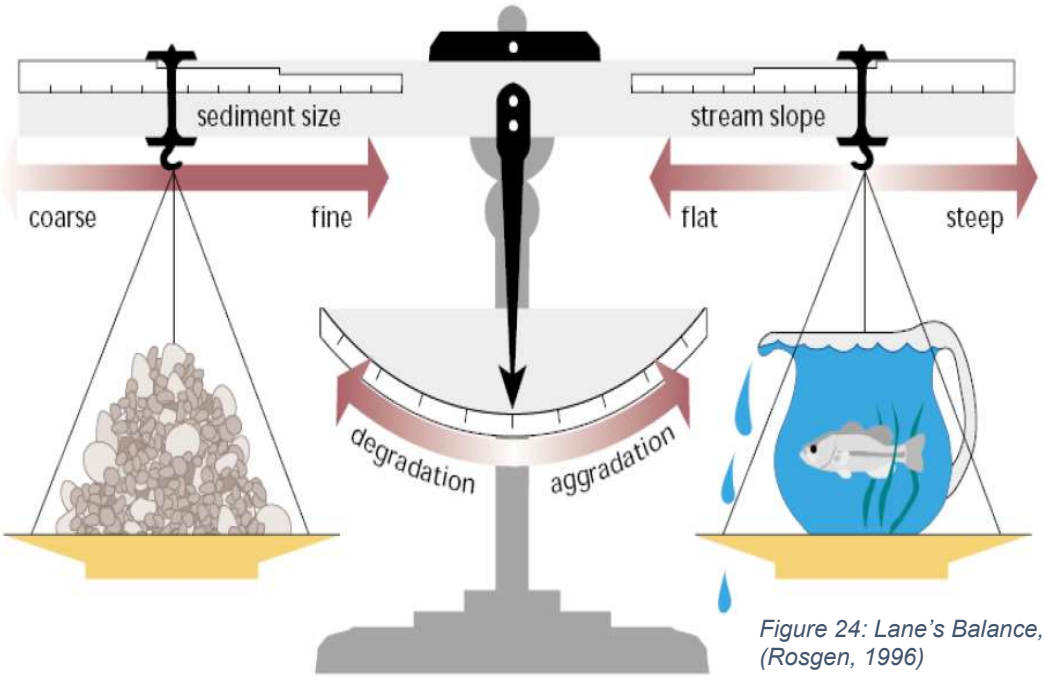


Figure 24: Lane's Balance, (Rosgen, 1996)

When in a state of dynamic equilibrium, a stream neither aggrades nor degrades and maintains consistent dimension, pattern, and profile while transporting the sediment and water supplied by its watershed (Mackin, 1948; Wolman & Leopold, 1957; Leopold & Maddock, 1963; Rosgen, 1996; Keane & Sass, 2017). Disturbances, whether natural or man-made that alter inputs of discharge, sediment load, sediment size, or channel slope in a fluvial system beyond a geomorphic threshold create disequilibrium within the system (Mackin, 1948; Lane, 1954; Leopold et al., 1964). Common anthropogenic disturbances to fluvial systems located in agriculturally dominated watersheds affecting the fluvial inputs listed above are:

- Change in land cover/use from natural vegetative cover to agricultural land uses
- Channelization, which is the linear reshaping or repositioning of an existing channel to facilitate rapid drainage of the immediately surrounding fields, may result in increased channel width, increased bed and bank slopes, increased bank height and a reduction of bank roughness due to vegetation removal (Simon & Hupp, 1987).
- The installation of flow through impoundments aimed at flood control by reducing peak flows while extending median flows during precipitation events (US-COE, 1998).

In an attempt to regain equilibrium - the most efficient transportation of water and sediment (Leopold & Maddock, 1953) – following a disturbance, a river will proceed through a number of sequential geomorphological changes as it attempts to adjust its dimension, pattern, and profile to fit the new flow and sediment regimes of its watershed. This series of adjustments following disturbance are generally known as channel evolution.

The Black Vermillion River (BVR) located in NE Kansas is one such agriculturally dominated fluvial system that has been significantly altered by the anthropogenic disturbances listed above (Figure 25). The BVR is in the process of channel evolution resulting from the disturbances noted above and serves as the study area for this research. The overall goal of this work is to document geomorphological changes the BVR channel has experienced over the past 15 years to better understand its channel evolution and better inform sediment production and restoration efforts.



Figure 25: Location of the BVR Watershed in NE Kansas (Sass & Keane, 2012)

Study Area Description

Three subwatersheds of the BVR are included in this study due to their inclusion in Sass & Keane (2012), as portions of the data collected at that time are utilized in this study. Sass & Keane (2012) was aimed at developing a tool for predicting annual streambank erosion rates and selected three subwatersheds within the upper BVR watershed for inclusion in their study: Black Vermillion Main Stem (MS), Irish Creek (IC), and North Fork (NF). Each subwatershed contained three study reaches generally

located in the upper, middle, and lower sections of each subwatershed. Unfortunately, of the original nine study reaches, only seven were able to be included in this study due to landowners' access permission (Figure 26).

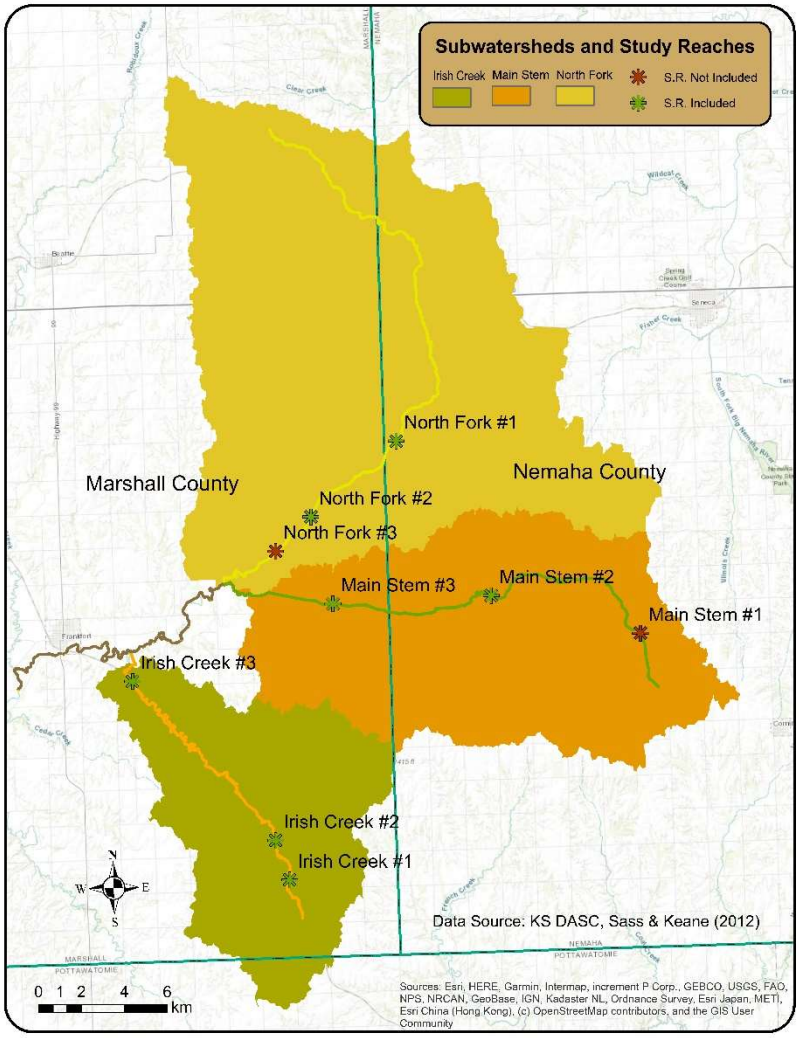


Figure 26: Subwatersheds and Study Reaches (Sass & Keane, 2012)

The entire Black Vermillion River Basin covers 1,383 km^2 and lies within the glaciated physiographic region of Northeast Kansas, which is a portion of the larger Glaciated Plains Region; however, the Irish Creek watershed in the southwestern portion of the BVR Basin is influenced by the Flint Hills Uplands Region that lies to the south (Sass & Keane, 2012). In the glaciated region of NE KS, a layer of glacial till ranging in depth from 30.5 m to 122 m in depth covers alternating layers of limestone (Permian and Pennsylvanian) and shale. Although the Flint Hills Uplands shares the same underlying geology of limestone and shale as the glaciated regions, it is not overlain with glacial till (KGS, 2007). Throughout the BVR Basin, riparian soils are

formed from alluvium parent material deposited by repeated flooding over the millennia (Sass, 2011). Soils at the study reaches are silt loams and silty clay loams having a high clay content ranging between 23 and 47% (NRCS, 2011). Table 7 indicates the major soil properties at each Sass & Keane (2012) study reach.

Table 7: Study Reach Soil Properties Adapted from Sass & Keane (2012) Study Reaches: Source: NRCS Soil Survey

Study Reach	Soil Name	Parent Material	Percent Clay (%)	Liquid Limit (%)	Bulk Density (g/cm^3)	Minor Association
MS1	Kennebec Silt Loam	Fine-silty alluvium	25.4	40.5	1.37	Wabash
MS2	Kennebec Silt Loam	Fine-silty alluvium	25.4	40.5	1.37	Wabash
MS3	Nodaway Silt Loam	Calcareous fine-silty alluvium	23	35.3	1.30	Wabash, Aquolls
NF1	Kennebec Silt Loam	Fine-silty alluvium	25.4	40.5	1.37	Wabash
NF2	Wabash Silty Clay Loam	Clayey alluvium	47.1	62.6	1.35	None
NF3	Nodaway Silt Loam	Calcareous fine-silty alluvium	23	35.3	1.30	Wabash, Aquolls
IC1	Kennebec Silt Loam	Fine-silty alluvium	25.4	40.5	1.37	Wabash
IC2	Kennebec Silt Loam	Fine-silty alluvium	25.4	40.5	1.37	Wabash
IC3	Wabash Silty Clay Loam	Clayey alluvium	47.1	62.6	1.35	None

The climate in NE Kansas is considered continental with most of the average 87.9 cm of rainfall (period of record 1970 - 2021) occurring between April and September (Aber, 2007). Annual precipitation at Frankfort, KS exceeded the annual average three times (2007, 2010 and 2019) over the 2007-2021 study period. In 2019, annual precipitation exceeded the average by 2.1 standard deviations (42.88 cm). In contrast, annual precipitation was below average every year between 2011 and 2018 (Figure 27).

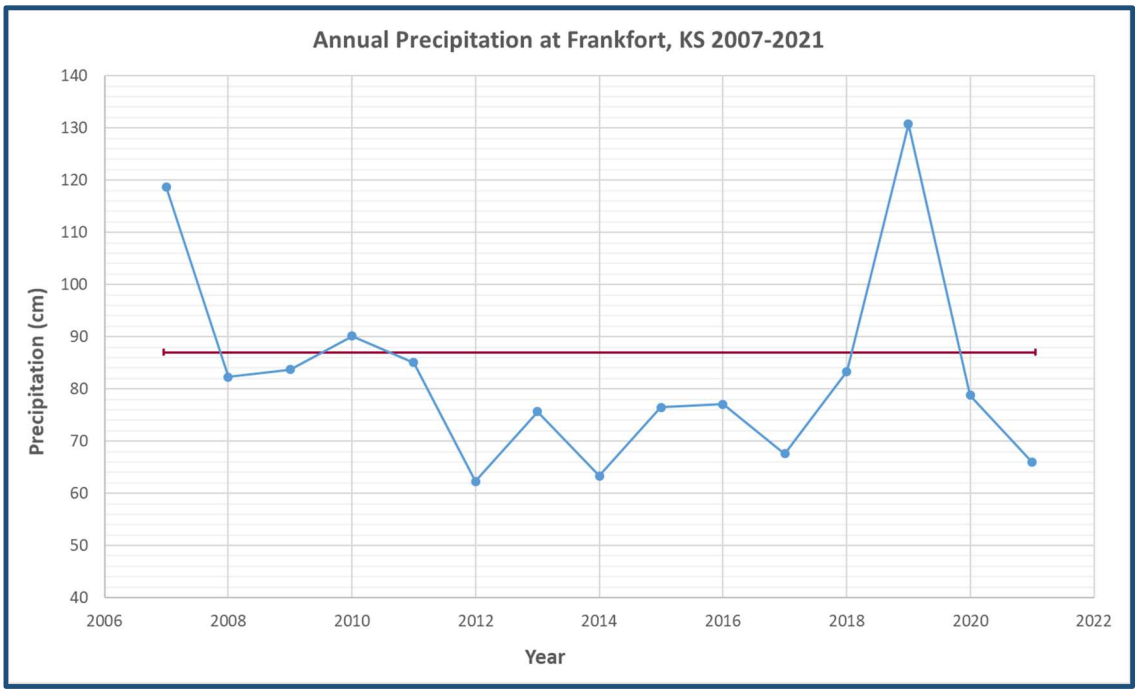


Figure 27: Annual Precipitation at Frankfort, KS 2007-2021 (NOAA, 2022)

BVR Watershed Change in Land Use

Prior to the late 1800s, row-crop agriculture in the BVR basin was concentrated on floodplains adjacent to rivers due to deep, fertile riparian topsoil and low-relief topography (Meade, 2009; USDA-SCS_KES, 1951). By the 1930s, when the population of Marshall and Nemaha Counties were at their highest, tillage, row-crop agriculture land use had become dominant in the BVR basin (Legends of Kansas, 2022; USDA-SCS_KES, 1951). Examination of National Landcover Data (NLCD) from the Multi-Resolution Land Characteristics Consortium indicate that total agricultural land use (cultivated fields plus hay/pasture) within the seven study reach watersheds included in this study ranges between 83 and 93% and remained unchanged from 2007 through 2019.

Changes in land use in the BVR watershed from native vegetation to agricultural uses in the late 19th and early 20th centuries resulted in an increase in discharge. The runoff coefficient is "the ratio of volume of water superficially drained during rainfall to the total volume of precipitation" for a given rain event (Machado, Cardoso, & Mortene, 2022). Qiao et al. (2017) found the runoff coefficient for tallgrass prairie, similar to what would have been present in the BVR watershed before European settlement, to be 0.044. The runoff coefficient for pastureland and cultivated land with clay and loam soils, as found in the BVR watershed, range between 0.30 and 0.55 (Chow, Maidment, & Mays, 1988). The increase in runoff coefficient means that prior to the conversion of land use to agriculture about 4.4% of rainfall flowed overland into BVR streams and rivers, while after the conversion, above ground stormwater runoff increased to between 30% and 50%. The increase in runoff coefficient along with extensive channelization has resulted in the BVR having approximately 40% higher storm discharges and a flashier hydrograph than pre-European settlement, which is characterized by discharges rising faster and receding more quickly than before (Sass & Keane, 2012).

The 1.5-year recurrence interval (RI) discharge (5016 ft^3/s, 142.04 m^3/s) was calculated from 67 years (1954-2020) of yearly peak stream discharge data using the formula: $RI = \frac{N+1}{rank}$. Where N = number of years in the period of record and *rank* = ranked order of peak annual discharges starting with the largest discharge. Discharge was measured at the USGS gauging station #6885500 approximately 3.8 km downstream of Frankfort, KS. Utilization of the 1.5-year RI in this study was due to its use in Keane & Sass (2017), who found the 1.5-year RI discharge to be consistent with field observed bankfull features and whose results will be included in the discussion;

however, the 1.5-year recurrence interval calculated by Keane & Sass 2017) was less (4,900 cfs) due to the yearly peak flows of the last decade being included in the calculation for this study. Keane & Sass (2017) employed the 1-5 year return interval in order to compare their results with other discharge curves for the ecoregion. During the 2007-2010 study period of Sass & Keane (2012), discharge exceeded the 1.5-year recurrence interval bankfull flow 12 times, an average of 4/year. Bankfull flows typically occur about once every 1.5 years. From 2011 through 2021, discharge exceeded bankfull 23 times, an average of 2.3/year, with nine occurring in 2019 alone, when annual precipitation was in excess of 130 cm. It is clear that over the past 14 years, bankfull flows as determined by the 1.5-year recurrence interval have become substantially more common than once every 1.5 years.

BVR Channelization

While channelization of the BVR has been done in a piecemeal fashion by farmers and private land owners since the early 1900s, the vast majority of channelization occurred between the 1950's and 1980's in conjunction with state and federal agencies such as the Soil Conservation Service (now NRCS) and the U.S. Army Corps of Engineers (Meade, 2009; Sass & Keane, 2016). Channelization increases channel gradient and sets in motion vertical adjustments such as upstream degradation and downstream aggradation as the stream attempts to adjust its slope back to the pre-channelization gradient (Simon & Rinaldi, 2006).

As incision caused by channelization migrates upstream and once enough time has passed with minimal additional disturbance, space for time substitution can be used to discern the various stages of channel evolution, with the lower reaches being further

along in the evolutionary process (Schumm et al., 1984; Simon & Hupp, 1986). In such a scenario, it would be expected to see higher amounts of active channel adjustment, incision and/or widening in the upper reaches and less in the lower reaches that have had more time to adjust. Keane & Sass (2017) speculated that this was the case within the BVR system.

Channelization of the BVR has shortened the portion of the river included in Sass & Keane (2012) from an estimated original length of 114.8 km to 89.3 km in 1998 (US-COE, 1998). To determine the amount of channelization in each subwatershed between 1967 and 2021, the centerline of each of the three subwatershed channels was determined using National Agriculture Imagery Program (NAIP) aerial photographs attained from the State of Kansas GIS Data Access and Support Center (KS DACS) and USGS Earth Explorer. Table 8 provides the amount of river length in each subwatershed that was lost to channelization between 1967 and 2021. The location and timing of channelized reaches between 1958 and 1988 created by Rob Daniels in 2008 and adapted from Mead (2011) is shown in Figure 16, p.46.

Table 8: Change in Subwatershed Centerlines between 1967 and 2021

Subwatershed Centerline Change (km)					
Subwatershed	1967	1985	2008	2021	Change 67-21
Main Stem	39.20	28.80	29.23	29.20	-10.00
Irish Creek	27.61	23.01	23.69	23.48	-4.13
North Fork	40.39	34.68	35.30	35.11	-5.28

The decrease in length due to channelization resulted in an increase in slope and stream power and led to basin-wide streambed degradation and incision, thus increasing sediment being delivered downstream (US-COE, 1998; Knighton, 2014;

Sass & Keane, 2012). Overall, the BVR flows from east to west emptying into the Big Blue River that was first dammed in 1959 by the United States Army Corps of Engineers creating Tuttle Creek Reservoir in order to facilitate flood control and flow management of the lower Missouri River (Keane & Sass, 2017; US-COE, 1998). Although originally designed for flood control, the State of Kansas has begun planning the use of flood control reservoirs such as Tuttle Creek as municipal water supplies (KWO, 2017); however, sedimentation has led to an estimated 47.9% capacity loss in the reservoir since its completion in 1961 (Rattanavong, 2019).

BVR Impoundments

Numerous “flow-through” flood control impoundments can be found in the BVR watershed in the form of small reservoirs and farm ponds (Sass, 2011). While these impoundments attenuate peak discharges increased by temporarily storing runoff, they increase the duration of median flows. Stormwater is released over a longer period as indicated by the extended rising and falling limbs of the storm hydrograph when compared to the pre-impoundment hydrograph (Brogan, 2018; Mei et al., 2018). In 2007, the controlled area calculated by Sass & Keane (2012) within the BVR watershed included in this study was 29%. Inspection and watershed analysis of 2018 NAIP imagery and KS DASC topographic data indicate the controlled area had increased to 39% due to the construction of new impoundments during the nine-year period. This increase could be partially due to an error in the calculation of the controlled area in 2007. Table 9 indicates the amount of controlled area in the drainage area for each study reach in 2007, when the study reach data was first collected, and 2018, the most

current high-resolution topographic data available. All but one study reach watershed experienced an increase in the amount of controlled area between 2007 and 2018.

Table 9: Change in Study Reach Watershed Controlled Area

Change in Study Reach Controlled Area 2007 - 2018						
Study Reach	Total Drainage Area	Controlled Area 2007 (km^2)	Percent of DA Controlled 2007	Controlled Area 2018 (km^2)	Percent of DA Controlled 2018	Percent Change
MS2	91.46	42.44	0.46	46.71	0.51	10.06%
MS3	160.47	70.17	0.44	77.85	0.49	10.95%
IC1	20.52	8.91	0.43	12.05	0.59	35.36%
IC2	34.17	18.94	0.55	21.83	0.64	15.25%
IC3	118.94	58.31	0.49	67.08	0.56	15.05%
NF1	156.13	40.89	0.26	44.65	0.29	9.21%
NF2	294.05	79.91	0.27	73.93	0.25	-7.48%

Channel Evolution Models

The disturbances discussed above have significantly altered the stormwater runoff and sediment regimes of the BVR subwatersheds, resulting in geomorphic channel adjustments in the BVR as it attempts to adjust its dimension, pattern, and profile to accommodate the new water and sediment inputs. In an attempt to regain equilibrium (the most efficient transportation of water and sediment (Leopold & Maddock, 1953) following a disturbance, a river channel will proceed through the sequential geomorphological adjustments discussed above, generally known as channel evolution. A number of channel evolution models (CEMs) have been proposed over the past four decades that seek to explain the process of stream adjustment or evolution in specific physiographic settings (Schumm et al., 1984; Simon & Hupp, 1986; Cluer & Thorne, 2014; Rosgen, 1996). However, some of these models have been shown to apply to a variety of physiographic settings (Cluer & Thorne, 2014).

Documentation of river channel evolution is dependent on observation over time, as adjustment following disturbance could take decades if not centuries. Evaluation of river systems using these models may help guide restoration efforts. As noted by Schumm et al. (1984, p.3), conservation and restoration efforts "will be most successful when implemented at the proper evolutionary stage of development...acting with the evolving river system rather than in opposition to it."

Keane & Sass (2017), a study aimed at using channel evolution models appropriate for the BVR as predictors of sediment yield, considered four CEMs:

- Schumm, Harvey, and Watson (1984) Channel Evolution Model
- Simon and Hupp (1986) Channel Evolution Model
- Cluer and Thorne (2014) Stream Evolution Model
- Rosgen (2006) Successional Scenarios

Note that while the channel sequences described by each model differ somewhat, they all attempt to predict the sequence of river and stream channel adjustment following disturbance. Channel adjustments occur in two dimensions, vertical and lateral. Vertical adjustments such as upstream incision and downstream aggradation dominate the initial response and result in a reduction of channel gradient over time (Thorne, 1999; Cluer & Thorne, 2014; Simon & Rinaldi, 2006). While vertical adjustment is still ongoing, lateral channel adjustment begins once critical bank height is reached and erosional processes such as excess shear stress, soil piping/seepage, pore pressure changes, and entrainment of bank toe material lead to mass failure of bank material. Steeper banks tend to experience slab failure; in contrast, shallow banks

ten to fail by rotational slump or pop-out failures at the base of the bank (Simon & Hupp, 1987; Dunne & Leopold, 1998; Fox et al., 2007).

Mass failures result in channel widening when the stream has the competence and capacity to entrain and transport the fallen material (Sass, 2011). The channel may continue to widen until near-bank flows no longer have the competence to remove failed bank material resulting in the formation of toe benches and/or aggradation of the streambed (Cluer & Thorne, 2014). Channel width stabilizes as bank toe benches and berms are built from slumped bank material and subsequently secured with vegetation, and a new quasi-equilibrium is attained once “banks and berms stabilize, and the energy slope adjusts to match local sediment transport capacity to the supply of sediment from upstream” (Cluer & Thorne, 2014 p.137; Schumm et al., 1984).

Although these adjustments following disturbance have been organized into a number of channel evolution models consisting of sequential “Stages” or “Stream Types”, it is important to note that channel evolution is more of a continuum rather than the discreet phases described in each model (Keane & Sass, 2017). “Stages” and/or “Stream Types” of the four CEMs and their descriptions are shown below in Table 10, adapted from Cluer and Thorne (2014), and expanded to include a Rosgen Successional Scenario #11 (Figure 28). Because of the measurable criteria in the Rosgen System as well as the nature of the data collected by Sass & Keane (2012) to be used in this study, the Rosgen (2006) Stream Succession Scenarios was the primary CEM considered when evaluating the channel evolution of the BVR over the past 14 years. In addition, the terms “channel evolution” and “stream succession” will be used interchangeably for the remainder of this document.

Table 10: CEMs with Stage/Type Descriptions

Schumm et al. 1984	Simon and Hupp, 1986	Cluer and Thorne, 2014 (SEM)		Rosgen, 2006 Suc. Scen. #11	Description
		0. Anastomosing (Braided Channel)			Pre-Disturbance, dynamically meta-stable network of anabranching channels and floodplain with vegetated islands supporting wet woodland or grassland.
I. Undisturbed	I. PreModified	Single Thread Channel	1. Sinuous	C	Dynamically stable and laterally active channel within a floodplain complex. Flood return period 1-5 yr. range
	II. Constructed		2. Channelized	G	Re-sectioned land drainage, flood control, or navigation channels.
II. Degradation	III. Degradation		3. Degrading	G	Incising and abandoning its floodplain. Featuring head cuts, knick points or knick zones that incise into the bed, scours away bars and riffles and removes sediments stored at bank toes. Banks stable geotechnically.
			3s. Arrested Degradation		Stabilized, confined or canyon-type channels. Incised channel in which bed lowering and channel evolution have been halted because non-erodible materials (bed rock, tight clays) have been encountered.
III. Rapid Widening	IV. Degradation and Widening		4. Degradation and Widening	G	Incising with unstable, retreating banks that collapse by slumping and/or rotational slips. Failed material is scoured away and the enlarged channel becomes disconnected from its former floodplain, which becomes a terrace.
				F	
			4-3. Renewed Incision		Further head cutting within Stage 4 Channel
IV. Aggradation	V. Aggradation and Widening		5. Aggrading and Widening	F	Bed rising, aggrading, widening channel with unstable banks in which excess load from upstream together with slumped bank material build berms and silts bed. Banks stabilizing and berming.
V. Stabilization	VI. Quasi-Equilibrium		6. Quasi-Equilibrium	C	Inset floodplain re-established. Quasi-equilibrium channel with two-stage cross section featuring regime channel inset within larger, degraded channel. Berms stabilize as pioneer vegetation traps fine sediment , seeds and plant propagules.
	VII [(1)]		7. Laterally Active		Channel with frequent floodplain connection develops sinuous course, is laterally active and has asymmetrical cross section promoting bar accretion at inner margins and toe scour and renewed bank retreat along outer margins of expanding /migrating bends.
		8. Anastomosing (Braided Channel)			Meta-stable channel network. Post-disturbance channel featuring anastomosed planform connected to a frequently inundated floodplain that supports wet woodland or grassland that is bounded by set-back terraces on one or both margins.

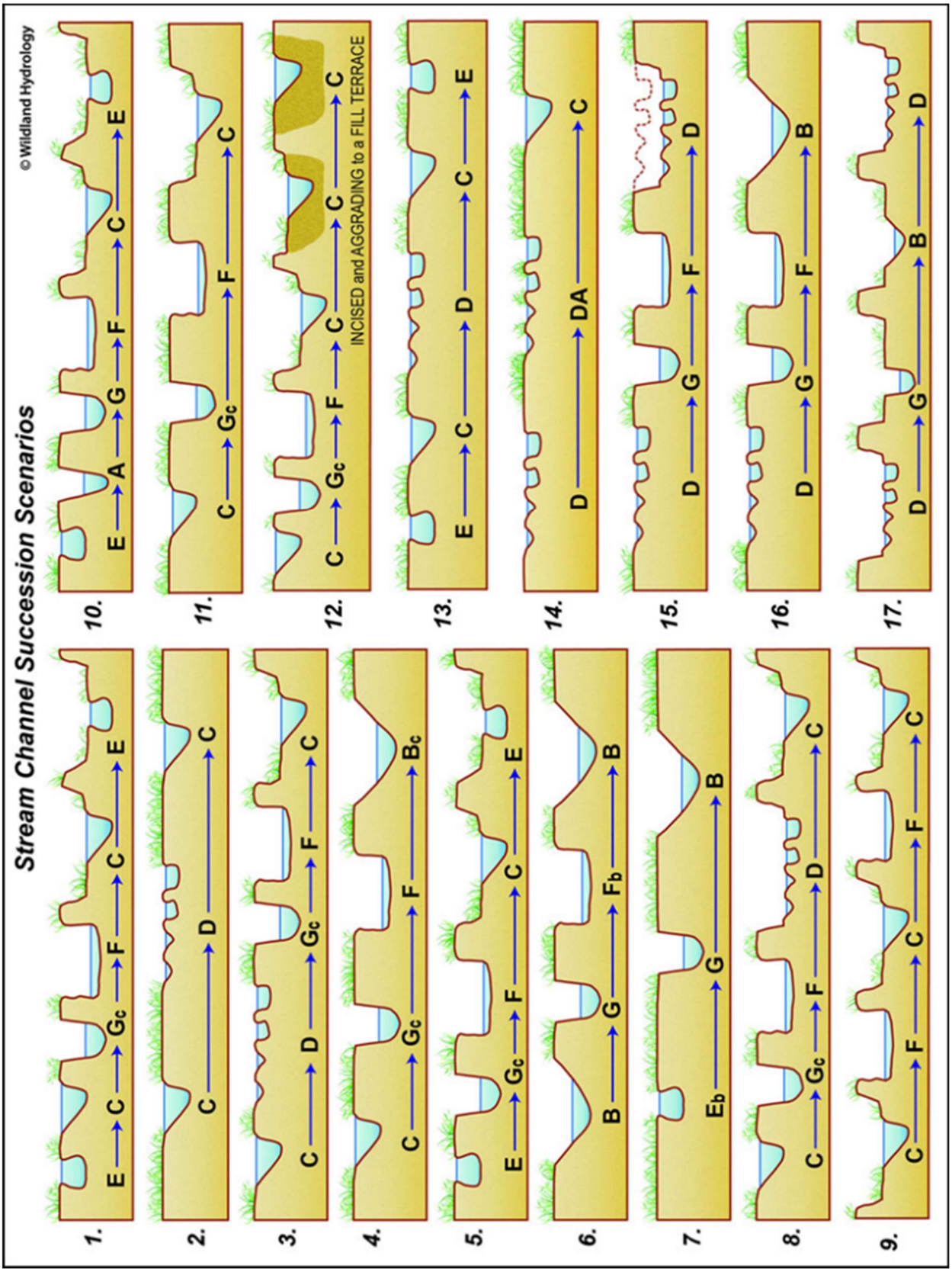


Figure 28: Rosgen Successional Scenarios (Rosgen, 2014)

Rosgen Successional Scenarios (1996, 2006, and 2014) are based on the 4-Level Rosgen (1994) Classification System first introduced in the article "*A classification of Natural Rivers*" in the journal *CATENA.* As the Rosgen Level II methodology of stream classification will be relied upon heavily in the discussion of channel evolution, it may be helpful to briefly discuss the system. Rosgen's Level II assessment for classification is conducted at a reach scale equal to approximately 20-30 times the bankfull width that includes at least one representative riffle cross section (Rosgen, 1994). The Rosgen (1996) Classification System consist of nine stream types denoted by the letters A through G and two additional types Aa+ and DA (Figure 29) (Rosgen, 1996), with stream types A, B, C, and E being stable stream types, type D being rarely stable, and types G and F being most often unstable, transitional stream types. As noted earlier, a "stable" stream does not aggrade or degrade and maintains a consistent dimension, pattern, and profile as it transports the water and sediment supplied by its watershed (Mackin, 1948; Leopold & Maddock, 1963; Rosgen, 1996). Level II assessment is based on five criteria of representative "reference reaches" (Rosgen, 1994):

1. **Entrenchment Ratio**, measured at a riffle cross-section, is the width at the flood-prone elevation/bankfull width, with the flood-prone elevation set at twice the maximum depth at bankfull (Figure 30).
2. **Width/depth ratio**, measured at the riffle cross-section, is bankfull width/mean depth, with channels having a low width/depth ratio being narrow and deep and channels having a high width/depth ratio being wider and shallower (Figure 30).
3. **Sinuosity** is the ratio of stream length to valley length and reflects the meander geometry characteristics of a reach with higher values indicating a more sinuous channel.

4. **D_{50}** is 50th percentile of the reach pebble count = dominant channel material
5. **Water surface slope** at bankfull discharge is estimated using the water surface slope at the beginning and end of the longitudinal profile, both at the head of a riffle.

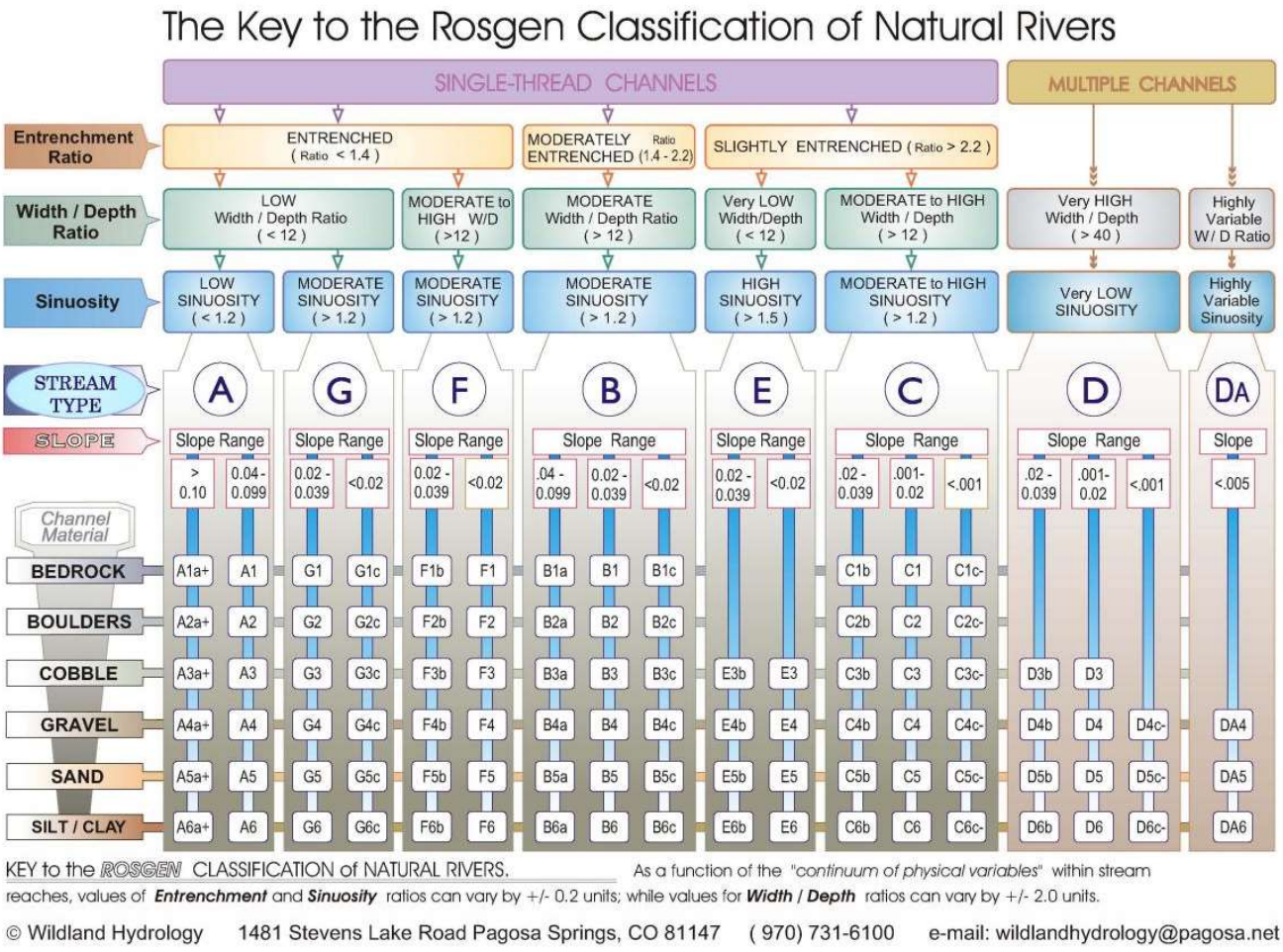


Figure 29: Key to Rosgen Classification System (Rosgen, 1996)

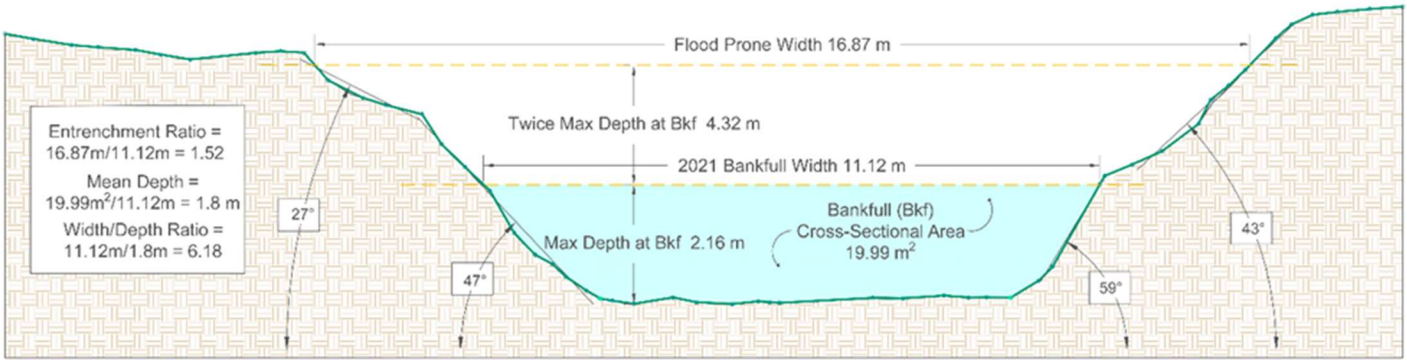


Figure 30: Rosgen Level II Classification Dimensions and Ratios of Irish Creek 1 2021 Riffle Cross Section

Rosgen (1996, 2006, and 2014) presented a number of sequences of channel adjustment following significant disturbances based on multiple real-world river systems known as “channel succession scenarios” (Figure 28) that are:

- Described using the Rosgen classification system stream types discussed earlier.
- Channel changes associated with these successional scenarios are the result of adverse consequences, such as accelerated sediment supply, accelerated bank erosion, degradation and/or aggradation from channel disturbance, and changes in discharge (Rosgen, 1996).
- Reflect a broader range of conditions, such as hydrology, boundary conditions, and vegetation, making them more in line with the SEM presented by Cluer & Thorne (2014).
- Based on the previously discussed measurable criteria related to channel dimension, pattern, and profile, which allows a more exact parameterization (Keane & Sass, 2017).

Keane (2004) conducted a three-year study of nearly 60 stable reference reach streams in Kansas and found in Eastern Kansas “many of the stable ‘C’ streams documented....were ‘C’ streams that had stabilized at a lower elevation inside of old “F” channels” (Keane & Sass, 2017 p. 1521). In addition, “Pre-European settlement streams in the Kansas Glaciated Region and BVR area seemed to classify as “C” type streams according to notes of the Kansas Territory Survey completed in 1857” (Keane & Sass, 2017 p. 1524). Based on these findings, Keane & Sass (2017) determined Rosgen successional scenario #11, “C”-“G_c”-“F”-“C” (Figure 28) to be the most common sequence in the eastern part of the state where the BVR is located.

BVR Stream Type in 2009

In 2009, all study reaches measured by Sass & Keane (2012) were classified as "$G4_c$", "$G5_c$", "F5" or "$B5_c$" type streams; however, it is noted that the reach classified as "$B5_c$" alternated between "$B5_c$" and "$G5_c$" (Table 11). The "C"-"Gc"-"F"-"C" Rosgen successional scenario is common in Eastern Kansas (Keane & Sass, 2017); therefore, the expected change from "Gc" to "F" and "F" to "C" would be the expected succession for all of the 7 study reaches included in this study. Indicators of incision/aggradation (max depth at bankfull, mean bankfull depth, cross-sectional area), and widening (bankfull width, bankfull cross-sectional area) as well as bank angle are considered here.

*Table 11: BVR Study Reach Characteristics and Rosgen Classification; using bankfull (1.5-yr) recurrence interval, adapted from (Sass & Keane, 2012): *Sass & Keane (2012) note IC3 alternated between B5c and G5c: Wbkf (Bankfull Width), D_{50} (Dominant Feature Particle Size Feature), W:D (Width/Depth Ratio), K (Sinuosity)*

Study Reach	Rosgen Stream Type	D_{50} (mm)	W_{bkf} (m)	W:D	Entrench-ment Ratio	Slope (m/m)	K	Reach Length (m)	Average Bank Height (m)
Main Stem 2	G5c	10.25	11.52	8.80	1.50	0.0014	1.20	472.74	4.60
Main Stem 3	F5	0.82	14.11	13.50	1.30	0.0007	1.20	414.53	5.73
Irish Creek 1	G4c	6.98	10.27	9.90	1.40	0.0014	1.30	376.43	5.15
Irish Creek 2	G4c	18.86	13.59	8.70	1.20	0.0017	1.30	510.24	6.74
Irish Creek 3	B5c*	0.35	13.05	7.70	2.10	0.0006	1.30	524.87	5.24
North Fork 1	G5c	2.92	13.90	7.10	1.60	0.0013	1.20	510.84	6.31
North Fork 2	G5c	2.78	19.54	10.90	1.50	0.0008	1.00	696.77	4.94

Availability of Data

The availability of datasets to aid in the evaluation of BVR channel succession was also beneficial. As noted, Sass & Keane (2012) collected data related to the dimension, pattern, and profile of the BVR channel at precise locations between 2007 and 2010, most of which were resurveyed in 2021 and used to evaluate channel succession.

Regarding the Rosgen (1996) classification, “channel type classification is based largely on riffle measures; while riffles are the most stable grade/elevation points/features along a stream, it does not mean they cannot or do not move or change (e.g., transverse bar formation). Fourteen years of instability is likely to shift bed features” (Keane, 2022).

In addition to the Sass & Keane (2012) data, digital elevation models (DEMs) were available for the entire study area from 2010 (2012 in Nemaha Co.) and 2018, a sizable portion of the 14-year study period (2007-2021). A DEM is a 3-dimensional digital representation of the bare earth topographic surface derived from light detection and ranging (LiDAR), a process similar to radar. DEMs are gridded data (raster), where each cell or pixel (1m x 1m in this case) contains an elevation value. DEMs from different times can be compared in order to determine geomorphic change. Every DEM has inherent error that is determined using checkpoints. Checkpoints are evenly distributed throughout the LiDAR survey area, and their position and elevation measured with high-accuracy GPS equipment. The GPS position and elevation values at each checkpoint are then compared to the values at the same points on the LiDAR-derived DEM to determine the error of each checkpoint. The root mean square error (RMSE) of all checkpoints is used as the DEM error.

Methods

The study area is based on three subwatersheds of the BVR selected for inclusion and reported in Sass & Keane (2012): 1) Irish Creek, 2) Black Vermillion Main Stem, and 3) North Fork. The goal of assessing river channel evolution within the Rosgen “C”-“Gc”-“F”-“C” successional scenario over the past 14 years within each of these three subwatersheds was achieved in two ways:

1. Geomorphic changes in channel dimension, pattern, and profile at seven of the original nine study reaches monitored between 2007 and 2009 was determined by resurveying, analyzing, and comparing:
    a. Two cross sections (one riffle/crossover and one pool)
    b. Reach longitudinal profile
    c. Study bank profiles (only study banks located at pools were included)
    d. Feature (pools and riffles) and study reach modified Wolman Pebble Counts (Wolman, 1954).
2. Geomorphic change along the entire BVR riverbank included in this study was assessed by comparing DEMs from 2010 - 2018 for portions of the BVR in Marshall County and from 2012 - 2018 in Nemaha County. This system-wide comparison helped determine if channel successional changes observed at the Sass & Keane (2012) study reaches can be found throughout the subwatershed (e.g., channel widening at the cross section would be indicated in the DoD by erosion outpacing deposition along the BVR riverbanks).

Geomorphic Changes in Dimension, Pattern and Profile at the Sass & Keane (2012) Study Reaches

Dimension

Of the 18 original cross sections, 14 were included in this study and resurveyed in 2021. In 2007, 4'-long steel (.5" rebar) right and left bank pins were installed at each of the 14 cross sections to mark the beginning and end of each cross section. Of these 28 pins, 25 were located using field notes, GPS coordinates, and a metal detector, and at least one bank pin was located at all 14 cross sections. At cross sections where only

one pin was located, the cross section was aligned perpendicular to the flow of the BVR, and a new pin location was established. When one of the original pins was missing due to streambank erosion, the new cross section was wider than originally measured by Sass & Keane (2012). Cross sections were surveyed using a Leica TC704 total station with an accuracy of 2 mm +2 ppm from left to right bank pins. For cross section stationing see Table 1, p. 13.

At cross sections where both right and left bank pins were located, the elevation difference between the left and right bank pins in 2007 documented by Sass & Keane (2012) was compared to the 2021 elevation difference between pins, and the differences ranged between .05 m and .0006 m, indicating the pins had not moved significantly since 2007. RiverMorph and AutoCAD were used to determine the cross-sectional changes in channel dimension between 2007, 2009 and 2021 at each of the 14 cross sections. Figure 30, p.88 illustrates a typical cross section.

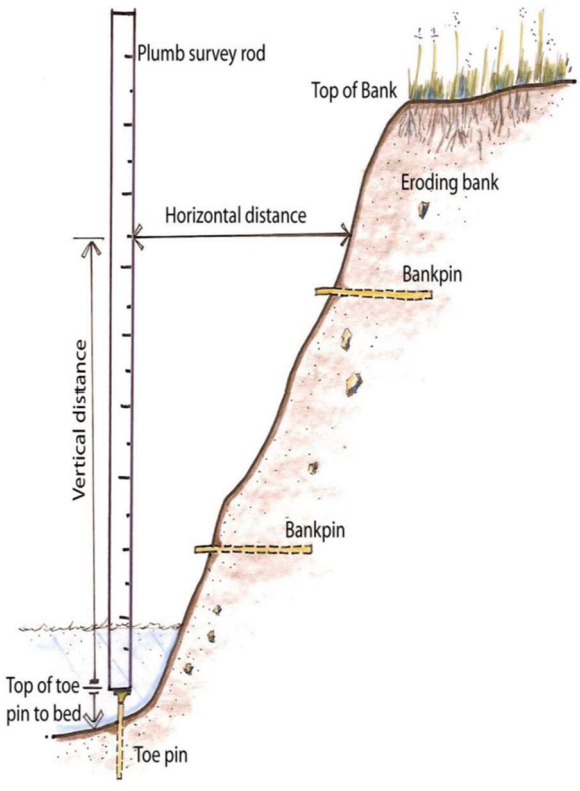


Figure 31: Illustration of Bank Profile (Sass, 2011)

Sass & Keane (2012) also collected bank profile data at two locations (study banks) within each study reach using a vertical toe pin and a number of horizontal bank pins (Figure 31), one at each pool and one at an additional location. None of the study bank toe or bank pins were located; however, the 2021 pool bank profiles were

determined using cross section data and toe pin stations from the original Sass & Keane (2012) field notes.

P*rofile and Pattern*

Sass & Keane (2012) surveyed longitudinal profiles at each of the seven study reaches equivalent to approximately 20 times the bankfull width, beginning and ending at the head of a riffle. Because the primary purposes of resurveying the longitudinal profile for this study was to estimate bankfull water surface slope and not bed feature change and to calculate reach sinuosity, an abbreviated longitudinal profile was conducted by taking a thalweg and water surface elevation every fifty feet (15.24 m). The water surface slope at bankfull was estimated using the elevation difference of the water surface elevation at the beginning and end of the longitudinal profile, both measured at the head of a riffle. Sinuosity was determined in ArcGIS using the beginning and ending points of the 2021 longitudinal profile collected with a Juniper Archer Field PC plus Hemisphere GPS with sub-meter accuracy.

Channel Material

Sass & Keane (2012) collected reach and feature (pool and riffle cross sections) modified Wolman Pebble Counts annually from 2007 to 2009. Current reach and feature pebble counts were collected in order to determine trends in dominant sediment size. The time of data collection could influence each pebble count particle size distribution. Sass & Keane (2012) conducted pebble counts in June or July when precipitation and streambank erosion are more common, which could result in more of the fine-grained bank material being present in the feature and reach pebble counts.

Pebble counts for this study were conducted in April of 2022 after a winter of little precipitation and low flow may have had time to remove fine-grained particles from the streambed eroded from banks and deposited the previous summer.

Summary of Variables and Ratios Collected at the Seven Sass & Keane (2012) Study Reaches

In summary, the variables and ratios related to dimension, pattern, and profile collected using the methods described above at the seven study reaches and their respective riffle and pool cross sections previously monitored from 2007 to 2009 in order to facilitate the evaluation of the BVR channel succession within the Rosgen “C”-“Gc”-“F”-“C” successional scenario are:

1. Bankfull width
2. Flood-prone area width
3. Cross sectional area
4. Maximum bankfull depth
5. Mean bankfull depth
6. Entrenchment ratio
7. Width/Depth ratio
8. Sinuosity
9. Slope
10. Pebble count D50 at features and reach
11. Riffle/Pool Right and Left Bank Angle

Geomorphic Change along the Entire BVR River Channel Using 2010-12 and 2018 DEMs

Patterns and estimated amounts of streambank erosion and deposition along the entire length of the BVR channel could provide insight into channel evolution by indicating if the amounts of erosion/deposition occurring at the study reach cross sections is representative of each subwatersheds’ entire channel. Estimate amounts

and patterns of erosion and deposition were evaluated by comparing publicly available LiDAR-derived DEMs with 1-meter resolution from 2010 and 2018 in Marshall County and from 2012 and 2018 in Nemaha County. The 2018 LiDAR and DEM dataset became available in January 2022 and is the first time such large scale, sequential LiDAR datasets have been made publicly available for northeast Kansas.

First, the BVR riverbanks were delineated. Water level at the time of LiDAR data collection does affect how much of the river bank is reflected in the subsequent DEMs, as water does not return topographic LiDAR pulses resulting in the bottom of the channel being an interpolation of the river's edge of water at the time of data collection (Miller, 2022). It was determined through simple observation of the channel bottom elevation at various locations that the water level was higher in the 2018 DEM; therefore, only the BVR banks above the water level of 2018 could be evaluated. The area between the top and toe of the riverbank was delineated using slope analysis of the 2018 DEM in ArcGIS.

The portion of each LiDAR-derived DEM within the BVR riverbank was extracted and used to create two digital elevation models of difference (DoD), one for Marshall County and one for Nemaha County. A DoD is created by simply subtracting the elevation values in each cell of the older DEM (2010 and 2012) from those in the corresponding cells of the newer DEMs (2018) resulting in a new raster dataset where areas of erosion have negative values and deposition positive values. The threshold for significant change or minimum level of detection (minLoD) was estimated using the root mean square error (RMSE) of the checkpoints of each DEM (Williams, 2012). The

2010, 2012 and 2018 DEMs had 54, 60 and 76 checkpoints, respectively. The minLoD was calculated as:

$$minLoD = \sqrt{(\varepsilon DEM_1)^2 + (\varepsilon DEM_2)^2}$$

Where εDEM_1 and εDEM_2 are the root mean square error (RMSE) of the checkpoints for each DEM being compared. The RMSE for the 2010 and 2018 DEMs were 0.10 m and 0.1438 m respectively resulting in a minLoD = **0.172 m** for the 2010-2018 DoD: therefore, only erosion and deposition < -0.172 m or > 0.17 m was considered significant (Williams, 2012). Similarly, the RMSE for the 2012 DEM was 0.065 m resulting in the minLoD = **0.154 m** for the 2012-2018 DoD.

As discussed in Williams (2012), a more rigorous approach to DoD production is the use of probabilistic thresholding at a user defined confidence interval, which is 95% for this study (Brasington, Rumsby, & McVey, 2000). "Probabilistic thresholding provides a technique to remove systematic bias throughout the filtering of elevation changes based on the confidence that detected change is real" (Williams, 2012 p. 8). For thresholding at the 95% confidence interval, equation 1 is revised to:

$$minLoD_2 = t\sqrt{(\varepsilon DEM_1)^2 + (\varepsilon DEM_2)^2} \quad (2)$$

Where *t* it the critical t-value for a two-tailed Student's t-distribution for a 95% confidence interval (1.96) and all other variables are as in equation 1 (Williams, 2012). Using equation 2, the $minLoD_2$ for the 2010-2018 DEM (Marshall Co.) and 2012-2018 (Nemaha Co.) DoDs were determined to be **0.343 m** and **0.306 m,** respectively. All estimated amounts of erosion and deposition were reported at the 68% and 95% confidence intervals (CI).

As a qualitative check of the DoDs, erosion and deposition reflected in the DoDs at the Sass & Keane (2012) cross section locations were compared to the combined 2007, 2009, and 2021 surveyed cross sections. The pattern of deposition on the right bank and erosion on the left bank at the IC3 cross section is reflected in the DoD (Figure 32). This was the case for other cross section/DoD comparisons as well.

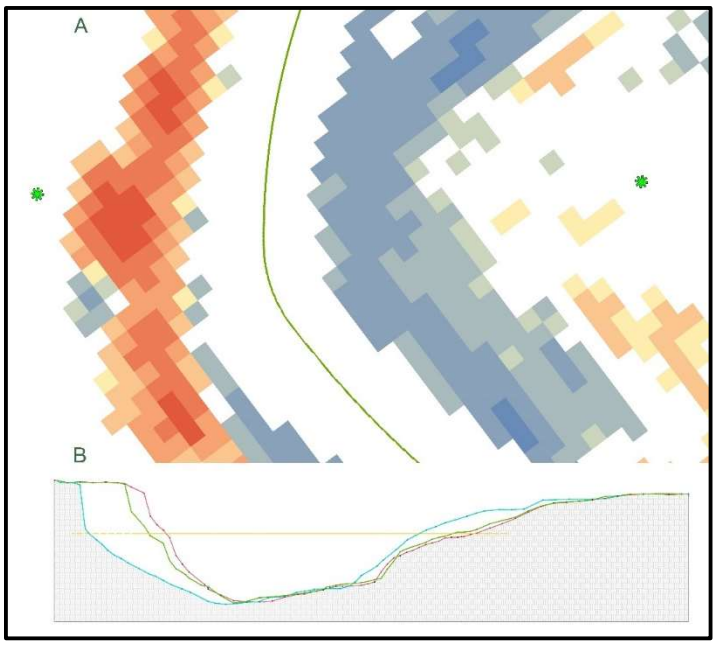


Figure 32: Irish Creek 3 Pool Cross-Section A) 2010-18 DoD, Red = Erosion and Blue = Deposition and B) Surveyed Cross Section, 2007 (red), 2009 (green) and 2021 (blue)

With LiDAR data such as that used to create the 2010-12 and 2018 DEMs, systematic errors may be introduced during data collection due to the limitations of the technology at the time of data collection or during post processing due to varying georeferencing information as well as point cloud classification and DEM generation methods. (Bretar, Pierrot-Deseilligny, & Roux, 2004; Goodwell et al., 2014; Lee, Yu, Kim, & Habib, 2007; Schaffrath et al., 2015). A number of corrections associated with systematic error were necessary, and these included error associated with 1) the geoid model used, 2) horizontal bias, and 3) coregistration of flight lines.

A Geoid is a model of global mean sea level utilized in the measurement of precise surface elevations. Geoid models are produced by the National Geodetic Survey and are updated every few years. The 2010, 2012, and 2018 LiDAR point clouds and DEMs available through KS GIS DASC were processed using GEOID03, GEOID09, and GEOID12B, respectively. Geoid correction was accomplished by first creating a geoid surface of the study area for each of the three geoid models by entering 10,000 random points within the study area into the National Geodetic Survey's interactive computation webpages (https://geodesy.noaa.gov/GEOID/GEOID12B/computation.html). The 03 (2010) and 09 (2012) geoid models were differenced from the 12B (2018), and the result added to the 2010 and 2012 DEMs. This process is explained in detail in *Chapter IV*.

There was an obvious horizontal offset between the 2010 and 2018 DEMs. Similar to the methodology of Schaffrath et al. (2015), the degree and direction of the horizontal bias was determined by comparing the x and y coordinates of 197 digitized points on well-defined structures, primarily buildings, points of cone-roofed grain silos and specific points on large impoundment levees. The 2010 DEM was adjusted 2.2 m at an azimuth of 152.59° from north. This process for horizontal bias was applied to the 2012 DEM using an initial thirty points; however, no horizontal bias was observed.

The final corrections were those associated with flight lines. LiDAR data is typically collected in strips along flight lines that overlap 10-30% (Schaffrath et al., 2015). Discrepancies between flight lines due to imprecise calibration parameters may lead to coregistration errors that are not detectable in stand-alone DEMs but become evident as strips of elevation bias when differenced with a more current and accurate

DEM (Schaffrath et al., 2015). Strips of elevation bias were present in the 2010-2018 Marshall County (Figure 33, A) and 2012-2018 Nemaha County DoDs and were corrected using methodology adapted from Schaffrath et al. (2015), where the DoD is corrected using an error surface derived from areas with little expected elevation change (Figure 33, B). This process of DoD flight line correction is discussed in more detail in *Chapter IV*.

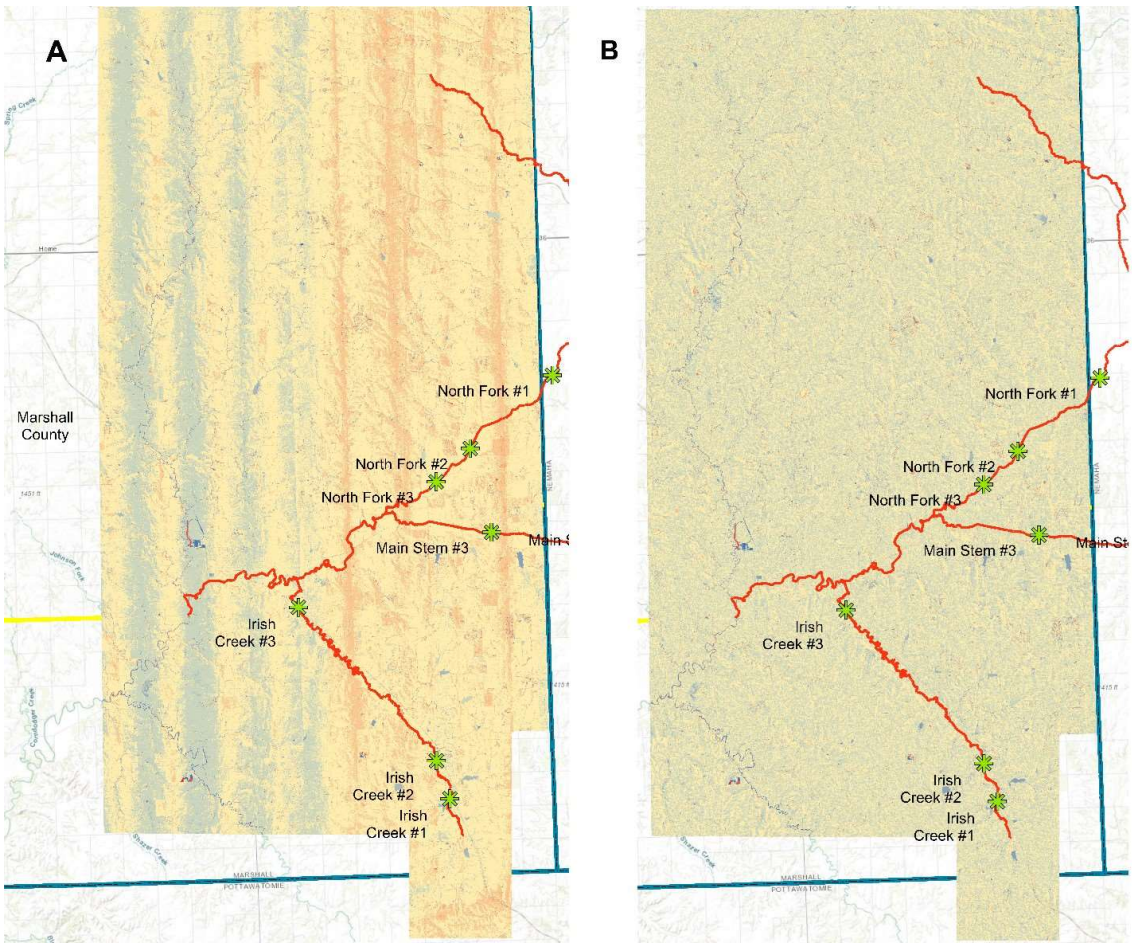


Figure 33: Flightline Correction for the 2010-2018 DoD (A) Uncorrected and (B) Corrected: See Figure 60, p. _for Legend: Darker red (erosion) and blue (deposition) strips indicate elevation bias due to poor flightline co-registration with lighter yellow and blue indicating little change

Patterns and Amounts of Erosion and Deposition along the BVR Channel

Data collected at the seven study reaches monitored between 2007 and 2009 provided understanding of channel changes at those specific locations as well as broad patterns of change between the upper, middle, and lower reaches of each subwatershed. Although for a shorter period of time, the DoDs created by comparing the 2010 (12) and 2018 DEMs provide understanding of system-wide geomorphic change by evaluating patterns of erosion and deposition along the entire BVR riverbank. As noted, the DoDs do not identify changes in streambed morphology below the water surface in 2018. Understanding of system-wide changes aid in determining if the patterns of streambank erosion and deposition observed at the study reach cross sections are reflective of the entire channel.

To evaluate patterns of erosion and deposition along the banks of the BVR channel, each subwatershed channel centerline was divided into 1-km segments. A 40-m buffer was then created for each segment and used to extract the portion of the DoD associated with each segment, which then allowed the calculation of streambank erosion and deposition along each segment. For each of the 1-km segments, a point was created at the segment midpoint and assigned the total amount of erosion and deposition for that segment as attributes. These attributes allowed each point to be sized proportionally based on either the amount of erosion or deposition in order to visualize the overall patterns of erosion and deposition along the BVR riverbanks and to identify areas or segments with high levels of erosion or deposition. In order to determine if the amounts of erosion and/or deposition of each segment have any correlation to the drainage area, the drainage area from the midpoint of each segment

was also calculated using ArcGIS. As noted, the DoD for Marshall County represents eight years of change between 2010 and 2018, while the DoD for Nemaha County represents only six years of change between 2012 and 2018.

Results and Discussion

For each study reach, channel succession within the Rosgen "C"-"G_c"-"F"-"C" successional scenario was assessed using the Rosgen (1996) classification system metrics as well as other indicators of incision, aggradation, and widening. System- wide patterns of geomorphic change were assessed by evaluating patterns of erosion and deposition along the entire BVR riverbank using the 2010-12 and 2018 DEMs.

Irish Creek

All three Irish Creek study reaches monitored by Sass & Keane (2012) were included in this study (Figure 26, p.74). Tables 12, 13, and 14 indicate the Rosgen Classification metrics, cross section data and pool study bank profile data used to evaluate the IC channel evolution at each study reach. It is important to note that bankfull elevation in 2021 was set to the same bankfull elevation determined by Sass & Keane (2012) for each study reach cross section.

Rosgen Classification Metrics for Irish Creek

Reach	Year	Ent Ratio	W/D ratio	Reach D_{50} (mm)	Slope	K	Class
IC1	07	1.47	9.36	6.98	0.0028	1.3	G5c
	09	1.61	7.54	0.23	0.0028		
	21	1.52	6.18	0.83	0.0021	1.1	G5c
IC2	07	1.22	11.48	3.00	0.0017	1.3	G4c
	09	1.22	10.28	0.93	0.0019		
	21	1.16	11.10	2.65	0.0017	1.3	G4c
IC3	07	1.54	7.73	0.35	0.00057	1.3	B5c*
	09	1.56	8.94	0.50	0.00072		
	21	2.48	10.10	0.32	0.0011	1.3	**

*Table 12: Irish Creek Rosgen Classification Metrics: Ent (Entrenchment), W/D (width/depth), D_{50} (Dominant Bed Material), k (Sinuosity): * Reach alternated between B5c and G5c, ** Cross section was no longer at riffle*

*Table 13: Irish Creek Cross Section Data: Wbkf (Bankfull Width), Wfpa (Width at Flood Prone Elevation), Dmean (Mean Bankfull Depth), Dmax (Maximum Depth at Bankfull), X-Sec Area (Bankfull Cross-Sectional Area), Bk Ang L and R (Bank Angle Left and Right Banks), D_{50} (Dominant Feature Particle Size Feature): *Cross section at IC3 no longer at riffle*

IC		Riffle Cross Sections								Pool Cross Sections							
Reach		Wbkf (m)	Wfpa (m)	Dmean (m)	Dmax (m)	X-Sec Area (m^2)	Bk Ang L	Bk Ang R	D_{50} (mm)	Wbkf (m)	Wfpa (m)	Dmean (m)	Dmax (m)	X-Sec Area (m^2)	Bk Ang L	Bk Ang R	D_{50} (mm)
IC1	07	9.28	13.68	1.00	1.40	9.24	36	36	0.24	9.15	11.61	1.66	2.42	15.22	44	63	1.60
	09	10.10	16.31	1.34	1.95	13.54	31	37	0.30	9.27	11.72	1.86	2.54	17.29	45	78	0.53
	21	11.12	16.87	1.80	2.16	19.99	47	43	1.00	11.22	13.24	2.05	2.47	23.03	54	84	1.85
IC2	07	12.06	14.57	1.05	1.42	12.61	43	76	18.86	17.54	22.94	1.82	3.14	31.91	62	36	0.36
	09	11.92	14.53	1.16	1.47	13.86	42	78	14.70	17.21	22.12	1.61	2.83	27.76	56	36	2.90
	21	13.21	15.31	1.19	1.58	15.70	41	81	16.54	16.75	22.19	1.68	2.72	28.16	48	36	2.65
IC3*	07	12.67	19.57	1.64	2.25	20.82	43	37	0.35	13.93	30.18	1.93	3.1	26.88	55	22	0.31
	09	14.16	22.38	1.58	2.36	22.39	20	37	0.5	14.49	30.18	2.04	3.5	29.56	51	19	0.55
	21	15.05	37.32	1.49	2.65	22.36	35	18	0.19	15.72	30.19	2.18	3.36	34.34	31	22	0.32

*Table 14: Irish Creek Sass & Keane (2012) Pool Data: Pool Cross Sectional Area and Bank Retreat Rates (*2010 data was not available): RB = Right Bank*

IC Pool Study Bank Profile X-Sec. Area and Bank Retreat

Reach	Cross Sectional Area (m^2)				Bank Height (m)	Bank Retreat Rate (m/yr)	
	2007	2009	2010	2021		07 - 10 (*09)	10 (*09) - 21
IC1 (RB)	7.81	9.66	10.59	17.60	5.38	-0.17	-0.12
IC2 (RB)	26.22	26.12	*	27.18	6.12	0.0082 *	-0.01
IC3 (LB)	9.11	11.87	13.55	23.27	4.83	-0.31	-0.18

Irish Creek 1

As IC1 was classified as "G4c" by Sass & Keane (2012) for the 2007-09 study period, the expected transition within the Rosgen "C"-"Gc"-"F"-"C" successional scenario would be to an early stage "F" type stream. IC1 experienced minor change in entrenchment ratio, sinuosity, or slope over the entire 14-year study period, which is to be expected, as the reference values for these variables are the same for both "Gc" and "F" type streams. The primary metric differentiating a "Gc" type stream from an "F" type

stream is an increase in width/depth ratio above 12; however, the IC 1 width/depth ratio declined from 9.63 in 2007 to 7.4 in 2009 and continued to decline to 6.18 by 2021 (Table 12). The decline in the width/depth ratio between 2007 and 2021 does not reflect the Gc to F succession. However, increases in riffle and pool bankfull width by 1.84 m and 1.63 m, respectively, and cross-sectional area by 10.75 m^2 (116%) and 7.81 m^2 (51.31%), respectively, do indicate the IC1 channel is widening as expected in the "Gc" to "F" succession (Table 13 and Figure 34). IC1 still classified as a "Gc" type stream in 2021

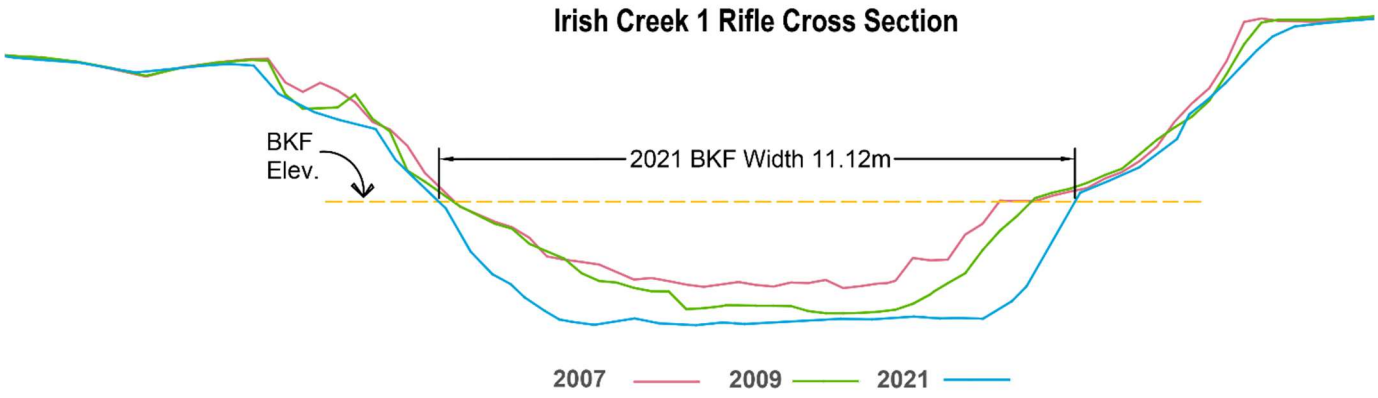


Figure 34: Irish Creek 1 Riffle Cross Section

Widening at the IC1 pool is further evidenced by study bank (right) retreat during the 2007-2010 period (0.17m/yr.) as well as the 2010-2021 period (0.12 m/yr.) (Table 14). The higher rate of bank retreat in the 07-09 period may be due to the large number of bankfull events that occurred during that time. The reach D_{50} at IC1 decreasing from 6.98 mm in 2007 to 0.83 mm in 2021 suggests increased bed material originating from fine-grained bank material upstream of the reach.

The declining width/depth ratio is due to continued incision outpacing widening at the IC1 riffle cross section evidenced by an increase in bankfull maximum depth and mean depth of 0.76 m and 0.8 m respectively (Figure 34, Table 13). However, a decrease in the rate of incision at the riffle from 0.275 m/yr (2007 - 2009) to 0.02 m/yr (2009 - 2021) coupled with a 0.17 m decrease in the maximum depth at the IC1 pool, indicating filling, suggest incision in the reach is waning and aggradation beginning. It is also important to note that the declining width/depth ratio is only at one riffle cross section within the reach, which may or may not be representative of the entire reach. As the channel at IC1 continues to widen and begins to aggrade, the channel should become wider and shallower leading to an increased width/depth ratio more reflective of an “F” type channel.

Irish Creek 2

Irish Creek 2 (IC2) located approximately 2.5 km downstream from IC1, was also classified as a “$G4_c$” type stream by Sass & Keane (2012); therefore, a transition to an “F” type channel would be likely. As expected within the “Gc” to “F” succession, there was little change in entrenchment ratio, sinuosity, and slope (Table 12). The entrenchment ratio remained steady between 2007 and 2009 at 1.22 before decreasing to 1.16 in 2021 indicating the channel had become slightly more entrenched. In 2007, the IC2 width/depth ratio was 11.48 characteristic of a late stage “Gc” stream type. Between 2007 and 2009, the width/depth ratio decreased to 10.28 due to degradation (incision) and narrowing of the IC2 riffle evidenced by an increase of cross-sectional area by 1.25 m^2 and a decrease in bankfull width by 0.14 m (Table 13). Between 2009 and 2021, the riffle cross section bed elevation did not significantly change, as the mean

depth only increased by 0.03 m, while the bankfull width increased by 1.29 m resulting in an increase in width/depth ratio to 11.10 indicating progression in the “Gc” to “F succession since 2009.

The IC2 pool cross section experienced a pattern of aggradation and narrowing over the 14-year study period, as maximum bankfull depth and cross-sectional area decreased by 0.42 m and 3.75 m^2, respectively, indicating channel aggradation, and the bankfull width narrowed by 0.79 m (Table 13). As shown in Figure 35, the right bank has remained relatively stable as evidenced by minor bank deposition in the 07-09 period (0.0082 m/yr.) and average retreat of 1 cm/yr over the 09-21 period (Table 14). In addition, a substantial portion of the decrease in bankfull width and area is due to the formation of a bench on the left bank that is stabilized with young woody and herbaceous vegetation. Stabilization of the bench may have contributed to the well-defined two-stage channel we see in the 2021 pool cross section (Figure 35). The reach D_{50} of 18.86 mm in 2007 and 14.70 mm in 2009 (Table 13) indicates the bed material at the riffle was not originating from the fine-grained bank material, providing more evidence of a lack of bank erosion within the reach.

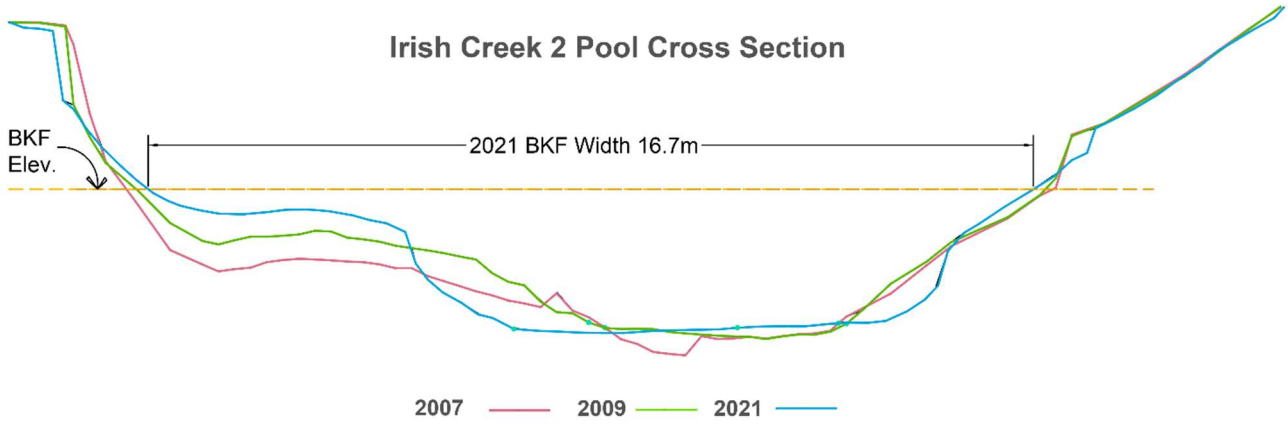


Figure 35: Irish Creek 2 Pool Cross Section

Irish Creek 3

Sass & Keane (2012) classified the IC3 reach as $B5_c$ based the entrenchment ratio of 1.54 in 2007 and 1.56 in 2009 falling within the "B" range of the Rosgen classification even though the width/depth ratio of 7.3 in 2007 and 8.94 in 2009 fell within "Gc" range (Table 12). Sass & Keane (2012) noted that the IC3 reach alternated between $B5_c$ and $G5_c$. In 2021, the Rosgen classification metrics indicate classification at the riffle to be a "C" type stream, when entrenchment ratio is given more weight as was done previously. From 2009 to 2021, the entrenchment ratio increased to 2.48 and the width/depth ratio increased to 10.10 (Table 12), which is common in confined "C" type streams that have stabilized inside of old "F" channels (Keane & Sass, 2017). However, in 2007-09 the "riffle" cross section was a crossover located just upstream of a meander bend. Since 2009, the pool associated with the bend has expanded upstream, and the cross section location is now within a pool, which is not used in the Level II Rosgen classification. Therefore, it is not appropriate to attempt Rosgen classification based on the 2021 cross section. Large woody debris and vegetation

stabilizing the right bank may have directed and concentrated flow towards the left bank resulting in streambed scour and extension of the downstream pool. It is clear the IC3 study reach does not have adequate, continuous flood plain throughout the reach providing more evidence the “C” classification is not appropriate for the reach.

The IC3 riffle cross section experienced incision and widening over the 14-year study period, with an increase in maximum bankfull depth of 0.40 m and an increase in the bankfull width and cross-sectional area of 2.38 m and 1.54 m^2, respectively (Table 13). As IC3 is located in an unchannelized, sinuous section of Irish Creek (Figure 26, p.74), the IC3 pool exhibited typical outer cut bank and depositional point bar progression over the 14-year period (Figure 32, p.97). The pool left (cut) bank experienced bank retreat of 0.31 m/yr. in the 2007-2010 period; however, that rate fell by approximately 42% to 0.18 m/yr. in the 2010-2021 period (Table 14). As with previous reaches, the lower rate of cutbank retreat in the 2010-21 period compared to the 2007-10 period may be due to the large number of bankfull events that occurred during the 2007-10 period. The pool incised and widened over the study period, with an increase in maximum bankfull depth by 0.21 m and an increase in bankfull width and cross sectional area by 1.79 m and 7.46 m^2, respectively.

Widening within the IC3 reach is further evidenced by the D_{50} remaining relatively constant for both riffle and pool cross sections at approximately 0.33 mm suggesting erosion of fine-grained bank material upstream of the cross sections throughout the entire study period. Decreases between 2009 and 2021 of already relatively low right (43°) and left (37°) bank angles at the riffle by 8° and 19° (Table 13), respectively, suggest the reach may be further along in the successional scenario or channel

evolutionary process, yet both riffle and pool incised over the study period. It is possible the reach is experiencing a retrogression to an earlier stage, or "short circuit" reflected in the Cluer & Thorne (2014) SEM.

Irish Creek System Wide

The Irish Creek DoD, calculated by subtracting the 2010 DEM from the 2018 DEM, only reflect 8 years of the 14-year period between the first and last cross section observations. However, the DoD does provide insight into patterns and estimated amounts of erosion and deposition along the Irish Creek banks. As noted earlier, erosion and deposition were calculated for each 1-km segment of the creek. For this discussion, erosion and deposition at the 68% CI was used. Overall, the Irish Creek channel had approximately 95% more erosion (3,998 m^3/km) per 1-km segment as deposition (2,048 m^3/km) over the 8-year period (Table 15). In addition, Irish Creek had the highest erosion per 1-km segment compared to the Main Stem (3,591 m^3/km) and North Fork (3,679 m^3/km) 1-km segments in Marshall County, even though it has the smallest drainage area of the three subwatersheds. Between 2007 and 2021, the Irish Creek subwatershed experienced the greatest increase in the area controlled by small impoundments resulting in IC1, IC2, and IC3 having 59%, 64% and 56% controlled area, respectively, (Table 9, p.81), with all three being higher than any other study reach. As discussed earlier, this increase in controlled area likely increased the duration of bankfull or near bankfull flows resulting in more geomorphic work being done annually than before control.

Keane & Sass (2017) utilized various channel evolution models and riverbank retreat rates reported in Sass & Keane (2012) to estimate the annual and total amount

of sediment expected to be produced as each subwatershed's channel undergoes adequate widening to allow a stable channel form at a new, lower elevation. Keane & Sass (2017) estimated the annual sediment yield of Irish Creek to be between 2,530 m^3/km and 1,058 m^3/km. It is important to note that deposition was not considered in the calculation of erosion rates used by Keane & Sass (2017); therefore, their results were compared to the estimated erosion in this research. For the 8-year period of the 2010-2018 DoD, the average annual erosion rate along the IC banks was 499.75 m^3/km (68%CI). This rather large discrepancy could be due to a number of factors, such as unidentified errors in the 2010 and 2018 DEMs and subsequent DoDs, erosion below the MinLoD thresholds not being included, deposition along the riverbanks not being considered by Sass & Keane (2012), or accelerated bank retreat rates between 2007 and 2010 due to the large number (12, average of 4 per year) of bankfull flow events compared to the number between 2010 and 2018 (14, average of 1.75 per year).

Table 15: Streambank Erosion and Deposition by Subwatershed

Bank Erosion and Deposition by Subwatershed												
			Confidence Level 68% (m^3)					Confidence Level 95% (m^3)				
	Reach	Length (km)	Ero	Dep	Net Ero/ Dep*	Ero/km Bank	Dep/km Bank	Ero	Dep	Net Ero/ Dep*	Ero/km Bank	Dep/km Bank
Marshall County (2010-2018)	Irish Creek	23	91,965	47,113	-44,852	3,998	2,048	81,825	35,906	-45,919	3,558	1,561
	Main Stem	9	32,320	19,075	-13,245	3,591	2,119	27,497	17,696	-9,801	3,055	1,966
	North Fork	15	55,180	70,119	14,940	3,679	4,675	46,660	58,442	11,783	3,111	3,896
Total		47	179,464	136,307	**-43,157**	3,818	2,900	155,982	112,044	**-43,937**	3,319	2,384
Nemaha County (2012-2018)	Main Stem	20	75,848	36,967	-38,881	3,792	1,848	68,536	28,158	-40,378	3,427	1,408
	North Fork	15	61,277	40,340	-20,936	4,085	2,689	54,723	33,139	-21,584	3,648	2,209
	Weyer	16	87,018	49,601	-37,416	5,439	3,100	77,377	41,697	-35,680	4,836	2,606
Total		51	224,142	126,908	**-97,234**	4,395	2,488	200,635	102,994	**-97,642**	3,934	2,019

*Negative values indicate erosion

Five of six cross sections monitored in the Irish Creek subwatershed from 2007 to 2021 showed increases in both bankfull width and bankfull cross sectional area,

indicating widening of the channel. In addition, all 1-km segments of the IC DoD analysis showed higher amounts of erosion than deposition indicating overall widening along the entire channel, thus providing evidence that channel changes at the cross sections are reflective of the entire Irish Creek channel (Figure 36). The estimated erosion within the 1-km segments where the IC1, IC2 and IC3 study reaches were located was 6,243 m^3, 3,696 m^3, and 2,047 m^3, respectively. The lower amount of erosion along the IC3 segment compared to IC1 and IC2 segments supports the suggestion by Keane & Sass (2017) of lower reaches being further along in the channel evolutionary process and experiencing less adjustment.

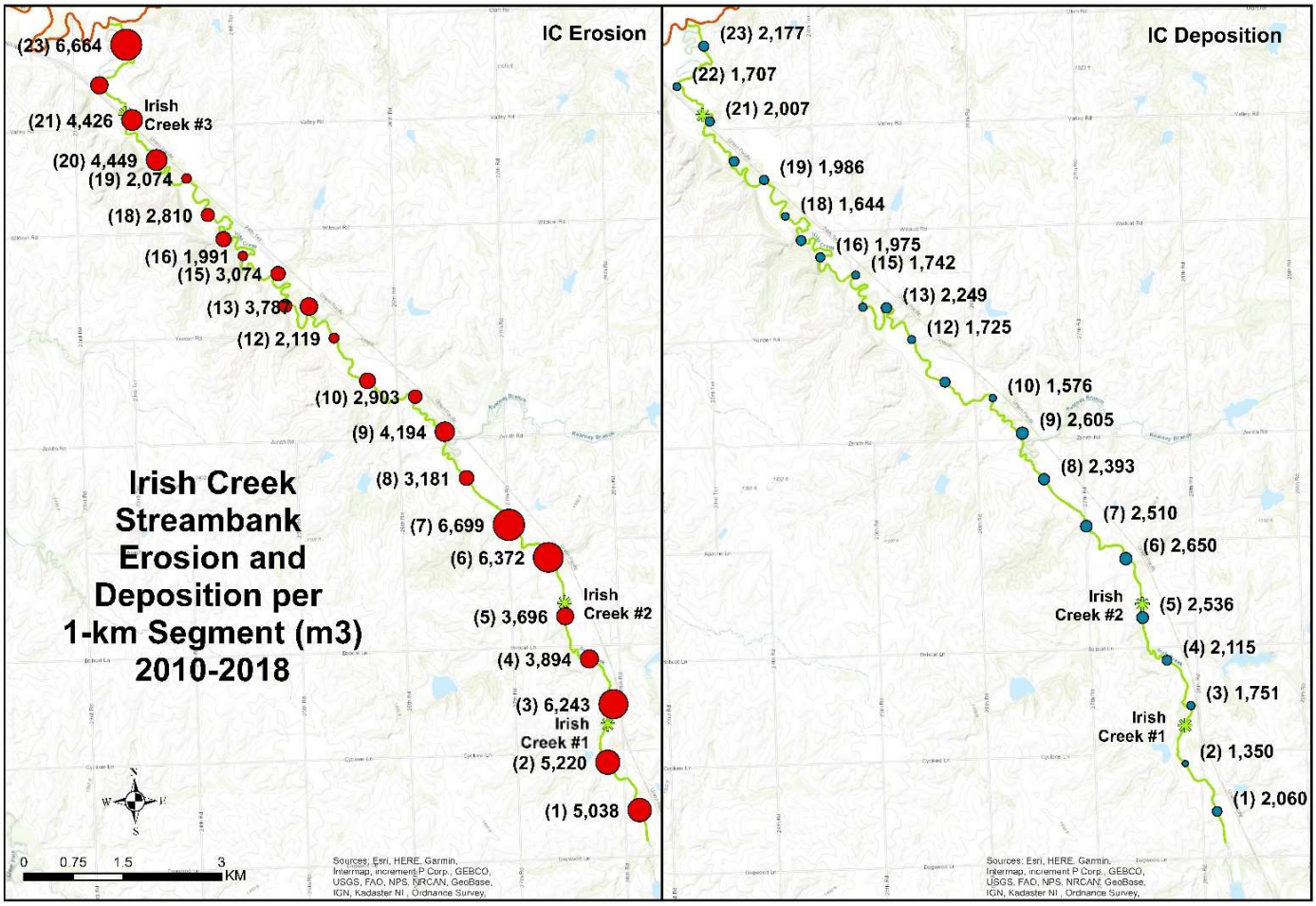


Figure 36: Irish Creek Erosion and Deposition 2010-2018: Size of Points are Proportional to the Amount of Erosion/Deposition in each 1-km Segment: Green Asterisks Indicate Sass & Keane (2012) Study Reaches

The pattern of decreasing channel adjustment moving downstream is also reflected in the cross sectional data, with IC1 in the upper watershed having a 116% increase in bankfull cross-sectional area between 2007 and 2021 and IC3 in the lower watershed having only a 7.4% increase in bankfull cross-sectional area for the same period. In addition, moving downstream, a modest negative correlation exists between drainage area and streambank erosion in the 2010-2018 per km DoD data for the first 19 segments (Figures 36 and 37). This pattern of decreasing adjustment downstream may be due to Irish Creek having one channelized reach in its lower watershed around 1977 and relatively little channelization otherwise. Incision caused by the 1977 channelized reach would be expected to migrate upstream resulting in more adjustment occurring in the upper watershed. Erosion increases within the four most downstream 1-km segments of IC with the most downstream segment (23) having the second highest amount of erosion. However, the high amount of erosion in segment 23 is primarily due to two areas of intense erosion along a total of approximately 100 m of streambank clearly visible in the 2018 aerial photo (Figure 38), which is bit surprising given the ample riparian woody vegetation along the segment.

The jump in erosion between segments 5 and 6 may be due to two tributaries flowing into the creek between the two points increasing the drainage area from approximately 34 km^2 to 60 km^2, resulting in a similar increase in discharge. Inspection of segments with the highest amounts of erosion revealed the bulk of erosion often occurred along a relatively small portion of each segment. For example, within the IC segment #7 (Figure 36), approximately 68% of the erosion within the 1-km segment occurred along a 200-m length of streambank containing two sequential cut banks with

little or no woody riparian vegetation (Figure 39). It is important to note that these two cutbanks have low radiuses of curvature of 15.85 m and 7.32 m and ratio to bankfull width of 0.69 and 0.32, respectively (bankfull width = 22.86m, estimated using Eastern KS regional curves). The radius of curvature is most often between 2 and 3 times bankfull width. Also note in Figure 39, comparison of the aerial photographs from 2010 and 2018 illustrate the erosion indicated by the 2010-18 DoD.

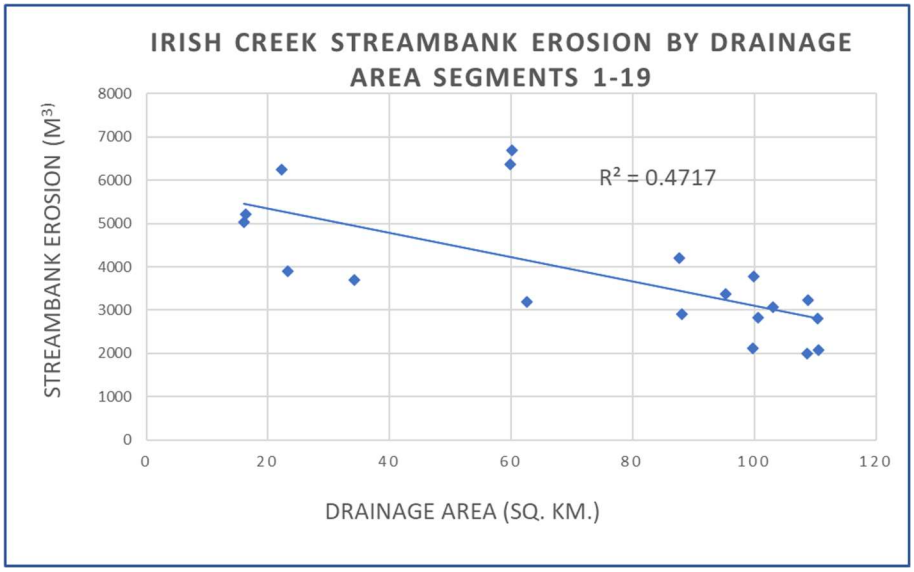


Figure 37: Irish Creek Streambank Erosion by Drainage Area: Segments 1-19

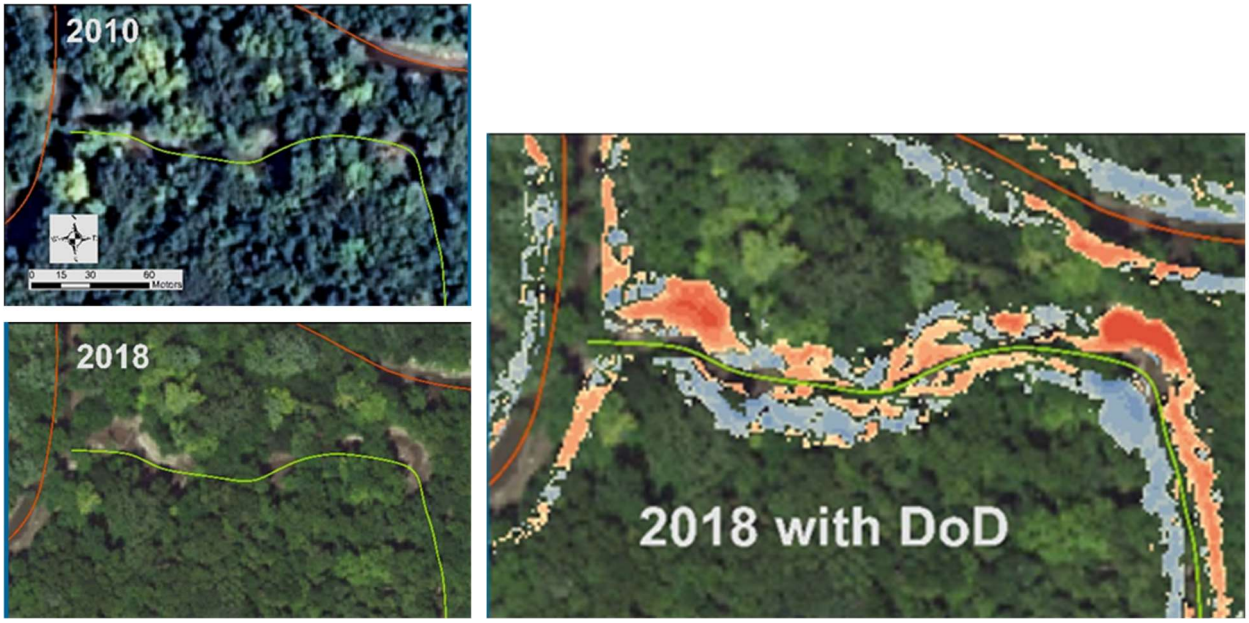


Figure 38: IC Areas of Severe Erosion: near the confluence of IC and the BVR Main Stem

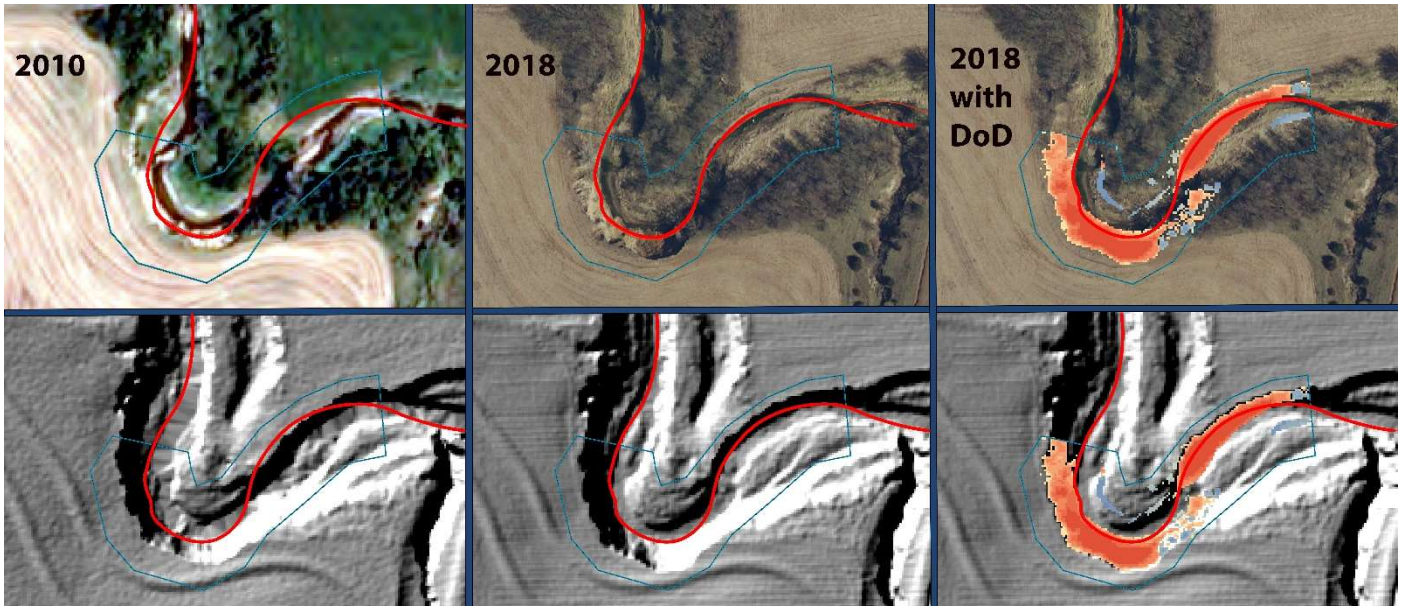


Figure 39: Eroding Bank within Irish Creek Segment 7: 2010 and 2018 aerial photos and DEM hillshade of a 200' length of streambank within segment 18 containing two cut banks producing approx. 70% of the segment's erosion

BVR Main Stem

As shown in Figure 26, p. 74, it is evident that the bulk of the extensive channelization along the BVR Main Stem has occurred since 1970, with a few small reaches channelized in the 1980s, while small reaches near the towns of Vermillion and Centralia and more extensive reaches in the headwaters were channelized prior to 1963. Channel length analysis in this study indicates that between 1967 and 1985, the Main Stem lost 10 km (25.5%) of its length (Table 8, p.77), with most of that loss occurring in the western portion of the subwatershed (Figure 40). Each of these instances of channelization would have set in motion upstream incision and downstream aggradation discussed earlier. It is possible that the extensive downstream channelization was in response to by the earlier, upstream channelization increasing both the amount of sediment and discharge being delivered downstream resulting in flooding amplified by aggradation (Schumm et al., 1984; Brookes, 1985).



Figure 40: Western Main Stem Channelization 1967-2021: Source NAIP

Two of the BVR Main Stem study reaches (MS2 and MS3) monitored by Sass & Keane (2012) were included in this study (Figure 40). Tables 16, 17, and 18 present the Rosgen Classification Metrics and additional measurements used to evaluate the MS channel evolution at each study reach.

Table 16: BVR Main Stem Rosgen Classification Metrics: Ent (Entrenchment), W/D (width/depth), D_{50} (Dominant Bed Material), k (Sinuosity), Class (Rosgen Stream Type)

Rosgen Classification for Main Stem							
Reach	Year	Ent. Ratio	W/D ratio	Reach D_{50} (mm)	Slope	K	Class
MS2	07	1.38	9.51	0.33	0.0013	1.2	G4c
	09	1.53	8.83	0.48	0.0012		
	21	1.5	9.90	0.63	0.0011	1.2	G4c
MS3	07	1.25	13.45	0.29	0.00072	1.2	F5
	09	1.35	11.52	1.50	0.001		
	21	1.24	12.61	1.53	0.001	1.2	F5

Table 17: BVR Main Stem Cross Section Data: Wbkf (Bankfull Width), Wfpa (Width at Flood Prone Elevation), Dmean (Mean Bankfull Depth), Dmax (Maximum Depth at Bankfull), X-Sec Area (Cross-Sectional Area), Bk Ang L and R (Bank Angle Left and Right Banks), D_{50} (Dominant Feature Particle Size)

MS		Riffle Cross Section								Pool Cross Sections							
Reach		Wbkf (m)	Wfpa (m)	Dmean (m)	Dmax (m)	X-Sec Area (m^2)	Bk Ang L °	Bk Ang R°	D_{50} (mm)	Wbkf (m)	Wfpa (m)	Dmean (m)	Dmax (m)	X-Sec Area (m^2)	Bk Ang L °	Bk Ang R°	D_{50} (mm)
MS2	07	11.13	15.37	1.17	1.51	13.01	43	28	10.25	10.08	18.40	1.57	2.09	15.79	35	49	1.12
	09	10.68	16.31	1.21	1.55	12.94	41	37	22.16	10.22	18.73	1.50	2.13	15.31	26	52	0.50
	21	12.18	18.24	1.23	1.49	14.99	28	43	20.22	13.63	22.08	1.30	2.09	17.77	32	20	0.84
MS3	07	14.12	17.66	1.05	1.48	14.81	54	30	9.13	11.82	19.98	1.50	2.16	17.75	27	35	0.38
	09	13.25	17.85	1.15	1.52	15.27	74	21	1.63	11.97	16.18	1.23	1.62	14.67	21	35	1.43
	21	14.37	17.85	1.14	1.58	16.36	41	30	14.01	13.44	18.11	1.32	1.71	17.83	19	32	0.92

*Table 18: BVR Main Stem Sass & Keane (2012) Pool Data: Study Bank Profile Cross Sectional Area and Bank Retreat Rates (*2010 data was not available)*

Pool Study Bank Profile X-Sec. Area and Bank Retreat							
Reach	Cross Sectional Area (m^2)				Bank Height (m)	Bank Retreat Rate (m/yr)	
	2007	2009	2010	2021		07 - 10 (*09)	10 (*09) - 21
MS2 (RB)	10.16	13.80	*	25.17	4.41	-0.4127 *	-0.21
MS3 (RB)	14.48	13.29	*	22.40	4.50	0.1322 *	-0.17

BVR Main Stem 2

Main Stem 2 (MS2) is a non-channelized reach classified by Sass & Keane (2012) as a $G5_c$ stream type in the Rosgen (1996) classification system. Therefore, the next expected transition in the Rosgen "C"-"Gc"-"F"-"Gc" successional scenario would be to an "F" stream type. Looking first at the Rosgen metrics in Table 16, we see that the width/depth ratio decreased from 9.51 to 8.83 between 2007 and 2009; however, between 2009 and 2021 the W/D ratio increased to 9.90 resulting in a net increase over

the entire 14-year study period, which is expected in a “G” to “F” succession. The entrenchment ratio increased from 1.38 to 1.5 indicating a reduction in entrenchment at the riffle cross section. Although 1.5 is slightly above the <1.4 reference for “G” type streams, the reach still would be classified as a “G” stream type given the width/depth ratio of 9.90.

The pool and riffle cross sections of the MS2 reach are located on the upstream and downstream ends, respectively, of a meander bend and both exhibit typical cut bank and depositional point bar geometry (Figure 41). Over the entire study period (2007-2021), both MS2 riffle and pool experienced widening due to erosion of the cutbank outpacing deposition on the inner bank, indicated by increases in bankfull width of 1.05 m and 3.55 m, respectively, and bankfull cross-sectional area of 1.98 m^2 and 1.98 m^2 (yes this is correct, just coincidence), respectively (Table 17). The rate of bank retreat on the right bank between 2007 and 2009 (0.41 m/yr.) dropped by approximately 50% during the 2009-2021 period to 0.21 m/yr (Table 18). While there was little change in bed elevation at the riffle over the 14-year study period (Figure 41), the pool cross section showed minor aggradation near the middle of the channel resulting in a decrease in bankfull mean depth by 0.20 m, which may be the beginning of mid-bar formation as the channel widens (Table 17).

At the riffle and pool, the bank angle on the eroding cut bank decreased by 13° and 32° respectively (Table 17 and Figure 41), with the vertical face bank angle remaining constant at approximately 80°. This reduction of bank angles is not expected in the “Gc” to “F” succession. However, the 2021 bank angles may be due to the presence of failed bank material that has not yet been removed by higher flows, as both

cut banks have signs of rotational slump, primarily large blocks of bank material along the bank slope topped with the same vegetation (Brome grass) as that at top of bank.

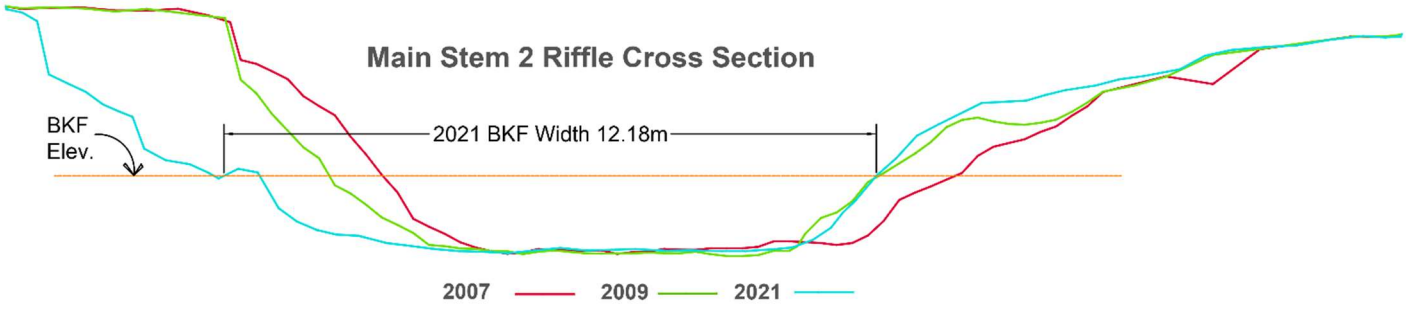


Figure 41: BVR Main Stem 2 Riffle, 2007, 2009, and 2021

BVR Main Stem 3

Main Stem 3, located in a channelized reach just south of Vermillion, KS was classified as an "F5" stream type in the Rosgen classification in the 2007-09 period. The next expected transition in the Rosgen "C"-"Gc"-"F"-"C" successional scenario would be to the stable "C" stream type at the new, lower elevation. There was no change in the water surface slope or sinuosity over the 14-year study period. The entrenchment ratio, the most important indicator of the "F" to "C" succession, increased from 1.25 to 1.35 from 2007 to 2009 before decreasing over the 2009-21 period to 1.24 (Table 16), which does not indicate a movement towards a "C" type stream. The width/depth ratio, at 13.45 in 2007, decreased to 11.52 in 2009 below the >12 reference width/depth for a "F" stream type indicating a regression to a late stage "G" stream type before increasing over the 2009-2021 period to 12.61, again in the "F" range (Table 16). This pattern of regressing then progressing in the width/depth ratio may indicate stage regression or "short circuit" followed by a progression of stage unique to the Cluer & Thorne (2014) SEM. It is important to note that width/depth ratio and entrenchment ratio

come from only one riffle cross section and in entrenched systems bed features are difficult to define and are prone to downstream migration.

In the 2007-09 period, the MS3 riffle experienced little bed elevation change and narrowed indicated by a 0.87 m decrease in bankfull width (Table 17 and Figure 42). Over the 2009-21 period, the riffle cross section continued to experience little bed elevation change yet widened resulting in a net increase in bankfull width and cross-sectional area of 0.25 m and 1.55 m^2, respectively, over the entire 14-year study period (Table 17). The MS3 riffle exhibited a pattern of bank retreat on one bank and deposition on the opposite bank. If this pattern continues in this straight, channelized section of the river, it should result in an increase in sinuosity and decrease in slope as a meander is formed and elongated. In contrast, the MS3 pool cross section experienced net aggradation and widening over the 14-year study period, with a decrease in bankfull maximum and mean depth of 0.45 m and 0.18 m, respectively, and an increase in bankfull width and cross sectional area of 1.62 m and 3.16 m^2, respectively (Table 17). All of the aggradation occurred between 2007 and 2009, as there was little change in the pool bed elevation between 2009 and 2021. In contrast, all of the widening occurred in the 2009-21 period, as the study bank experienced bank retreat of -0.17 m/yr. between 2009 and 2021 (Table 18)

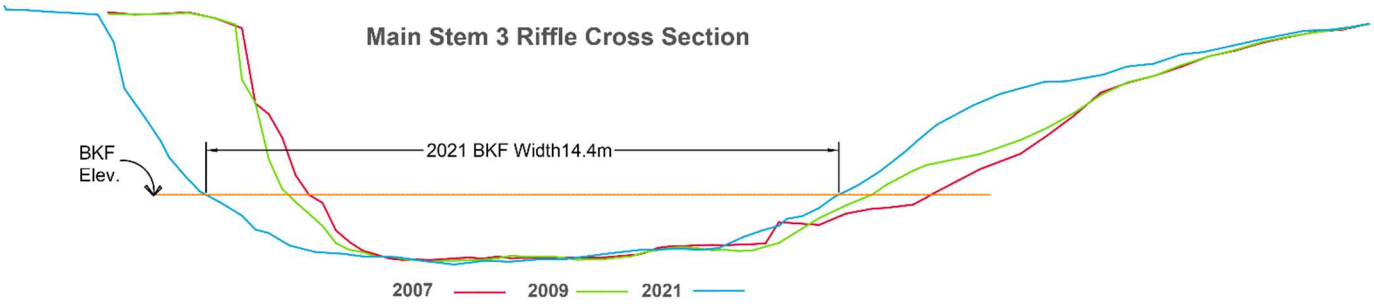


Figure 42: BVR Main Stem 3 Riffle Cross Section: 2007, 2009, and 2021

BVR Main Stem System Wide

The portion of the BVR MS included in this study begins approximately 29 km in length upstream from the confluence of the BVR Main Stem and North Fork, with approximately 9 km lying in Marshall County and 20 km in Nemaha County. As noted, a DoD was created for Marshall County for the 8-year period between 2010 and 2018 and for Nemaha County for the 6-year period between 2012 and 2018. The DoD was then separated into 1-km segments for analysis. All four cross sections monitored in the BVR MS experienced widening over the 2007-2021 study period evidenced by increases in both bankfull width and bankfull cross-sectional area. This pattern of widening was found throughout the BVR MS, with 26 of 29 1-km segments having more erosion than deposition over the 14-year study period (Figure 43).

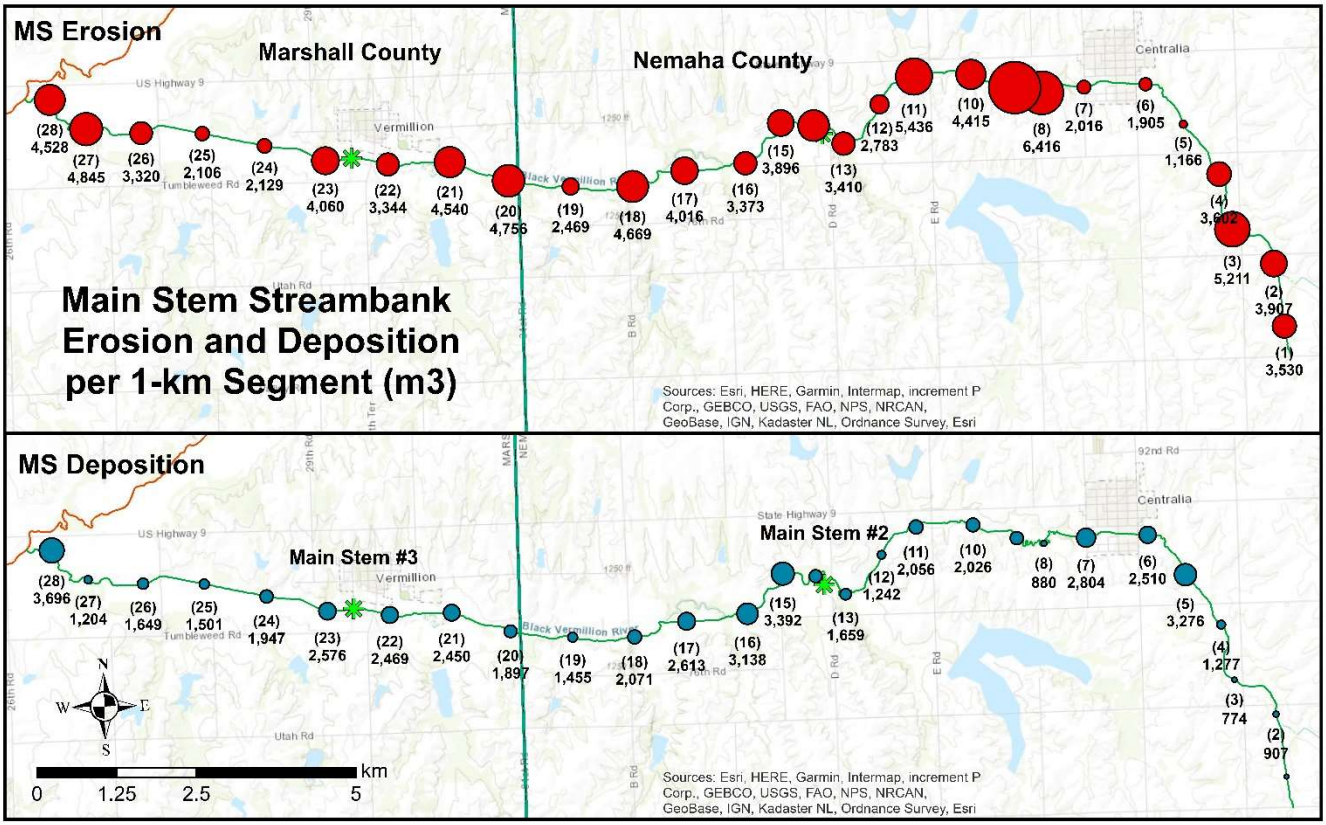


Figure 43: BVR Main Stem Erosion and Deposition 2010 (12) - 2018: Point size is proportional to the amount of erosion/deposition in each 1-km segment: reaches (#) is segment number

In Marshall County, average MS bank erosion per 1-km segment (3,591 m^3/km) between 2010 and 2018 was approximately 70% higher than deposition (2,119 m^3/km) (Table 15, p.110). Even though the MS Nemaha Co. DoD represented two years less of change (2012-2018), average erosion (3,792 m^3/km) was 6% higher than that of Marshall Co. and 105% higher than Nemaha deposition per km (1,848 m^3/km). In addition, the annual average erosion per km of MS streambank in Marshall County (2010-2018) was 449 m^3/km/y, while in Nemaha County (2012-2018) the annual average was 632 m^3/km/y. The higher yearly average of erosion per km of bank length in Nemaha Co. may be an indication of more channel adjustment occurring in the upper watershed as incision works its way up the channel.

Amounts of erosion and deposition in each 1-km segment may be affected by the timing of channelization along the channel, given that approximately one-third of the BVR MS channel has been channelized in a piecemeal fashion since 1967, with most occurring since 1971 (Figure 16, p. 46). Each of these instances of channelization would have resulted in increased channel bed slope and set in motion upstream incision and downstream aggradation associated with the oversteepening of a reach (Schumm et al., 1984). Another factor that may affect the erosion rate at a given location is the presence of woody vegetation. Sass (2011) found the mean rate of retreat in BVR study banks with woody vegetation was 0.16 m and those without woody vegetation was 0.41m between 2007 and 2010. The effects of presence, amount, and density of woody vegetation on bank erosion rates will be discussed in detail in Chapter IV.

Of the four BVR MS 1-km segments with the highest amounts of erosion (8, 9, 10, and 11, Figure 43), three contain relatively short cut banks with little or no woody

vegetation and high amounts of erosion similar to that in IC segment #7 (Figure 36, p. 110) discussed earlier. However, within segment 9 is an example of how instream large woody debris can affect stream geomorphology. Within MS segment 9, an area of large woody debris accumulated between 2012 and 2013, and by 2018, the stream channel shifted to the northwest around the debris.

North Fork

The North Fork (NF) of the BVR is the largest of the three subwatersheds included in Sass & Keane (2012) and covers approximately 313.4 km^2. The confluence of the BVR MS and NF is located approximately 14 km upstream of Frankfort, KS. As with the BVR MS, the NF has been heavily channelized, with the bulk of its channelization occurring in or prior to the 1950s (Figure 16, p.46); however, a few reaches in in the mid-watershed were channelized in the 1970s, and a few reaches in the upper watershed were channelized in the 1970s and 1980s. Weyer Creek is the largest tributary of the NF and also experienced widespread channelization, primarily since the 1970s (Figure 16). Two of the original three NF study reaches monitored by Sass& Keane (2012) were included in this study (NF1 and NF2) (Figure 26, p.74). Tables 19, 20, and 21 indicate the Rosgen Classification Metrics and additional measurements used to evaluate the NF channel evolution at each study reach.

Table 19: North Fork Rosgen Classification Metrics: Ent (Entrenchment), W/D (width/depth), D_{50} (Dominant Bed Material), k (Sinuosity), Class (Rosgen Stream Type)

Rosgen Classification Metrics for North Fork							
Reach	Year	Ent. Ratio	W/D ratio	Reach D_{50} (mm)	Slope	K	Class
NF1	07	1.68	7.26	1.13	0.0022	1.2	G5c
	09	1.37	8.97	0.9	0.0019		
	21	1.39	10.60	1.08	0.0019	1.1	G4c
NF2	07	1.5	10.89	0.34	0.0008	1	G5c
	09	1.69	9.36	0.75	0.0008		
	21	1.51	10.33	0.65	0.0008	1	G5c

Table 20: North Fork Cross-Sectional Data: (Bankfull Width), Wfpa (Width at Flood Prone Elevation), Dmean (Mean Bankfull Depth), Dmax (Maximum Depth at Bankfull), X-Sec Area (Cross-Sectional Area), Bk Ang L and R (Bank Angle Left and Right Banks), D_{50} (Dominant Feature Particle Size)

North Fork		Riffle Cross Sections								Pool Cross Sections							
Reach		Wbkf (m)	Wfpa (m)	Dmean (m)	Dmax (m)	X-Sec Area (m^2)	Bk Ang L	Bk Ang R	D_{50} (mm)	Wbkf (m)	Wfpa (m)	Dmean (m)	Dmax (m)	X-Sec Area (m^2)	Bk Ang L	Bk Ang R	D_{50} (mm)
NF1	07	10.82	18.23	1.49	2.01	16.10	36	27	2.92	13.23	25.53	1.94	2.92	25.67	15	31	0.13
	09	13.36	18.37	1.49	1.95	19.86	44	25	0.50	16.41	26.93	2.06	3.12	33.80	25	38	0.50
	21	14.73	20.52	1.39	1.90	20.40	65	33	15.78	19.30	27.69	1.83	2.86	35.26	44	45	0.60
NF2	07	19.60	29.39	1.80	2.38	35.29	36	23	2.78	20.23	33.53	1.92	2.90	38.75	33	20	1.05
	09	18.26	30.80	1.95	2.56	35.69	40	20	0.47	21.01	33.38	2.03	2.95	42.68	32	16	0.97
	21	17.14	25.86	1.66	2.23	28.44	33	25	0.50	21.00	36.27	2.08	3.15	43.67	22	16	0.54

*Table 21: Sass & Keane (2012) North Fork Pool Study Bank Profile Cross Sectional Area and Bank Retreat Rates (*2010 data was not available: Right bank (RB) and left bank (LB) of each pool cross section was measured*

Pool Study Bank Profile X-Sec. Area and Bank Retreat							
Reach	Cross Sectional Area (m^2)				Bank Height (m)	Bank Retreat Rate (m/yr)	
	2007	2009	2010	2021		07 - 10 (*09)	10 (*09) - 21
NF1 (RB)	28.70	36.67	*	35.09	5.39	-0.74 *	0.02
NF1 (LB)	53.92	57.96	*	68.42	6.65	-0.30 *	-0.13
NF2 (RB)	56.78	55.33	53.54	45.25	5.41	0.20	0.14
NF2 (LB)	25.69	33.66	32.69	40.70	5.29	-0.44	-0.14

North Fork 1

Sass & Keane (2012) classified North Fork 1 (NF1) as a G5c in the Rosgen (1996) classification; therefore, the next expected transition in the Rosgen "C"-"Gc"-"F"-"Gc" successional scenario would be to an "F" stream type. In 2007, the first year the NF1 riffle was surveyed, the entrenchment ratio was in the range of a "B" stream type at 1.68; however, by 2009, the NF1 riffle cross section had become more entrenched as the entrenchment ratio fell to 1.37, which is within the "G" stream type range (Table 19). Between 2009 and 2021 the NF1 entrenchment ratio remained in the entrenched range with a slight increase to 1.39, which is expected in the "Gc" to "F" succession, as both have a reference entrenchment ratio of < 1.4.

In 2007, the width/depth ratio was 7.26 as expected within the "Gc" classification. The "Gc"-"F" succession is primarily evidenced by an increase in width/depth ratio over the 2007-09 and 2009-21 periods to 8.97 and 10.60 respectively (Table 19). Over the 14-year study period, the increase in width/depth ratio was due to a pattern of widening and slight aggradation at the riffle cross section, indicated by an increase in bankfull width and bankfull cross-sectional area of 3.91 m and 4.3 m^3, respectively, coupled with a decrease in bankfull mean depth and cross-sectional area of 0.10 m and .05 m respectively (Table 20). The relatively minor fluctuation in the bankfull mean and maximum depth may be due to bed feature migration. In 2021, there was a depositional gravel bar on the left side of the channel (right side of Figure 44) resulting in the riffle D_{50} of 15.78 mm that was not present in the 2007-2009 period as evidenced by the 2007 and 2009 cross sections (Figure 45) and D_{50} of 2.92 mm and 0.05 mm,

respectively. The gravel could have originated from a bedrock outcrop just upstream of the study reach.



Figure 44: North Fork 1 Riffle Cross Section: Looking upstream

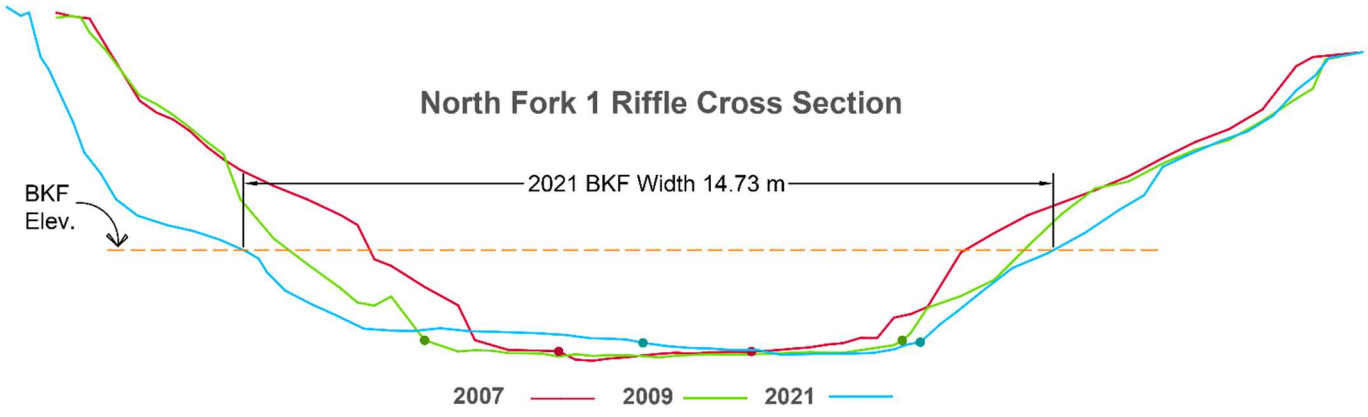


Figure 45: North Fork 1 Riffle Cross Section: 2007, 2009 and 2021: Points indicate edge of water

In contrast to the NF1 Riffle, the NF1 pool cross section experienced incision between 2007 and 2009, with an increase in bankfull mean and maximum depth of 0.12 m and 0.2 m, respectively. The pool also widened in the 2007-09 period with a 3.18 m increase in bankfull width and 8.13 m^2 increase in bankfull cross-sectional area (Table 20). However, in the 2009-21 period, the pool cross section aggraded slightly while continuing to widen resulting in net bed aggradation and significant channel widening for the entire 14-year study period indicated by a decrease in bankfull mean depth of 0.11 m and an increase in bankfull width and cross-sectional area of 6.07 m and 9.56 m^2, respectively. In Figure 46, note the channel thalweg shifted from near the right bank in the 2007-09 period to the left bank in the 2009-21 period. The channel shift could be due to rotational slump of the right bank, as the pattern of concave erosion above bankfull and convex deposition below bankfull on the right bank is typical of such mass failure, or the downstream migration of the meander bend immediately upstream, which is evident when comparing aerial images from 2008 and 2021 (Figure 47).

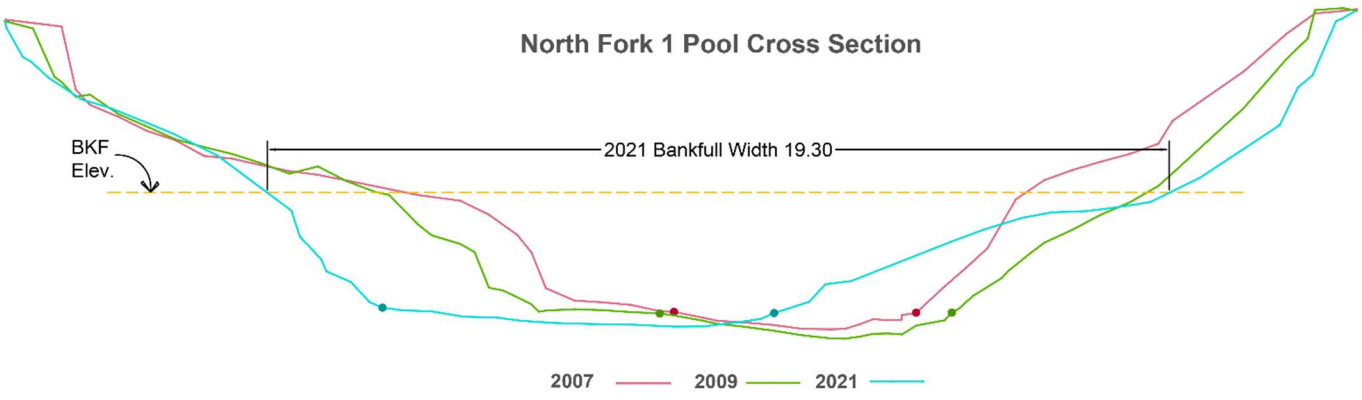


Figure 46: NF1 Pool Cross Section 2007, 2009, 2021: Points indicate edge of water

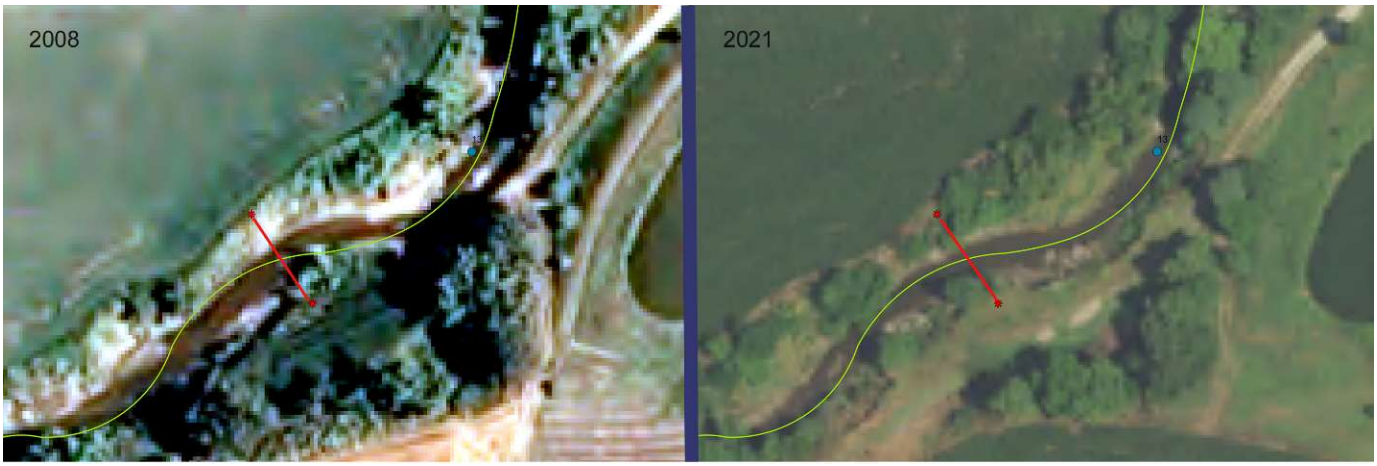


Figure 47: NF1 Pool Cross Section: Downstream Meander Migration: Green line indicates centerline in 2021

North Fork 2

North Fork 2 (NF2) is located approximately 6 km downstream of NF1, in a channelized, very straight reach evidenced by a sinuosity of 1.0, and was also classified as a “G5c” by Sass & Keane (2012); therefore, the next expected transition in the Rosgen “C”-“Gc”-“F”-“Gc” successional scenario would be to an “F” stream type. The NF2 riffle cross section remained consistently entrenched over the 14-year study period with an entrenchment ratio of 1.5, 1.69, and 1.51, in 2007, 2009 and 2021 respectively which would be expected in the “G” to “F” succession. However, the width depth ratio declined over the same time period from 10.89 to 10.33 (Table 19), which is not reflective of the “G” to “F” succession. Of note at the NF2 Riffle cross section is the aggradation that occurred on both the riverbanks and riverbed between 2009 and 2021 resulting in a decrease in bankfull width, mean depth, maximum depth, and cross sectional area of 2.46 m, 0.14 m, 0.15 m, and 6.85 m^2, respectively (Figure 48, Table 20). The NF2 riffle cross section also experienced overbank deposition, as both left and right bank pins were buried, 0.16 m and 0.76 m, respectively. Aggradation of both bed

and banks resulting in a lower width/depth ratio is not reflective of the “G” to “F” succession.

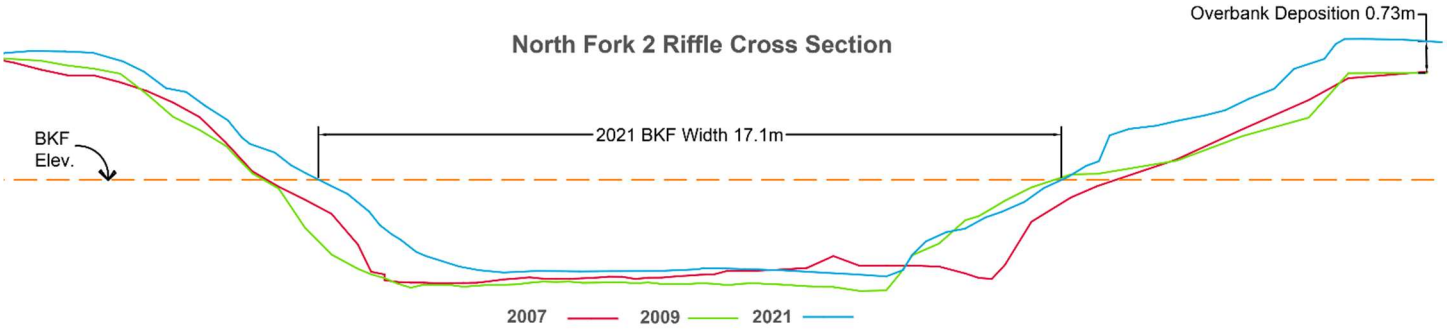


Figure 48: North Fork 2 Riffle Cross Section 2007, 2009, 2021

Over the entire 14-year study period, the NF2 pool cross section experienced minor incision and widening with an increase in bankfull maximum depth and mean depth of 0.29 m and 0.16 m, respectively, and an increase in bankfull width and cross-sectional area of 0.77 m and 4.92 m^2, respectively (Table 20). However, the channel shifted to the left bank with the rate of bank retreat on the left bank equaling the rate of deposition on the right bank (Table 21). The DoD created from the 2012 and 2018 DEMs indicated the reach experienced higher amounts of deposition than erosion over the 6-year period suggesting the riffle cross section is more reflective of the reach, which is discussed in greater detail in the next section.

North Fork System Wide

The North Fork begins approximately 35 km in length upstream from the confluence of the BVR Main Stem and North Fork, with approximately 19 km lying in Marshall County and 16 km in Nemaha County. As noted, a DoD was created for Marshall County for the 2010-2018, 8-year period and for Nemaha County for the 2012-2018, 6-year period. Unlike the BVR Main Stem and Irish Creek, along the North Fork

banks in Marshall County, the average bank deposition per km (4,675 m^3/km) was approximately 27% more than erosion (3,679 m^3/km) (Table 15, p.109). However, this was not the case for the entire North Fork Channel. Figure 49 below illustrates that upstream of the confluence of the North Fork and Weyer Creek (segments 61-83) - a tributary that flows from the east - the patterns of erosion and deposition were similar to that of IC and MS, with erosion being greater than deposition within 20 of 24 1-km segments. While downstream of that point (segments 52-60), there is a noticeable jump in deposition for all 1-km segments, with all segments having greater deposition than erosion. These results initiated further investigation of Weyer Creek.

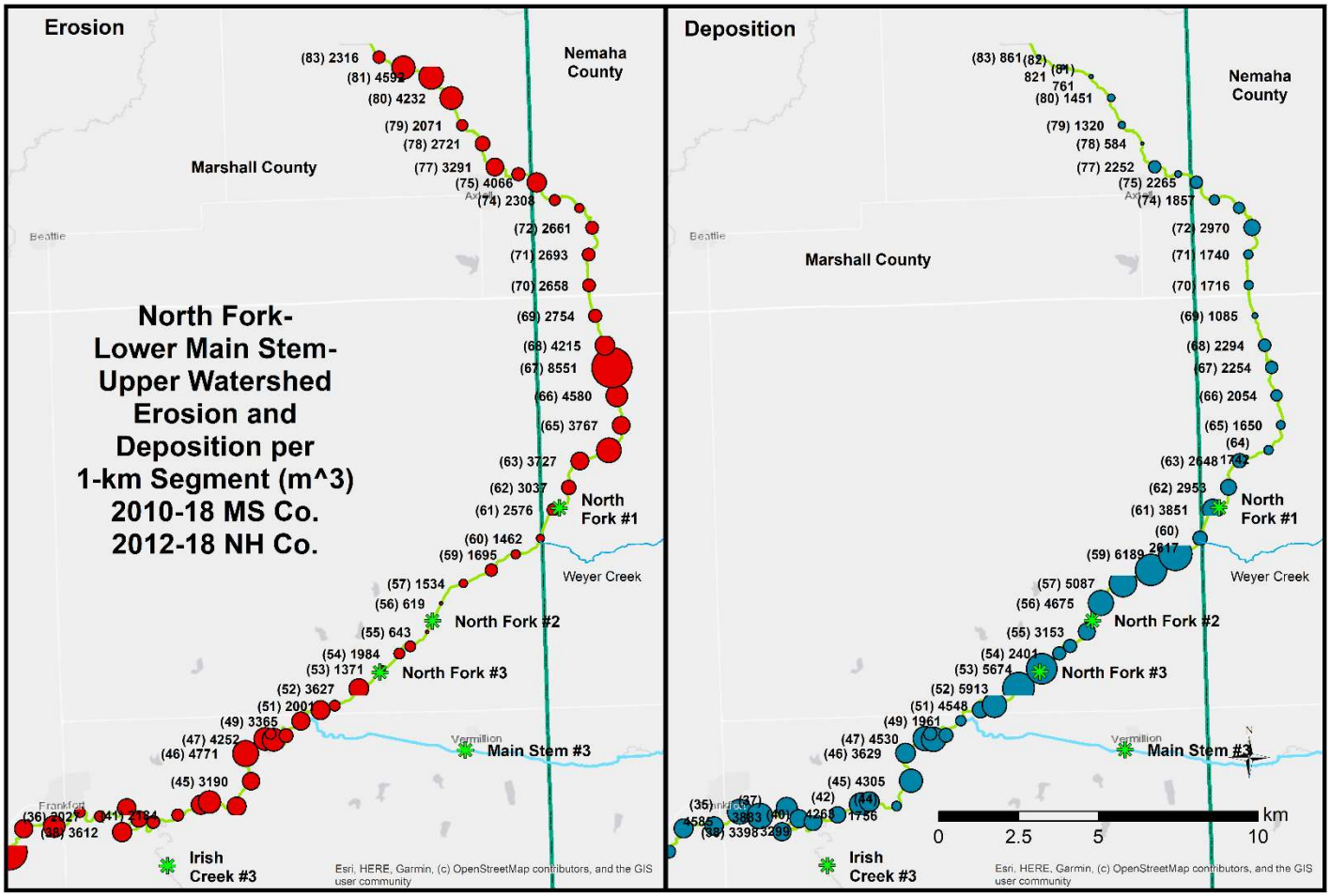


Figure 49: North Fork Erosion and Deposition 2010 (12) - 2018: Point size is proportional to the amount of erosion/deposition in each 1-km segment: reaches (#) is segment number

In order to assess sediment originating from Weyer Creek, a 2012-2018 DoD was created for the banks of Weyer Creek using the same methodology employed with the three subwatersheds revealing that Weyer Creek had substantially higher erosion per km (5,439 m^3/km) than any of the other channels regardless of DoD time period (Table 15, p.109). Deposition along Weyer Creek averaged 3,105 m^3/km. For an 8-year period, Irish Creek with a drainage area of 121.81 km^2 produced an estimated 44,852 m^3 of sediment from bank erosion (erosion less deposition), while for a 6-year period, Weyer Creek with a drainage area one-third the size of IC (47.80 km^2) produced an estimated 49,601 m^3 (Table 15, p. 109). Figure 16 (p.46) shows the bulk of channelization along Weyer Creek was done in the 1970s and 1980s, which is more recent than much of the channelization within the BVR watershed and may be responsible for the high rate of streambank erosion along the creek. Upon inspection of the Weyer Creek 2012 and 2018 DEMs and DoD, a channelized reach was discovered that had occurred more recently than 2008 (Figure 50).

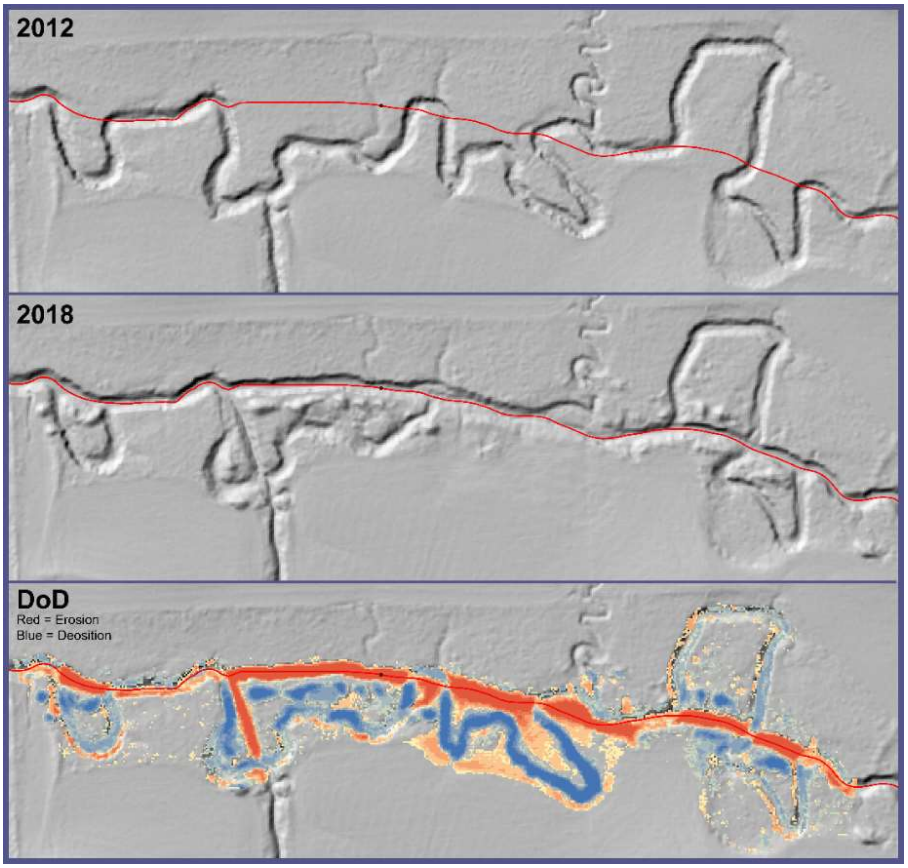


Figure 50: Weyer Creek Reach Channelized between 2012 and 2014: Red line indicates approx. centerline in 2018

According to NAIP aerial images, the channelization occurred sometime between 2012 and 2014, and reduced a 1,200-m length of stream channel to approximately 500m. Between 2012 and 2018, this channelized reach and the area associated with the old channel produced an estimated 4,579 m^3 of sediment between 2012 and 2018, approximately 9% of the total Weyer Creek sediment yield. The NF1 and NF2 cross sections suggest increased deposition downstream of the NF/Weyer Creek confluence. The NF1 riffle and pool cross sections upstream of the Weyer Creek/NF confluence experienced bank erosion as indicated by increases in bankfull cross-sectional area. In contrast, the NF2 cross sections downstream of the confluence experienced deposition on the streambed and banks resulting in a loss of cross-sectional area at the riffle, which was determined to be more characteristic of the reach.

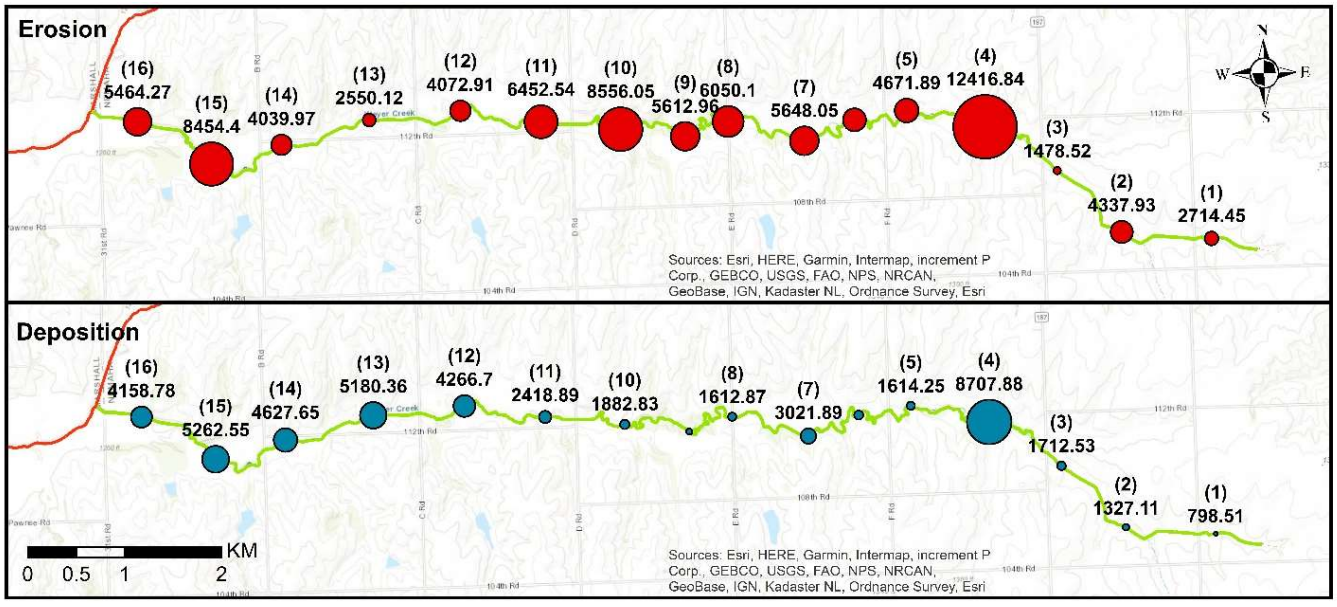


Figure 51: Weyer Creek Erosion and Deposition 2012 - 2018: Point size is proportional to the amount of erosion/deposition in each 1-km segment: reaches (#) is segment number

Deposition along the NF2 reach may be partially due to a decrease in slope compared to NF1 from .0019 to .0008 resulting in a decrease in mean boundary shear stress, velocity, and stream power. As river competence is closely related to velocity, the velocity at NF1 and NF2 was calculated using Manning's equation:

$$\bar{u} = \frac{kAR^{\frac{2}{3}}S^{\frac{1}{2}}}{n}$$

Where: $\bar{u}$ = Bankfull mean velocity (m/s)
k = Unit conversion factor (1 for SI units)
R = Hydraulic radius
S = Bankfull slope
n = Manning's roughness coefficient

Manning's roughness coefficient was determined using Rosgen (2008) Figure 2-31 *Manning's "n" by Stream Type* " using the Average bankfull value for smaller rivers with controlling vegetative influence" curve. Bankfull mean velocity at the NF1 and NF2 riffle cross sections was calculated using the equation above. For the "G5" stream type, the estimated Manning's n was 0.064. Estimated bankfull mean velocity at the NF1 and NF2 2021 riffle cross sections was 0.807 m/s and 0.589 m/s, respectively. Reach NF1 can transport particles approximately <= 67 mm at bankfull discharge while reach NF2 is only able to transport particles approx. <= 28 mm at bankfull (Figure 52).

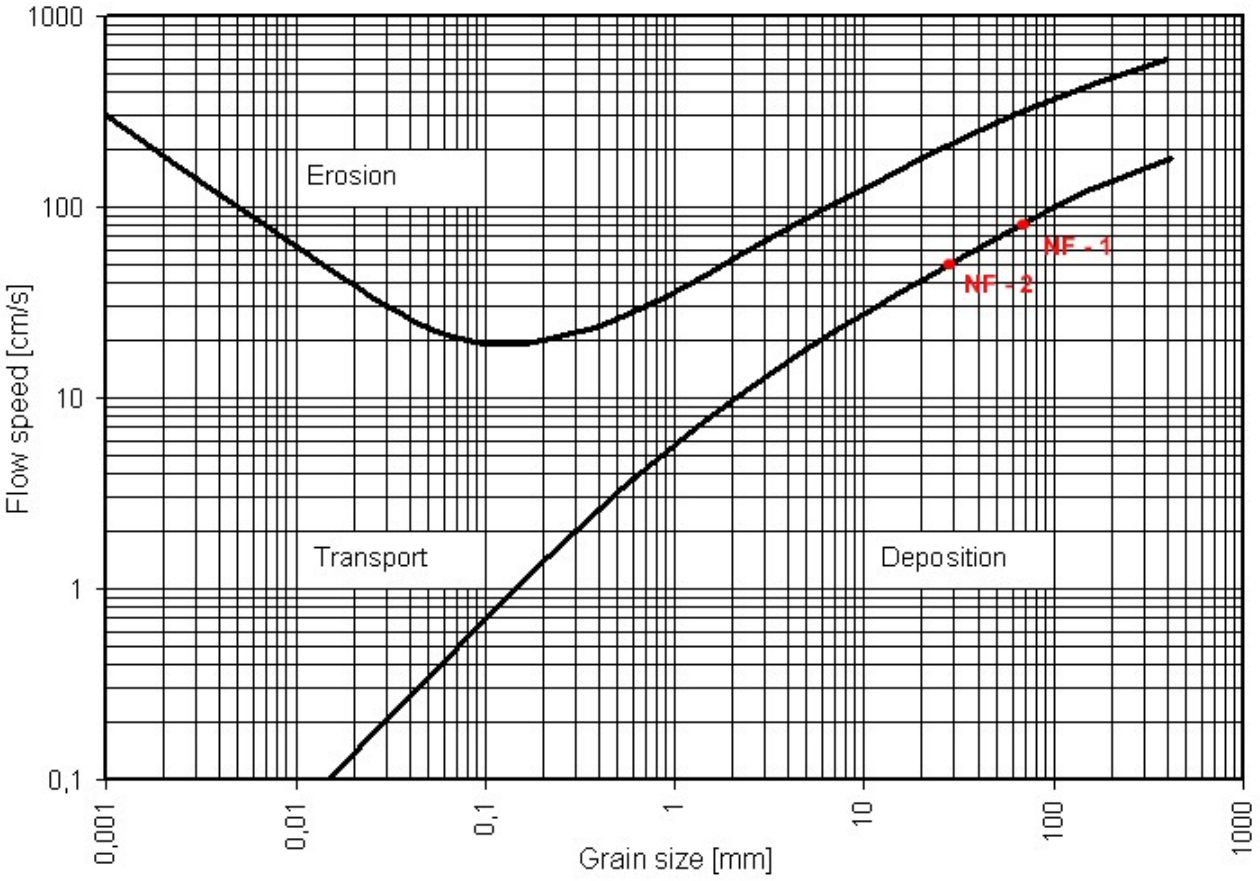


Figure 52: Hjulström-Sundborg diagram with NF1 and NF2 Competence: (Hjulstrom, 1935)

Deposition along the NF2 study reach may also have been facilitated by an increase in bank vegetation between 2010 and 2018 (Figure 53), which would have also increased the roughness coefficient. As woody vegetation has increased along the NF2 riverbanks, they have become more efficient sediment traps by increasing roughness and reducing velocity resulting in higher deposition (Trimble, 1999). Figure 53 below shows how dramatically bank vegetation, especially woody vegetation, has increased within the NF2 reach channel from 2008 through 2019. It may be important to note that in 2008, an herbaceous conservation buffer was present along the NF2 reach; however, by 2019, this buffer had been removed and returned to tillage agriculture, yet woody bank vegetation had been allowed to grow within the channel.

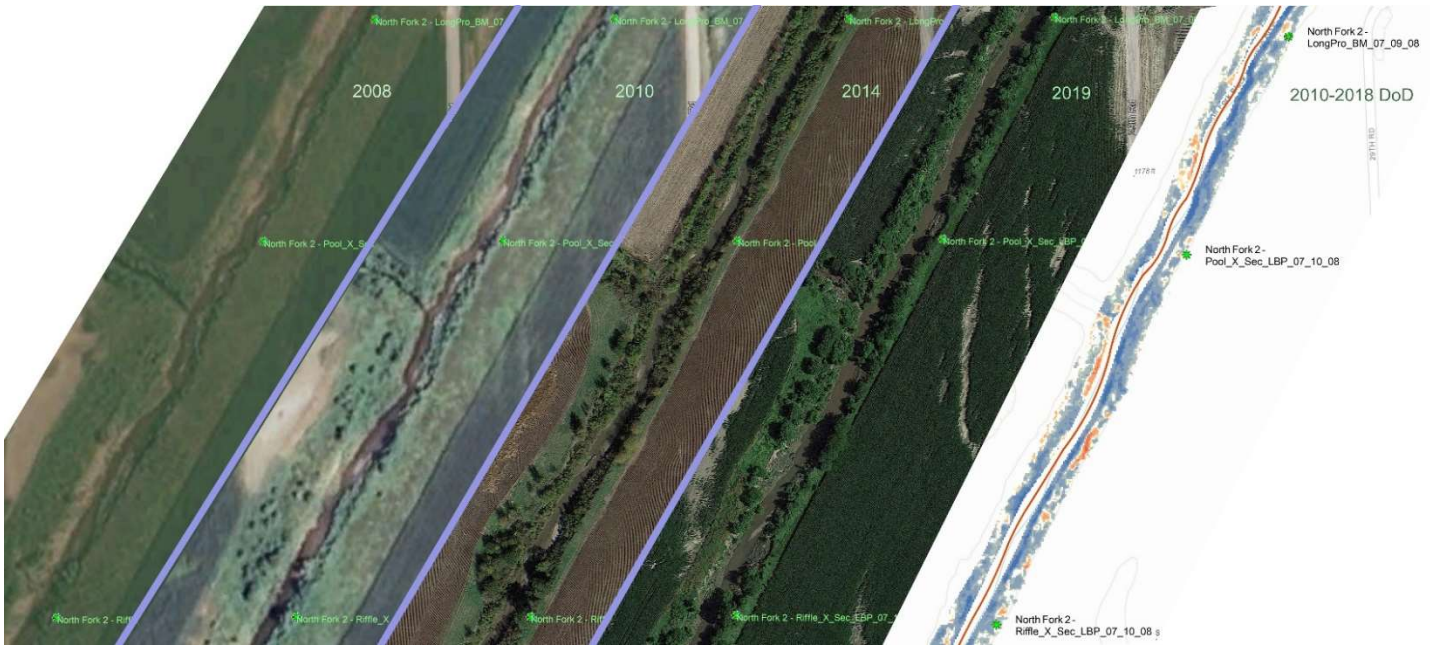


Figure 53: North Fork 2 Increase in Woody Vegetation 2008 – 2019: (Right) NF2 2010-18 DoD with pool and riffle cross section locations showing extensive deposition throughout the reach

Summary and Conclusions

Human induced geomorphological channel adjustment of the BVR began with the conversion of natural tallgrass prairie to agriculture in the late 19th century and was compounded and/or complicated with the practice of widespread channelization that began mid-20th century. These changes to the BVR watershed and channel led to increased discharge and slope and thus stream power, resulting in the BVR progressing through a sequence of geomorphological adjustments – generally known as channel evolution - as it attempts to adjust its dimension, pattern, and profile to the new flow and sediment inputs. This study utilized cross sectional, longitudinal profile, study bank profile, and pebble count data collected annually from 2007 to 2010 and again in 2021 along with publicly available sequential LiDAR-derived DEMs of the study area to evaluate channel evolution over the past 14 years. As noted, this study primarily utilizes the Rosgen (1996, 2006, and 2014) Level II Classification System and successional

scenarios to evaluate channel change at the seven study reaches due to its measurable criteria and use in Sass & Keane (2012), the source of a portion of the data used in this study. However, the Rosgen successional scenarios share many characteristics of other prominent channel evolution models (e.g., Schumm et al. (1984), Simon & Hupp (1986), Cluer & Thorne (2014)), as all of these channel evolution models follow the general pattern of: 1) incision 2) incision and widening 3) rapid widening with aggradation and 4) the establishment of quasi-equilibrium at a new, often lower, elevation.

The “C”-“Gc”-“F”-“C” Rosgen successional scenario is the most common in NE Kansas (Keane & Sass, 2017). Of the seven study reaches included in this study, Sass & Keane (2012) found one “F” stream type, five “G4/5c” stream types and one a “B5” stream type; however, it was noted the study reach determined to be a “B5c” at the riffle cross section alternated between “B5c” and “G5c”. At the six of seven study reaches determined to be “G” type streams, the expected transition would be to an “F” type stream. Within the Rosgen (1994) classification system and successional scenarios, the “G” to “F” succession is primarily indicated by an increase in the riffle cross section width/depth ratio above 12, which is achieved as incision ceases and aggradation begins while channel widening continues. This transition from a phase of incision and widening to rapid widening or aggradation and widening is also characteristic of the other CEMs noted above.

Four of six study reaches determined by Sass & Keane (2012) to be a “G” type stream in 2009 experienced an increase in the width/depth ratio at their riffle cross sections between 2009 and 2021 as expected in the “G” to “F” succession. The two

riffle cross section having a decrease in width/depth ratio both experienced widening between 2009 and 2021; however, they also experienced continued incision resulting in a reduction of the width/depth ratio, which is not characteristic of the “G” to “F” succession.

The MS3 study reach was determined to be an “F” type stream in 2009, therefore the next expected transition would be to a stable, “C” type stream, which is indicated by an increase in the entrenchment ratio above 2.2. The reference width/depth ratio for “F” and “C” streams is < 12 so little or no change was expected. Between 2007 and 2009, the width/depth decreased into the “G” range before returning to the “F” range between 2009 and 2021. The slight decrease in both entrenchment ratio and width/depth ratio over the entire 14-year study period does not indicate a movement towards a stable, “C” stream type. The MS3 reach may have or be experiencing a channel evolution short circuit characteristic of the Cluer & Thorne (2014) SEM. There were signs of the “F” to “C” succession within the MS3 study reach, as the pool experienced aggradation and both riffle and pool experienced a reduction in bank angles.

Looking at all riffle and pool cross sections included in this study, 12 of 14 cross sections experienced widening over the entire 14-year study period. Six of 14 cross sections experienced incision; however, the rate of incision at these cross sections over the last 11 years is significantly less than between 2007 and 2009 indicating a waning or cessation of incision. Five of 14 cross sections (3 pools and 2 riffles) experienced aggradation with the remaining three cross sections having no appreciable change in bed elevation. The mix of cross section incision and aggradation suggests the BVR’s channel evolution is between a phase of incision and widening and a phase of

aggradation and widening or may be the result of localized influence creating short circuits within the channel evolution. In addition, six of seven pool study bank profiles monitored experienced a reduction in annual bank retreat rate over the last decade when compared to the bank retreat rates between 2007 and 2010.

Sequential LiDAR-derived DEMs from Marshall County and Nemaha County covering a sizable portion of the entire 14-year study period were utilized to determine if the changes documented at the seven Sass & Keane (2012) study reaches were indicative of each of the three subwatersheds overall. Digital elevation models of difference (DoDs) were created from 2010 and 2018 DEMs in Marshall County and 2012 and 2018 DEMs in Nemaha County facilitating the estimation of riverbank erosion and deposition along the entire length of each subwatershed for the respective time periods. To evaluate patterns of erosion and deposition along each subwatershed channel, each channel was divided into 1-km segments and erosion and deposition within each segment calculated. It is important to note that DoD analysis does not include any geomorphic change of the riverbed, as only the banks are included in the analysis. The lidar-derived DEMs and DoDs may be more indicative of change system-wide than the two cross sections at each study reach, which are sensitive to bed feature migration.

Within the IC and MS subwatersheds, nine of ten cross sections experienced widening over the 14-year study period. In agreement with the cross-sectional data, the 8-year (6-year in Nemaha Co.) DoD analysis indicated that within 59 of 62 1-km segments along the IC and MS channels, erosion was greater than deposition indicating channel widening and a net production of sediment from each subwatershed. In the IC

watershed, erosion did have a modest correlation with drainage area (drainage area-weighted erosion decreased with drainage area), which is not surprising given the lack of channelization since mid-century except for one reach in the lower watershed channelized in the late 1970s. Erosion along the MS channel did not show any correlation with drainage area, which may be due to the large number and wide distribution of reaches channelized in the 1970s and 1980s.

DoD analysis within the NF subwatershed was perhaps the most surprising. Upstream of Weyer Creek confluence, the largest tributary of the NF, the pattern and amounts of erosion and deposition were similar to IC and MS. However, downstream of Weyer Creek there was a noticeable, dramatic increase in the amount of deposition within each 1-km segment, which instigated further investigation of sediment being produced by Weyer Creek. DoD analysis indicated Weyer Creek with a drainage area of 48 km^2 had the highest erosion per 1-km segment (5,439 m^3) of any subwatershed. In addition to the excessive amount of sediment being produced by Weyer Creek, deposition downstream of Weyer Creek may be facilitated by a reduction in slope and a significant increase in woody vegetation within the channel over the past decade (Figure 53, p. 133).

Understanding and projecting erosion within the BVR could better inform restoration efforts aimed at reducing sediment being delivered to the Tuttle Creek Reservoir. However, both the traditional methods used by Sass & Keane (2012) and the LiDAR-derived DoDs used in this study to estimate amounts of erosion and deposition along riverbanks have limitations that may introduce error into the calculations. Cross sections are sensitive to local influences such as large woody

debris, episodic mass failure, local changes in land use, and channelization and may not be reflective of the entire reach in which they are located. Undetected or uncorrectable errors within legacy DEMs due to varying surveying techniques, changes in technology used for data collection, point cloud generation and classification, and DEM creation, and changing georeferencing data may result in systematic error in the final DoD used to estimate geomorphic change. However, future DoD analysis should be more accurate as technology improves, becomes more consistent, and more meta data are provided for subsequent datasets.

Questions arise from the results of this study that highlight the need for further research within the BVR watershed. Will the widening seen in each of the three tributaries continue at the same rate or increase if these channels have indeed entered into a phase of rapid widening? If the rate were to increase, even more sediment would be produced, at least until the channel reaches adequate width to attain equilibrium at a new, lower elevation. In addition, if the DoD created in this study along the North Fork is correct downstream of Weyer Creek, channel capacity has been reduced along the North Fork and much of the Main Stem included in this study, which raises even more questions. Will this cause localized flooding and will farmers tolerate it? Does this pattern of excessive deposition continue downstream of Frankfort? Is the excessive deposition downstream of Weyer Creek a pulse of sediment from Weyer Creek and will it work its way downstream eventually? Further monitoring of the BVR using both traditional methods as well as future data derived from remote sensing techniques could help answer these questions while informing restoration efforts with the goal of reducing the amount of sediment being produced and delivered to Tuttle Creek Reservoir.

CHAPTER IV - Quantification of the Effects of Woody Riparian Vegetation on Black Vermillion River Streambank Erosion and Deposition Utilizing Repeat LiDAR-Derived Elevation Data

Introduction

Traditional riverbank surveying methods used to measure erosion and deposition include erosion pins, recurrent cross-sections, bank profiles, and longitudinal profile surveying. Traditional methods provide only two-dimensional data with the resolution dependent on the number of permanent pins installed or the number of points collected at each cross section and/or the total number of cross sections, and “their accuracies may be affected by several factors, such as subaerial processes”, which are land-based processes above the waterline such as mass wasting (Couper et al., 2002; Duro et al., 2018). While differential leveling with a self-leveling laser is the most accurate traditional surveying technique, it limits coverage and is labor intensive. Total station and GPS systems increase coverage and efficiency but not necessarily accuracy. The accuracy of most high-accuracy GPS systems and total stations ranges from millimeters to a few centimeters; however, the spatial and temporal resolution of surveying with these traditional methods may be sensitive to episodic, intermittent, or localized erosion (e.g., Brasington et al, 2000) (Duro et al., 2018). For example, if large woody debris falls into the stream near a given cross section, localized accelerated bank erosion caused by the woody debris could cause the cross section to no longer be representative of the overall reach. When monitoring cross sections and longitudinal profiles at a reach scale, traditional methods may be the most accurate and appropriate;

however, newer remote sensing techniques may be more appropriate when attempting to quantify geomorphic change over large, continuous areas of riverbank.

Fluvial systems are “continuous systems that vary across multiple space and time scales...” (Marcus & Fonstad, 2010), and therefore, require continuous data in order to understand the full range of river functions and structure (Lane et al., 1994). Prior to the last decade, the vast majority of data used in fluvial geomorphology was collected via the traditional field surveying methods noted above; however, new remote sensing technologies can provide researchers with data that is of higher quality in terms of spatial extent as well as temporal resolution (Mirijovsky & Vavra, 2012). The complete three-dimensional complexity of riverbanks over large areas, and how they change over time, can currently be surveyed by a number of remote sensing techniques (Duro et al., 2018). This research focuses on the use of the active remote sensing technique of Light Detection and Ranging (LiDAR) to evaluate change along the Black Vermillion River (BVR) channel in Northeast Kansas.

LiDAR scans are collected from an airborne platform by emitting thousands of laser pulses directed towards the target of interest, which in this case, is a riverine landscape. In vegetated areas, each pulse will have multiple returns with the last return representing the ground. The round-trip travel time is then recorded for each return within each pulse. Simultaneously, the aircraft’s position and attitude (roll, pitch, and yaw) are recorded using a global positioning system (GPS) and inertial measurement unit (IMU) (Kessler et al., 2012). Return times combined with position and attitude of the aircraft allow for accurate estimation of horizontal and vertical positions of points and objects on the ground (Kessler et al., 2012). The LiDAR data is processed into a

point cloud, from which ground points can be filtered and used to construct raster digital elevation models (DEMs) that represent the “bare earth” surface. LiDAR-derived DEMs collected at different times can be compared by subtracting the earlier DEM from the latter DEM to create a digital elevation model of difference (DoD) that provides estimates of volume change within a given geographical area.

Areas of erosion and deposition along riverbanks can be identified when applying this technique to river channels. The use of LiDAR has become popular in the field of fluvial geomorphology due to its ability to provide detailed, accurate three-dimensional models of terrestrial elements in riverine landscapes that lie above the water surface (Marcus & Fonstad, 2010), as most LiDAR surveys do not penetrate water. LiDAR has been used to estimate riverbank volume change at both the reach (Moretto et al., 2012; Anderson & Pitlick, 2014) and catchment/watershed (Kessler et al., 2012; Schaffrath et al., 2015; DeLong et al., 2022) scales, and may now be used to assess other factors influencing river geomorphology, such as riparian vegetation. Accuracy of LiDAR-derived DEMs may be affected by aircraft elevation, aircraft speed, laser pulse rate, and laser footprint as well as the manner of data processing (Kessler et al., 2012). Methodology has been developed to correct many systematic errors created during LiDAR data collection and processing (Kessler et al., 2012; Schaffrath et al., 2015). The primary goals of this research are threefold:

(1) Identify and correct systematic errors introduced during data collection and processing in repeat LiDAR-derived DEMs of the BVR basin and their subsequent DoDs.
(2) Use the DoDs to estimate amounts and patterns of erosion and deposition along the banks of 151 km of the BVR and three of its tributaries.

(3) Quantify the effect of the presence, amount, and density of woody vegetation on rates of erosion and deposition along the banks of the BVR and three of its tributaries.

Sedimentation of Tuttle Creek Reservoir

Streambank erosion has been shown to account for between 30 and 80 percent of total sediment loading in incised rivers and streams (Wilkin & Hebel, 1982; Lawler, Grove, Couperthwaite, & Leeks, 1999; Sekely et al., 2002; Sass & Keane, 2012), which has led to sediment being the greatest water quality problem in the United States (U.S.) (Darby & Simon, 1999). The seemingly ubiquitous incision of rivers and streams in the Midwestern U.S. is primarily due to anthropogenic alterations to rivers and their watersheds, which have led to a dramatic increase in the volume and velocity of water entering rivers and streams. In the Midwest, over 90 percent of the original prairies were plowed, approximately 95 percent of the wetlands drained, and 70 percent of the forests cleared over the last 150 years (Whitney, 1994). In addition, the practice of channelization (the linear reshaping or repositioning of an existing channel to facilitate rapid drainage of the immediately surrounding fields) began in the late 1800s and reached its peak in the mid-20th century. Channelization shortens the channel resulting in increased bed and bank slopes and decreased channel roughness leading to increased stream energy often resulting in degradation and incision upstream of the channelized reach and aggradation downstream (Schumm et al., 1984).

The Black Vermillion River (BVR) and its watershed in Northeast Kansas (Figure 54) is a river that has experienced the anthropogenic alterations described above. The transition of approximately 90 percent of the landcover in the BVR watershed from

native tallgrass prairie with some gallery forest to agricultural land uses has resulted in runoff increasing from approximately 4 percent to between 30 and 55 percent (Chow et al., 1988; Qiao et al., 2017). This increase in runoff has resulted in BVR discharges increasing by 40 percent compared to estimated predevelopment discharges (US-COE, 1998; Sass, 2011). Altered flow regimes within the BVR watershed and channel set in motion a series of geomorphological changes known as channel evolution or succession that generally follow a pattern of incision followed by incision and widening followed by rapid widening with aggradation and finally the attainment of quasi-equilibrium at a new, often lower, elevation (Schumm et al., 1984; Simon & Hupp, 1987; Rosgen, 1996; Cluer & Thorne, 2014). Previous studies and Chapter III found the upper reaches of the BVR to be somewhere near the end of the incision and widening phase and beginning of the rapid widening with aggradation phase and the lower BVR to be within the rapid widening with aggradation phase leading to pervasive and excessive streambank erosion throughout the system (Keane & Sass, 2017).



Figure 54: Black Vermillion Watershed, Northeast Kansas (Sass & Keane, 2012)

Excessive sediment caused by channel adjustment to anthropogenic watershed and river channel alterations may have a number of impacts noted by Sass & Keane (2012):

- Sedimentation of reservoirs (Beach, 1994; Hargrove, Johnson, Snethen, & Middendorf, 2010)
- Loss of water storage capacity (Beach, 1994; Hargrove et al., 2010; Williams, & Smith, 2008)
- Higher treatment costs (Boggess, Miranowski, Alt, & Heady, 1980)
- Increase in ambient water temperature (Naiman & Décamps, 1997)
- Decrease in dissolved oxygen (Ringler & Hall, 1975)
- Loss of Stream Habitat (Odum, 1971; Naiman & Décamps, 1997)
- Decrease in aesthetics (Riley, 1998)
- Increase in bank erosion and flooding potential (Knighton, 2014; Rosgen, 1996)

A prime example of reservoir sedimentation is Tuttle Creek Reservoir in Northeast KS that covers an area of approximately 49.4 km^2 during normal conditions and 214.8 km^2 at full flood capacity (US-COE, 2011). Tuttle Creek Reservoir was originally designed for flood control and management of the lower Missouri River by impounding up to 524,613,846 m^3 of water (US-COE, 1998); however, since it became operational in 1962, sediment delivered by the Big Blue River and its tributaries has led to a 47.9% decrease in storage capacity (Figure 55) (Rattanavong, 2019). The State of Kansas has begun planning for the use of Tuttle Creek as a municipal water supply, and in order to increase its capacity, U.S. Army Corps of Engineers is planning on beginning a pilot project in 2023 that will use water injection dredging to agitate sediment from the bed of Tuttle Creek Reservoir delivering it through the exit gates and downstream. However, the environmental consequences of delivering excessive sediment downstream are unknown (Llopis-Jepsen, 2022).

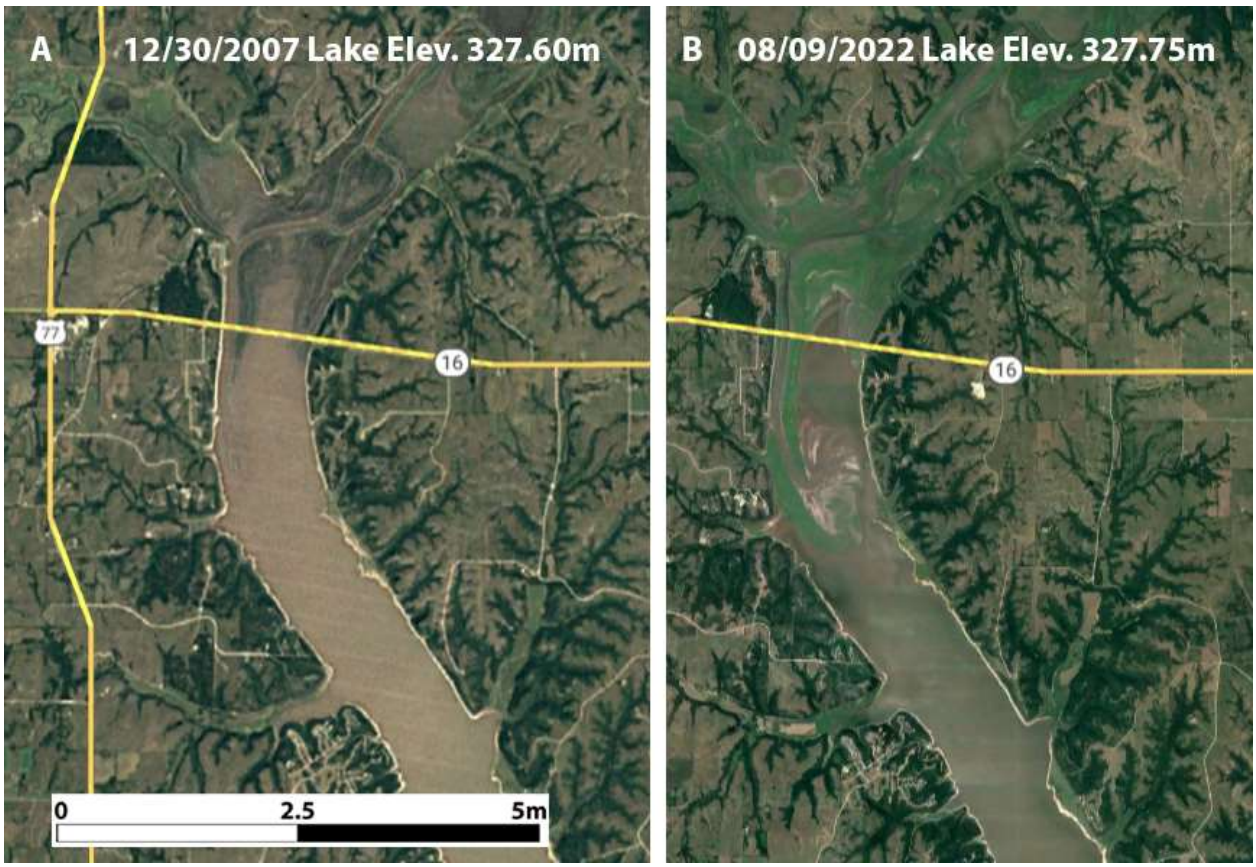


Figure 55: Sedimentation of Tuttle Creek: 2007 to 2022: Source: Google Earth

The BVR flows into the Big Blue River, which empties into Tuttle Creek Reservoir. The BVR only accounts for approximately 6% of the Tuttle Creek Reservoir watershed. However, the BVR is physiographically similar to much of the Big Blue River's watershed; therefore, the evaluation of streambank erosion along the BVR riverbanks may add to the overall understanding of sediment being delivered to Tuttle Creek Reservoir.

In agricultural watersheds such as the BVR's, riparian forest buffers provide a management tool for reducing streambank erosion and thus downstream reservoir sedimentation. The role of riparian woody vegetation stabilizing streambanks and protecting them from the erosive force of flowing water is well documented (Schultz,

Colletti, & Isenhart, 2000; Zaimes, Schultz, & Isenhart, 2006). It is suggested in the literature that woody vegetation lessens erosion rates by increasing roughness when within the channel resulting in higher dissipation of energy in the water column and by increasing cohesion by increasing tensile strength within the root-soil matrix (Schumm, 1973; Thorne, 1990; Gurnell, 1997; Genet et al., 2005; Pollen, 2007; Sass & Keane, 2012). “Riparian vegetation in the Black Vermillion watershed has been reduced significantly over the past 60 years...” (Sass & Keane, 2012). Utilizing the traditional river surveying methods, Sass & Keane (2012) found erosion rates of banks void of woody vegetation (0.48 m/yr.) to be almost three times higher than when at least some woody vegetation was present (0.18 m/yr.) at 18 study banks within 9 study reaches located throughout the upper BVR watershed studied between 2007 and 2010 (Figure 56). However, it is unclear if the changes observed at these 18 study banks are reflective of all BVR riverbanks.

Study Area

The entire Black Vermillion River Basin covers 1,382 km^2 and lies almost entirely within the glaciated physiographic region of Northeast Kansas, which is a portion of the larger Glaciated Plains Region; however, the Irish Creek watershed in the southwestern portion of the BVR Basin is influenced by the Flint Hills Uplands Region that lies to the south (Figure 56) (Sass & Keane, 2012). The BVR watershed lies almost entirely in Marshall and Nemaha Counties and within the glaciated region of northeast KS, where a layer of glacial till ranging in depth from 30.5 m to 122 m in depth covers alternating layers of limestone (Permian and Pennsylvanian) and shale. Throughout the BVR Basin, riparian soils are formed from alluvium parent material deposited by repeated

flooding over the millennia and range in clay content from 23 and 47 percent (NRCS, 2011; Sass & Keane, 2012). The climate in NE Kansas is considered continental with most of the average rainfall occurring between April and September (Aber, 2007). The average annual precipitation for the BVR Basin (period of record 1970 - 2007) was 87.9 cm with a standard deviation of 20.4 cm (Sass & Keane, 2012).



Figure 56: BVR Subwatersheds with Sass & Keane (2012) Study Reaches

Prior to the late 1800s, row-crop agriculture in the BVR basin was concentrated on floodplains adjacent to rivers due to deep, fertile riparian topsoil and low-relief topography (USDA-SCS_KES, 1951). By the 1930s, when the population of Marshall and Nemaha Counties were at their highest, tillage, row-crop agriculture land use had become dominant in the BVR basin (Legends of Kansas, 2022). The prevalence of row-crop land use has led to extensive channelization within the catchment, as farmers attempt to facilitate the rapid drainage of their fields. While channelization of the BVR has been done in a piecemeal fashion by farmers and private land owners since the early 1900s, the vast majority of channelization occurred between the 1950's and 1980's in conjunction with state and federal agencies such as the Soil Conservation Service (now NRCS) and the U.S. Army Corps of Engineers (Meade, 2009; Sass & Keane, 2016). Channelization of the BVR has shortened the river from an estimated 114.8 km original length to a measured length of 89.3 km in 1998 (US-COE, 1998). Figure 16, p.46 illustrates the timing and extent of channelization in the BVR upper watershed.

A total of 151 km of the Black Vermillion River (BVR) and its tributaries will serve as the study area (four study channels) for this research, including the entire length of the BVR's primary channel and three of its tributaries (Figure 56). The BVR's primary channel (83 km channel length) includes a portion of the Main Stem and all of the North Fork and will be referred to as the North Fork-Lower Main Stem (NF-LMS) study channel. The three tributaries included as study channels are Irish Creek (IC) (23 km), Weyer Creek (WC) (16 km) and the Main Stem (MS) upstream of the North Fork/Main Stem Confluence (29 km). Cross-sectional and bank profile data collected at nine study

reaches in the upper BVR basin (Figure 56) by Sass & Keane (2012) will be considered. The entire BVR system is relatively low gradient with estimated water surface slopes ranging from 0.0028 to 0.0008 (Sass & Keane, 2012).

The BVR system is typified by incised channels with bank heights ranging from 5.2 m at the Irish Creek 1 study reach to over 8 m in the lower watershed, with dominant bank angles ranging from 20 to 84 degrees. Many steep bank angles are the result of rotational slump or fall, which are the two types of mass wasting most common in Northeast KS (Sass & Keane, 2012). In addition to numerous steep, high banks, most of the BVR and its tributaries flow through remote, privately owned land making the surveying of large sections of the river problematic. Active remote sensing techniques such as LiDAR allow for the quantification of geomorphic change along the riverbanks in a safe and relatively rapid manner (Kessler et al., 2012).

Methods and Methodological Results

Before final DoDs could be produced from repeat LiDAR-derived DEMs and used to estimate amounts of erosion and deposition along the BVR riverbanks, systematic errors needed to be corrected. Figure 57 shows the process for the removal of errors and generation of final BVR riverbank DoDs from 2010 and 2018 for Marshall County and from 2012 to 2018 for Nemaha County.

LiDAR Data

Publicly available LiDAR datasets of large areas are becoming increasingly available, and the datasets used in this study were accessed through the State of Kansas Data Access and Support Center (DASC). Vendor generated LiDAR classified

point clouds and DEMs were available for 2010 and 2018 for Marshall County and for 2012 and 2018 for Nemaha County, with the 2018 data first becoming available on 01/03/2022. The LiDAR point clouds for each year were classified into a number of classes that included ground points; however, building and vegetation classes were not included.

The 2010 Marshall Co. LiDAR data was collected by Surdex Corporation, Chesterfield, MO with a Leica ALS-5011MPIA aerial LiDAR sensor system in February of 2010, with a nominal point spacing of 1.4 m on the ground. Pulse rate and LiDAR footprint were not included in the metadata. “Bare earth” DEMs were processed by the vendor using proprietary software using geoid model 03 and NAD83 UTM Zone 14 coordinate system. In addition, accuracy was assessed by the vendor using 54 checkpoints over a variety of groundcovers; however, neither the individual check point coordinates and elevations nor method and equipment used for point data collection were given in the brief “LiDAR Accuracy Report”. The 2010 overall checkpoint root mean square error ($RMSE_{(z)}$) reported in the Accuracy Report was 0.10 m resulting in a fundamental vertical accuracy ($RMSE_{(z)} * 1.96$) of ± 0.196 m.

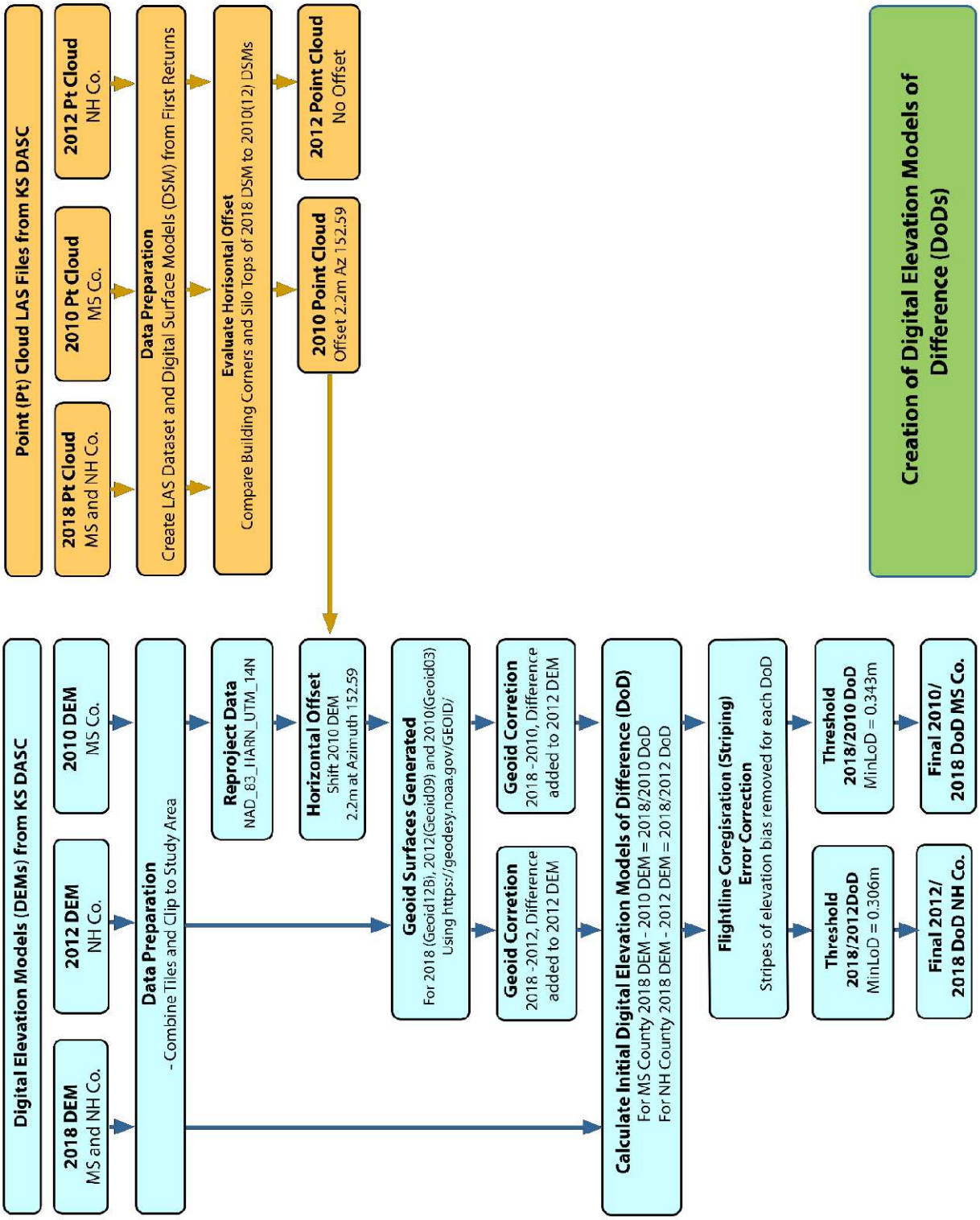


Figure 57: Process for Creation of BVR Riverbank DoDs

The 2012 LiDAR data was acquired by Aero-Metric, Inc. Sheboygan, WI in March, and April of 2012 using Optech Gemini and Leica ALS70 airborne LiDAR systems at a nominal altitude of 2,400 m above ground, with a laser pulse rate of 70kHz and nominal point spacing of 1.4 m. DEMs were generated by the vendor using proprietary software and geoid model 09. The vendor collected location and elevation data on 208 checkpoints using Rapid Static GPS techniques over a variety of land covers and reported RMSE of 0.065 m and std. deviation of 0.63 resulting in a fundamental vertical accuracy of ± 0.1274 m. Horizontal (NAD 83/07 UTM Zone 14) and vertical (NAVD88) coordinates as well as reported vertical checkpoint errors were given in the 2012 metadata.

The 2018 LiDAR data was collected by Atlantic, Inc., Huntsville, AL between March 1, 2018, and April 26, 2018, using a Leica ALS70-HP system, with a pulse rate of 256 kHz and nominal point spacing of 0.71 m. The vendor-generated DEMs utilized geoid model 12B and NAD 83(HARN) UTM Zone 14 coordinate system. The vendor collected 104 ground survey points including 28 LiDAR control points and 76 checkpoints on both vegetated and non-vegetated areas and reported the UTM coordinates, elevations, and elevation errors in their metadata; however, horizontal errors and methods and equipment used for collecting ground survey points were not given. The RMSE for all checkpoints was calculated to be 0.1438 m resulting in a fundamental vertical accuracy of ± 0.2818 m.

Systematic error and bias may be introduced at a number of points during LiDAR data collection and processing and are frequently due to each LiDAR data set being

created within a unique methodology. The 2018 Project Report from Atlantic, Inc. Huntsville, Al. states:

“Consideration should be given by the end user of this dataset to the fact that this LiDAR dataset was developed differently and separately than previous LiDAR datasets that may be available for this geographic location. It is likely that the data in this project was created using different geodetic control, a different Geoid, newer LiDAR technology and more up-to-date processing techniques.”

Previous studies have developed methodology for identifying and correcting systematic errors associated legacy DEMs and subsequent DoDs created with LiDAR data (Schaffrath et al., 2015). Corrections associated with horizontal offset and Geoid model used were applied to the 2010 and 2012 DEMs before DoDs were generated, and correction associated with poor flight line co-registration were applied to the 2010-18 (Marshall Co.) and 2012-18 (Nemaha Co.) DoDs (Kessler et al., 2012; Williams, 2012; Schaffrath et al., 2015). It is important to note that for both the 2010-18 DoD and the 2012-18 DoDs, DEMs supplied by the vendor were used, after corrections, instead of interpolating DEMs directly from points classified as ground points in the LiDAR point clouds, which were also available. Hereafter, the vendor supplied DEMs will be referred to as user DEMs. Kessler et al. (2012) interpolated DEMs using a variety of interpolation methods from data with a similar resolution to the data used in this study and found less than 2 percent standard error in DoD volume calculations due to the interpolation method used, which is supported by other studies (e.g. (Bater & Coops, 2009; Guo, Li, Yu, & Alvarez, 2010). Therefore, I deferred to the interpolation methods used by each of the vendors. (Kessler et al., 2012).

Horizontal Correction

Perhaps because horizontal offset between sequential DEMs can be difficult to quantify, many studies either report the manufacturer minimum error or simply ignore horizontal error (Hodgson & Bresnahan, 2004; Kinzel, Wright, Nelson, & Burman, 2007; Schaffrath et al., 2015). Horizontal errors were not addressed, or even mentioned, in any of the 2010, 2012 or 2018 LiDAR project/accuracy reports.

An initial, uncorrected DoD was created for Marshall (MS) and Nemaha (NH) Counties by subtracting the earlier user DEM (2010 MS and 2012 NH) from the later user DEM (2018). Figure 58 shows the DoD legend that applies to all DoDs in this study. In the Marshall Co. DoD, the river channel and every ravine showing erosion on one aspect and deposition on the opposite evidenced systematic, ubiquitous horizontal error (Figure 59, A). The 2012-2018 DoD for the Nemaha Co. study area did not have the pattern of horizontal elevation bias seen in the 2010-2018 DoD. To facilitate the assessment of horizontal offset between the 2010 and 2012 user DEMs and the 2018 DEM, digital surface models (DSMs) were created for each year from the classified LiDAR point clouds (used by the vendor to produce the user DEMs) using all first returns in Quick Terrain Modeler. DSMs differ from DEMs in that they include natural and man-made structures above the earth's surface such as buildings and tree canopies.

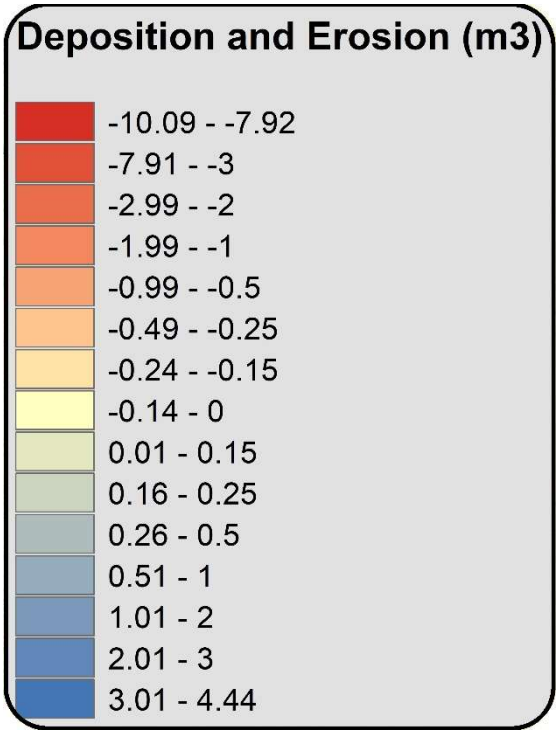


Figure 58: DoD Legend

For each area used in the horizontal offset analysis containing buildings and structures, the DSMs were classified in ArcGIS into two elevation classes such that the buildings and other high structures (> 2 m) were well defined (Figure 60, B and C). A number of points on well-defined structures were digitized in ArcGIS on each of the three DSMs for comparison (Schaffrath et al., 2015). For this study, building corners, points of cone-roofed silos, and a few distinct features of large impoundment levees were used as horizontal offset points. Figure 60 illustrates an area where three building corners were used for horizontal offset points in the 2010 and 2018 DSMs. Lines were created in ArcGIS between each set of corresponding points, from which the magnitude (distance) and angle (direction) of the vector between each set of points could be determined. Initially, a set of 50 points in the Marshall Co. study area (2010-2018) and 30 points in the Nemaha Co. study area (2012-2018) were identified and compared.

Point comparison in the Nemaha Co. did not suggest systematic horizontal bias. Systematic offset was evident in the point comparison of the 2010 and 2018 DEMs. For a more accurate estimation of the systematic horizontal offset between the 2010 and 2018 DEMs, the number of correction point pairs was increased to 197. The distance of offset had a range between 1.8 m and 2.6 m with an average of 2.20 m, and the direction of the offset ranged from 130.58 to 169.51 with an average azimuth of 152.59. The 2010 DEM was shifted by the average horizontal offset distance and direction to better align with the 2018 DEM, which did alleviate the pervasive deposition on one aspect and erosion on the opposite for most of the riverbank noted earlier (Figure 59, B).

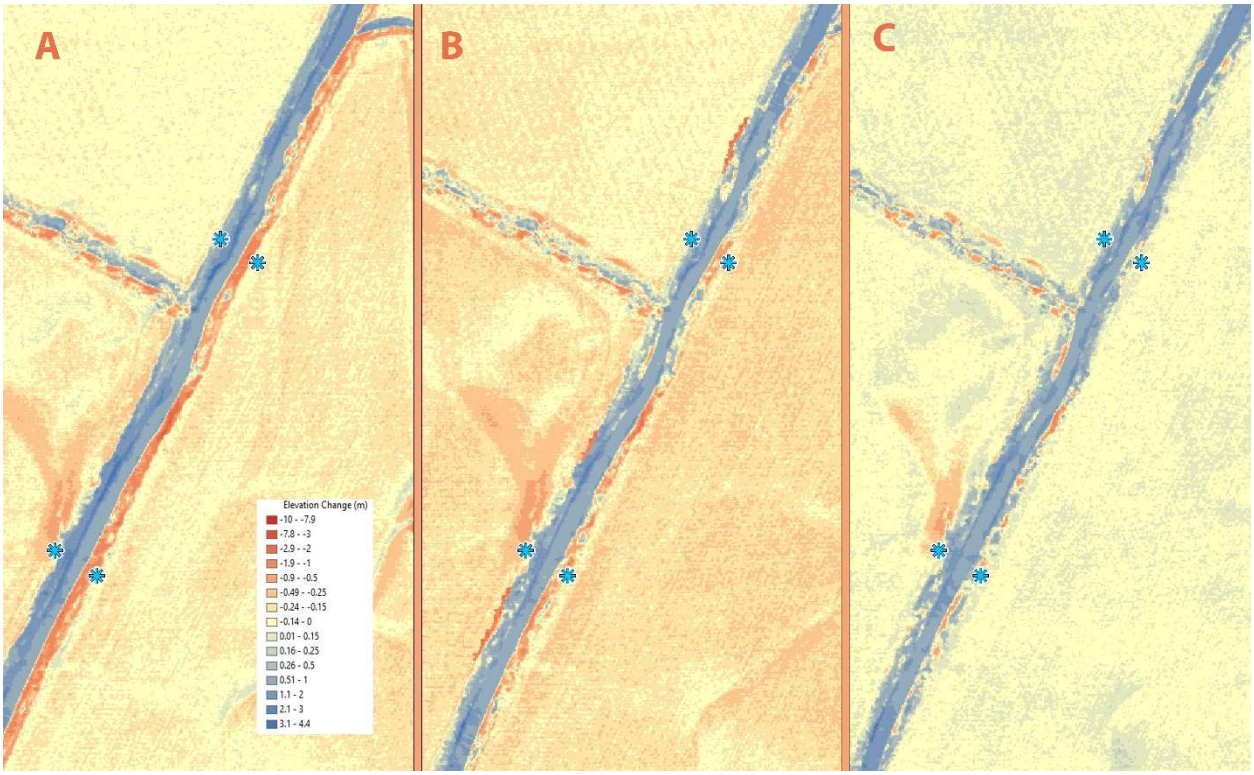


*Figure 59: DoD Correction at Sass & Keane (2012) Study Reach **North Fork 2**: A) Raw uncorrected DoD B) DoD after 2010 DEM horizontal offset and Geoid used corrections and C) after DoD correction for poor flight line coregistration*

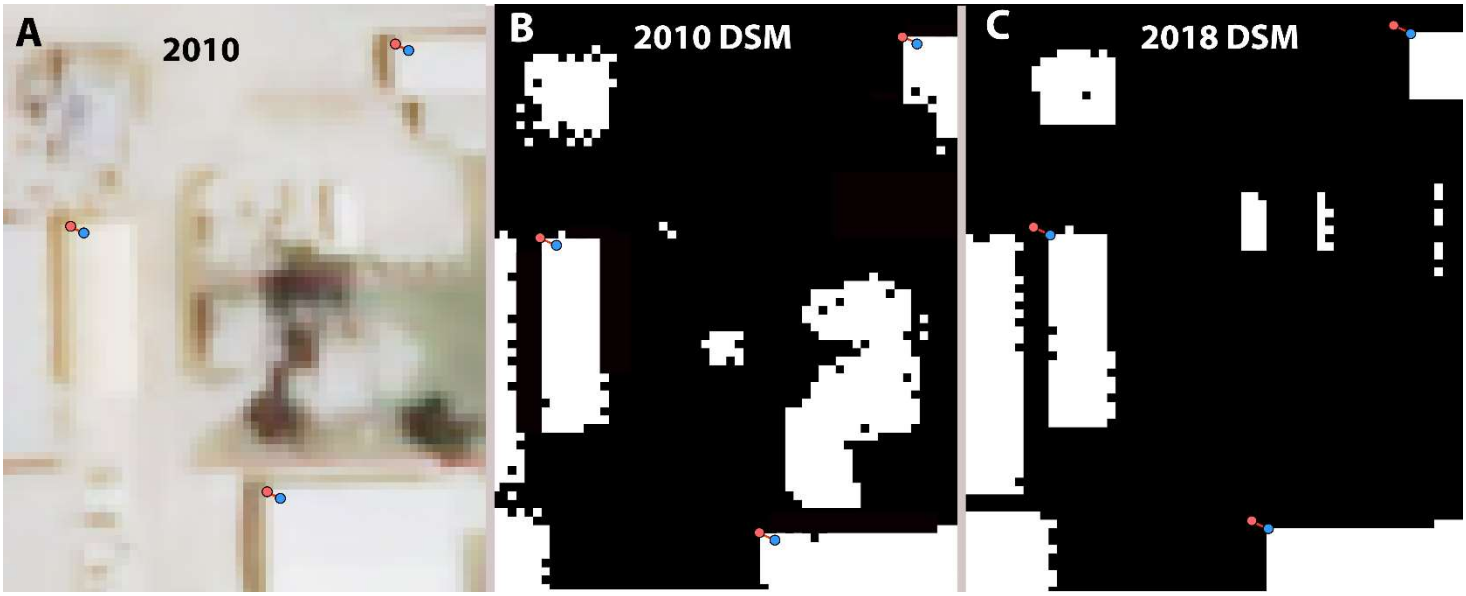


Figure 60: Horizontal Offset Points: (A) 2010 NAIP aerial image with red points indicating building corners (B) 2010 DSM, red points at building corners and (C) 2018 DSM, blue points at building corners: Distance and direction between points was used to determine horizontal offset.

Geoid Correction

According to NOAA's National Ocean Service, "The geoid is a model of global mean sea level that is used to measure precise surface elevations" (NOAA, 2022b), and the National Geodetic Survey (NGS) has released a number of updated models since 1996 (NGS, 2022). DEM and LiDAR dataset metadata indicated different geoid models were applied when converting ellipsoid heights to orthometric heights for each user DEM (GEOID03 in 2010, GEOID09 in 2012 and GEOID12B in 2018). The vertical offset associated with the use of different geoid models DEMs was corrected by first creating a surface of geoid models 03 and 12B for the Marshall Co. (MS) study area and geoid models 09 and 12B for the Nemaha Co. study area. For the Marshall Co. study area, the geoid03 and 12B surfaces were created by generating 10,000 random points (Figure 61) within the study area and entering them into the NGS's Geoid03 and Geoid21B interactive calculators that produce tables of elevation difference between each point and the Geoid surface being referenced (see: https://geodesy.noaa.gov/GEOID/).

In ArcGIS, surfaces were interpolated using IDW (inverse distance weighting) with points created from the NGS tables of geoid elevations, then differenced using the raster calculator tool. The same process was repeated for the Nemaha Co. study area but only using 7,500 random points, as the area is smaller. The Geoid 03-12B difference surface ranged between -0.034 m to 0.082 m (Figure 61), and the Geoid 09-12B difference surface ranged between -0.025 m to .0004 m. The Geoid03-12B and 09-12B difference surfaces were then added to the horizontally corrected 2010 and the 2012 DEMs, respectively.

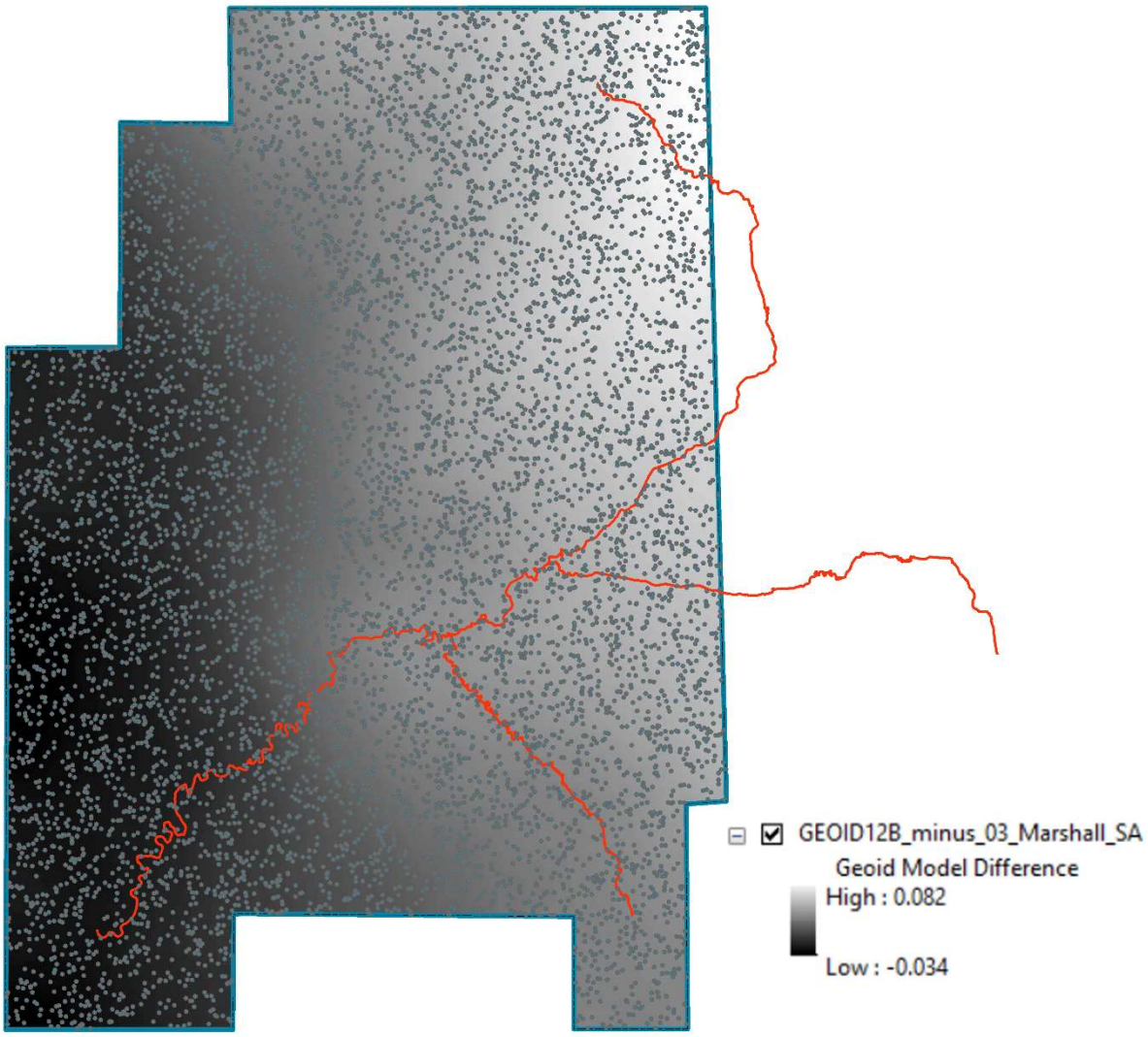


Figure 61: MS Co. Study Area Geoid 03-12B Difference Surface with Random Points

Accuracy Assessment

Before generating revised DoDs with the horizontally and Geoid corrected 2010 DEM and the Geoid corrected 2012 DEM, the DEMs were assessed for vertical accuracy to the extent possible without additional independent checkpoints. The RMSE and fundamental vertical accuracies discussed earlier were the result of analysis on raw LiDAR data performed and provided by the vendor. The 2018 metadata provided UTM coordinates and elevations for 104 checkpoints consisting of LiDAR control points,

vegetated area points and non-vegetated points. Of the 104, 52 checkpoints fell within the area of the available 2010 LiDAR data and were used for accuracy assessment for the 2018 and 2010 DEMs.

For the 2018 user DEM, the elevations of checkpoints given in the metadata were compared to the corresponding point elevations of the 2018 user DEM mosaicked from tiles downloaded from KS DASC, which were not altered or corrected in any way. While the metadata indicated the vendor checkpoint error analysis was based on a DEM surface, there were some slight differences in the reported DEM elevations and downloaded DEM elevations. The difference in the 2018 reported checkpoint elevations and the 2018 user DEM ranged between -0.119 m and 0.156 m with an average of 0.015 m. To assess DEM accuracy over time, the 2010 user DEM elevations were extracted to the 2018 checkpoints. Comparison of the 2010 user DEM checkpoint elevations to the elevations reported in the 2018 metadata resulted in errors ranging from -0.368 m to 0.393 m with a median of 0.025 m and average of 0.038 m, which is well below the vendor guaranteed error of ± 0.15 m and indicates good agreement between the two DEMs. It is important to note that only a portion of the checkpoints were taken on hard surfaces, which are less likely to experience elevation change.

For the 2012 DEM, accuracy between reported and user DEM error and accuracy across time was assessed using 40 checkpoints from the 2012 LiDAR project collected over a range of land covers, for which the 2012 metadata provided checkpoint coordinates, elevations, and elevation errors. The reported error for the 40 checkpoints was compared to the corresponding point elevations on the 2012 user DEM resulting in differences ranging from -0.145 m to 0.029 m with an average of 0.02 m, again below

the vendor guaranteed error. For accuracy assessment over time between the 2012 and 2018 user DEMs, the 2018 user DEM elevations were extracted to the 2012 checkpoints. Vertical checkpoint errors between the 2012 checkpoint elevations and the 2018 user DEM elevations ranged from -0.349 m to 0.209 m with a median of -0.032 m and average of -0.028 m.

For a more qualitative assessment of the alignment between the corrected 2010 and 2012 user DEMs and the 2018 user DEM, three cross sections from the Sass & Keane (2012) study reaches surveyed with a differential laser level in 2007 and total station in 2021 were compared to the same cross sections on the 2010 and 2018 user DEMs. Two cross sections were located in the Marshall Co. study area (Irish Creek 3 and North Fork 2) and one in the Nemaha Co. Study area (BVR Main Stem 2) (Figure 56, p.147). Left and right bank pin horizontal locations for each cross section were collected using a Juniper Archer Field PC plus Hemisphere GPS with sub-meter accuracy. The points were entered into ArcGIS and the cross section data exported from an interpolated line created between the left and right bank pins in 3D Analyst. All four cross sections were imported into Civil 3D for comparison. The cross sections surveyed in 2007 and 2021 utilized an arbitrary elevation of 30.48 m for the left bank pin. For comparison, the left bank pin elevations of the 2010 and 2018 DEM cross Sections were set to 30.48 m and the remaining points adjusted accordingly. While the user DEM cross sections are not as detailed, they do fit within the cross sections surveyed in 2007 and 2021 using traditional surveying methods (Figure 62).

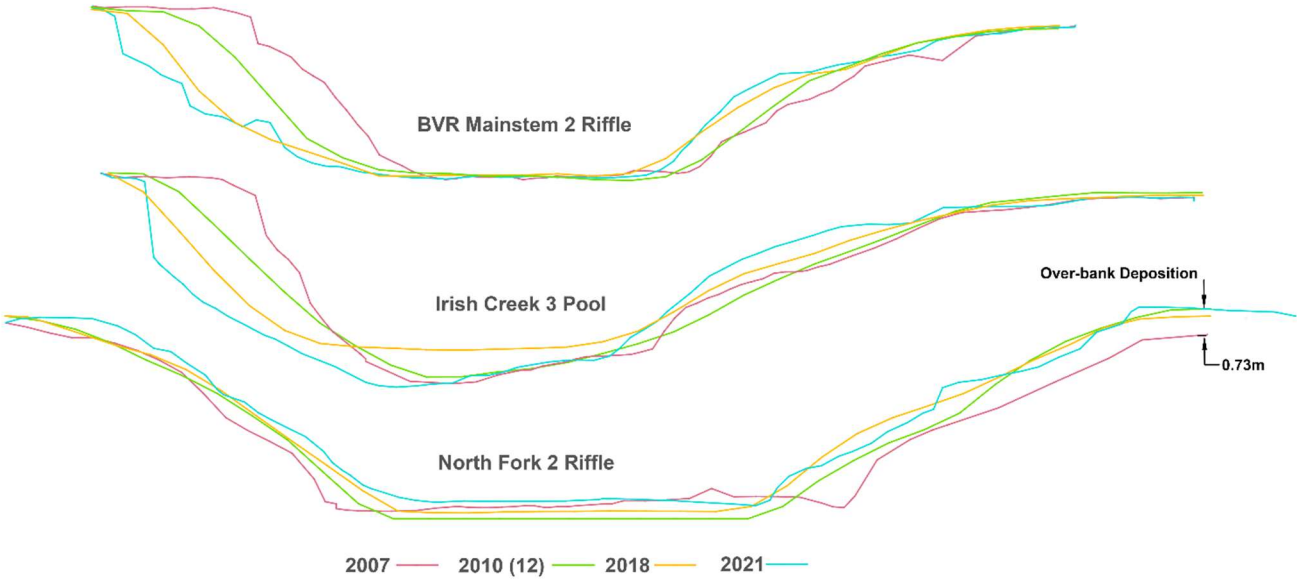


Figure 62: Comparison of 2007 and 2021 traditionally surveyed cross sections and 2010 and 2018 DEM generated cross sections at three Sass & Keane (2012) study reaches (Figure 56, p.147)

Flight Line Co-Registration Error

Semi-final DoDs for Marshall (2010-18) and Nemaha (2012-18) Counties were produced with the corrected 2010 and 2012 DEMs and 2018 DEM. While patterns of erosion and deposition at a local scale no longer indicated systematic horizontal bias, at the county scale, large stripes of elevation bias running north and south were severely evident in the 2010-18 DoD (Figure 63, A) and somewhat evident in the 2012-18 DoD. Such strips of elevation are unlikely due to any natural erosional or depositional processes. Vendors generally collect LiDAR datasets in strips along flightlines that overlap approximately 30% (Schaffrath et al., 2015). This pattern of elevation bias strips was also seen in the data of Schaffrath et al. (2015) and was contributed to the poor coregistration of flightlines during data collection. Poor coregistration occurs when imprecise determination of calibration parameters leads to discrepancies between flightlines known as coregistration error. Such errors are common in older “legacy”

datasets such as those from 2010 and 2012 (Schaffrath et al., 2015). Coregistration errors were not evident in the 2010 and 2012 individual DEMs but were revealed in the DoDs when differenced from the more recent and likely more precisely calibrated 2018 data (Schaffrath et al., 2015).

The most accurate methods for correcting strips of elevation bias include recalibration of the raw GPS and IMU (inertial measurement unit) data, and another utilizes the “local slope and local elevation differences between adjacent points in the flightline overlap area to realign flightlines” (Schaffrath et al., 2015 p. 337). Unfortunately, neither the flight line nor raw data necessary for such methods were available. Following the methods of Schaffrath et al. (2015), correction surfaces for both study areas were generated from random points (728,465 for Marshall Co. and 384,149 for Nemaha Co.) created in areas where it is believed little substantial elevation change had occurred. In the BVR watershed and along the BVR riverbanks, the predominant landcover is terraced row crop fields. For this study, areas of little change were determined using two criteria 1) areas of low slope (< 8%) and 2) areas with little change in slope (< 2%) between the earlier 2010-12DEMs and the later 2018 DEM. Steep areas within each DEM were omitted, as they are more likely to experience surface erosion. Areas with a notable change in slope (> 2%) were also omitted, as it is believed these areas are likely to have experienced erosion or deposition either due to natural processes or farmer’s grading equipment. Slope difference between the earlier (2010-12) and the latter 2018 DEMs was determined on a cell-by-cell basis.

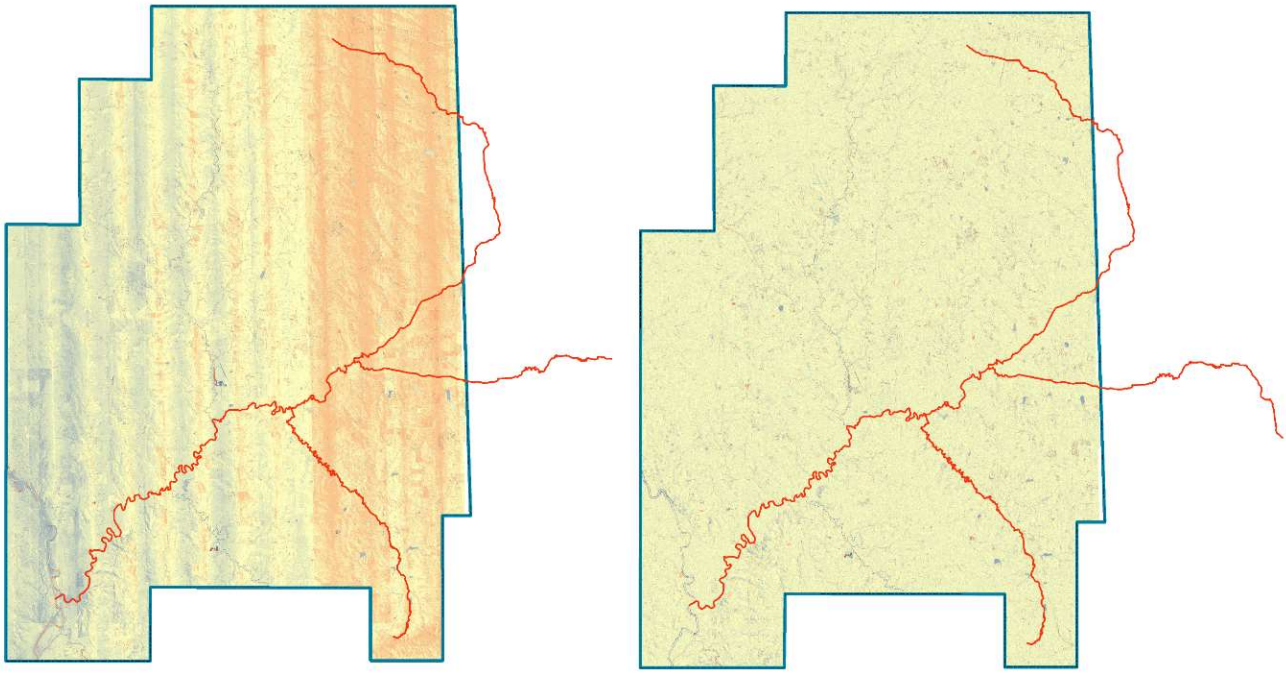


Figure 63: 2010 - 2018 DoD, A) stripes of elevation bias due to poor flightline coregistration and B) Corrected: See Legend Figure 58, p. 154: Dark red (erosion) and blue (deposition) indicate elevation bias due to poor flightline co-registration, while lighter yellow and blue indicate areas of little change.

In Figure 64, the pink color represents areas with less than 2 percent change in slope between the 2010 and 2018 DEMs where random points were generated. Figure 64 illustrates A) a relatively flat field where little change in slope has occurred, B) a terraced field where change in slope, likely due to erosion, had occurred at the edge of each terrace, and C) areas of severe changes in slope likely due to the regrading of fields and drainage areas using heavy equipment.

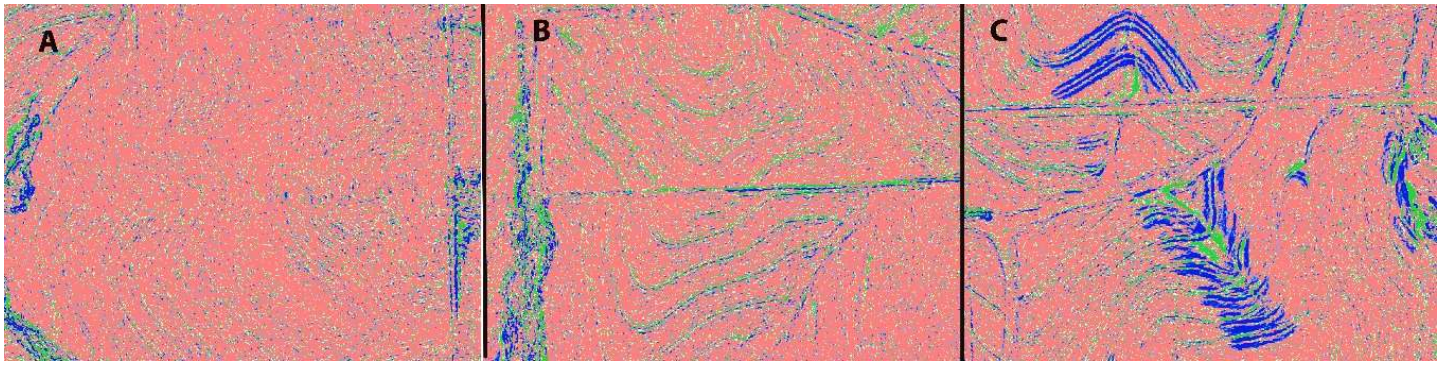


Figure 64: Examples of Change in Slope in BVR Agricultural Fields, A) where little has changed over the field, B) slight change along edge of field terraces and C) Change due to grading with heavy equipment.

Areas within 100 m of the BVR riverbank were also excluded, as areas of evenly distributed deposition resulting from overbank flooding had been observed, especially along the North Fork channel. The process of creating random points in areas believed to have experienced little elevation change was repeated for the 2012-2018 DoD. The DoD values were extracted to the random points and error surfaces generated in GIS using the spherical model of ordinary kriging (method of interpolating continuous surface from a set of points) with a 5 m-fixed search radius and a minimum of 12 points (Schaffrath et al., 2015), which was then subtracted from the respective DoDs (created with the horizontally and Geoid corrected user DEMs). The final DoDs (Figure 63, B) no longer had evidence of striping, yet retained the elevation variability along the river channel (Figure 59, p.156, C) (Schaffrath et al., 2015). At North Fork 2 shown in Figure 59, the riffle cross section surveyed between 2007 and 2021 supports the large amount of deposition seen along the reach (Figure 48, p.127).

DoD Error Propagation, Probabilistic Thresholding & Riverbank Volume Change

Every DEM contains inherent error. When assessing the accuracy of a DoD, the error from both DEMs being used must be considered and propagated. While spatially variable error propagation is possible, it requires the coordinates and errors for each checkpoint, which was not available for the 2010 data; therefore, a spatially uniform approach was used. When subtracting two DEMs to produce a DoD, the root sum square of error can be used as an estimate of the combined error then used as the minimum level of detection (MinLoD) (Williams, 2012):

$$MinLoD_1 = \sqrt{(\varepsilon DEM_1)^2 + (\varepsilon DEM_2)^2} \quad (1)$$

Where εDEM_1 and εDEM_2 are the root mean square error (RMSE) of the checkpoints for each DEM being compared. The RMSE for the 2010 and 2018 DEMs were 0.10 m and 0.1438 m respectively resulting in a $MinLoD_1$ = **0.172 m** for the 2010-2018 DoD: therefore, only erosion and deposition < -0.172 m or > 0.17 m was considered significant (Williams, 2012). Similarly, the RMSE for the 2012 DEM was 0.065 m resulting in the $minLoD_1$ = **0.154 m** for the 2012-2018 DoD. Equation 1 represents the 68% confidence interval (*t* = 1).

As discussed in Williams (2012), a more rigorous approach to DoD production is the use of probabilistic thresholding at a user defined confidence interval, which is 95% for this study (Brasington et al., 2000). "Probabilistic thresholding provides a technique to remove systematic bias throughout the filtering of elevation changes based on the confidence that detected change is real" (Williams, 2012 p. 8). For thresholding at the 95% confidence interval, equation 1 is revised to:

$$MinLoD_2 = t\sqrt{(\varepsilon DEM_1)^2 + (\varepsilon DEM_2)^2} \quad (2)$$

Where *t* it the critical t-value for a two-tailed Student's t-distribution for a 95% confidence interval (1.96) and all other variables are as in equation 1 (Williams, 2012). Using equation 2, the $MinLoD_2$ for the 2010-2018 DEM (Marshall Co.) and 2012-2018 (Nemaha Co.) DoDs were determined to be **0.343 m** and **0.306 m,** respectively. All estimated amounts of erosion and deposition were reported at the 68% and 95% confidence intervals. Final DoDs reflecting application of $MinLoD_1$ and $MinLoD_2$ were generated using the geomorphic change detection (GCD) add-in for ArcGIS (see:

gcd.joewheaton.org), which automates the process of applying uniform error propagation and thresholding.

The riverbanks for the BVR primary channel and three additional tributaries included in this study were manually digitized primarily using slope grids created from the 2018 DEM in ArcGIS. It was determined through trial and error that isolating slopes ≥ 15% (8°) was best at bank delineation when visually compared to hillshade and aerial maps. The highest water breaklines were used as bottom of bank when present in the DEMs; however, the only portion of the BVR and tributaries included in this study large enough for the use of breaklines were the portions of the North Fork-Lower Main Stem (NF-LMS) in Marshall Co. After the top of bank was determined, an additional 2-m buffer was added to ensure the inclusion of the entire top of bank. The portion of the thresholded DoDs within each riverbank was extracted (clipped). Each extracted riverbank DoD was separated into areas of erosion and deposition facilitating the extraction of volume change using zonal statistics in ArcGIS. Since the DoD resolution was 1m x 1m, the elevation change (m) for each 1-m cell was equal to the volume change (m^3). To determine overall patterns of erosions and deposition along each channel, each channel centerline was divided into 1-km segments, buffered, and the portion of the respective DoD extracted before zonal statistics were used to calculate the amount of erosion and deposition in each 1-km segment.

Volume Change within Woody Vegetation Classes

Figure 65 shows the process for assessing the presence of woody riparian vegetation on BVR riverbank erosion and deposition discussed below.

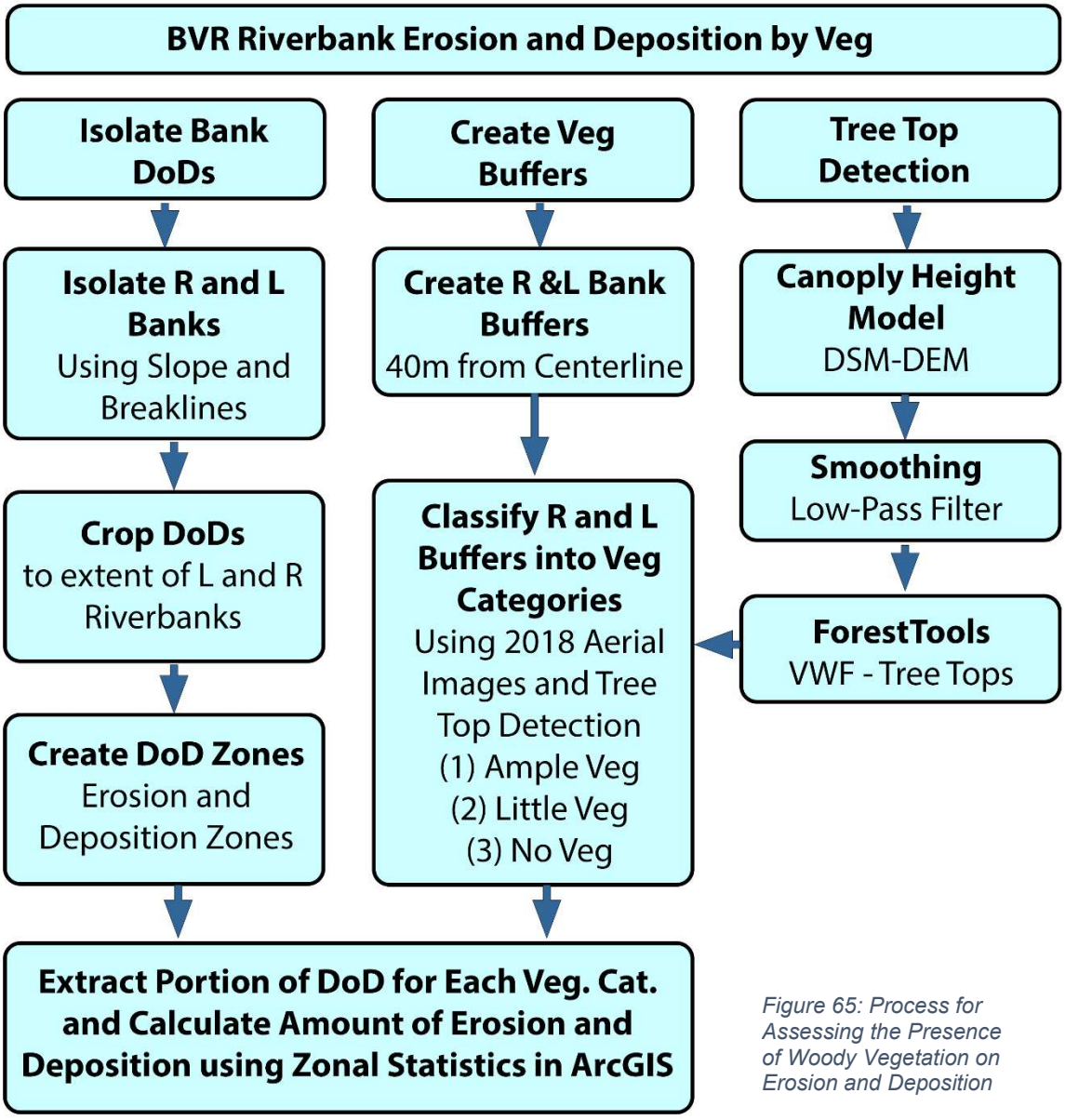


Figure 65: Process for Assessing the Presence of Woody Vegetation on Erosion and Deposition

While assessing the effect of the presence and amount of woody vegetation on 18 study banks throughout the upper BVR system (Figure 3, p.12), Sass & Keane (2012) classified the riparian vegetation at each study bank into three categories: 1) *No woody vegetation* "included those banks influenced by tillage agriculture, brome pasture, and shallow-rooted herbaceous plants only", 2) *Little woody vegetation* "included some woody vegetation, corridor widths usually less than two rows of trees with little age or species diversity", and 3) *Ample woody vegetation* included those areas with strong influence from surrounding large riparian vegetation" (Sass & Keane, 2012). A right and left bank 40-m buffer was created for NF-LMS, IC, MS and WC and classified into the three categories used in Sass & Keane (2012) (Figure 66), and classification was based on the bank condition in 2018. To assist with the vegetation classification, individual treetop detection analysis was conducted using the R package "ForestTools" and a high-resolution canopy height model (CHM) generated from each LiDAR dataset. A 1-m resolution CHM was generated in Quick Terrain Modeler by subtracting each year's DEM from

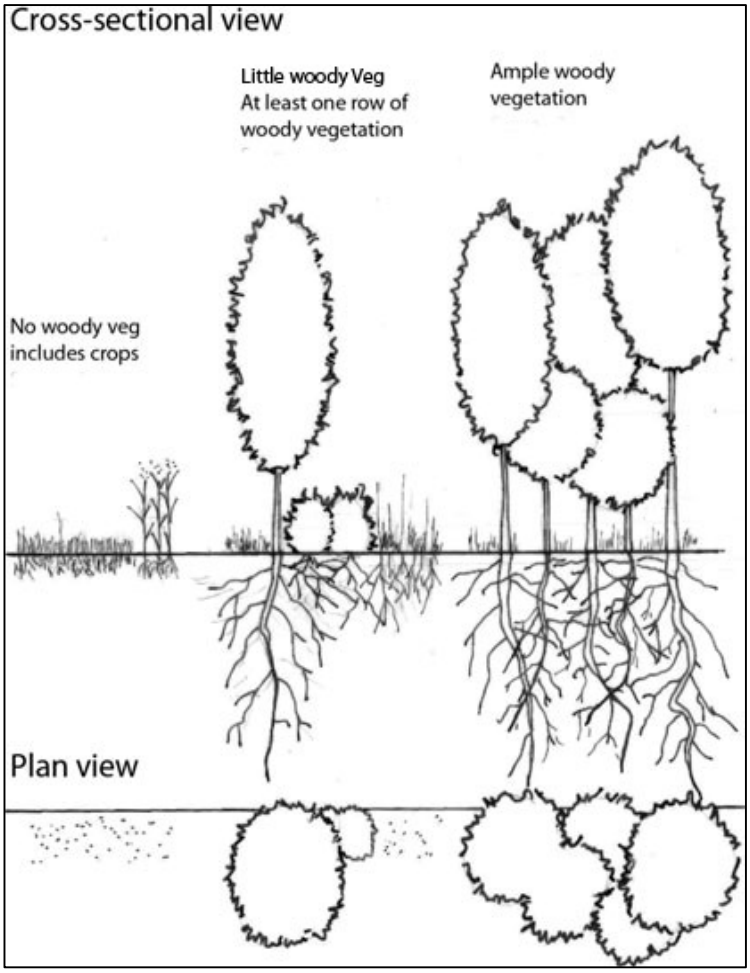


Figure 66: Vegetation Categories adopted from Sass & Keane (2012)

its respective DSM, previously generated for the horizontal offset analysis, and then applying a low pass filter in ArcGIS, which has been shown to reduce errors of commission in individual tree crown detection (Lindberg & Hollaus, 2012; Silva et al., 2022). Smoothing was made even more necessary because the LiDAR data was collected during leaf-off conditions.

ForestTools implements a *variable window filter* (vwf) algorithm consisting of a moving circular window of varying size that scans canopy heights within the window of each cell and if that cell is found to be the local maxima, it is tagged as a treetop (Plowright, n.d.). The radius of the window for each cell is a function of the cell's height and is dependent on the assumption that a relationship exists between tree heights and tree crown spread (Popescu & Wynne, 2004). The window size function was determined by regressing the average height to the average crown spread of the 18 tree species found in the BVR riparian corridor by Sass & Keane (2016, Table 5, p. 68), resulting in the equation (R^2 = 0.85):

$$Crown\ radius\ (m) = 0.5486 \times Tree\ Height(m) + 1.7136$$

ForestTools was run on the 2010, 2012 and 2018 CHM generating a point shapefile of treetops for each year. Because the window was set using approximate heights and crown spread of mature trees, the vwf would not be effective in detecting smaller, younger trees; therefore, a minimum height of 4.5 m was set in ForestTools. It is important to note the treetop point shapefiles were only visually and qualitatively assessed using NAPI aerial images from each year (Figure 67).



Figure 67: Woody Vegetation Classification Assisted by Individual Tree Top Point Analysis

Once the right and left bank buffers of each study channel had been classified into one of the three vegetation categories, amounts of erosion and deposition in the 2010-18 and 2012-18 DoDs within each category were summarized in ArcGIS.

Effect of Understory and Overstory Density on Erosion and Deposition Rates

As noted earlier, ample riparian vegetation has been shown to stabilize banks and protect banks from the erosive forces of flowing water (Schumm, 1973; Thorne, 1990; Gurnell, 1997; Genet et al., 2005; Pollen, 2007; Sass & Keane, 2012); however, the results of Chapter III show a number of severely eroding banks with ample mature riparian vegetation yet little understory vegetation (e.g., Irish Creek 1 pool (Figure 68) and Main Stem 2 riffle and pool). In contrast, low rates of bank erosion were observed at cross sections where low, dense, and young woody vegetation was present along the bank (e.g., Irish Creek 2 pool and riffle (Figure 68) and North Fork 1 riffle right bank). It was hypothesized that the density of understory woody vegetation is negatively

correlated to bank erosion rates. If such a correlation did exist, it could help guide restoration efforts by providing evidence for the need to restore understory woody vegetation even when ample mature riparian vegetation is present. The effect of both understory and overstory riparian vegetation density on riverbank erosion and deposition was evaluated.

Two principal LiDAR point cloud vertical stratum metrics often used when analyzing forest density and structure, are overall relative point density (ORD) and normalized relative point density (NRD), and both assume that as vegetation density increases so does the likelihood of interaction with LiDAR pulses (Campbell, Dennison, Hudak, Parham, & Butler, 2018). With ORD, the number of points between heights *i* and *j* is divided by the total number of points within a defined area; however, with NRD the number of points in a given stratum is only compared to the total number of points in that stratum and below (Campbell et al., 2018):

$$ORD_{(ij)} = \frac{\Sigma_i^j n}{\Sigma_o^k n} \qquad (1) \qquad\qquad NRD_{(ij)} = \frac{\Sigma_i^j n}{\Sigma_o^j n} \qquad (2)$$

NRD is theoretically more robust with varying canopy conditions and densities (USDA, 2021); however, overhead canopy is less influential in leaf-off conditions, as was required for all three LiDAR datasets included in this study. All three LiDAR datasets were collected in late winter (February through April) when herbaceous understory vegetation would be at its lowest, although dead stems and debris from the previous summer's growth could still be present. Therefore, to capture primarily woody understory vegetation density, the understory stratum was set between 1.25 m to avoid

herbaceous litter and fallen limbs and 4.5 m, which is near the approximate mature height for some of the larger understory woody species observed by Sass & Keane (2016) (e.g., *Cornus drumundii, Zanthoxylum americanum).* The overstory was set as greater than 4.5 m, and as always with the uppermost stratum, the ORD and NRD are the same measure (Campbell et al., 2018). The density of the treetops determined using ForestTools was also considered as a measure of more mature riparian vegetation density, given the tree sizes used in the window size function in the variable window filter.

To facilitate the calculation of the understory and overstory NRD, a normalized point cloud was created using above ground level (AGL) analysis in Quick Terrain Modeler, where all ground points are changed to zero and all other point elevations become distance above the ground plane. Next, 3-m resolution point count grids indicating the number of points in each stratum were created for all necessary stratum (all points, points above 4.5 m, all points below 4.5 m and points between 1.25 m and 4.5 m) using the *clipping pane filtering* and *generate grid statistics* tools in Quick Terrain Modeler. Subsequently, 3-m resolution maps of the understory and overstory NRD maps were generated with the point count rasters using equation 2 in ArcGIS raster calculator. Figure 68 shows understory density along the IC1 and IC2 Sass & Keane (2012) study reaches.

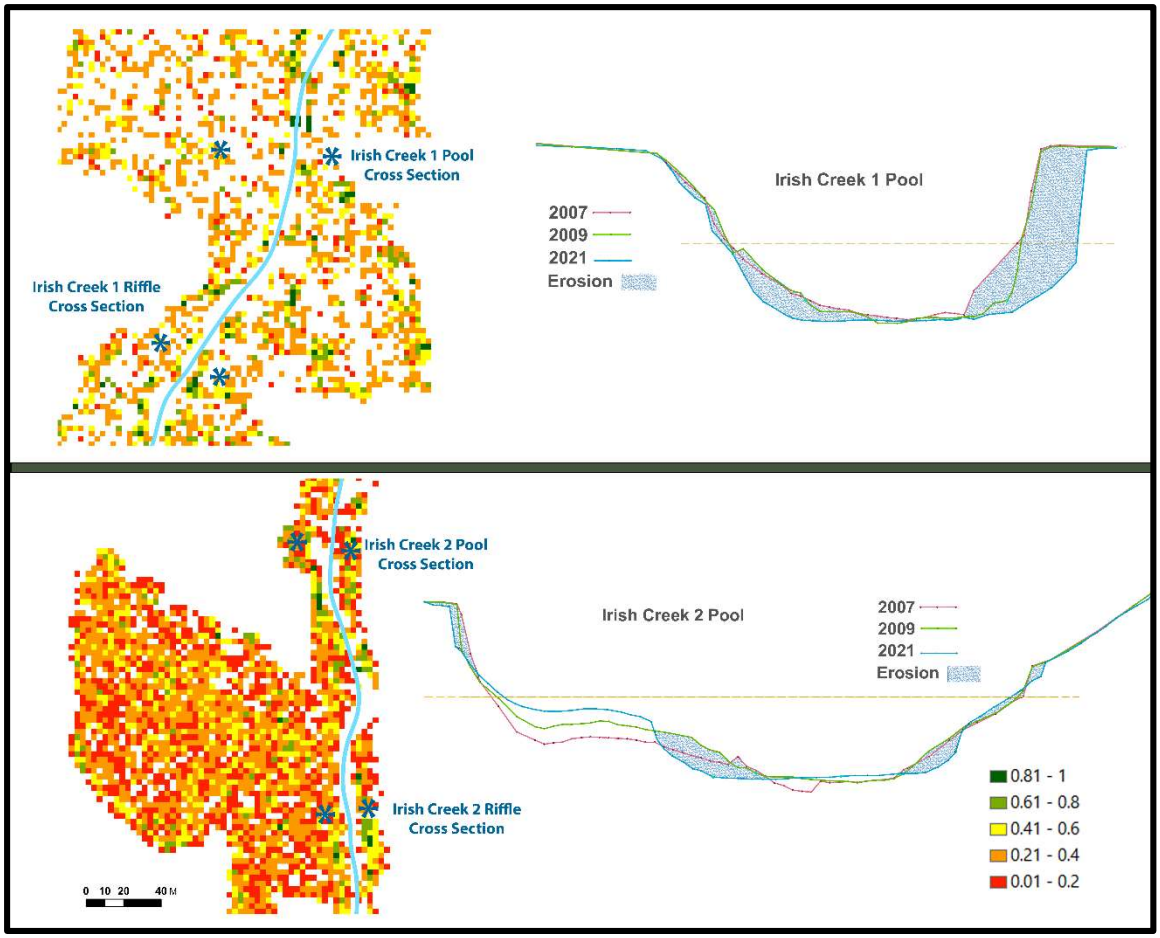


Figure 68: Understory NRD and Pool Cross Sections at IC1 and IC2 (Red (top) and Blue (lower) asterisk indicate approximate location of cross sections)

To facilitate assessment of the relationship, if any, of overstory and understory vegetation density along each channel to erosion and deposition, each channel centerline was divided into 100 m segments. From this divided centerline, right and left bank buffers were generated. For the understory NRD, right and left bank buffers were offset from the centerline to 4 m beyond the top of bank for each segment and included vegetation density at the top of bank as well as along the riverbank where slopes allowed for in-channel vegetation. For the overstory NRD and tree top density, the 100-m segments were buffered 15 m beyond the top of left and right banks, as larger, mature trees would have a more extensive root structure than lower, dense vegetation.

For each of the right and left bank 100-m segments, the amounts of erosion and deposition (dependent variables) were extracted from each of the DoDs. In addition, the variables associated with point cloud density listed in Table 22 (independent variables) were calculated from the point count and NRD raster grids for each 100-m left and right bank segment and each year (2010, 2012 and 2018) in ArcGIS. An initial Pearson correlation matrix was generated for all variables for each of the four channels (NF-LMS, MS, IC, and WC). When significant correlation was observed with either erosion or deposition, a stepwise linear regression was conducted using all independent variables.

Table 22: NRD and Tree Top Density Independent Variables

Variable	Description
Ttop_Den (2010, 2012, and 2018)	Tree top density = number of tree tops in a given 15-m buffer polygon / area of the polygon
Change_Ttop_Den	Change in tree top density from 2010 to 2018 for areas in MS Co. and from 2012 to 2018 in NH Co.
Under_NRD (2010, 2012, and 2018)	NRD = number of lidar points between 1.25m and 4.5m / total numer of points at or below 4.5m
Und_NRD_Change	Change in understory NRD from 2010 to 2018 for areas in MS Co. and from 2012 to 2018 in NH Co.
Over_NRD (2010, 2012, and 2018)	NRD = average NRD for each right and left bank 15m buffer
Over_NRD_Change	Change in overstory NRD from 2010 to 2018 for areas in MS Co. and from 2012 to 2018 in NH Co.

Results and Discussion

Repeat LiDAR scans of large areas provide an opportunity to monitor river geomorphology at a system-wide scale and will undoubtedly become more accurate and widely available as improving technology allows for more efficient and less costly data collection and processing. Horizontally and Geoid-corrected LiDAR-derived DEMs from 2010 (Marshall Co.) and 2012 (Nemaha Co.) were differenced from a 2018 DEM to created DoDs for each county that were further corrected for poor co-registration of flight lines. The DoDs were then thresholded at the 68 and 95 percent confidence intervals to produce final DoDs, which were then used to assess how the presence and density of woody riparian vegetation may affect riverbank erosion and deposition rates. It is important to note that besides representing 25 percent less time, the Nemaha Co. 2012-18 DoD represents 36% fewer bankfull flows (1.5-year recurrence interval, period of record 1954-2020) than the Marshall Co. 2010-18 DoD. Of the 13 bankfull flows that occurred between 2010 and 2018, five happened before 2012.

Volume Change

Table 23 displays the amount of erosion and deposition at the 68 and 95 percent CI for each study channel for both the Marshall Co. DoD (2010-18) and the Nemaha Co. DoD (2012-2018). Figure 69 also illustrates deposition and erosion for each study channel in Marshall and Nemaha Counties at 95% CI. Note that total net erosion for the Marshall Co. study area (2010-2018) increased when the MinLoD was raised from 0.17 m (CI 68%) to 0.343 m (CI 95%), due to deposition (15%) being more sensitive to the MinLoD increase than erosion (10%). Net erosion increased in Nemaha Co., but only by a small amount. For both study areas and similar to the results of Kessler et al.

(2012), deposition being more sensitive to an increase in the MinLoD indicates “a larger portion of small elevation changes are attributed to deposition and thus deletion of areas with small changes in elevation results in an increase in volume change” (Kessler et al., 2012 p. 203). In contrast, the majority of large elevation changes resulted from erosion (Kessler et al., 2012). This pattern of deposition and erosion is expected in the BVR, as riverbank deposition is the result of suspended sediment settling out on the receding limb of the storm hydrograph and large amounts of riverbank erosion result from mass wasting (fall and rotational slump), where large amounts of bank material can move in a relatively short time (Sass & Keane, 2012). It is important to report volume change, especially deposition, at the 68% CI, as it is unlikely that all deposition lost when the MinLoD is increased is error.

Table 23: Erosion and Deposition by Subwatershed and County

Bank Erosion and Deposition by Subwatershed

			Confidence Level 68%					Confidence Level 95%				
	Sub-watershed	Length (m)	Ero (m^3)	Dep (m^3)	Net Ero/ Dep (m^3)	Ero/km (m^3)	Dep/km (m^3)	Ero (m^3)	Dep (m^3)	Net Ero/ Dep (m^3)	Ero/km (m^3)	Dep/km (m^3)
Marshall County (2010-2018)	Irish Creek	23	91,965	47,113	-44,852	3,998	2,048	81,825	35,906	-45,919	3,558	1,561
	Main Stem	9	32,320	19,075	-13,245	3,591	2,119	27,497	17,696	-9,801	3,055	1,966
	NF-LMS	68	346,384	390,560	44,176	5,094	5,744	313,675	335,240	21,566	4,613	4,930
Total		100	470,668	456,748	**-13,921**	4,707	4,567	422,997	388,842	**-34,154**	4,230	3,888
Nemaha County (2012-2018)	Main Stem	20	75,848	36,967	-38,881	3,792	1,848	68,536	28,158	-40,378	3,427	1,408
	NF-LMS	15	61,277	40,340	-20,936	4,085	2,689	54,723	33,139	-21,584	3,648	2,209
	Weyer Creek	16	87,018	49,601	-37,416	5,439	3,100	77,377	41,697	-35,680	4,836	2,606
Total		51	224,142	126,908	**-97,234**	4,395	2,488	200,635	102,994	**-97,642**	3,934	2,019

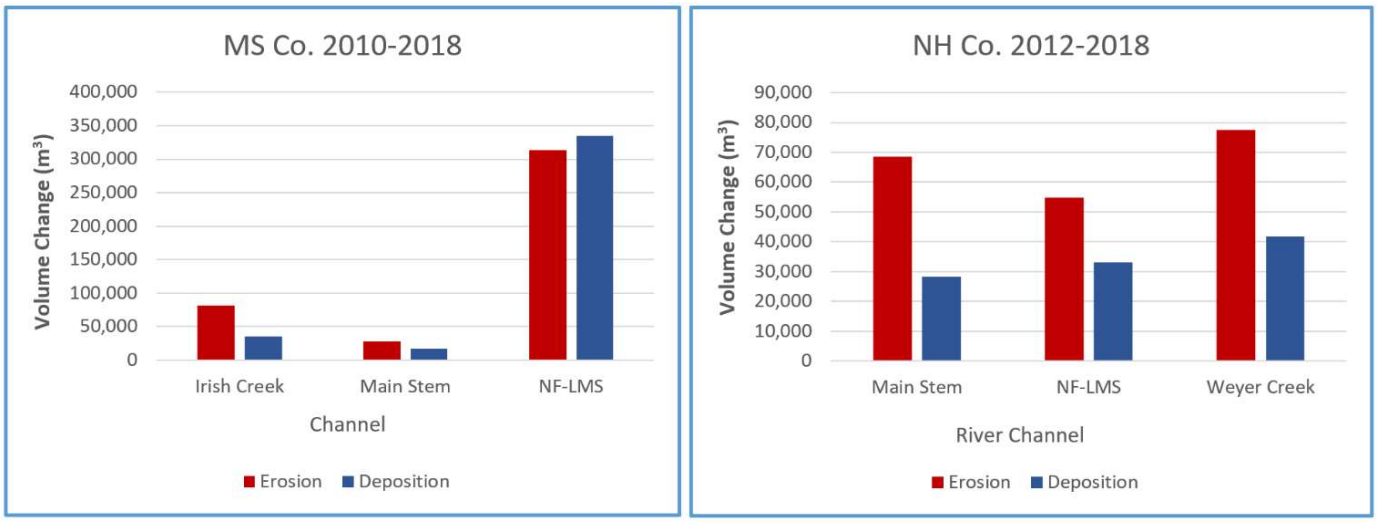


Figure 69: Volume Change for Marshall and Nemaha Co. DoDs at the 95% CI

Calculating erosion and deposition for each 1-km segment of each study channel allows comparison of erosion and deposition rates among the various study channels. Patterns and amounts of erosion and deposition for Irish Creek (IC), Main Stem (MS) and Weyer Creek (WC) were discussed in detail in Chapter III; however, for Chapter IV, the North Fork study channel was expanded to include the entire BVR primary channel consisting of the North Fork plus the Main Stem downstream of the North Fork-Main Stem confluence (Figures 70 and 72). Considering the Marshall and Nemaha Co. DoDs together, all three tributaries, MS, IC, and WC, had a net negative volume change of -50,179 m^3, -45,919 m^3 and -35,680 m^3, respectively, for a total of -131,778 m^3. Within Marshall Co., the NF-LMS experienced high erosion and deposition per 1-km segment, 4,613 m^3 and 4,930 m^3 respectively, resulting in net deposition of 21,566 m^3. It is important to note that when calculating net erosion/deposition along the NF-LMS channel in Marshall Co., 100% of the deposition is discounted from NF-LMS erosion, yet much of the deposited material likely originated from sources upstream other than the banks of the NF-LMS channel including fields, gullies, and banks of tributaries

(Kessler et al., 2012). Within Nemaha Co., the NF-LMS rate of erosion and deposition per 1-km segment are more in line with the three tributaries, as erosion is approximately 1.5 times greater than deposition. Within some segments, high rates of erosion and deposition may be due directly to human disturbance (Figure 71).

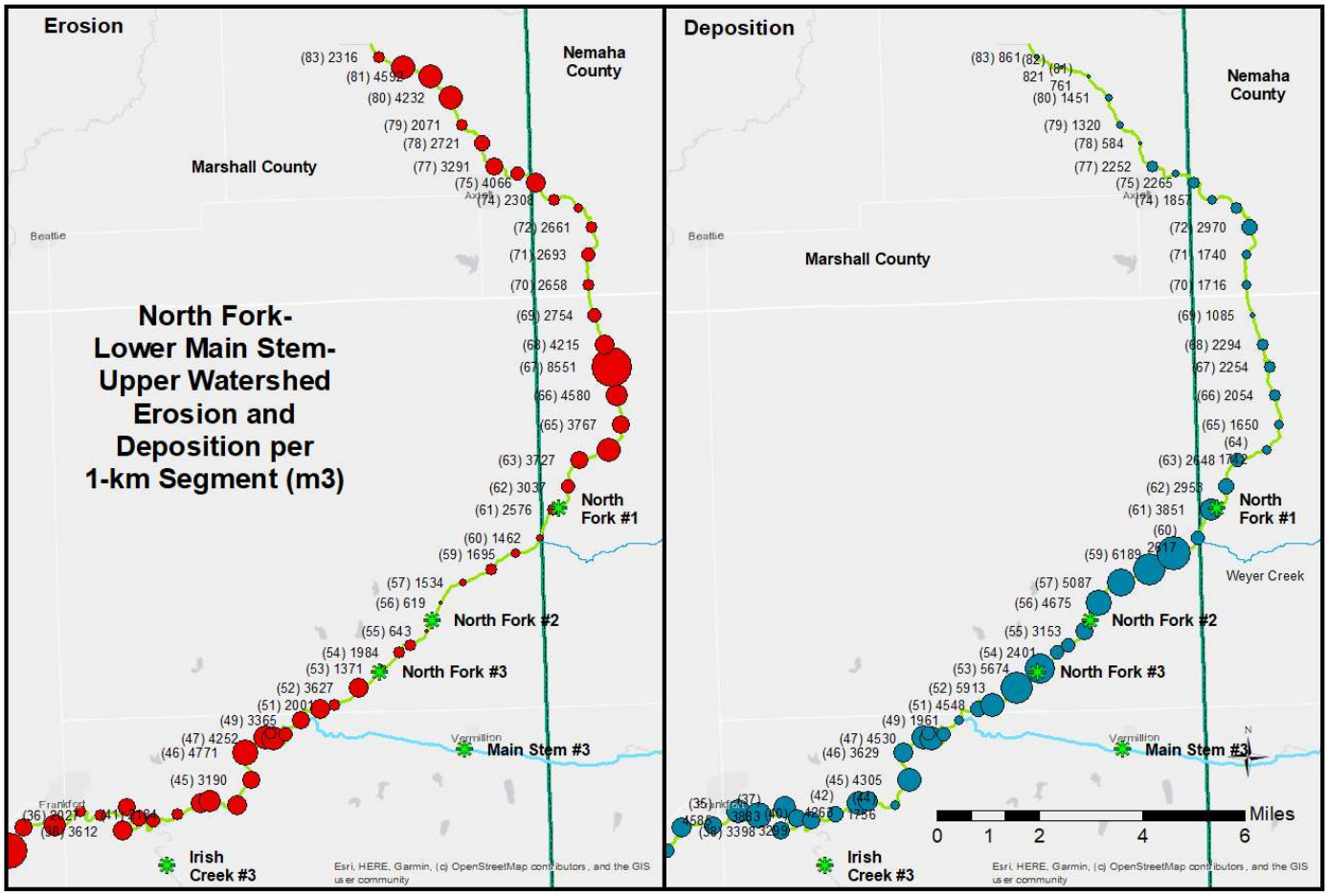


Figure 70: NF-LMS Erosion and Deposition (CI 95%) Upstream of Frankfort (#) is segment number.



Figure 71 Examples of Human Induced Erosion and Deposition: A) Debris pile from the removal of riparian vegetation resulting in deposition along northeast riverbank and B) Area of severe erosion due to grading along river for unknown reasons.

As seen in Figure 70, deposition outpacing erosion along the NF-LMS banks begins downstream of the confluence of the NF-LMS and Weyer Creek, which was shown in Chapter III, to be producing excessive sediment. The high rate of deposition indicated in the vicinity of the North Fork 2 Study Reach in Figure 59, p.156 is supported by the pool and riffle cross sections surveyed between 2007 and 2021 (Chapter III). High 1-km rates of erosion and deposition in the NF-LMS in Marshall Co. are skewed by an area with high rates of erosion in the lower watershed (segments 18-21, Figure 72) and an area further downstream with high rates of deposition (segments 1-7, Figure 72). Figure 73 shows an area of high erosion within 1-km segment #19 of Figure 72 due to downstream meander migration and sinuosity development. Segments showing heavy deposition (Figure 72, Segments 1-7) are located within a low lying and flood prone portion of the Tuttle Creek Wildlife Area managed by the Kansas Department of Wildlife

& Parks and thus protected against direct human alteration of the riverbanks and riparian corridor.

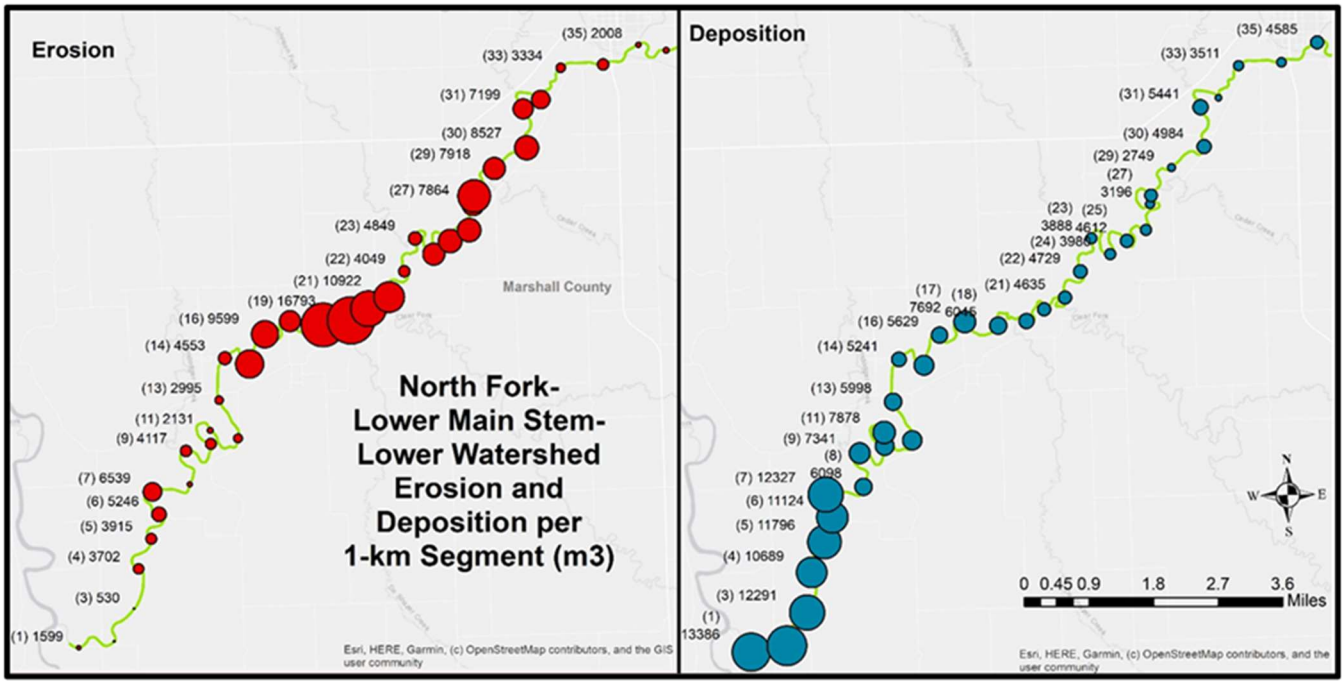


Figure 72: NF-LMS Erosion and Deposition (CI 95%) Downstream of Frankfort (#) is segment number.

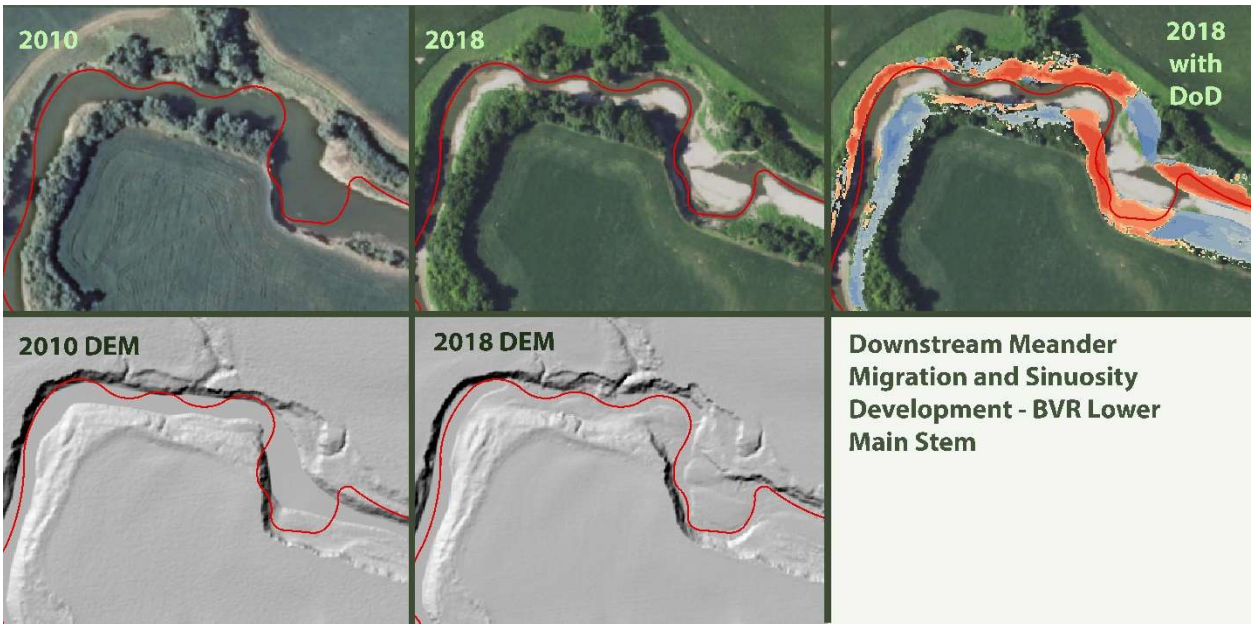


Figure 73: NF-LMS Area of High Erosion due to Downstream Meander Migration and Sinuosity Development (Segment 19 of Figure 74): Red line is approximate flow line in 2018.

Weyer Creek produced the highest amount of erosion per-km of any study channel (4,836 m^3) and produced just 22.3% less net erosion than IC even though its water shed is 61% smaller and the DoD represented two fewer years of change. High rates of erosion along Weyer Creek may be due to numerous instances of human-caused disturbance found throughout the channel. For example, Figure 74 illustrates a reach of WC that was channelized sometime between 2012 and 2014 shortening a 1,200-m length of river to approximately 500 m, which likely led to channel adjustment both up and downstream.

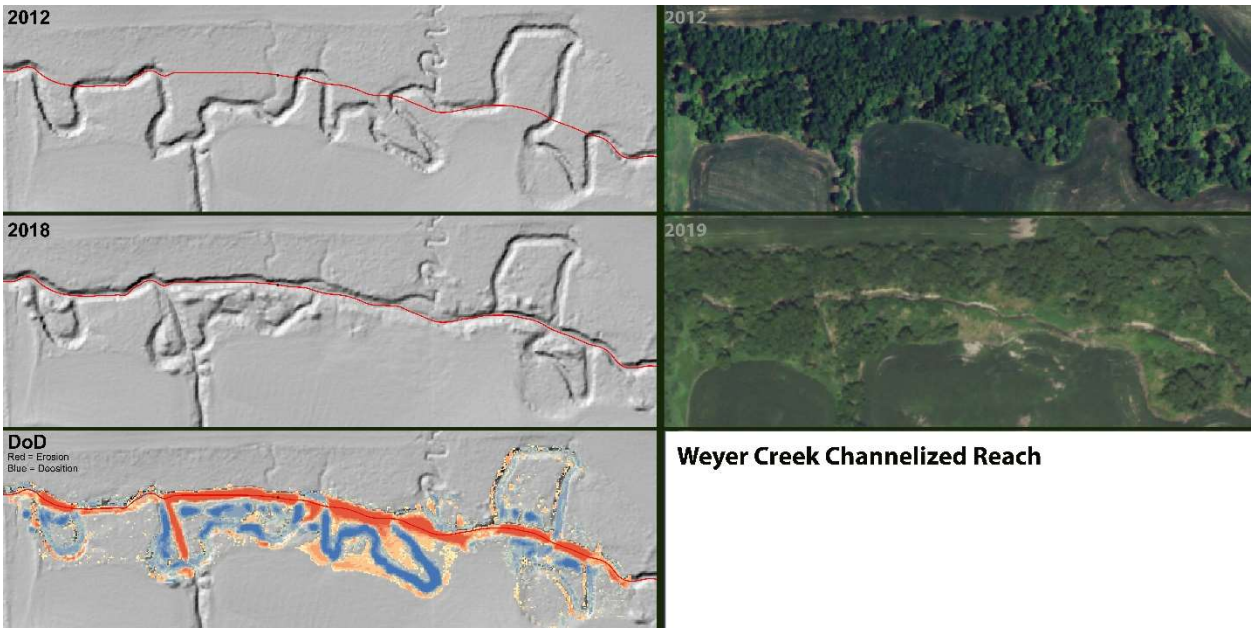


Figure 74: Channelized Reach of Weyer Creek: Red line is approximate flow line in 2018.

Keane & Sass (2017) utilized various channel evolution models and riverbank retreat rates reported in Sass & Keane (2012) to estimate the annual and total amount of sediment expected to be produced as each subwatershed's channel undergoes adequate widening to allow a stable channel form at a new, lower elevation. Keane & Sass (2017) estimated the annual sediment yields of Irish Creek, Main Stem and North

Fork were compared to rates of erosion in this study. Keane & Sass (2017) estimated the annual sediment yield of Irish Creek to be between 2,530 m^3/km and 1,058 m^3/km. However, for the 8-year period of the 2010-2018 DoD, the average annual erosion rate along IC was estimated to be 500 m^3/km (CI 68%). The difference between Keane & Sass (2017) sediment yield estimates and erosion estimates in this study for Main Stem and North fork were similar to that of Irish Creek. This rather large discrepancy could be due to a number of factors, such as unidentified errors in the 2010 and 2018 DEMs and subsequent DoD, erosion below the MinLoD thresholds not being included, or unusually high bank retreat rates between 2007 and 2010 due to the large number (12) of bankfull flow events during that time.

Volume Change by Amount of Woody Vegetation

Tables 24 and 25 and Figures 75 and 76 show amounts of erosion and deposition within each study reach and vegetation category for Marshall Co. (2010-2018) and Nemaha Co. (2012-2018). Looking first at Table 24 and Figure 75, we see that in Marshall Co., erosion per meter along banks with no woody vegetation is 2.88 times higher than erosion per meter along banks where little or ample woody vegetation is present. However, this may be a bit misleading, as the rate of erosion per meter of no woody vegetation in the NF-LMS study channel is influenced by the area of high erosion in the lower watershed (Figure 72, Segments 14-31) discussed earlier. Moving downstream between segments 32 and 31 of Figure 72, the drainage area, and associated discharge, jumps 45% due to the large tributary Robidoux Creek that was not included in this study, due to time constraints, resulting in a much larger channel

with higher banks. In this lower section of the NF-LMS study channel, areas void of woody vegetation within sinuous reaches produce large amounts of erosion that are not indicative of the channel upstream of the Robidoux-Main Stem confluence. IC and MS also have high rates of erosion per meter of bank with no woody vegetation compared to ample and little vegetation; however, these study channels only contain 11 percent of the total bank length in Marshall Co. with no woody vegetation. In addition, erosion along no woody vegetation banks in IC and MS originates from a few severely eroding banks.

Table 24: Marshall County Erosion and Deposition by Amount of Riparian Woody Vegetation

Marshall County Erosion and Deposition by Bank Vegetation 2010-2018										
			68% (m^3)				95% (m^3)			
Veg	Study Channel	Length (m)	Dep	Ero	Dep/m	Ero/m	Dep	Ero	Dep/m	Ero/m
Ample	IC	28,897	30,061	53,231	1.04	1.84	24,808	47,973	0.86	1.66
	MS	6,624	8,325	9,922	1.26	1.50	5,829	6,614	0.88	1.00
	NF-LMS	47,085	136,238	102,173	2.89	2.17	114,323	90,553	2.43	1.92
	Total	82,606	174,624	165,326	**2.11**	**2.00**	144,960	145,140	**1.75**	**1.76**
Little	IC	16,523	15,946	32,777	0.97	1.98	12,390	29,483	0.75	1.78
	MS	9,892	13,605	16,939	1.38	1.71	10,962	14,222	1.11	1.44
	NF-LMS	68,356	193,955	138,534	2.84	2.03	163,836	121,819	2.40	1.78
	Total	94,770	223,505	188,249	**2.36**	**1.99**	187,187	165,524	**1.98**	**1.75**
No	IC	1,410	929	5,958	0.66	4.23	738	5,734	0.52	4.07
	MS	1,214	549	5,506	0.45	4.54	406	5,227	0.33	4.31
	NF-LMS	20,578	70,451	111,457	3.42	5.42	64,189	105,950	3.12	5.15
	Total	23,201	71,929	122,921	**3.10**	**5.30**	65,333	116,911	**2.82**	**5.04**

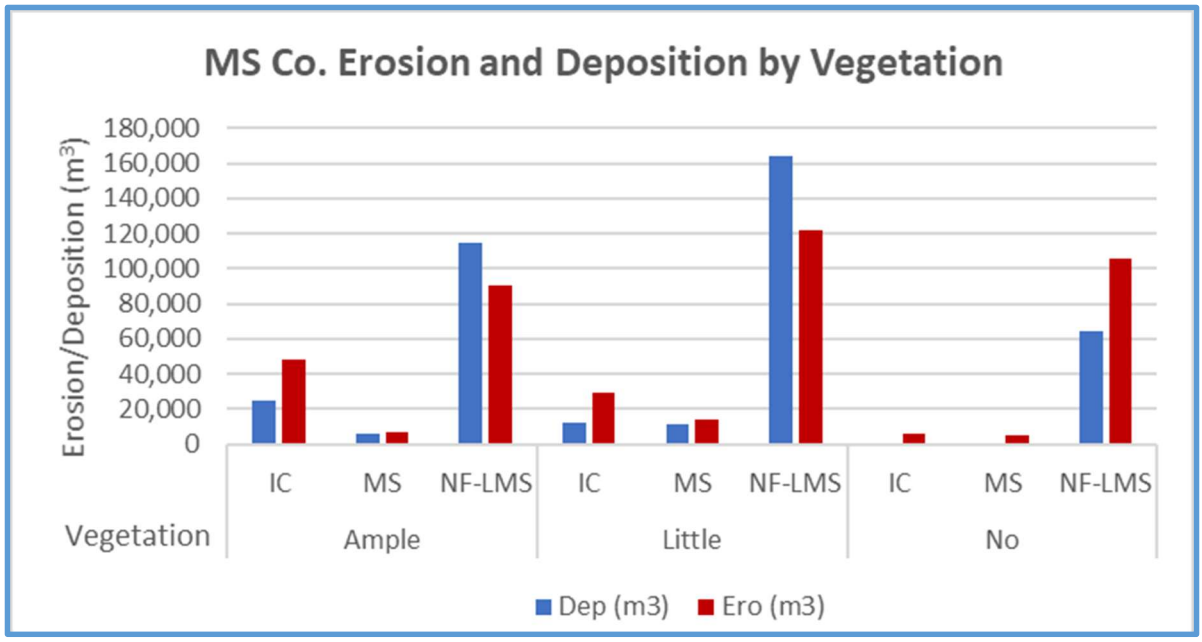


Figure 75: Marshall Co. Erosion and Deposition by Amount of Vegetation (CI 95%)

Rates of deposition per meter of bank length in Marshall Co. are consistently less than erosion except in the NF-LMS ample and little vegetation categories. In the IC and MS study reaches, we see the rate of deposition per meter is significantly lower along banks with no woody vegetation compared to banks with ample or little vegetation. In contrast, in the NF-LMS the rate of deposition per meter along banks with no woody vegetation is higher than when little or ample vegetation is present. As with the NF-LMS rate of erosion along banks with no woody vegetation, the rate of deposition is likely elevated due to the area of high deposition in the lowest part of the watershed (Figure 72, Segments 1-7). In the lower BVR watershed flooding is more common, which may be compounded by "back watering" of Tuttle Creek Reservoir when water

levels are high. Many banks in the lower watershed have experienced high amounts of deposition while being void of woody vegetation.

Looking at Table 25 and Figure 76, the rate of erosion per meter of bank length along banks with no woody vegetation in Nemaha Co. is higher than banks with ample and little woody vegetation by 30% and 57% respectively; however, this difference is significantly less than in Marshall Co. This difference may be due to the fact that the MS, WC and NF-LMS study channels in Nemaha Co are either head waters or in the upper watershed where the channels are smaller and/or the fact that the Nemaha Co. DoD represents two fewer years of change and five fewer bankfull events than the Marshall Co. DoD. In the MS study channel, erosion per meter along banks with ample vegetation is higher than when little vegetation is present. Figure 77 shows the MS2 Sass & Keane (2012) study reach with ample riparian vegetation and significant amounts of erosion. In addition, Figure 78 shows how patterns of erosion on one bank and deposition on the opposite bank observed at the pool and riffle cross sections between 2007 and 2021 (Chapter III) agree with same patterns seen in the 2012-2018 DoD.

Table 25: Nemaha County Erosion and Deposition by Amount of Woody Vegetation

Nemaha County Erosion and Deposition by Bank Vegetation 2010-2018										
			68% (m^3)				95% (m^3)			
Veg	Bank	Length (m)	Dep	Ero	Dep/m	Ero/m	Dep	Ero	Dep/m	Ero/m
Ample	Weyer	6,338	5,832	16,174	0.92	2.55	4,592	14,005	0.72	2.21
	MS	11,850	13,274	24,114	1.12	2.03	10,173	21,876	0.86	1.85
	NF-LMS	5,064	7,717	8,852	1.52	1.75	6,224	7,757	1.23	1.53
	Total	23,253	26,823	49,140	**1.15**	**2.11**	20,990	43,638	**0.90**	**1.88**
Little	Weyer	8,822	16,044	22,373	1.82	2.54	13,525	19,574	1.53	2.22
	MS	24,061	21,761	38,924	0.90	1.62	16,474	34,411	0.68	1.43
	NF-LMS	16,122	21,774	26,262	1.35	1.63	17,926	22,658	1.11	1.41
	Total	49,005	59,579	87,559	**1.22**	**1.79**	47,924	76,643	**0.98**	**1.56**
No	Weyer	15,026	17,542	36,095	1.17	2.40	13,825	31,754	0.92	2.11
	MS	4,428	3,769	13,737	0.85	3.10	2,825	12,863	0.64	2.90
	NF-LMS	9,247	13,100	27,617	1.42	2.99	11,061	25,589	1.20	2.77
	Total	28,702	34,411	77,450	**1.20**	**2.70**	27,711	70,206	**0.97**	**2.45**

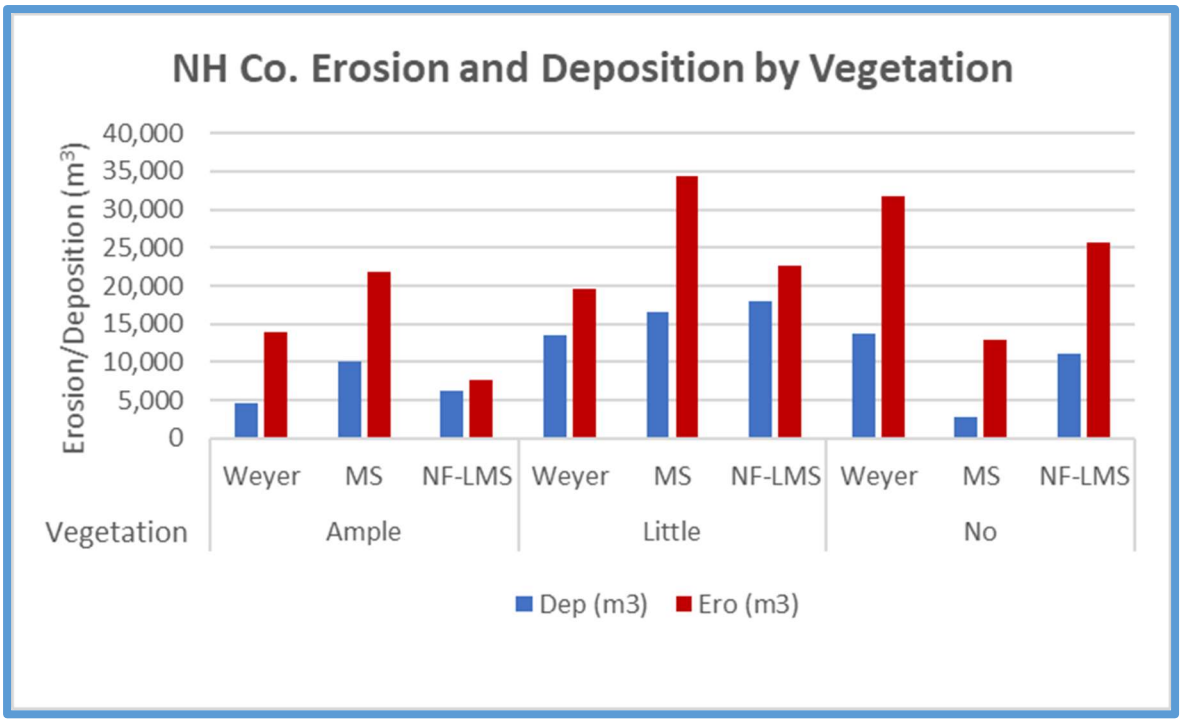


Figure 76: Nemaha Co Erosion and Deposition by Amount of Vegetation (CI 95%)



Figure 77: Sass & Keane (2012) Main Stem 2 Study Reach with 2012-2018 DoD

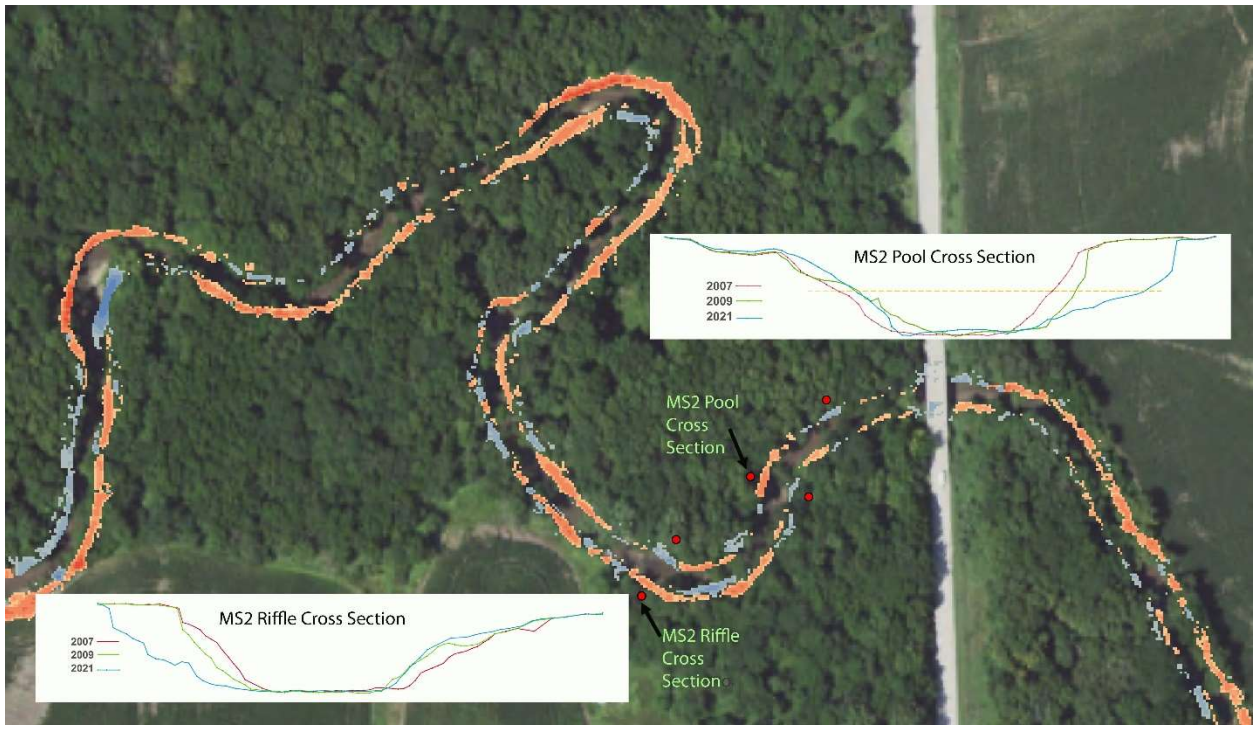


Figure 78: Sass & Keane (2012) Main Stem 2 Cross Sections with 2012-2018 DoD

Perhaps the most notable element of Table 25 is that along the WC study channel, the rate of erosion per meter of bank is almost the same across all vegetation categories. This amount of pervasive erosion throughout the entire WC channel may be due to the high degree of human disturbance seen through the channel noted earlier. In addition to the channelized reach discussed earlier, numerous other instances of human disturbances can be seen along WC. Figure 79 shows a second, smaller area of channelization along WC conducted by the landowner in late 2012 or early 2013.

Figure 80 shows a reach along Weyer Creek where the riparian buffer was removed from the north side of the creek sometime between 2012 and 2019, and the 2012-18 DoD indicates severe erosion along the same bank. Removal of riparian vegetation between 2012 and 2017-19 can also be seen at a number of other locations along WC.

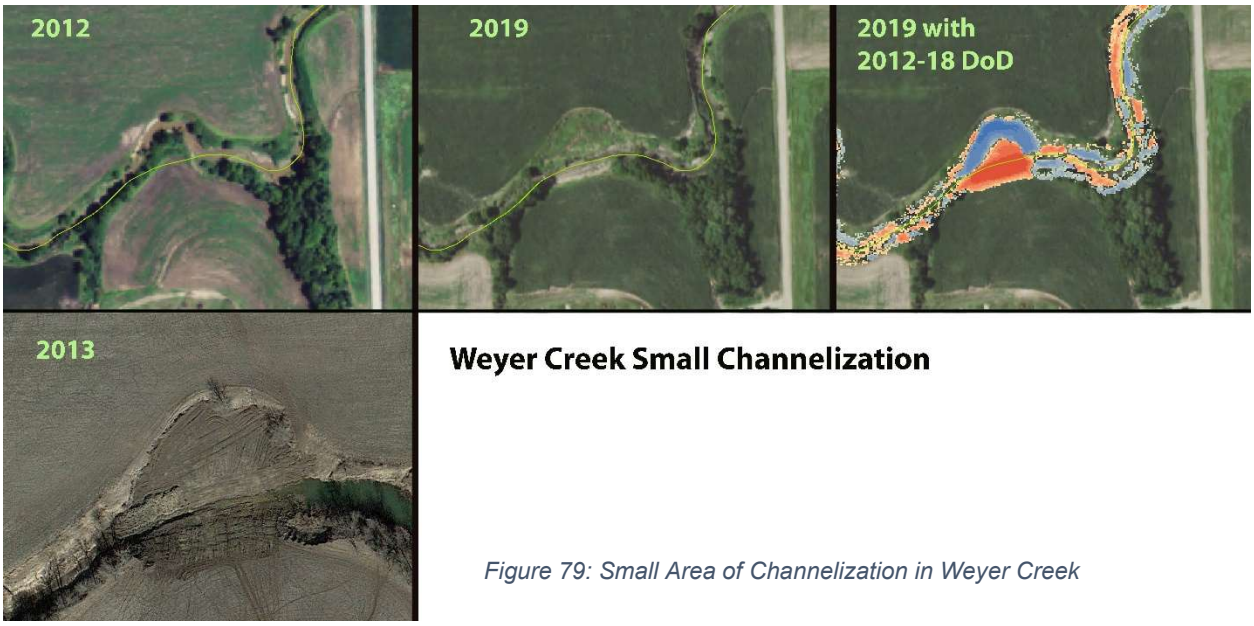


Figure 79: Small Area of Channelization in Weyer Creek



Figure 80: Area of Weyer Creek with Riparian Vegetation Removed and High Erosion

Sass & Keane (2012) monitored 18 study banks within 9 study reaches throughout the upper BVR watershed (7 having no woody vegetation, 5 having little

vegetation, and the remaining 6 having ample veg) and found annual bank retreat rates of -0.45 m, -0.11 m, and -0.13 m, respectively. As with the comparison of overall sediment yields to erosion calculated in this study, the Sass & Keane (2012) annual bank retreat rates for every vegetation category were significantly higher than rates of erosion calculated with LiDAR data in this study. In Marshall Co., the annual rate of bank retreat at banks with no, little, and ample vegetation, was 0.13 m, 0.04 m, and 0.04 m, respectively and in Nemaha Co. 0.08 m, 0.05 m, and 0.06 m, respectively. Note the difference between the vegetation categories is not as extreme in Nemaha Co., which includes Weyer Creek (not included in Sass & Keane, 2012) and the upper reaches of the Main Stem that were shown to be experiencing high rates of erosion even when ample riparian vegetation is present.

Overall, along banks void of woody vegetation, erosion rates are higher and deposition rates lower; however, a large amount of erosion is still occurring in areas with ample vegetation, especially in the IC and NF-LMS study channels, which may be due to the channel evolution of the BVR. As noted in Chapter III, the BVR is in the process of adjusting to changes in its flow regime resulting from changes in land use and channelization. Evidence of widening coupled with evidence of waning incision and aggradation suggest the channel is moving from a phase of incision and widening to rapid widening with aggradation. Widening of the channel results in increasing width/depth ratios, and “as the W/D ration value increases (i.e., the channel grows wider and shallower), the hydraulic stress against the banks also increases and bank erosion is accelerated” (Rosgen, 1996 p. 5-22). This increase in near-bank hydraulic stress leads to undercutting of woody vegetation resulting in the vegetation becoming large

woody debris within the channel, which was observed in numerous locations throughout the BVR during this research. In addition, in-channel large woody debris may result in accelerated, localized bank erosion by increasing near-bank velocities as water is directed around the debris.

Effect of Understory and Overstory Vegetation Density

For erosion and deposition along each study channel, a Pearson correlation matrix was generated for each of the two dependent (erosion and deposition) and all independent (Table 22, p.174) variables associated with the 100-m left and right bank equal distance segments. Looking first at erosion, after conducting the Pearson correlation, while a few independent variables did show a statistically significant correlation ($p < .05$) with erosion, the correlation coefficients (R) were exceptionally low, and no further investigation was made. With deposition, Irish Creek, Main Stem, Weyer Creek, and portion of the North Fork-Lower Main Stem, results of the correlation analysis was similar to that of erosion, where some statistically significant correlation was found but with low R values.

The only exception was a moderate correlation between deposition and several of the independent variables in the Marshall Co. NF-LMS data. A stepwise regression using all variables resulted in a model consisting of the understory and overstory Normalized Relative Density (NRD) and change in tree top density variables with an R^2 of 0.35. This result was not surprising since deposition as well as a dramatic increase in in-channel vegetation along the northern end of the NF-LMS in Marshall Co. was observed in Chapter III (Figure 53, p.133). Overall, the hypothesis that erosion rates are negatively correlated to understory vegetation density was rejected. Closer

examination of the understory NRD map and DoDs revealed many instances where the understory NRD indicated dense understory, yet severe erosion occurred (Figure 81).

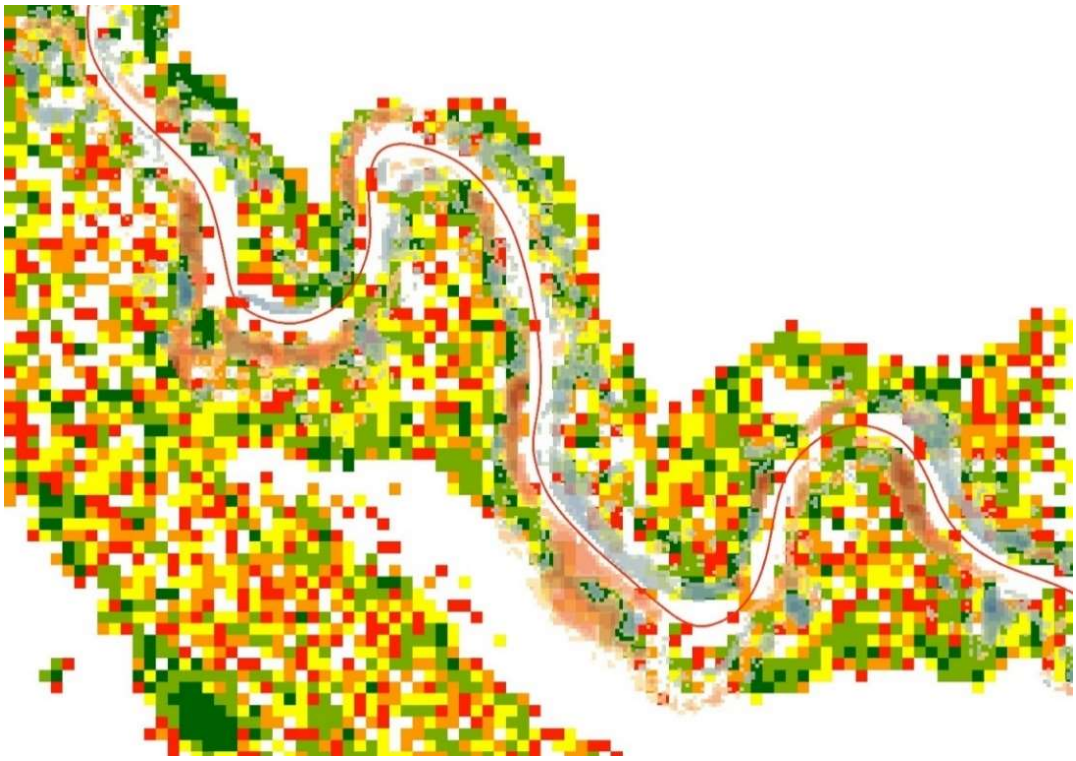


Figure 81: Area along Irish Creek NRD Map Overlain with 2010-2018 DoD

Conclusion

The three BVR tributaries included in this study, Irish Creek, Weyer Creek and the Main Stem upstream of the North Fork confluence) all had negative net volume change (erosion), In contrast, the North Fork-Lower Main Stem, the main channel, experienced net deposition, due primarily to two areas of high deposition 1) downstream of the North Fork/Weyer Creek confluence and 2) in the lowest portion of the watershed where the BVR empties into the Big Blue River. The portion of the North Fork upstream of its confluence with Weyer Creek experienced net erosion similar to the three tributaries included in this study. Further investigation of other large BVR tributaries

such as Robidoux Creek may be warranted given the large amount of sediment being produced by the other tributaries.

Overall, when banks void of woody vegetation were isolated, the rates of erosion are higher and deposition lower compared to banks with ample or little woody vegetation, with little difference in erosion rates between banks in the ample and little vegetation categories. Even though overall erosion rates of banks where woody vegetation was present are lower than of banks void of woody vegetation, banks with large amounts of erosion can be seen in areas with little and ample vegetation especially in the Irish Creek and Main Stem subwatersheds. Although the presence of understory and overstory vegetation can be estimated using LiDAR, there are numerous other factors influencing streambank erosion that are not discernible from the LiDAR data, such as root density, root depth, bank material, pattern, and bank angle, height, and cohesion.

In addition, no correlation between overstory or understory NRD (a measure of vegetation density) and erosion was found. Erosion in highly vegetated areas may be due to where the BVR is in its channel evolution. As discussed in Keane & Sass (2017) and Chapter III, the BVR is adjusting its form due to anthropogenic alterations to its watershed that have increased the volume and velocity of water entering the system. The data suggest that the BVR has entered a phase of rapid widening and will continue to adjust its dimension, pattern, and profile until a new quasi-equilibrium is attained at a new, lower elevation. Restoration efforts aimed at decreasing the sediment being delivered to the Tuttle Creek Reservoir by increasing or restoring riparian vegetation may slow this progression but will likely not stop the channel evolution. Bank erosion

that ends up as sediment in Tuttle Creek will likely only subside once the river has claimed enough real-estate to allow for stable bank angles and an adequate floodplain at the new, lower elevation.

While amounts of erosion and deposition estimated using LiDAR data contain uncertainty, the DoDs produced do provide better identification of areas of excessive erosion and deposition than methods previously used by the KWO, especially in areas of dense, overhanging woody riparian vegetation. The process of creating DoDs along riverbanks could easily be applied to the entire Tuttle Creek Reservoir watersheds within the coverage area of the 2010, 2012, and 2018 LiDAR data.

CHAPTER V - Evaluating the Use of Structure-from-Motion Photogrammetry to Seasonally and Annually Monitor Black Vermillion River Erosion "Hotspots"

Introduction

Beginning in the 1940s and continuing into the 1980s, the U.S. Army Corps of Engineers (USACE) in conjunction with the Bureau of Reclamation invested in building numerous reservoirs throughout Kansas with the primary purpose of flood control. State and local governments subsequently added water supply storage to the purpose of many reservoirs resulting in federal reservoirs providing municipal and industrial water supply for more than two-thirds of the state's residents (Hargrove, 2008). The initial expected life span of federal reservoirs in KS ranged between 150 and 200 years; however, excessive sedimentation has reduced the projected lifespans of KS reservoirs by 50 to 100 years (deNoyelles & Jakubauskas, 2008). Tuttle Creek Reservoir in NE Kansas is a prime example of loss of storage capacity due to sedimentation.

Tuttle Creek Reservoir covers an area of approximately 49.4 km^2 during normal conditions and 214.8 km^2 at full flood capacity (US-COE, 2011). The reservoir was designed to facilitate flood control and flow management of the lower Missouri River by impounding up to 524,613,846 m^3 of water (US-COE, 1998); however, the State of Kansas has begun planning for the use of Tuttle Creek Reservoir as a municipal water supply. Since it became operational in 1962, sediment delivered by the Big Blue River and its tributaries has led to a 47.9% decrease in storage capacity (Rattanavong, 2019), the fourth largest decrease of any reservoir in the state (deNoyelles & Jakubauskas, 2008). Figure 82 shows an increase in sediment in the north end of Tuttle Creek

Reservoir between 2007 and 2022 (Note the lake elevation was almost identical on both dates). The U.S. Army Corps of Engineers is planning a pilot project in 2023 that will use water injection dredging to agitate sediment from the bed of Tuttle Creek Reservoir delivering it through the exit gates and downstream. The environmental consequences of delivering such large amounts of sediment downstream are unknown (Llopis-Jepsen, 2022).

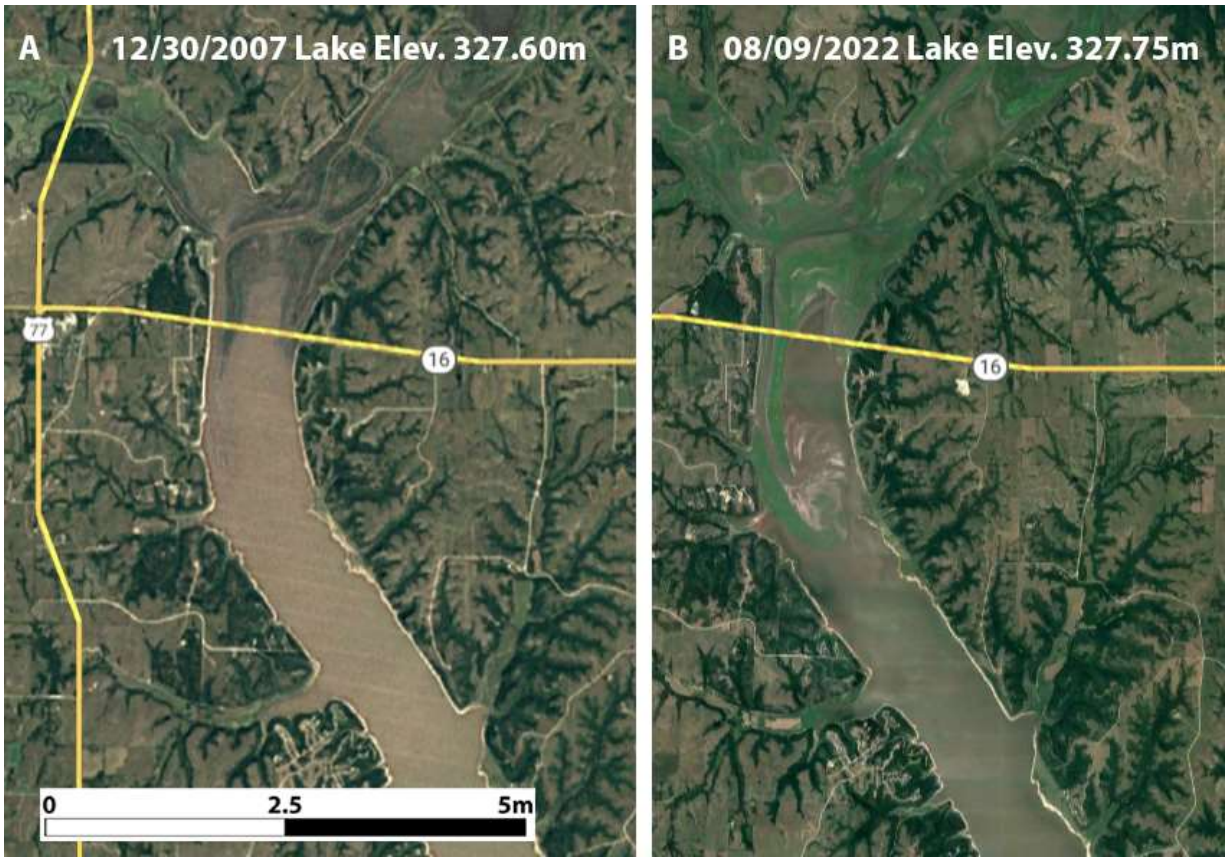


Figure 82: Sedimentation of Tuttle Creek Reservoir 2007-2022 (Source: Google Earth)

Tuttle Creek Reservoir Watershed Erosion "Hotspots"

In 2017, the Kansas Water Office (KWO) prepared the *Tuttle Creek Watershed Streambank Erosion Assessment: ArcGIS Comparison Study: 1991, 2002, 2003 vs.*

2015 Aerial Photography, with the aim of identifying areas of excessive streambank erosion termed “hotspots”. The assessment was used to guide stabilization and riparian restoration efforts within the Tuttle Creek Reservoir watershed (Figure 83) funded with a $1.2 million loan from the Kansas Water Pollution Control Revolving Loan Fund (KWO, 2017). The goal of the assessment was to identify areas of “aggressive movement” defined as areas of bank retreat greater than 2,000 sq.ft. (186 m^2) between the earlier years (1991, 2002 and 2003) and 2015. These areas were determined by drawing polygons in ArcGIS following the 2015 streambank and then closing the polygons following one of the earlier streambanks. In order to determine the volume of lost bank material, the area of each polygon was multiplied by the estimated bank height at that location, which was extrapolated from only five survey locations, three on the Big Blue River and one on each of two tributaries, the Little Blue River and the Black Vermillion River (BVR). Hotspots were identified on the three rivers noted, and an interactive map of the hotspots is available at https://kwo.ks.gov/projects/streambank-stabilization-projects. This research focuses on erosion hotspots identified along the BVR.

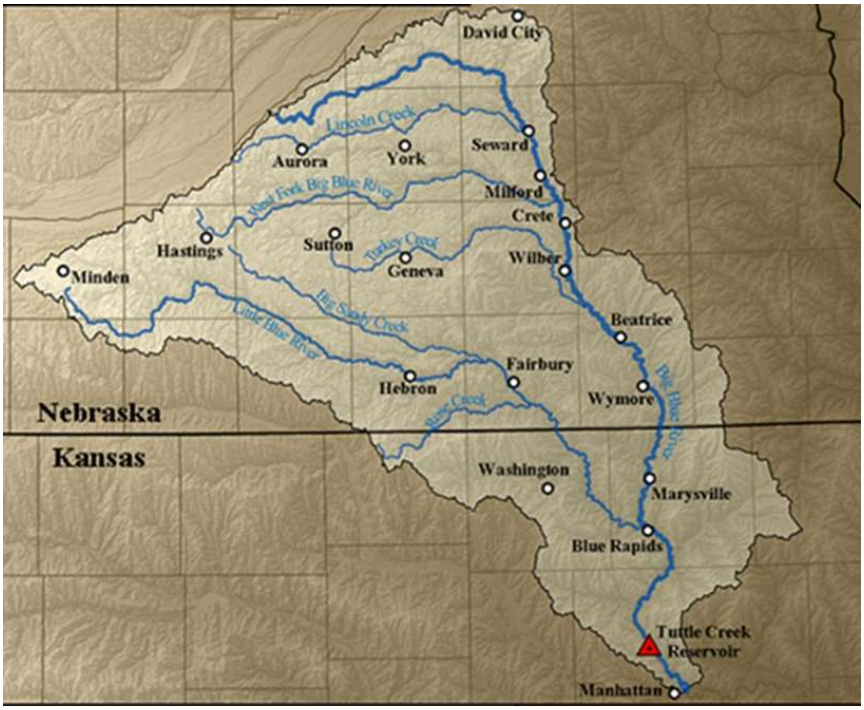


Figure 83: Tuttle Creek Reservoir and Big Blue River Watershed (Big Blue River, N.D.)

The analysis of repeat LiDAR-derived digital elevation models (DEMs) from 2010 (12) and 2018 discussed in Chapter III and IV may provide a more accurate and complete method of identifying areas and amounts of high erosion along the BVR riverbanks. The 2010-2018 digital elevation model of difference (DoD) was compared to the BVR erosion hotspots identified by the KWO 2017 assessment and it became clear that numerous areas of high erosion were missed. Figure 84 shows a 37,699 sq. ft. (3,502 m^2) area of bank retreat almost 20 times the threshold established that was missed. In addition, the LiDAR-derived DoD allows the identification of areas of high erosion in areas of dense, overhanging woody riparian vegetation, not visible in aerial photographs.

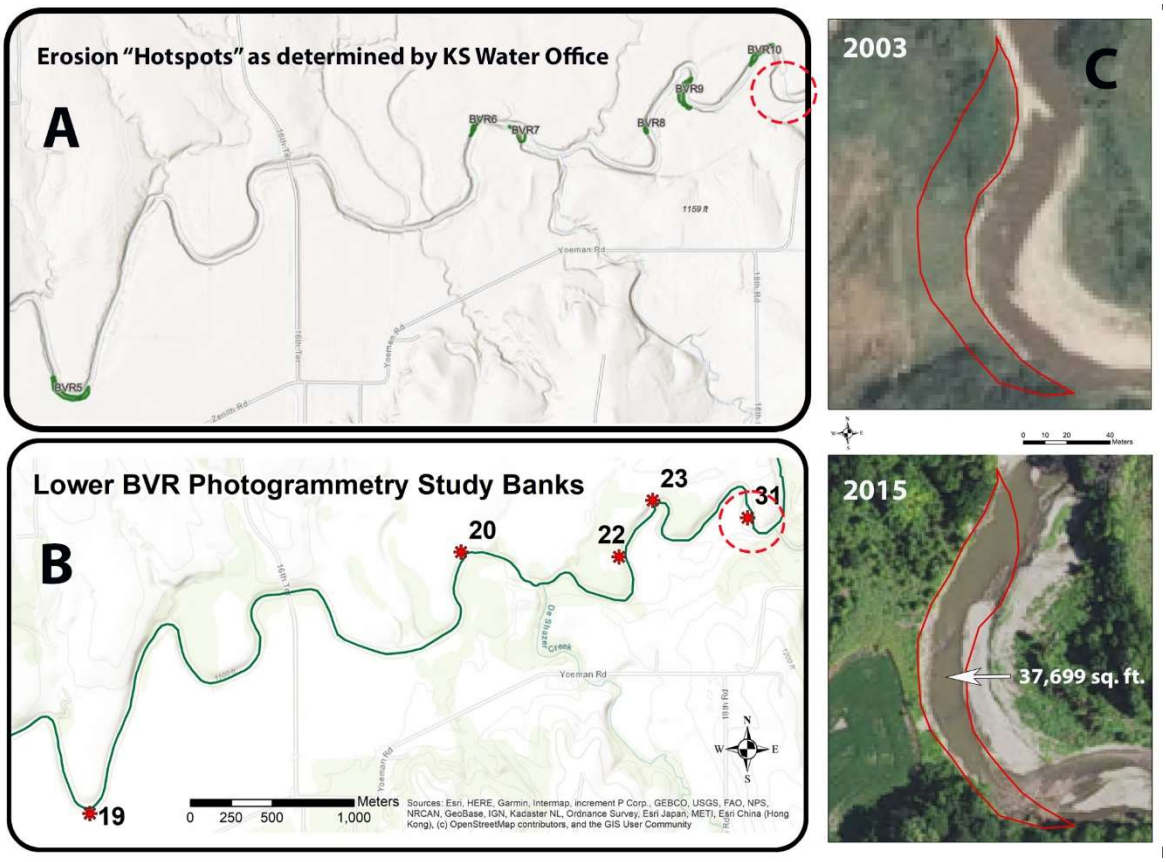


Figure 84: Missed Erosion Hotspot in KWO Assessment (A) Erosion hotspots identified by the KWO, (B) Study banks for this study (C) Aerial photos of area missed by the KWO Assessment (KWO, 2017; KS DASC, N.D.)

Identifying erosion hotspots with the LiDAR analysis provides estimations of bank erosion and deposition over many years; however, once identified, there may be a need for monitoring banks at a finer temporal scale due to changing precipitation and river flow patterns caused by climate change. The climate in NE Kansas is considered continental with most of the 87.9 cm average rainfall (period of record 1970-2021) occurring between April and September (Aber, 2007; Sass & Keane, 2012). In northeast KS, the amount of overall annual precipitation is not expected to increase dramatically over the next century; however, precipitation is expected to fall in more extreme precipitation events separated by longer periods of drought leading to an increase in the number of bankfull and greater flows and a decrease in base flows (Wasko & Sharma, 2017; Steiner et al., 2018; USGCRP, 2018).

This pattern of increasing high flows is already evident in the BVR gauge data. Based on 70 years of gauge data, bankfull discharge defined as the 1.5-year return interval was determined to be 142.03 m^3/sec (5,016 cfs); however, between 2007 and 2021 discharge equaled or exceeded bankfull 34 times or an average of 2.4 times per year, a dramatic increase from occurring on average every 1.5 years. Monitoring BVR erosion hotspots at a fine, seasonal temporal scale could aid in the estimation of future bank erosion resulting from these changing flow patterns. The relatively new remote sensing technique of Structure-from-Motion (SfM) photogrammetry could provide a means for monitoring erosion hotspots at a finer temporal scale and more extensive spatial scale with lower costs and data collection times than traditional river surveying methods.

Use of SfM to Monitor Riverbank Geomorphic Change

Prior to the last decade, the vast majority of data used in fluvial geomorphology was collected via the traditional field surveying methods, such as the use of differential lasers, total stations, and GPS systems to survey river cross sections and longitudinal profiles. However, new remote sensing technologies can provide researchers with data that is of higher quality in terms of spatial accuracy and resolution as well as temporal resolution (Mirijovsky & Vavra, 2012). Currently, several remote sensing techniques can be used to survey the three-dimensional complexity of large areas of riverbanks, such as terrestrial laser scanning (TSL) , airborne light detection and ranging (LiDAR), also known as airborne laser scanning (ALS), and Structure-from-Motion Photogrammetry (SfM) (Duro et al., 2018). This research focuses on Structure from Motion SfM photogrammetry that facilitates the extraction of topographic information from aerial imagery (Marteau et al., 2017). "The core concept of SfM is the science of photogrammetry, using photographs to make quantitative measurements of the scene they represent" (Dietrich, 2014 p.1). SfM has lower costs, shorter data collection times, and comparable (often higher) accuracies than ALS (Dietrich, 2014; Fonstad, Dietrich, Courville, Jensen, & Carbonneau, 2013; Mirijovsky & Langhammer, 2015) and TLS (Prosdocimi, Calligaro, Sofia, Dalla Fontana, & Tarolli, 2015; Hamshaw et al., 2017). SfM requires only a mid-grade single-lens reflex (SLR) camera ($1,000) for terrestrial surveying, or a high-end recreational grade unmanned aerial vehicle (UAV) ($2,000) for aerial surveying. In contrast, a TLS can be upwards of $10,000 and a LiDAR-capable drone upwards of $25,000.

It is important to note that all but one of the studies cited thus far that utilized SfM to monitor river geomorphology were conducted on montane, gravel-bed, and often braided rivers/streams with relatively low banks (e.g. Dietrich, 2015; Mirijovsky & Langhammer, 2015; Tamminga et al., 2015; Hamshaw et al., 2017; Marteau et al., 2017; Langhammer & Tereza, 2018), which are very different from the cohesive, often vertical banks of the BVR that can reach a height of 8m in the lower watershed. Duro (2018) utilized SfM to evaluate bank retreat on a 1.2 km restored bank of the Meuse River in the Netherlands achieving high accuracy when compared to ALS and RTK GPS. Although the cohesive, vertical banks of the Meuse River are more similar to the banks of the BVR, the maximum height was only 3.5m, which is less than half the height of the maximum BVR bank height. In a recent study, Lazell et al. (2022) utilized UAV surveys in conjunction with traditional surveying methods to monitor the effectiveness of erosion control structures along the Cottonwood River in eastern KS. The Cottonwood River is larger than the BVR; however, it does lie within in the Flint Hills physiographic region, which is physiographically similar to the glaciated region of KS.

While the aim of Chapter IV was to provide a continuous, system-wide assessment of patterns and amounts of erosion utilizing repeat 1-m resolution LiDAR derived DEMs, the primary goal of Chapter V is to evaluate the use of SfM to estimate volume change of erosion “hotspots” along the high and often vertical banks of the BVR channel over a 1.5-year study period as well as on an annual (leaf-off to leaf-off) and seasonal basis at a .03 m resolution between Nov. 2020 and July 2022.

Study Area

The BVR Basin covers 1,382 km^2 and lies entirely within the glaciated physiographic region of Northeast Kansas, which is a portion of the larger Glaciated Plains Region; however, the Irish Creek watershed in the southwestern portion of the BVR Basin is influenced by the Flint Hills Uplands Region that lies to the south (Figure 85) (Sass & Keane, 2012). The BVR lies almost entirely in Marshall and Nemaha Counties, where a layer of glacial till ranging in depth from 30.5 m to 122 m in depth covers alternating layers of limestone (Permian and Pennsylvanian) and shale. Throughout the BVR Basin, riparian soils are formed from alluvium parent material deposited by repeated flooding over the millennia ranging in clay content from 23 to 47 percent (NRCS, 2011; Sass & Keane, 2012).

Flow data for the BVR was available from one USGS gauging station (#6885500) located approximately 3.8 km downstream of Frankfort, KS, which is the approximate midpoint of the BVR main channel and is used in this study to distinguish between the upper and lower BVR watersheds. Flow data collected for the study period between November 2020 and July 2022 is shown below in Figure 86.



Figure 85: Black Vermillion Watershed Location in NE KS (Sass & Keane, 2012)

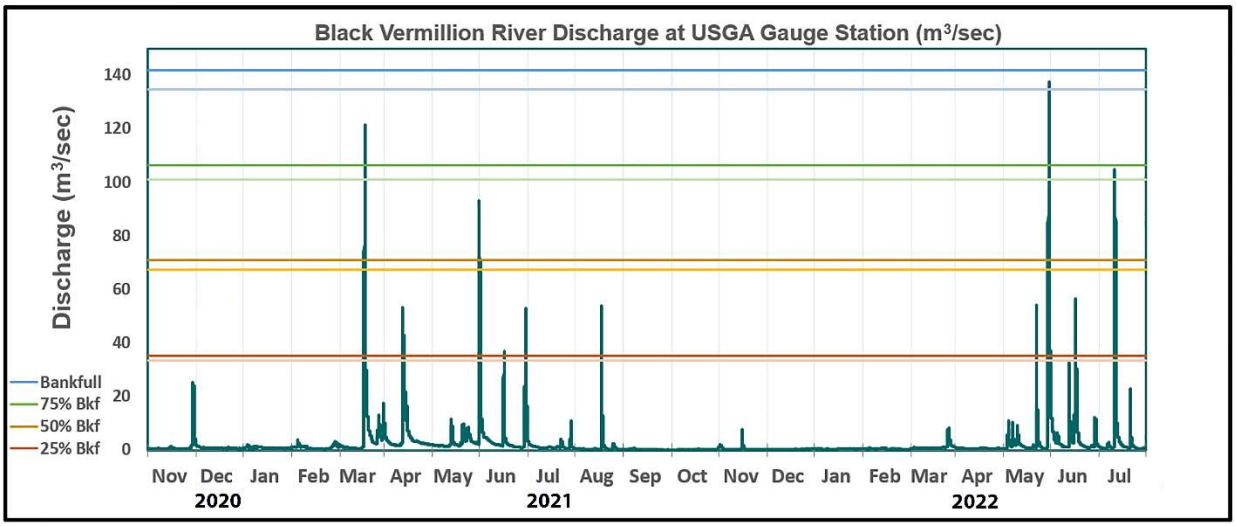


Figure 86: USGS gauging station (#6885500) Discharge Data 2020 - 2022

Methods

Site Selection

The BVR system is typified by incised channels with bank heights ranging from approximately 5 m in the upper watershed to over 8 m in the lower watershed, with dominant bank angles ranging from 20 to 84 degrees (Chapter 1). Many steep bank angles are the result of rotational slump or fall, which are the two types of mass wasting erosional processes most common in Northeast KS (Sass & Keane, 2012). In addition to numerous steep, high banks, most of the BVR and its tributaries flow through remote, privately owned land making the detailed surveying of riverbanks such as those to be included in this study with traditional survey methods difficult. As noted, SfM photogrammetry can be used for detailed surveying of up to hundreds of meters of riverbank using an inexpensive and less labor-intensive alternative to traditional surveying methods. However, in order to monitor the banks in every season using SfM, the banks must have little or no overhanging woody vegetation and little vegetation of

any kind on the bank face. Most erosion hotspots identified by the KWO 2017 Assessment meet these criteria. Google Earth was used to identify additional portions of the BVR riverbank that seemed to be actively eroding and were void of overhanging vegetation (Figure 87). In most cases, these areas are immediately adjacent or in close proximity to row crop fields or large areas of grass or other low, non-woody vegetation. Initially, 43 possible study banks were identified.

Nine study banks ranging in length between 30m and 186m were chosen for monitoring with SfM (Figure 88); however, these sites were not as evenly distributed throughout the BVR watershed as initially planned due to lack of landowners' access permission. Six sites were located in the lower BVR watershed (downstream of Frankfort, KS) and three in the upper watershed. Five of six study banks in the lower watershed were in close proximity to one another; however, as seen in Figure 89 below, this area was shown in the Chapter IV LiDAR analysis to be an area of high erosion between 2010 and 2018 containing a number of banks ideal for monitoring with SfM.



Figure 87: Typical BVR Riverbank with no Overhanging Riparian Vegetation (Source: Google Earth)

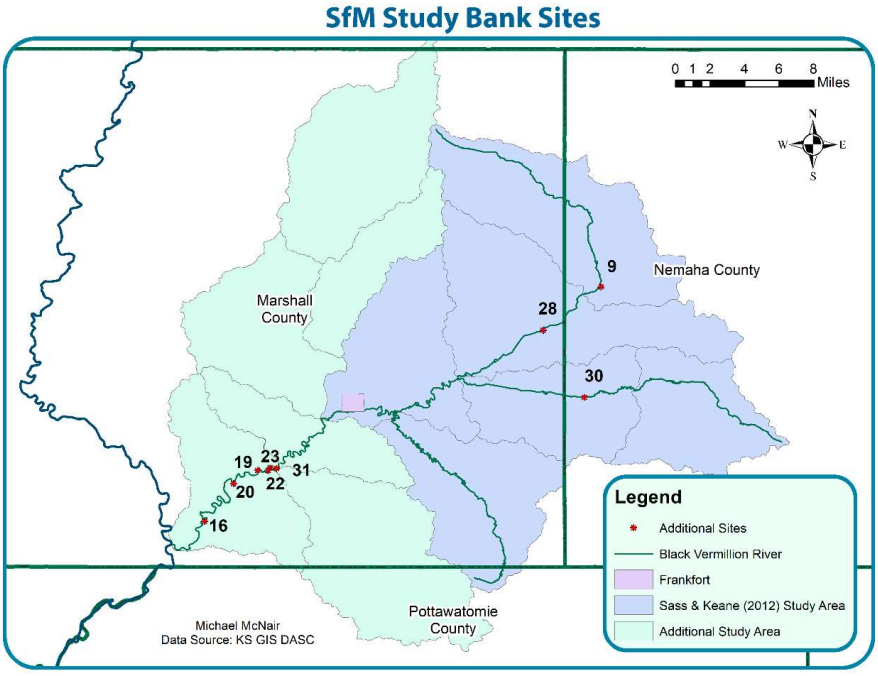


Figure 88: Structure-from-Motion Study Banks and Study Area

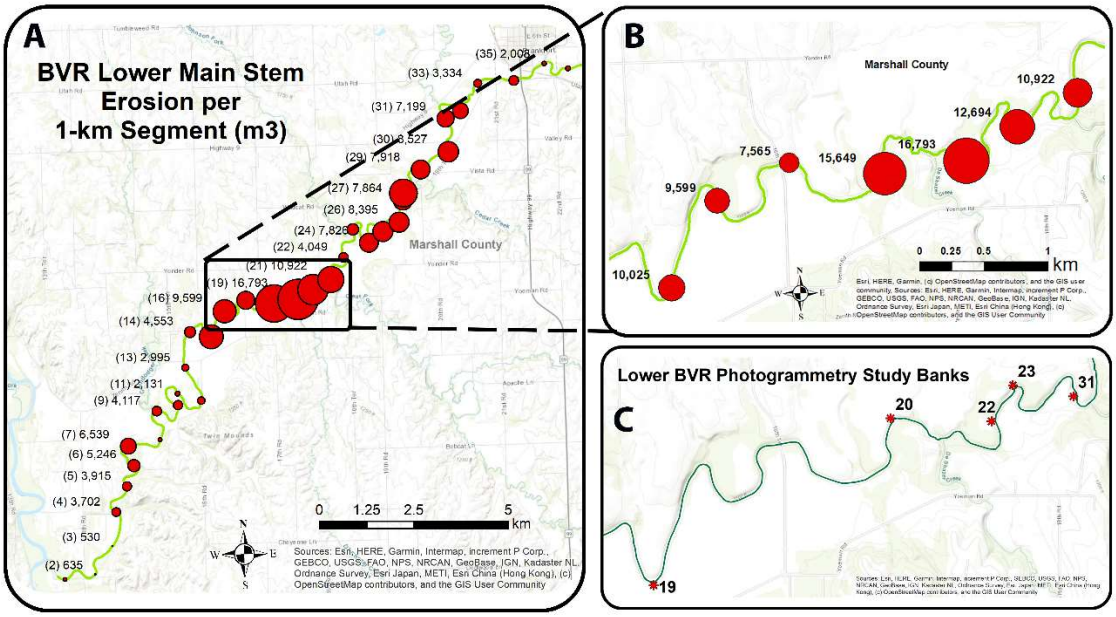


Figure 89: Area of High Erosion in Lower BVR: (A and B) Erosion per 1-km River Length Calculated in Chapter III (C) SfM Study Banks

Soils characteristics at the nine study banks are shown in Table 26. Clay content ranges from 25.3% to 46.7%, with study banks 19 and 28 having the highest.

Table 26: BVR SfM Study Bank Soil Properties

Soils at SfM Study Banks					
Study Bank	**Soil Name**	**Parent Material**	**Percent Clay (%)**	**Liquid Limit (%)**	**Bulk Density (g/cm^3)**
9	Kennebec silt loam	Alluvium	26.3	40.6	**1.37**
16	Nodaway silt loam	Fine-silty alluvium	25.3	39.7	1.29
19	Wabash silty clay loam	Silty and clayey alluvium	46.7	60.6	1.35
20	Nodaway silt loam	Fine-silty alluvium	25.3	39.7	1.29
22	Nodaway silt loam	Fine-silty alluvium	25.3	39.7	1.29
23	Nodaway silt loam	Fine-silty alluvium	25.3	39.7	1.29
28	Wabash silty clay loam	Silty and clayey alluvium	46.7	60.6	1.35
30	Kennebec silt loam	Alluvium	26.3	40.6	1.37
31	Nodaway silt loam	Fine-silty alluvium	25.3	39.7	1.29

SfM Photogrammetry Process

As one of the goals of this study is to assess SfM photogrammetry as a low-cost alternative to TLS and ALS, a relatively inexpensive unmanned aerial vehicle (UAV) was chosen, the DJI Phantom 4 Pro+ V2.0, which cost approximately $2,000 with accessories. This drone has several features that make it a good choice for photogrammetry such as a mechanical shutter that eliminates distortion associated with a rolling shutter, a 20-MP, 1” CMOS sensor, three-axis gimbal stabilization, waypoints smart mode that allows for precise, automated missions, and GLONASS satellite positioning.

At each SfM study bank, five ground control points (GCPs), which is sufficient given the largest area surveyed was approximately 1 hectare (2.47 acres), and between five and eight checkpoints (CKPs) were installed using 4’-long .5” diameter steel rods with survey caps (Figure 90) (Civil Tracker, 2023). The GCPs and checkpoints were evenly distributed, not linearly aligned, located at various elevations, clearly visible from multiple angles, and when collecting images, marked with 12”x12” black and white checkerboard tiles

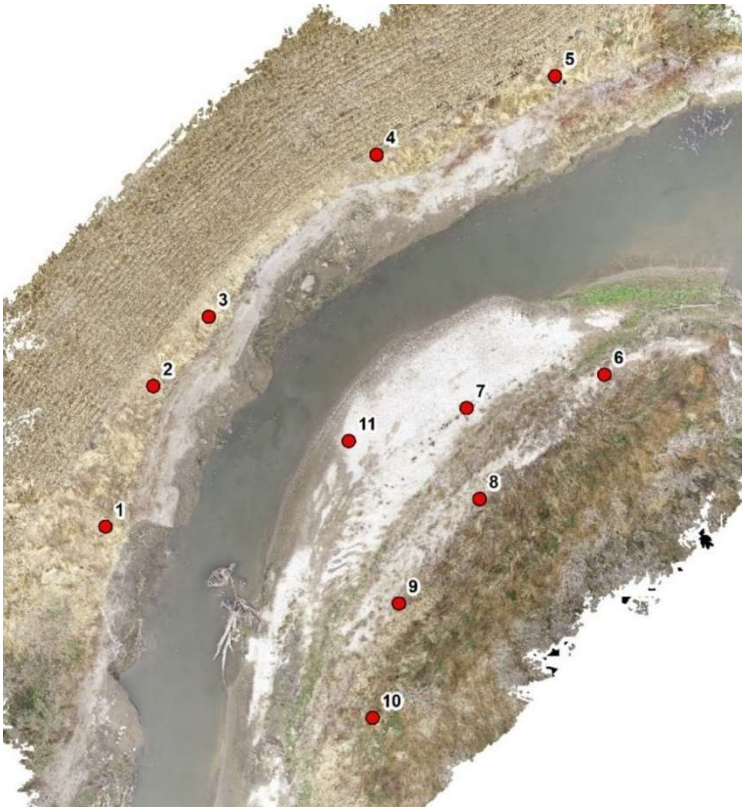
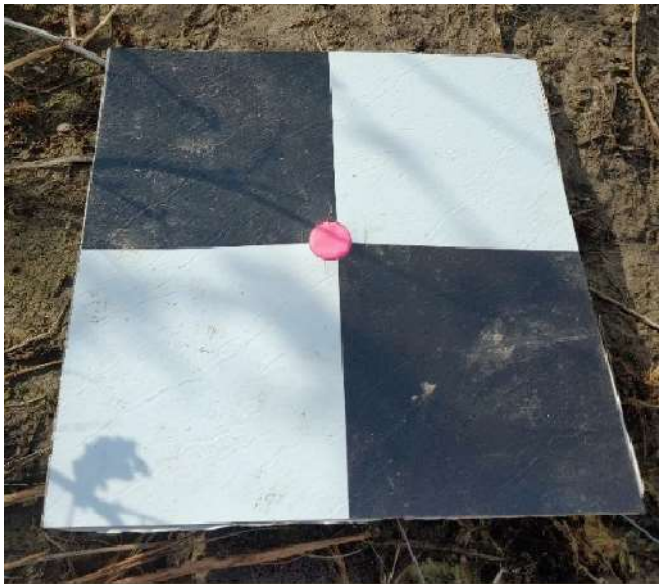


Figure 90: Typical GCP Placement



(Figures 90 and 91). All points were surveyed with a Leica TC704 total station with an accuracy of 2 mm +2 ppm. The difference between and use of GCPs and CKPs is discussed later in this document.

Figure 91: Ground Control Point 12"x12" Marker

Flight plans for automated UAV image collection were created in DJI Flight Planner and transferred to the Phantom 4 Pro V2.0 using the Litchi online Mission Hub and software application. Two flight plans were created for each study bank, one for collecting nadir images and one for oblique images (Figure 92 A and B). Note, the nadir flight plan covers an area significantly larger than the bank of interest in order to facilitate the optimal distribution of GCPs. As the nadir view alone is not well suited for vertical or overhanging portions of the riverbank (Rossi, Mancini, Dubbini, Mazzone, & Capra, 2017), oblique images were collected with gimbal angles ranging from -35° to -65° (nadir angle -90°) increasing convergent camera geometry along the study bank, shown to provide better imagery for SfM UAV surveys (Dietrich, 2014; James & Robson, 2014). Nadir images were collected at altitudes ranging from 23 m to 30 m and oblique images at altitudes from 12 m to 18 m with a minimum 80% forward and/or 80% side overlap.

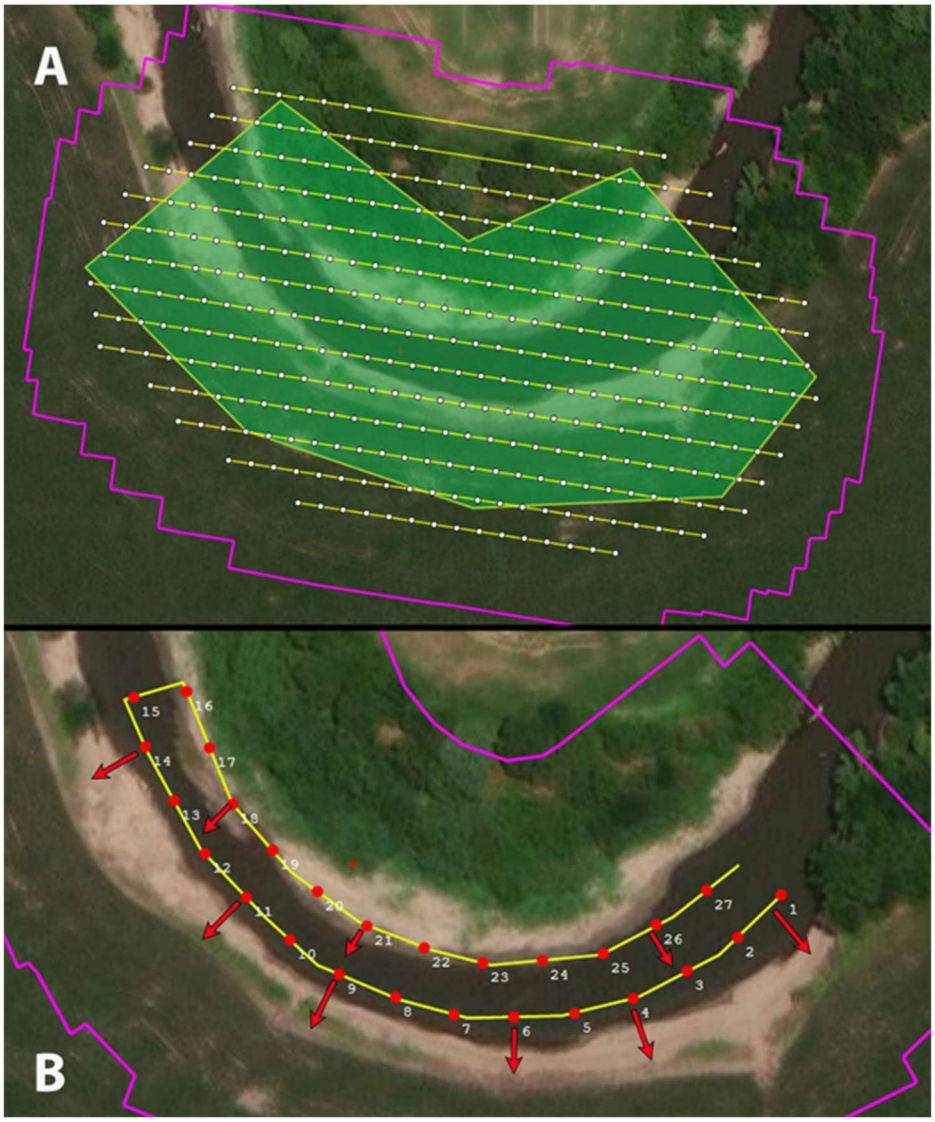


Figure 92: Automated Flight Planning using DJI Flight Planner: (A) Nadir and (B) Oblique

Images were processed into dense point clouds using Agisoft Metashape 2.0.1 using the default settings for high quality, dense point clouds. Metashape uses the five GCPs to register the point cloud to the exact same location each time with a 7-parameter transformation including three rotation parameters (roll, pitch, yaw), three translation parameters (x, y, z) and one scale parameter that minimizes the GCP's X, Y and Z errors (Fonstad et al., 2013; Dietrich, 2016). In contrast to GCPs, CKPs are not used in the SfM photogrammetry process and serve only to assess the accuracy of the

produced point cloud by comparing the surveyed coordinates of each CKP to that of the constructed model. For each model constructed from the images collected during each UAV survey, Metashape produces a “Processing Report” that includes the root mean square error (RMSE) of the X, Y, XY, and Z CKP errors as well as numerous other survey data.

Quick Terrain Modeler 8.4.0 was used to crop each study bank’s point clouds to the same horizontal and vertical extents. Upon selection, all of the SfM study banks had no or very little vegetation; however, a number of the study banks experienced varying levels of herbaceous vegetation growth over the study period. Investigation of river flows at the BVR USGS gauging station near Frankfort, KS indicated that in the year prior to this study (2019), the river experienced seven bankfull (determined by the 1.5-year return interval) or greater flows due to excessive spring and early summer rains. In addition, approximately 20 km of the lower BVR, where six of nine study banks were located, was completely under water for several months of 2019. These excessive flows and flooding most likely led to scouring of the BVR riverbanks, especially in the lower watershed. Bank vegetation removal from the cropped point clouds was done with a number of tools in Quick Terrain Modeler, primarily the “above ground level” analysis tool using the first point cloud containing little or no vegetation as the “ground” level. Figure 93 illustrates this process on study bank 31.

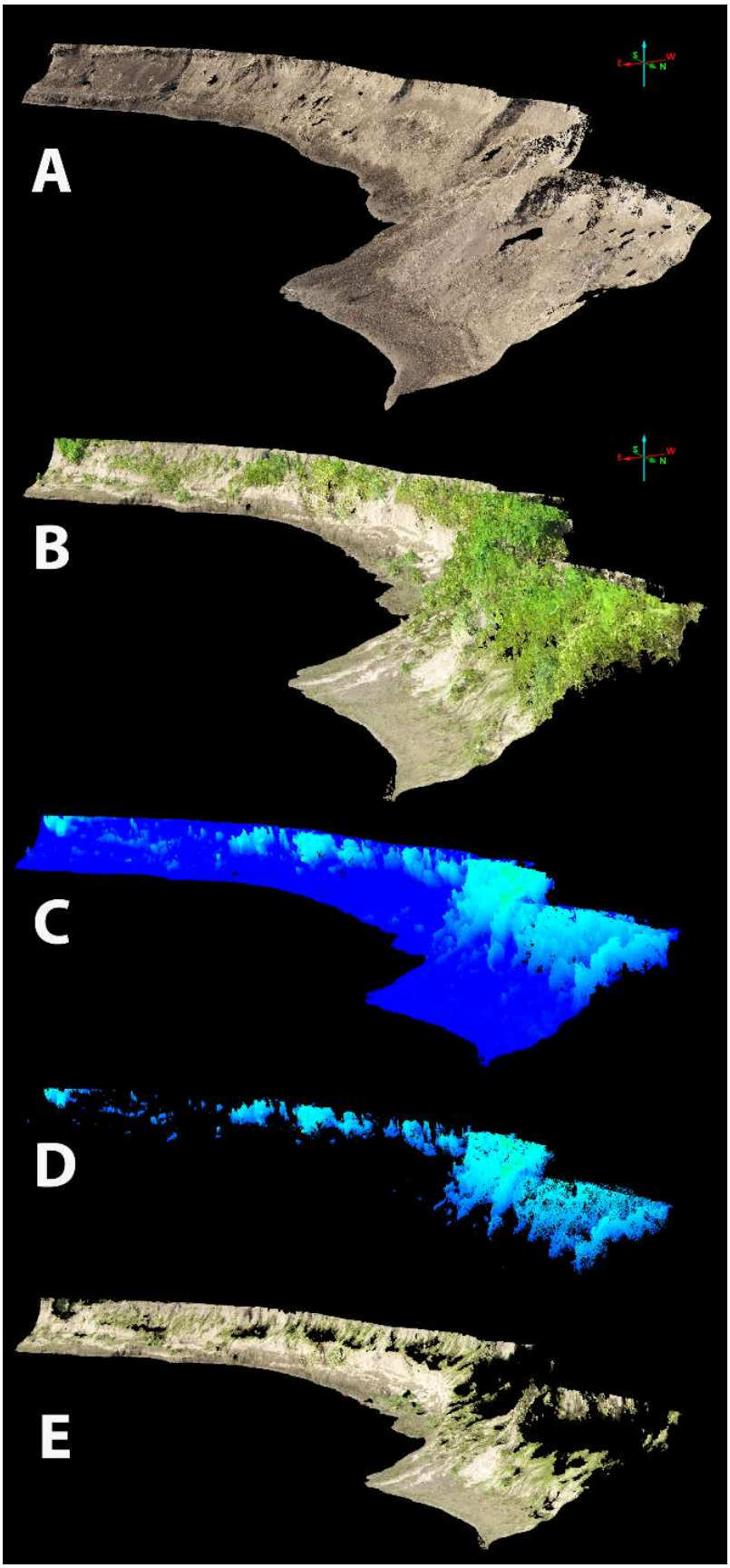


Figure 93: Process of Removing Bank Vegetation: (A) 03/21 point cloud containing little vegetation (B) Vegetation established over the summer growing season (C) Above ground analysis in Quick Terrain Modeler using earlier point cloud as ground level (D) isolated vegetation (E) Summer point cloud with vegetation removed

Volume Change & Evaluating the Use of SfM to Monitor Erosion Hotspots

Tables 27 and 28 provide the month and year of image collection at each of the nine study banks as well as the periods for which volume change was calculated and the use of SfM was assessed. Generally, the first four UAV surveys began in late 2020 and continued every two to three months through July of 2021, with the final two surveys being conducted in February, May, and July of 2022. Note that no UAV survey was completed at study bank 9 in late summer of 2021 due to landowner actively grading the field and riverbank immediately adjacent to the study bank with heavy equipment; therefore, study bank 9 was not included in the assessment of periods 3 and 4. No UAV survey was completed in July of 2022 for study bank 22 due to complete coverage of the bank with herbaceous vegetation and study bank 28 due to technical difficulties; therefore, these banks were not included in the period 5 assessment.

Table 27: SfM Image Collection Dates

SfM UAV Survey Dates (m/yr)						
Study Bank	**Date 1**	**Date 2**	**Date 3**	**Date 4**	**Date 5**	**Date 6**
31	12/20	3/21	5/21	7/21	2/22	7/22
30	11/20	1/21	4/21	7/21	5/22	7/22
28	11/20	2/21	5/21	7/21	5/22	*
23	11/20	1/21	4/21	7/21	2/22	7/22
22	11/20	1/21	4/21	7/21	5/22	*
20	11/20	2/21	6/21	9/21	5/22	7/22
19	11/20	1/21	4/21	7/21	5/22	7/22
16	12/20	2/21	4/21	7/21	5/22	7/22
9	11/20	1/21	4/21	*	5/22	7/22

Table 28: SfM Evaluation Periods

Period	Dates
1	1 and 2
2	2 and 3
3	3 and 4
4	4 and 5
5	5 and 6

Combined Error Estimation

Before the cropped and cleaned study bank point clouds were used to calculate volume change for each of the periods noted above, the combined error of each pair of point clouds was estimated with a 95% confidence interval probabilistic threshold using the root sum square of each point cloud's CKP's RMSE and the critical t-value (1.97) for the two-tailed Student's t-distribution associate with the 95% confidence interval (CI) using the formula:

$$U_{crit} = t\sqrt{(\varepsilon PtCloud_1)^2 + (\varepsilon PtCloud_2)^2} \quad (1)$$

Where $\varepsilon PtCloud_1$ and $\varepsilon PtCloud_2$ are the root mean square error (RMSE) of the point cloud checkpoints being compared, which may be either the Z errors (vertical) or XY errors (horizontal) depending on the projection direction of the analysis (this will be discussed later in detail) (Figure 94) and t = 1.96, the t-value associated with the 95% CI. The combined errors were used to establish a minimum level of detection (MinLoD) and/or calculate overall uncertainty. The ability to maintain consisitently low checkpoint errors at each study bank throughout the study was critical for accurate calculaiton riverbank volume change. Assessing checkpoint errors over the entire study period was the first of two ways the use of SfM to monitor BVR erosion hotspots was evaluated.

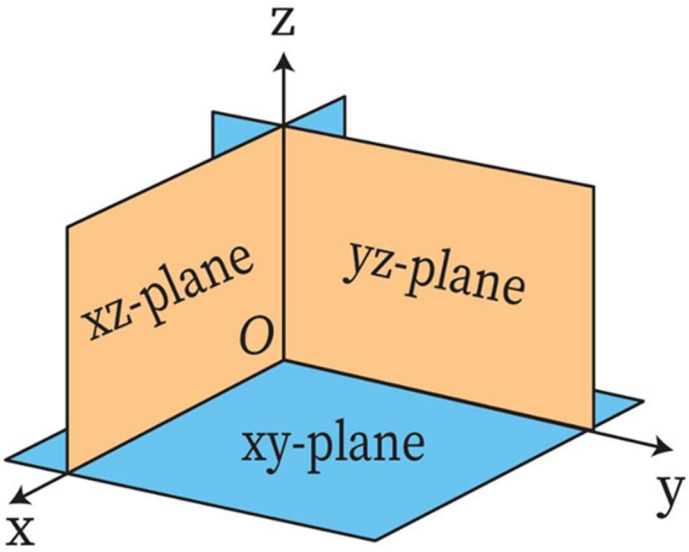


Figure 94: Projection Directions and Planes (Bartleby, 2023)

Volume Change Calculations Using CloudCompare

Initially, volume change calculations were generated for each time period in the z-projection direction (vertical) onto the XY-plane (Figure 94) using ArcGIS. Each point cloud was transformed into a 0.03 m-resolution raster digital elevation model (DEM) using the LAS to Raster tool, which interpolates any voids within the point clouds. For each pair of DEMs being compared, the earlier DEM was subtracted from the later DEM creating a digital elevation model of difference (DoD). The DoD was then thresholded using the estimated combined Z error as the minimum level of detection (MinLoD) before amounts of erosion and deposition were extracted. However, a better alternative to calculating volume change in ArcGIS was discovered using CloudCompare.

CloudCompare (CC) is an open-source point cloud processing software that can calculate volume change directly between two point clouds. CC is able to compare two point clouds by computing a 2.5D grid then deducing a number of statistics such as total volume change, amount added (deposition), amount subtracted (erosion), percentage of matching cells (cells that have a valid value for both point clouds), and grid surface area (CC, 2015). CC calculates volume change using the formula:

$$dV = grid\ step\ \times grid\ step \times difference\ in\ height \quad (2)$$

Where *dV* = total volume change, *grid step* = cell size and the difference in height (elevation) is the average height (y value when y-projection direction is specified) of points within each cell. Only the cells that have a valid height value for both point clouds are included in the volume calculation, with empty cells or cells for which only one height value is defined being ignored (CC, 2015).

The CC volume calculation tool allows a variety of treatments of voids in point clouds (in the case of this research, voids created when vegetation is removed) prior to execution of the tool. Two of these treatments are relevant to this research: 1) leaving the voids empty and 2) interpolating the voids using Delaunay triangulation. Interpolation increases the number of cells with a valid height value for both point clouds, when the point clouds have the same extents. However, interpolation introduces varying levels of uncertainty or error depending on the size and orientation of the voids, elevations along the edges of the voids, and actual surfaces where voids are present that may lead to an over or under estimation of erosion and/or deposition.

CC also allows voids resulting from the removal of vegetation to be left empty, which results in very accurate calculation of erosion and deposition in areas where no voids are present in either point cloud being compared; however, a portion of the actual change may be excluded or missed. For example, when there is a vegetated area on an earlier point cloud resulting in a void in that point cloud when vegetation is removed, then erosion during a given time period causes the removal of that vegetation as well as a portion of the bank underneath on the subsequent point cloud, change in that area would not be included in the volume change calculation. The presence or establishment of vegetation over each study period on the study banks that leads to voids in SfM point clouds is one of the primary limiting factors when using SfM to monitor erosion and/or deposition along the BVR riverbanks.

After learning CloudCompare (CC) allows for the calculation of volume change using the horizontal, y-projection direction, onto the XZ-plane (Figure 94), it was thought that a different approach that determines volume change in a horizontal projection could

be more accurate for several reasons. With the BVR steep, often-vertical banks that are undercut in some areas, evaluation of change in a horizontal direction would be more sensitive to fine-scale, local variations in the bank face, thus providing more accurate volume change calculations. In addition, it was noticed that many point cloud voids due to vegetation removal were on horizontal portions of the bank that are more pronounced in the nadir view (vertical view) than when viewing the bank elevations (horizontal view). As CC only allows the horizontal projection direction to be set in either the X (east/west) or Y (north/south) direction in the volume calculation tool, in order to conduct volume change analysis with a horizontal projection direction specified, the banks would need to be rotated to face either directly north or east. North was chosen, and all point clouds of each study bank were rotated along the Z-axis to face due north using the Translate/Rotate tool in CC (Figure 95) before running the volume calculation tool.

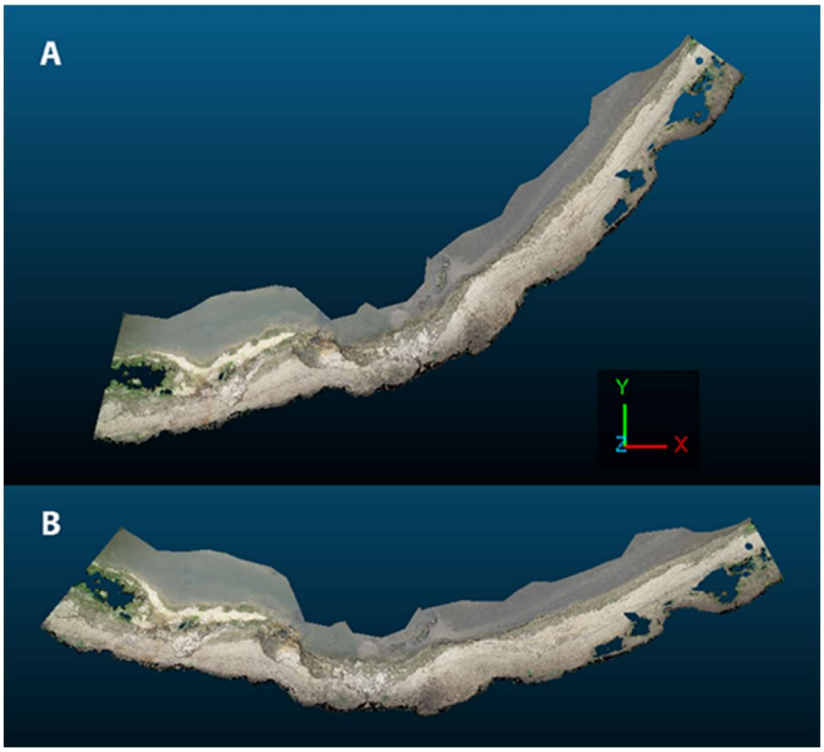


Figure 95: Rotation of SfM Study Bank along the Z-Axis to Face Due North (A) Before rotation and (B) After rotation

As an initial investigation, the CC volume calculation tool was run using the point clouds from the first and last UAV survey dates of all nine study banks, leaving the voids empty and using the Z-projection direction, which is the same projection used in the ArcGIS approach. It is important to note that the point clouds of the seven study banks surveyed on the last UAV survey date in July of 2022 contained the highest percentage of voids. The point clouds were then rotated to face directly north (Figure 95), and the volume calculation ran again with the Y-projection direction specified. With all nine study banks, the percentage of matching cells, one of the CC volume calculation tool output variables, was greater when using the Y-projection direction, with the average percentage of matching cells for all nine study banks increasing from 53.7% (Z-projection) to 67.6% (Y-projection).

It is assumed that the increase in the percentage of matching cells, along with the other reasons noted above, would result in more accurate calculation of volume change. In addition, the number of voids in point clouds resulting from the removal of vegetation that is reflected as the reciprocal of the percentage of matching cells represents a limiting factor for the use of SfM to monitor BVR riverbanks. Therefore, the percentage of matching cells between each pair of point clouds when executing the CC volume calculation tool was the second variable assessed to evaluate the use of SfM to monitor BVR erosion hotspots.

Even though volume change had already been calculated in the Z direction using ArcGIS, volume change for all periods was recalculated with both empty and interpolated voids using the CC Y-projection direction method, which are the results reported in the Results and Discussion section of this study. Volume change

calculations were generated at a fine temporal (seasonal) scale between each set of subsequent collection dates (periods noted in Table 28) for each study bank. In addition, volume change was calculated between the first and last date of each study bank, and as herbaceous vegetation is at a minimum in the winter and spring months, leaf-off to leaf-off volume change was calculated using the first and fifth dates. Volumes of erosion and deposition were normalized using the “surface area” output (area of study bank elevation) from the CC volume calculation tool in order to facilitate the comparison of erosion and deposition rates between study banks while considering both study bank length and height. Since the CC volume calculation tool does not allow for the application of a minimum level of detection as the ArcGIS method does, uncertainty (+ -) for the entire bank elevation surface was calculated by multiplying the surface area by the combined XY error of each pair of point clouds being compared.

Results and Discussion

Table 29 shows study bank characteristics related to streambank erosion and mass wasting, the final point clouds with vegetation removed and the DEMs created in ArcGIS were used to extract accurate study bank heights and bank angles at the beginning and end of the study period. ArcGIS was also used to determine the drainage area (DA) using the watershed tool and radius of curvature of each study bank. Note the lengths of the three study banks in the upper watershed (9, 28 and 30) tend to be shorter than study banks located in the lower water shed (16, 19, 20, 22, 23, and 31), due to the upper channel, being significantly smaller, narrower, and more tree-lined resulting in fewer banks being good candidates for monitoring with SfM. However, study banks heights did not vary significantly between the upper and lower watersheds,

as, the bank height of the study bank with the least DA (Study Bank 30, DA 115 km2) was only 2% shorter than the study bank with the largest DA (Study Bank 16, DA 1,368 km2).

Bankfull width at each SfM study bank was estimated using regional curves developed for Eastern Kansas (U.S. EPA, 2005). Note in Table 29 that only one of the SfM study banks has a radius of curvature between 2 and 3, which is typical of most rivers.

Table 29: SfM Study Bank Characteristics

SfM Study Bank Characteristics								
Study Bank	**Bank Length (m)**	**Bank Height (m)**	**Drainage Area (km^2)**	**Bank Angle 12/20 (°)**	**Bank Angle 07/22 (°)**	**Radius of Curvature (R_c) (m)**	**Bankfull Width (m)**	**R_c Ratio (R_c/W_{bkf})**
31	83.54	4.69	1,129	38.90	66.93	37.96	63.43	0.598
30	47.49	5.16	115	50.03	39.60	16.28	28.79	0.566
28	51.02	5.03	251	42.87	45.93	32.7	37.71	0.867
23	86.39	7.36	1,279	59.13	58.23	72.22	66.23	1.090
22	65.72	5.29	1,280	32.73	34.60	65.97	66.25	0.996
20	130.89	6.93	1,308	66.57	67.83	50.25	66.75	0.753
19	186.97	7.40	1,316	43.90	45.97	67.22	66.89	1.005
16	143.03	5.28	1,368	35.07	35.13	183.91	67.79	2.713
9	27.13	4.65	118	59.53	78.53	23.47	29.04	0.808

Although the volume changes reported in this study result from CC volume change analysis with the Y-projection direction specified (XZ-plane DoDs), the XY-plane DoDs created in ArcGIS will also be used in this discussion. Figures 96 and 97 below show the legends for the XZ-plane DoDs and XY-plane DoDs and apply to all subsequent DoDs. Selected study bank point clouds, XY-plane DoDs, and XZ-plane DoDs are used during the following discussion; however, all point clouds and DoDs for each study bank are shown in Appendix B.

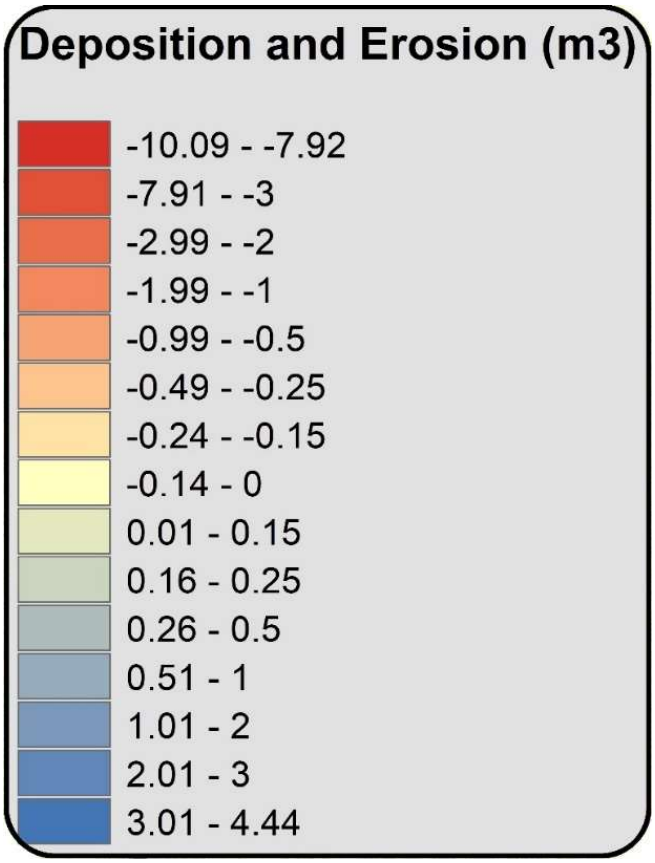


Figure 96: XY-Plane DoD Legend

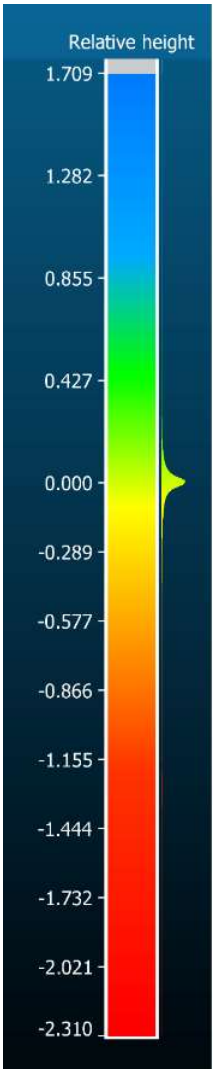


Figure 97: XZ-Plane DoD Legend

Evaluation of Checkpoint XY Errors over the Study Period

At the onset of the study between five and eight checkpoints were installed at each study bank site; however, over the course of the study, some checkpoints were lost to excessive deposition and vandalism. Some checkpoints were extremely hard to locate in the summer months due to thick growth of herbaceous vegetation, especially on the meander point bars opposite the study banks (Figure 98). At least 3 CKPs were located and marked at each UAV survey with an average of four CKPs per survey over the entire study. For the 51 UAV surveys conducted at the nine study bank sites, the

XY RMSE ranged from 0.0013 m to 0.0222 m with an average of 0.0121 m. It is also important to note that the UAV survey RMSEs did not increase significantly over the study period (Figure 99).

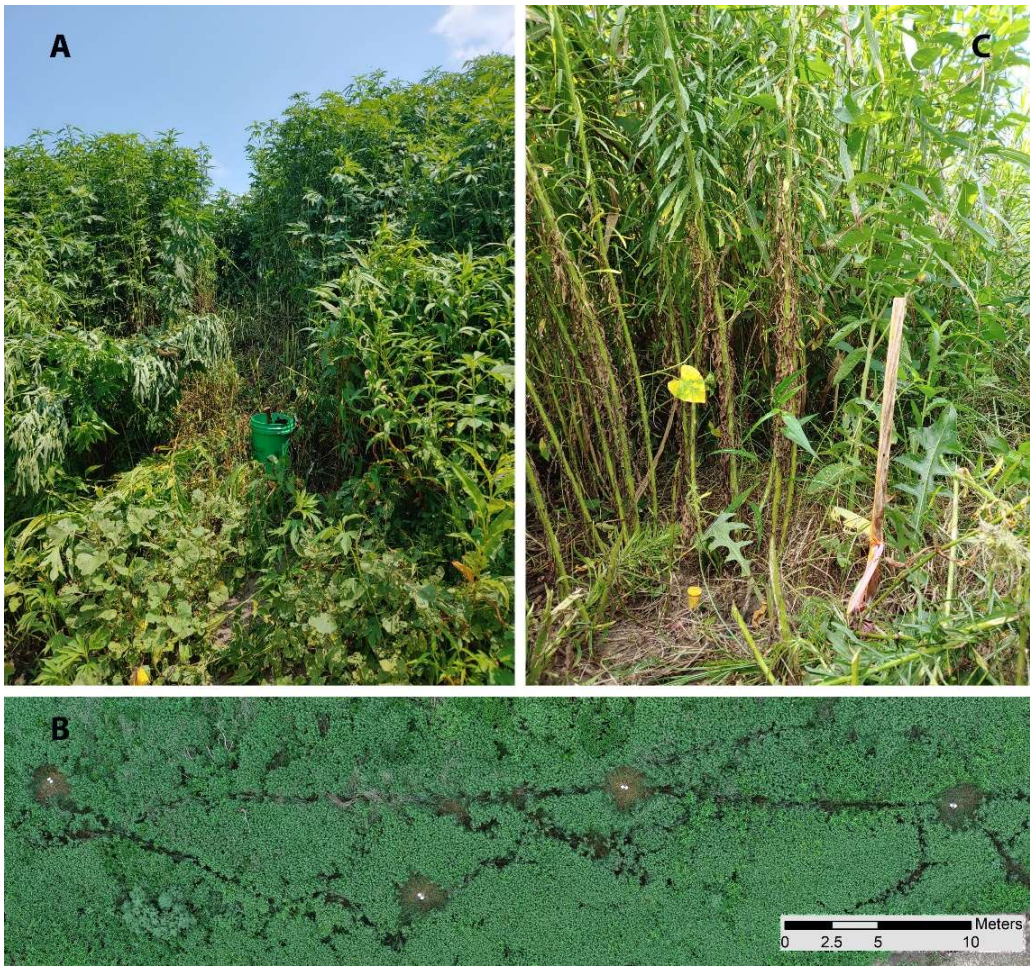


Figure 98: Ground Control Points in Summer (A) Cleared herbaceous vegetation (B) Typical GCP in summer (C) Aerial view of GCP in summer on point bar.

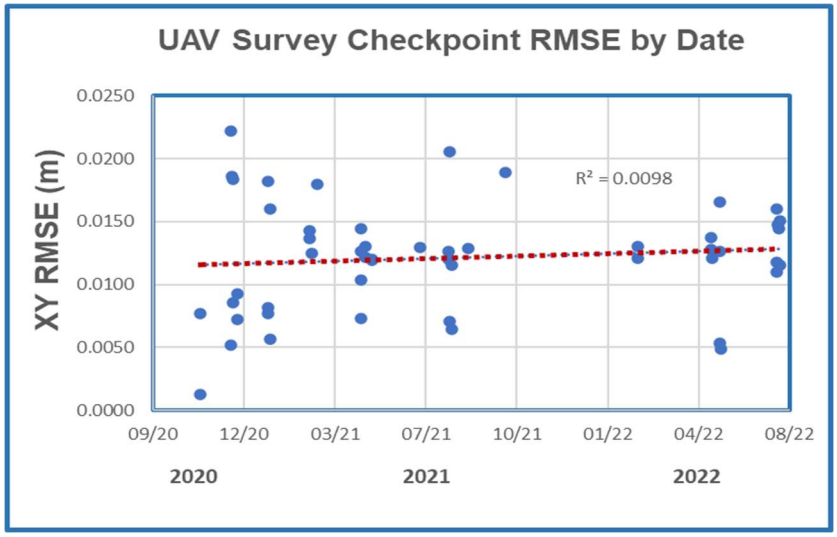


Figure 99: UAV Survey XY RMSE by Date

The low RMSEs resulted in the estimated combined XY error (Equation 1) of the 58 point cloud pairs compared using CC ranging from 0.0078 m to 0.0268 m with an average of 0.0175 m. These low XY RMSEs and combined CKP errors over the entire study period illustrate the ability to produce very accurate repeat SfM UAV surveys and point clouds over a 1.5-year study period.

Percentage of Matching Cells when Calculating Volume Change with Empty Voids in CC

When calculating volume over the entire study period in CC, the percentage of matching cells when point cloud voids (due to the removal of vegetation from study bank (SB) point clouds) were left empty ranged between 44% (SB16) and 88% (SB30) with an average of 71% (Table 30). In contrast, the percentage matching cells when volume was calculated from leaf-off to leaf-off conditions ranged from 74% (SB22) to 95% (SB19) with an average of 86% (Table 31). The higher percentages during leaf-off conditions indicate more accurate calculations of erosion and deposition could be made compared to when the later survey was conducted in the summer. In leaf-off conditions, all but one bank had a percentage of matching cells above 80%. In contrast, only three of seven study banks surveyed in the summer of 2022 (30, 19, and 9) maintained a percentage of matching cells of 80% or higher. However, with these three study banks, the summer vegetation was concentrated at one end of the bank leaving areas experiencing erosion exposed, which allowed for the accurate calculation of erosion in those areas (Figures 100 and101). Study banks with the lowest percentage of matching cells over the entire study period (16, 20, and 23) experienced vegetation over the

entire bank face, making accurate calculation of volume change difficult but also indicating that little change had taken place (Figures 102).

Table 30: CC Volume Change Entire Study Period

CC Volume Change Empty Voids-Entire Study Period												
					Total Erosion/Deposition (m^3)				Ero-Dep /m^2 Bank Face (m^3)			
Study Bank	Begin Date	End Date	% Cell Match	Surface Area (m^2)	Ero	Dep	Net Change	+ -	Ero/m^2 Face	Dep/m^2 Face	Net/m^2 Face	+ -
9	12/20	07/22	0.80	113.73	43.07	1.50	**-41.57**	2.46	0.38	0.01	**-0.37**	0.022
16	12/20	07/22	0.44	721.42	33.68	44.42	**10.74**	12.60	0.05	0.06	**0.01**	0.017
19	12/20	07/22	0.84	1074.48	742.99	17.41	**-725.59**	25.31	0.69	0.02	**-0.68**	0.024
20	11/20	07/22	0.56	766.65	113.49	4.62	**-108.87**	20.59	0.15	0.01	**0.44**	0.027
22	11/20	05/22	0.74	321.84	22.68	19.35	**-3.33**	5.87	0.07	0.06	**-0.01**	0.018
23	11/20	07/22	0.49	573.36	75.26	6.09	**-69.17**	6.80	0.13	0.01	**-0.12**	0.012
28	11/20	05/22	0.86	241.70	57.84	5.15	**-52.68**	3.29	0.24	0.02	**-0.22**	0.014
30	12/20	07/22	0.88	207.61	232.74	0.33	**-232.41**	2.89	1.12	0.00	**-1.12**	0.014
31	12/20	07/22	0.75	344.38	408.33	0.91	**-407.41**	6.04	1.19	0.00	**-1.18**	0.018
Average			**0.706**	**Totals**	**1,730.07**	**99.78**	**-1,630.29**					

CC Volume Change Interpolated Voids-Entire Study Period												
					Total Erosion/Deposition (m^3)				Ero-Dep /m^2 Bank Face (m^3)			
Study Bank	Begin Date	End Date	% Cell Match	Surface Area (m^2)	Ero	Dep	Net Change	+ -	Ero/m^2 Face	Dep/m^2 Face	Net/m^2 Face	+ -
9	12/20	07/22	0.92	113.73	45.99	4.52	**-41.47**	2.46	0.40	0.04	**-0.36**	0.022
16	12/20	07/22	0.98	721.42	43.83	175.11	**131.28**	12.60	0.06	0.24	**0.18**	0.017
19	12/20	07/22	0.99	1074.48	827.93	101.10	**-726.83**	25.31	0.77	0.09	**-0.68**	0.024
20	11/20	07/22	1.00	766.65	147.62	66.98	**-80.64**	20.59	0.19	0.09	**-0.11**	0.027
22	11/20	05/22	1.00	321.84	26.56	38.01	**11.45**	5.87	0.08	0.12	**0.04**	0.018
23	11/20	07/22	0.99	573.36	91.53	71.31	**-20.22**	6.80	0.16	0.12	**-0.04**	0.012
28	11/20	05/22	1.00	241.70	61.31	8.75	**-52.57**	3.29	0.25	0.04	**-0.22**	0.014
30	12/20	07/22	0.94	207.61	246.05	0.80	**-245.24**	2.89	1.19	0.00	**-1.18**	0.014
31	12/23	07/22	0.99	344.38	462.27	9.30	**-452.97**	6.04	1.34	0.03	**-1.32**	0.018
Average			**0.977**	**Totals**	**1,953.09**	**475.88**	**-1,477.20**					

Table 31: CC Volume Calculations Leaf-off to Leaf-off Conditions

CC Volume Change Empty Voids: Leaf-off 2020 to Leaf-off 2022												
					Total Erosion/Deposition (m^3)				Ero-Dep /m^2 Bank Face (m^3)			
Study Bank	Begin Date	End Date	% Cell Match	Surface Area (m^2)	Ero	Dep	Net Ero/Dep	+ -	Ero/m^2	Dep/m^2	Net/m^2 Face	+ -
9	12/20	05/22	0.93	114.60	30.76	5.92	**-24.84**	2.19	0.268	0.052	**-0.217**	0.019
16	12/20	05/22	0.86	631.79	33.15	109.19	**76.04**	9.62	0.052	0.173	**0.120**	0.015
19	12/20	05/22	0.95	1029.94	402.44	71.21	**-331.23**	23.27	0.391	0.069	**-0.322**	0.023
20	11/20	05/22	0.89	685.91	63.16	57.44	**-5.72**	17.92	0.092	0.084	**-0.008**	0.026
22	10/20	05/22	0.74	239.44	22.68	19.35	**-3.33**	4.36	0.095	0.081	**-0.014**	0.018
23	10/20	02/22	0.88	510.30	63.29	12.63	**-50.66**	6.21	0.124	0.025	**-0.099**	0.012
28	11/20	05/22	0.86	208.73	57.84	5.15	**-52.68**	2.84	0.277	0.025	**-0.252**	0.014
30	12/20	05/22	0.83	183.29	127.71	1.88	**-125.83**	1.80	0.697	0.010	**-0.687**	0.010
31	12/20	02/22	0.82	284.49	183.08	7.68	**-175.40**	4.23	0.644	0.027	**-0.617**	0.015
Average			**0.862**	**Totals**	**984.11**	**290.46**	**-693.66**					

CC Volume Change Interpolated Voids: Leaf-off 2020 to Leaf-off 2022												
					Total Erosion/Deposition (m^3)				Ero-Dep /m^2 Bank Face (m^3)			
Study Bank	Begin Date	End Date	% Cell Match	Surface Area (m^2)	Ero	Dep	Net Ero/Dep	+ -	Ero/m^2	Dep/m^2	Net/m^2 Face	+ -
9	12/20	05/22	0.92	113.98	31.55	6.08	**-25.47**	2.18	0.277	0.053	**-0.223**	0.019
16	12/20	05/22	1.00	733.91	39.00	126.76	**87.76**	11.17	0.053	0.173	**0.120**	0.015
19	12/20	05/22	0.99	1079.91	434.56	84.07	**-350.49**	24.40	0.402	0.078	**-0.325**	0.023
20	11/20	05/22	1.00	766.65	76.13	69.67	**-6.46**	20.03	0.099	0.091	**-0.008**	0.026
22	10/20	05/22	1.00	321.84	26.56	38.01	**11.45**	5.87	0.083	0.118	**0.036**	0.018
23	10/20	02/22	1.00	576.26	59.73	18.19	**-41.54**	7.01	0.104	0.032	**-0.072**	0.012
28	11/20	05/22	1.00	241.70	61.31	8.75	**-52.57**	3.29	0.254	0.036	**-0.217**	0.014
30	12/20	05/22	0.96	211.15	132.23	2.62	**-129.60**	2.08	0.626	0.012	**-0.614**	0.010
31	12/20	02/22	1.00	347.17	198.43	14.61	**-183.82**	5.16	0.572	0.042	**-0.529**	0.015
Average			**0.983**	**Totals**	**1,059.51**	**368.76**	**-690.75**					

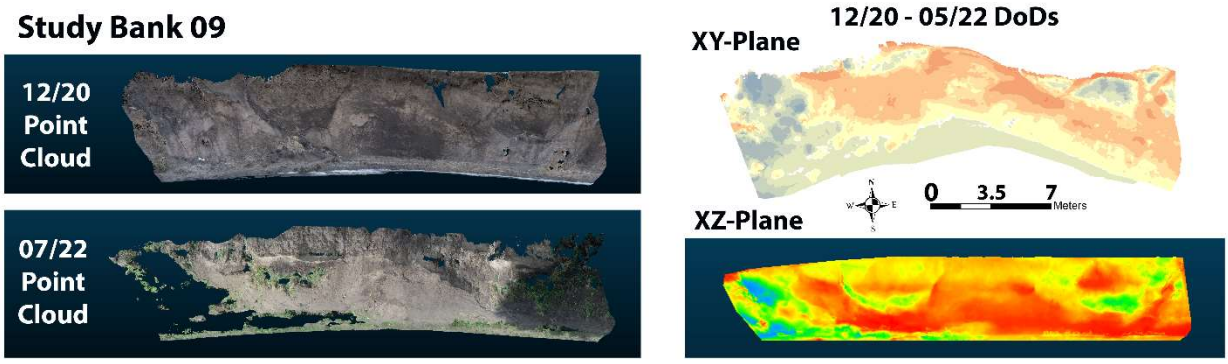


Figure 100: Study bank 09 Point Clouds from 12/20 and 07/22: Example of vegetation concentrated in one area.

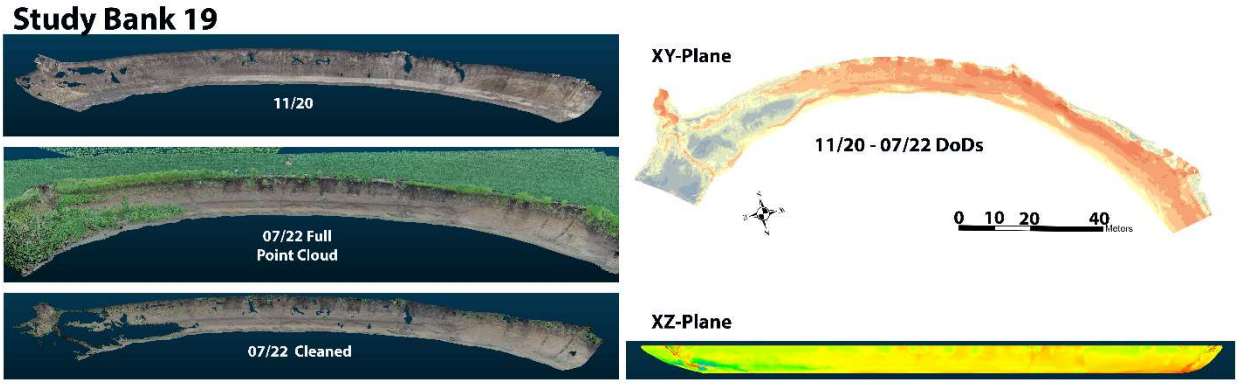


Figure 101: Study Bank 19 Point Clouds from 11/20 and 07/22: Example of vegetation concentrated in one area.

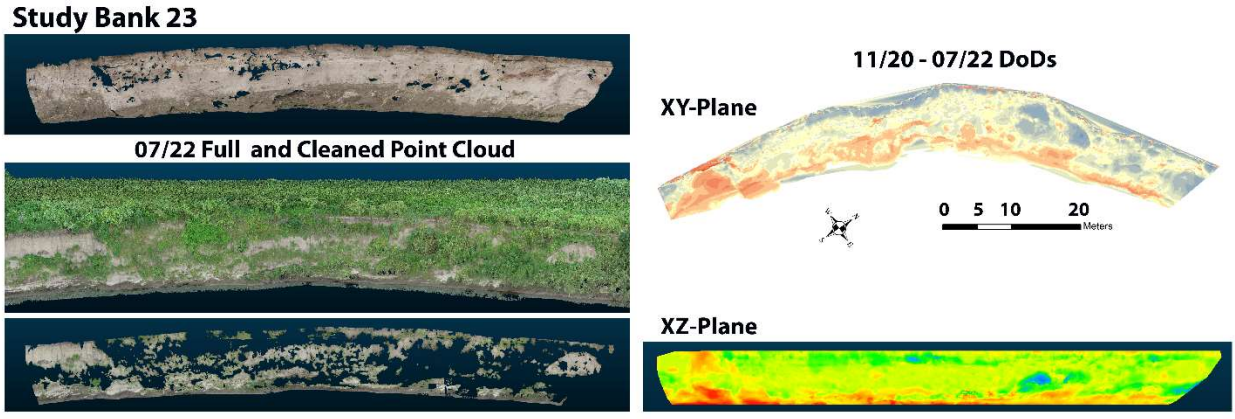


Figure 102: Study Bank 23 Point Clouds from 11/20 and 07/22: Example of vegetation spread over entire SB

Volume Change

Sensitivity of Deposition to Interpolation

The data suggests that deposition may be more sensitive to interpolation. When calculating volume change between the first and last UAV survey dates of each study bank, the total interpolated volume of erosion from all nine study banks was approximately 13% greater than with empty voids, while deposition was 377% greater. In addition, as the percentage of matching cells decreases when voids are left empty, the percent difference between the volume of erosion and deposition calculated with empty voids and the volume calculated with interpolated voids increases. However, as seen in Figure 103, this increase is far more pronounced with deposition suggesting it is more sensitive to the interpolation of voids.

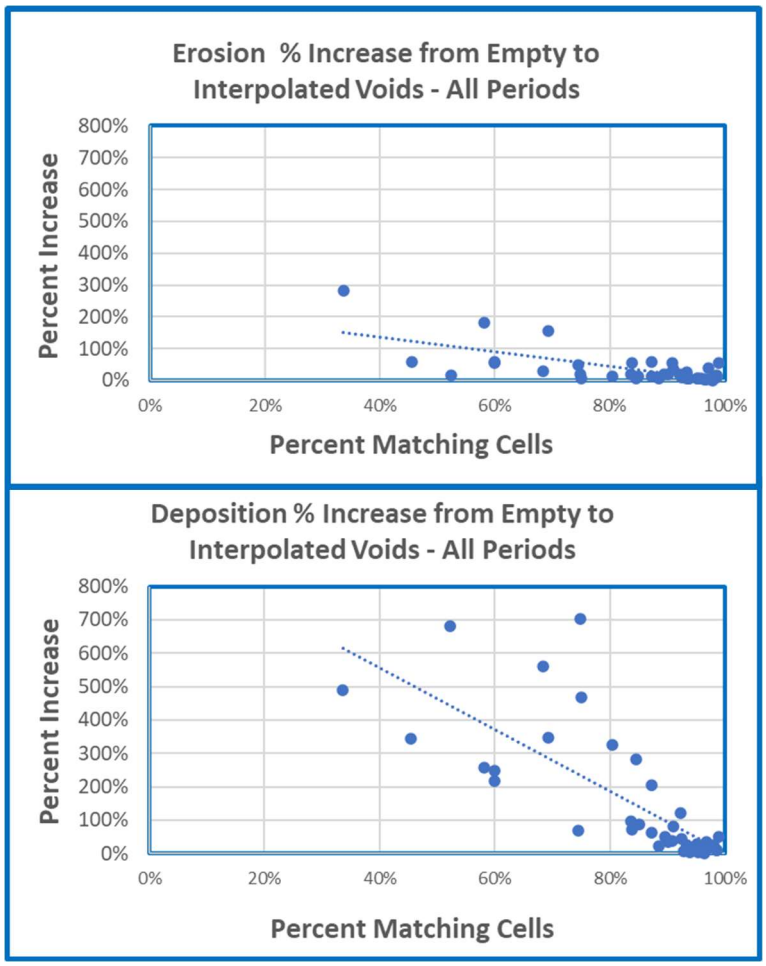


Figure 103: Percentage increase of erosion and deposition from empty to interpolated voids by percentage matching cells.

It is reasonable to assume that vegetated areas would experience deposition due to the vegetation acting as a sediment trap by increasing roughness and reducing velocity allowing more sediment to settle out, and therefore interpolated voids would indicate deposition. However, the

increase in deposition from empty voids to interpolated voids seemed excessive. One reason may be the concave shape of vegetated banks. On a concave riverbank where vegetation is present on a later UAV survey point cloud and little change had taken place, the void resulting from the removal of the vegetation would be interpolated as a flat surface that would be higher than the actual bare earth resulting in overestimation of deposition in that area (Figure 104).

Visual comparison of interpolated DoDs to their corresponding point clouds when voids are present show that areas where high erosion has occurred tend to be areas that are not being interpolated, while areas requiring interpolation indicate high amounts of deposition. Three examples are shown below in Figure 105, where areas of erosion in red correspond to areas not interpolated and areas of deposition in green and blue tend to correspond to areas that are void in the later point clouds and therefore interpolated. While volumes calculated with empty voids as well as interpolated voids were reported, amounts calculated with interpolated voids contain far more uncertainty.

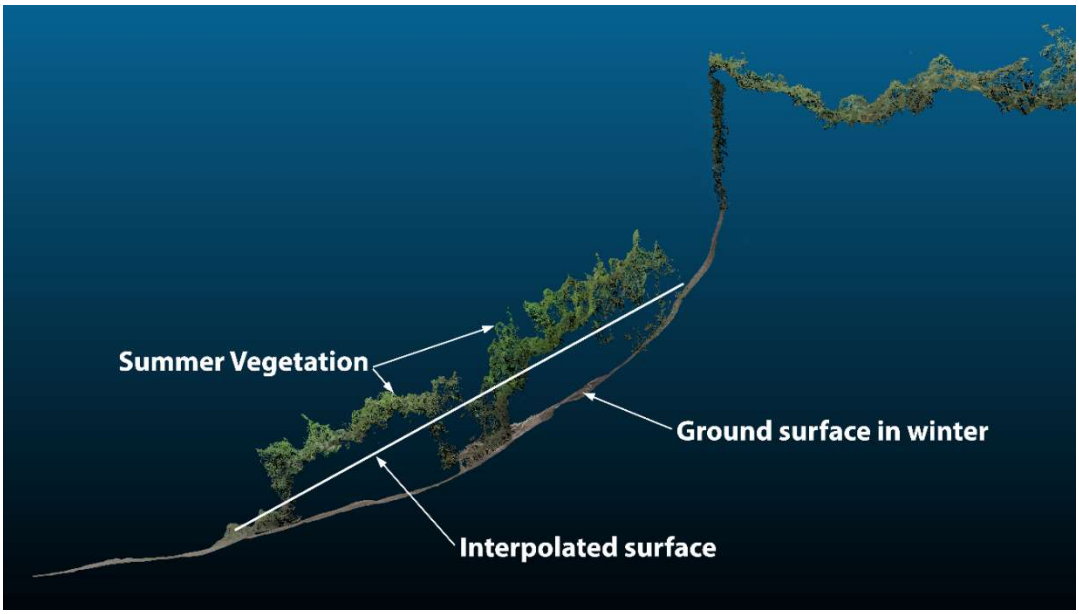


Figure 104: Cross Section of a Concave Portion of SB16: Interpolated void would likely lead to an overestimation of deposition.

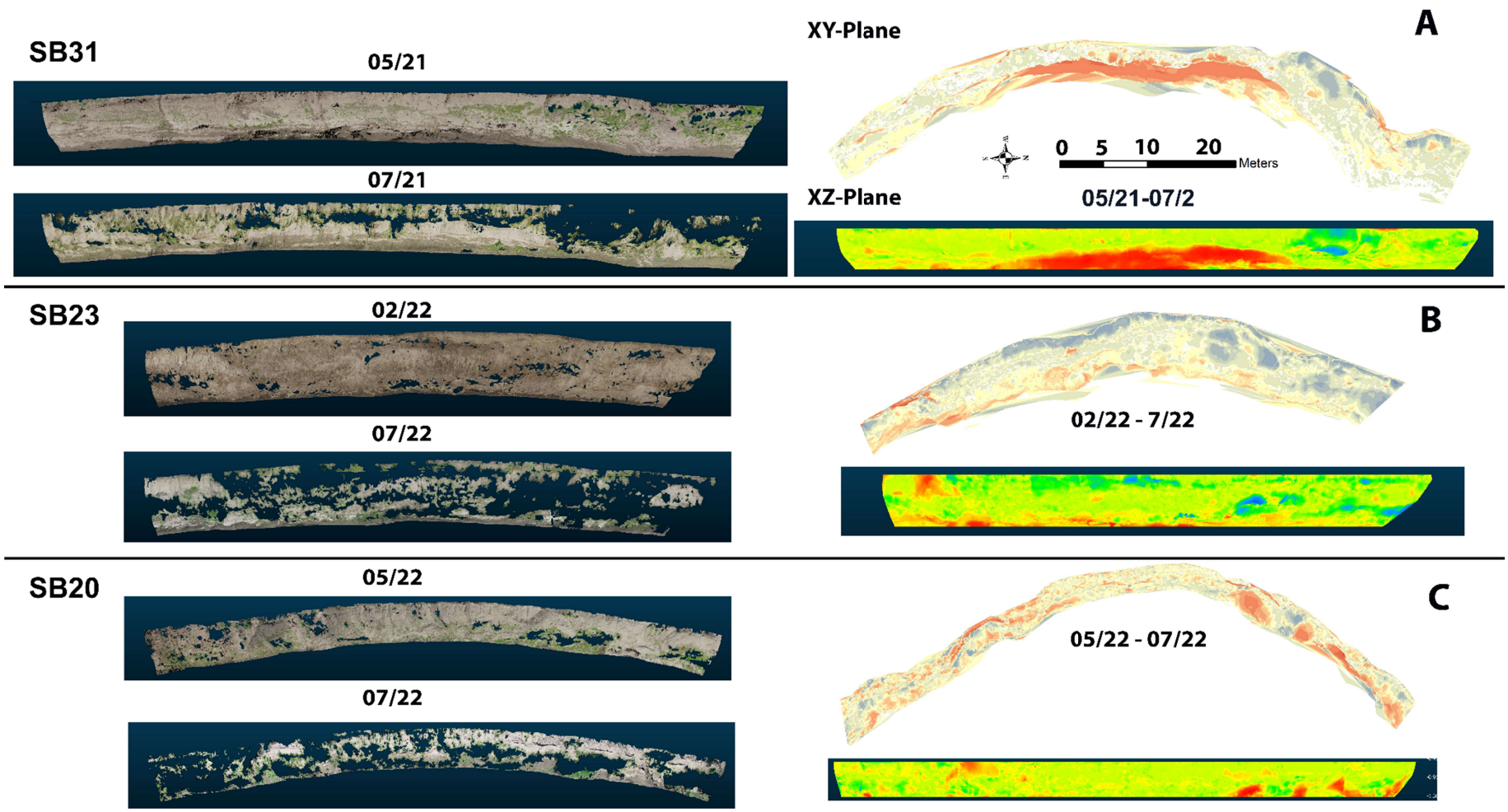


Figure 105: Three examples illustrating interpolated voids resulting in deposition and non-interpolated areas showing erosion.

Volume Change Calculations for Entire Study Period and Leaf-off to Leaf-off Conditions

Table 30 shows total and normalized erosion, deposition, and net volume change for each study bank over the entire study period. As noted, study banks 28 and 22 were not surveyed in July of 2022. Table 31 shows the same data for all banks from leaf-off to leaf-off conditions, but some low herbaceous vegetation growth had begun on some banks surveyed in May of 2022. Although the percentage of matching cells when calculating volume change was greater in leaf-off conditions indicating more accurate calculations, two high flows (one bankfull and one .75-bankfull) resulted in high amounts of erosion between February and July of 2022, with 45%-50% of the total erosion for actively eroding banks occurring in the summer of 2022 (Figure 106). Therefore, the remainder of this discussion will focus on volume change over the entire study period. The nine study banks, with a total length of only 822 m, experienced an estimated -1,730 m^3 (Int. -1,953 m^3) of erosion over the 19-month study period. However, not all study banks actively eroded during the study period, as study bank 16 experienced net deposition of 10.74 m^3 (Int. 131.28 m^3) and study bank 22 may have also experienced net deposition as the volume calculated with empty voids resulted in very minor erosion, but when voids were interpolated, net deposition (11.45 m^3) was indicated.

Study banks 19, 31, and 30 had the highest amounts of total erosion of -726 m, -407 m^3, and -232 m^3 (Int. -727 m^3, -453 m^3, -245 m^3), respectively, and bank erosion rates per square meter of bank face of -0.68 m^3, -1.18 m^3, -1.12 m^3 (Int. -0.68 m^3, -1.32 m^3, -1.18 m^3), respectively. It is important to note that study bank 30 with a drainage area (DA) of only 115 km^2 had a similar rate of erosion per m^2 bank face as

study bank 31 with a DA of 1,129 km^2. In addition, the average rate of erosion per m^2 bank face of the three study banks in the upper watershed (-0.57 m^3) was significantly higher than the six study banks in the lower watershed (-0.35 m^3) suggesting higher rates of channel adjustment in the upper watershed as suggested in Keane & Sass (2017).

The data also suggests that the ratio of radius of curvature to bankfull width (Rc/BkfW) could be an influencing factor on overall study bank change. The Rc/BkfW has an expected value between 2 and 3 (Langbein & Leopold, 1966; Williams, 1986). Study bank 16 with a Rc/BkfW of 2.7 is the only study bank to experience net deposition over the entire study period (Tables 29 and 30). In contrast, study banks 30 and 31 with the lowest Rc/BkfWs of 0.57 and 0.60, respectively, had the highest rates of erosion per meter bank face of -1.18 m^3 and -1.32 m^3, respectively. The remaining study banks had Rc/BkfWs ranging between 0.87 and 1.09 with net erosion per square meter bank face ranging between -0.68 m^3 and -0.012 m^3.

Given the episodic nature of mass wasting erosional processes common in the BVR system, the time frame of this study may not be adequate to reflect long-term erosion rates at the study banks that experienced little or no change. Of the study banks experiencing net erosion over the study period, banks 20, 23, and 22 had the lowest rates of erosion per m^2 bank face of -0.14 m^3, -0.12 m^3, -0.01 m^3 (Int. -0.11 m^3, -0.04 m^3, 0.04 m^3); however, the DoD derived from 2010 and 2018 LiDAR data in Chapter 2 indicate these study banks as well as study bank 16 that showed net deposition experienced significant amounts of erosion between 2010 and 2018 (Figure 107).

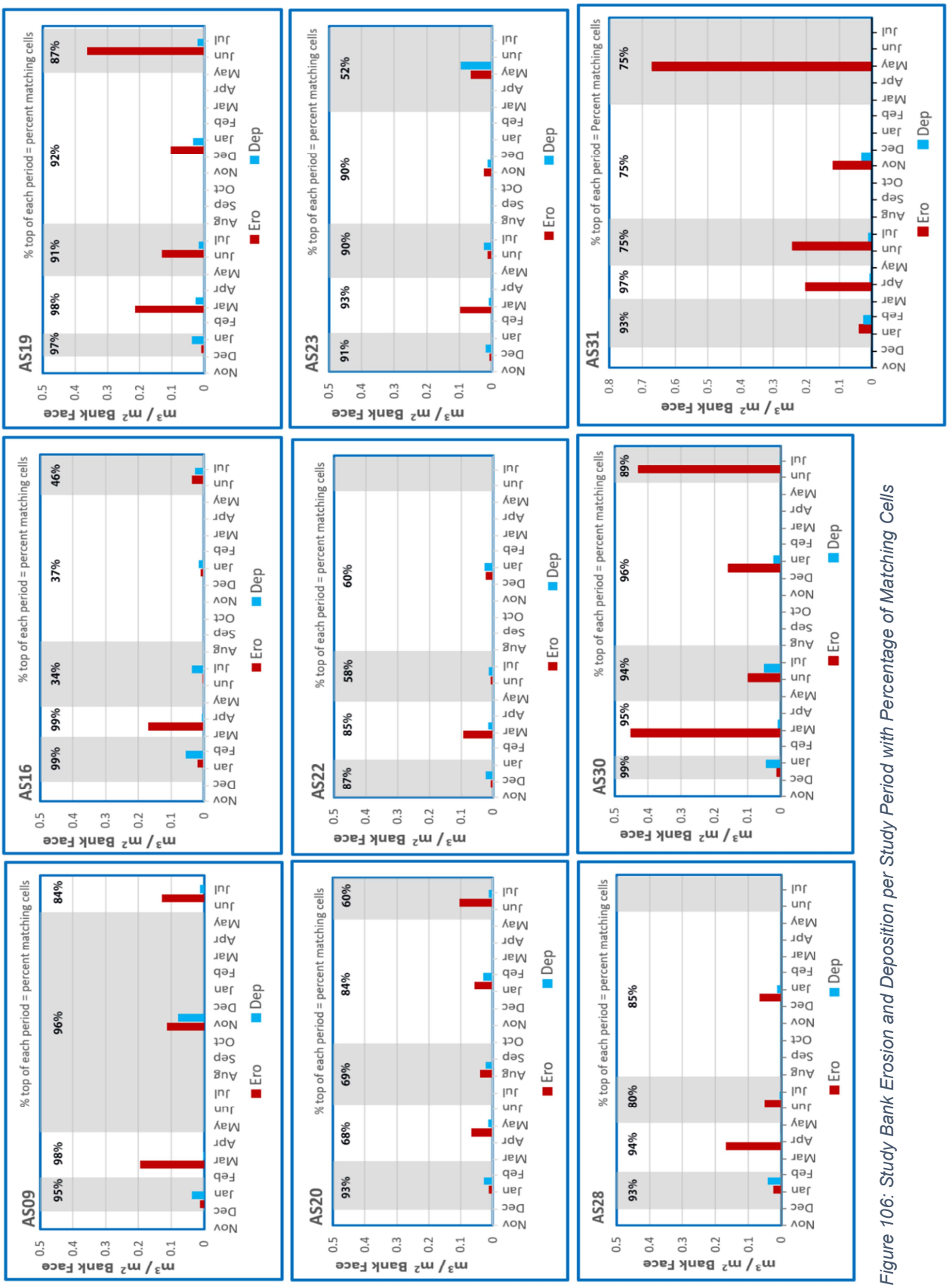


Figure 106: Study Bank Erosion and Deposition per Study Period with Percentage of Matching Cells

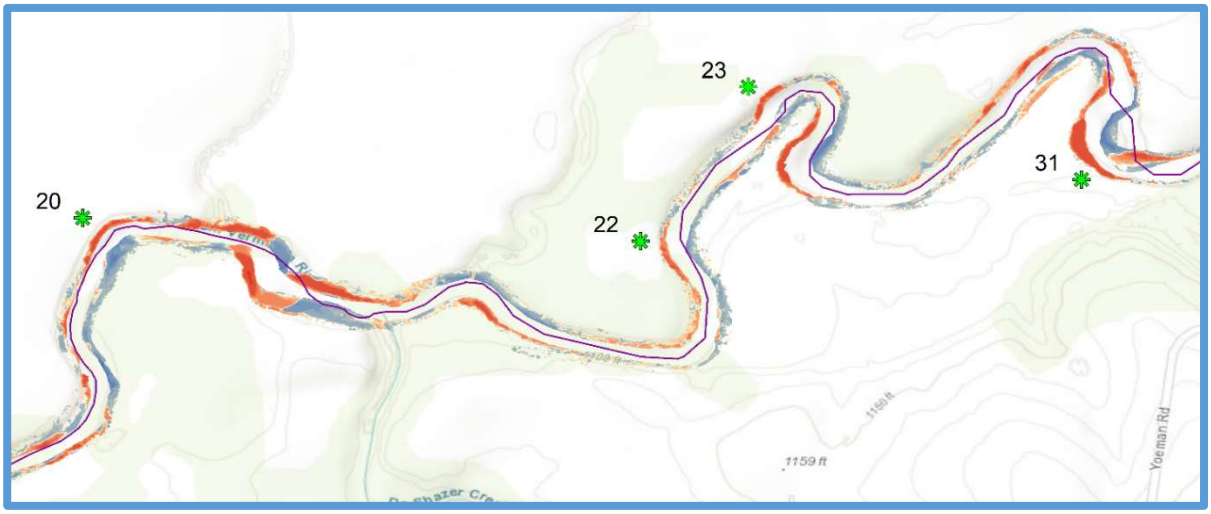


Figure 107: Chapter II 2010-2018 DoD with SfM Study Banks

Use of SfM to Monitor BVR Erosional Hotspots at a Fine Temporal Scale

For this section, percentage of matching cells and volume change will be discussed concurrently. The first period (Table 28, p.210) the BVR erosion hotspot study banks were monitored was the winter of 2020-2021. Study banks were surveyed in late-November and December of 2020 and again later in the winter on dates ranging from late January to early March. In 2020, due to the extensive flooding and numerous high flows during the summer of 2019, the study banks were void of any growing vegetation but did have some minor amounts of vegetative debris from the previous growing season. Vegetation debris remained minimal for the second UAV survey as evidenced by matching cell percentages ranging from 87% to 99% with an average of 94% for all nine study banks (Figure 106), which indicates very good feasibility of using SfM to monitor banks over these winter months.

All study banks except one experienced net deposition during this winter period primarily due to the in-channel erosional processes of freeze thaw and dry ravel, as there were no flows above low flow during this period (Figures 86, p.202 and 106; Appendix C). These low-flow, in-channel erosional processes are evidenced by an accumulation of darker material over the entire bank surface with concentration within the rills and small gullies along the bank face as well as at the toe of the study banks seen in late winter point clouds, and this accumulation of winter deposition is also evident in the blue and green colors of the DoDs (Figure 108). Quantities of deposition during these winter months were not large, ranging from 0.026 m^3 to 0.056 m^3 (Int. 0.029 m^3 to 0.066 m^3) per square meter of bank face and totaling approximately 156 m^3 (Int. 188 m^3) for all nine study banks (Figure 106 and Appendix C).

To assess the use of SfM to monitor erosion hotspots and determine study bank volume change for the second evaluation period in the Spring of 2021, the next round of image-collecting UAV surveys was conducted in late April and May, except for study bank 20 that was surveyed in June of 2021 and will not be included in this period's assessment. An approximately 75%-bankfull flow in late March (Figure 86, p.202) removed the winter's loose deposition as well as much of the vegetation debris from the previous summer resulting in even cleaner banks than in the first, initial UAV surveys (Figures 109 and 110), which is evidenced by a higher percentage of matching cells than the previous period in the DoDs of five of eight study banks (Figure 106). The percentage of matching cells ranged from 85% to 99% with an overall average of 95% when conducting this period's volume change calculations in CC with empty voids. As with the winter period, the high percentages of matching cells suggest the use of SfM to

monitor banks and determine amounts of both erosion and deposition was accurate for this spring period. The early season near bankfull event in March of 2021 led to net erosion far greater than the previous winter's deposition, with net erosion rates

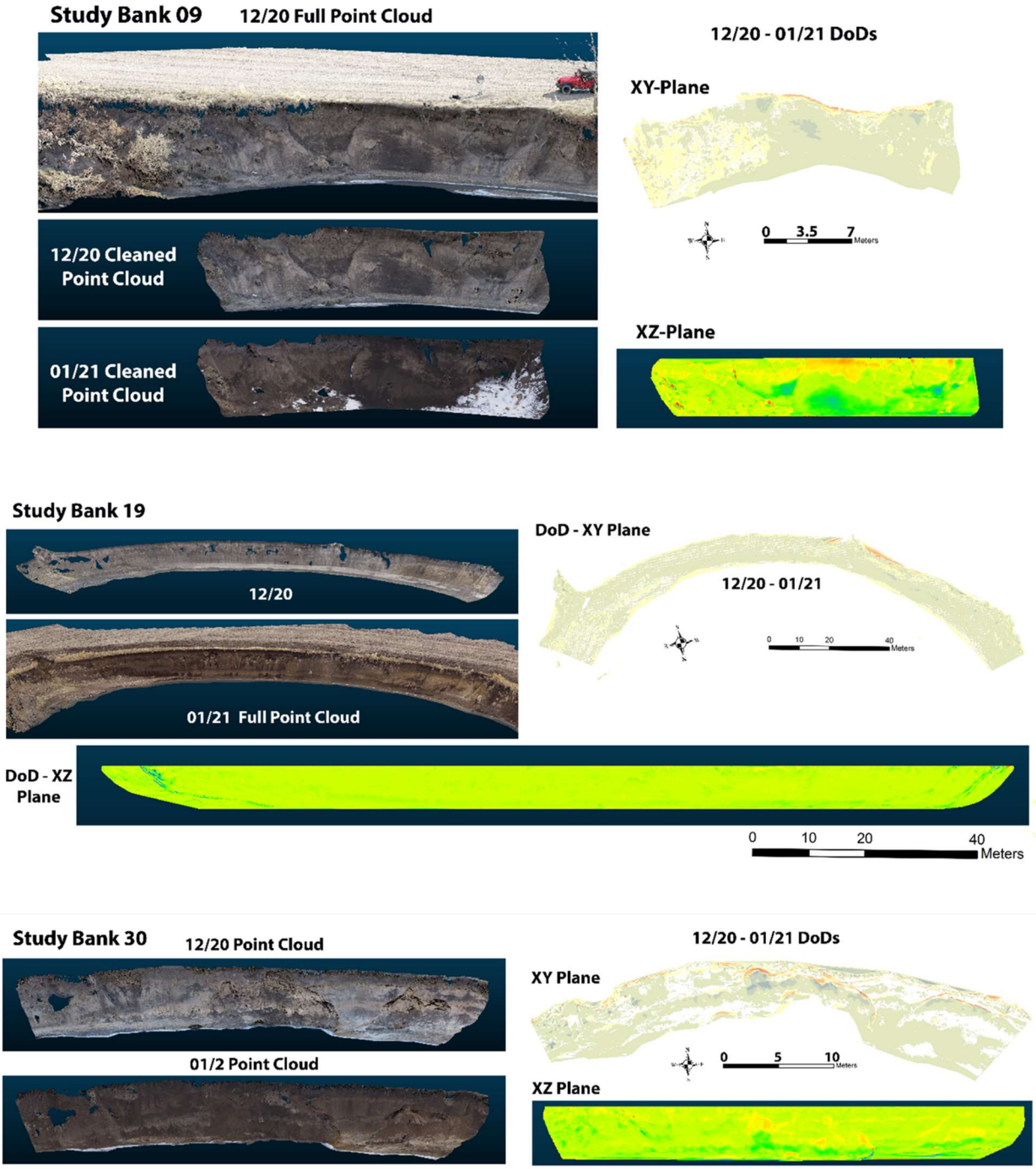


Figure 108: Three examples of the accumulation of winter deposition from freeze-thaw and dry ravel

ranging from -0.053 m^3 to -0.445 m^3 (Int. 0.077 m^3 to -0.468 m^3) per square meter of bank face and total erosion of approximately 731 m^3 (Int. 791 m^3) for all eight study banks included in this period's assessment. The high-water mark of the March high flow event was clearly evident on study bank 19's 04/21 point cloud as well as its 01/20 - 04/21 DoD (Figure 111).

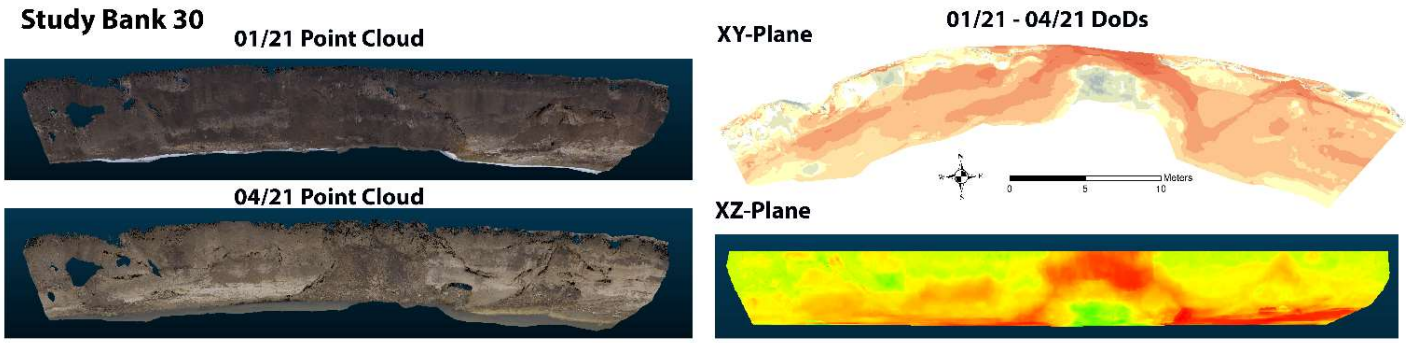


Figure 109: Study Bank 30's Second (Winter) Period: Removal of winter deposition and additional erosion

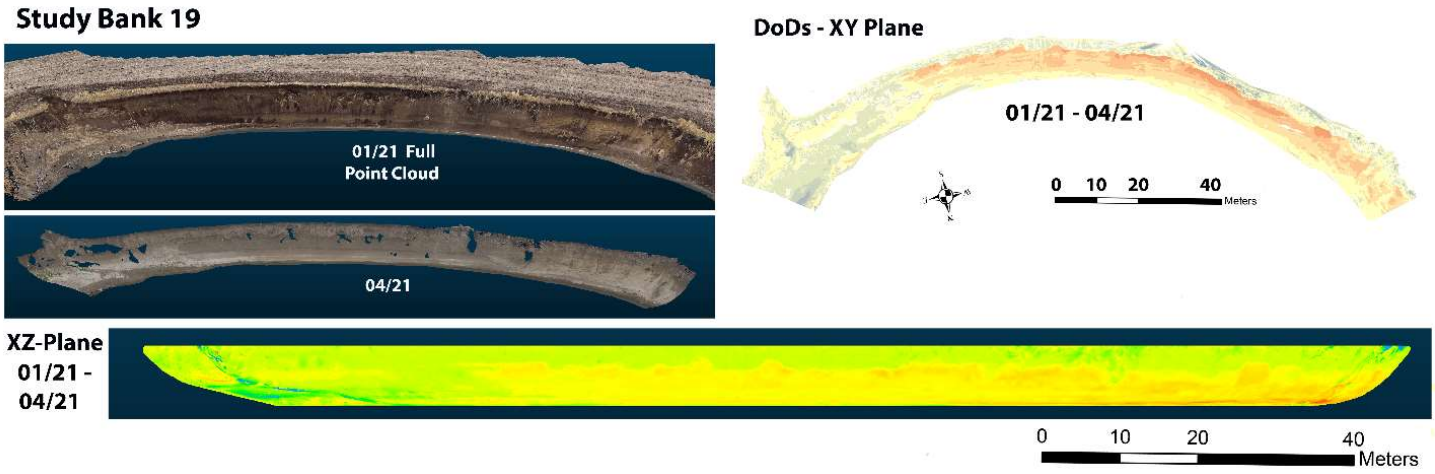


Figure 110: Study Bank 19's Second (Winter) Period: Removal of winter deposition and additional erosion

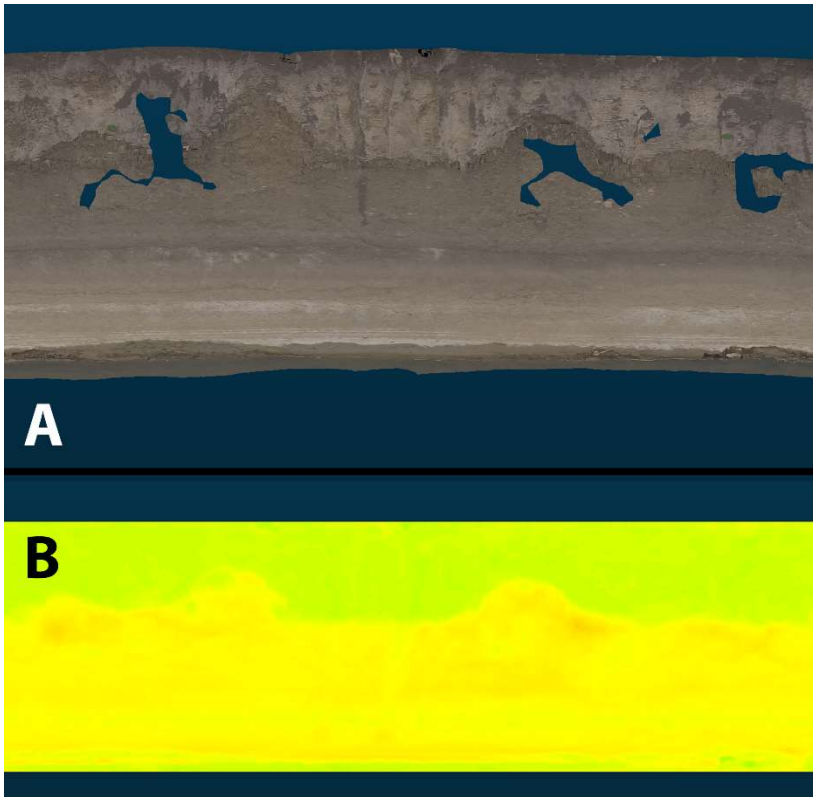


Figure 111: March 2021 High Flow Water Line on Study Bank 19: (A) 04/21 point cloud and (B) 01/21-04/21 XZ-plane DoD

Six of nine study banks (31, 30, 28, 23, 22, and 19) were resurveyed in late-July and study bank 16 in mid-August. Study bank 20, which had been surveyed in June, was resurveyed in mid-September. Study bank 9 was not resurveyed in the late summer of 2021 due to the landowner's active regrading of the field and gulley immediately adjacent to the study bank using heavy equipment. During this summer period, study banks 30, 23, and 19 experienced little vegetation as evidenced by matching cell percentages in the CC volume calculation tool ranging between 90% and 94%. Study banks 28 and 31 experienced vegetation cover of 20% and 25% (80% and 75% matching cells), respectively. However, at the two latter study banks, the establishment of vegetation was concentrated at one end of the study bank, with the

majority of the study bank remaining vegetation free and experiencing erosion (Figure 112). Study banks 16, 22 and 20 experienced vegetation growth scattered all along the entire bank face, with cell matching percentages of 34%, 58%, and 69%, respectively. The 66% vegetative cover of study bank 16 that was established during this period was the highest of any bank for the entire study period (Figure 113).

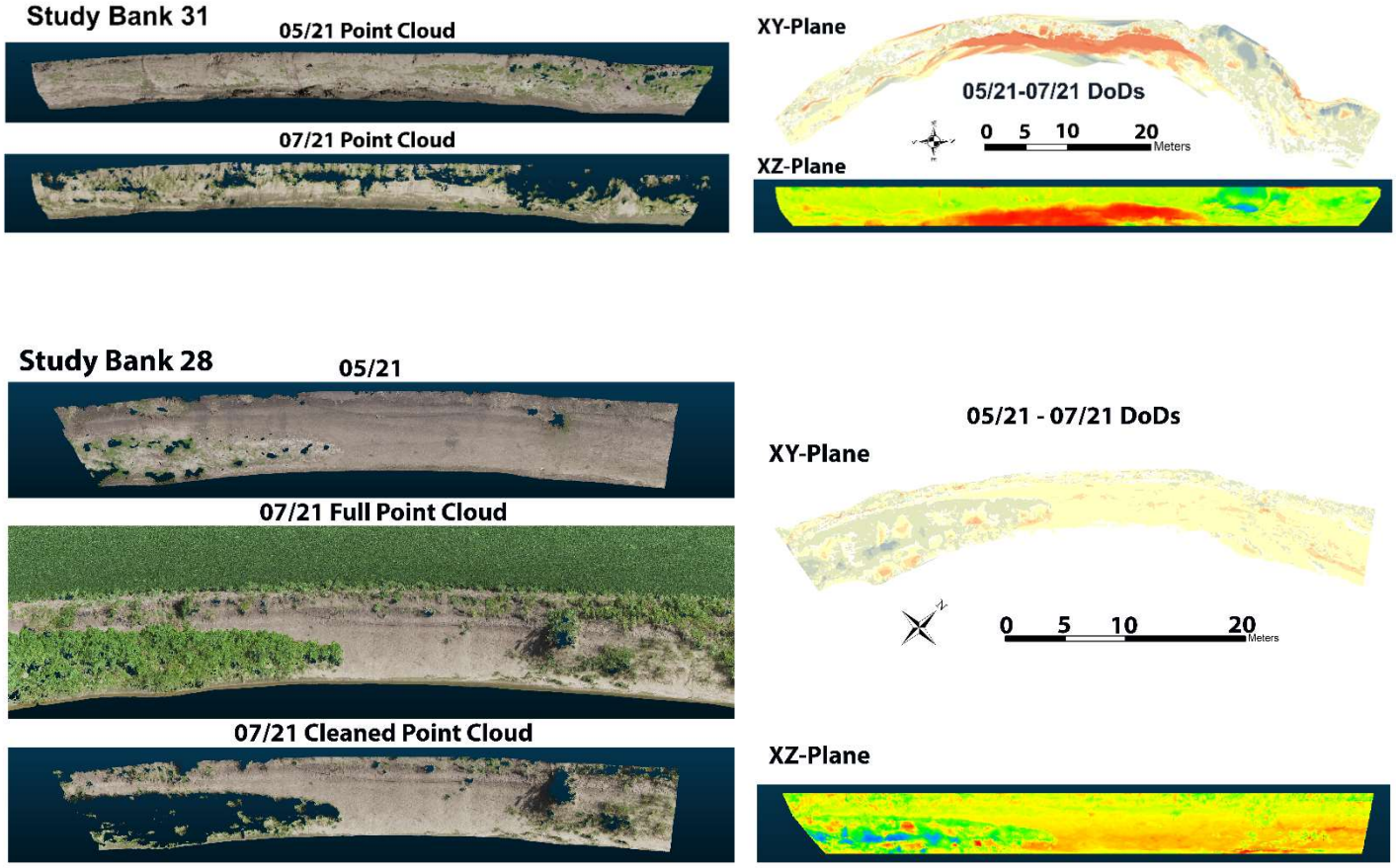


Figure 112: Two Examples of Vegetation Concentrated at One End of Study Bank: (28 and 30) during the summer of 2021.

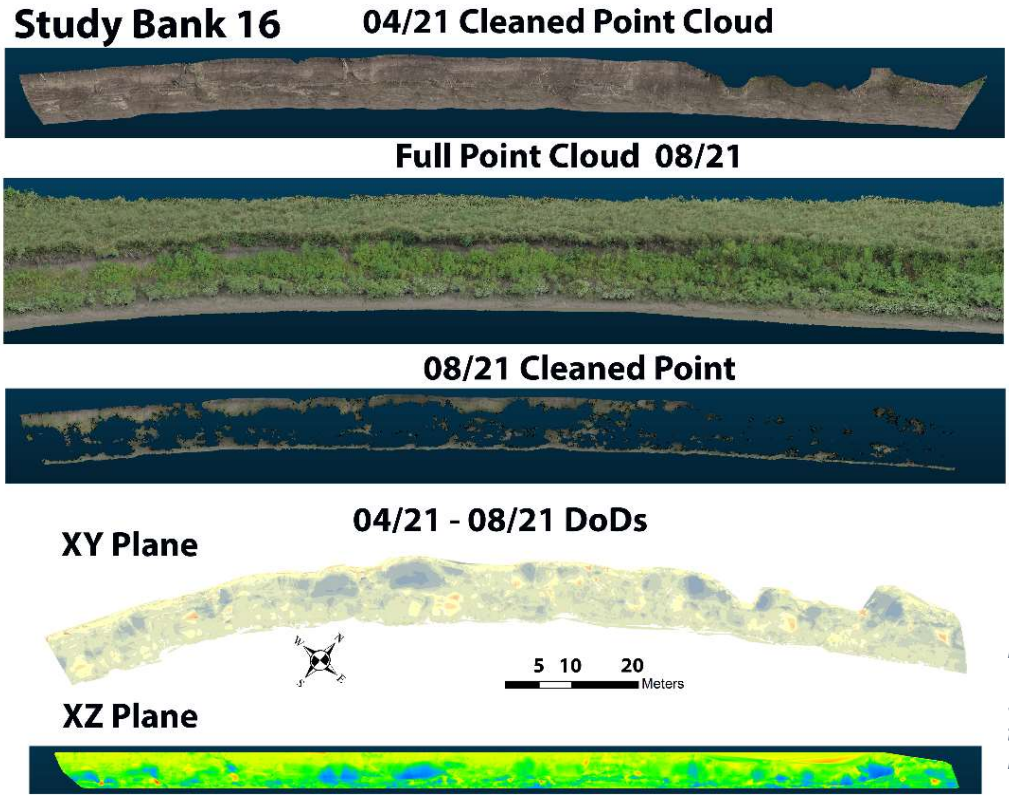


Figure 113: Example of Vegetation of Entire Study Bank: SB16 during the summer of 2021, Period 3

During this summer period, the river flow was dominated by low flow conditions, with only one river flow exceeding 0.5 bankfull discharge and three exceeding 0.25 bankfull discharge (Figure 86, p.202). Nonetheless, study banks 31 and 19 experienced significant rates of net erosion of -0.23 m^3 and -0.11 m^3 (Int. -0.2 0 m^3 and -0.015 m^3) per square meter of bank face, respectively and total erosion of -83.97 m^3 and -142.01 m^3 (Int. 88.56 m^3 and 157.71 m^3), respectively. Study banks 30, 28, and 20 experienced minor net erosion ranging between -0.02 m^3 and -0.05 m^3 (Int. -0.001 m^3 and -0.05 m^3) per square meter of bank face; however, the erosion for study bank 20 was less than the overall uncertainty (+ -) (Appendix C). Total erosion at all study banks for this period was approximately 303 m^3 (Int. 336 m^3). Volume change calculations for

study banks 23, 22 and 16 resulted in very low rates of deposition all less than the overall uncertainty for each study bank (Appendix C).

Simultaneous inspection of the two point clouds used for assessment during this summer period for each of the study banks with cell matching percentages of 75% and greater in CC revealed that all areas of active erosion during the period were present in each point cloud. In addition, the bank toe and upper bank were visible around most areas where vegetation had established on each study bank and had not retreated suggesting these areas had not experienced erosion. The data and visual inspection suggests that even when cell matching percentages are low, SfM is effective in monitoring areas of active erosion, which as one would expect, do not establish herbaceous vegetation over the growing season. In contrast, SfM may not be effective at estimating amount of deposition that are more likely to occur along vegetated banks due to the vegetation acting as a sediment trap, as these areas are excluded from volume calculation when the voids are left empty and interpolation of voids on concave banks likely result in the overestimation of deposition (Figure 104, p.225).

The next round of UAV surveys was conducted in late winter and spring of 2022, with study banks 31 and 23 being surveyed in February and all other study banks being surveyed in late May. During this period that included fall, winter, and spring, the only flow events of any significance were a flow in mid-August 2021 and another mid-May 2022 both between 0.25 and 0.50 bankfull discharge (Figure 86, p.202). This 5th round of UAV surveys was completed just before the only (near) bankfull event of the entire study period that occurred on May 26, 2022. Study bank 9 was resurveyed in May; however, as it had not been surveyed since April of 2021, it was not included in this

period's assessment. The percentage of matching cells between corresponding point clouds remained high for study banks 30, 23, and 19 at 96%, 90%, and 92%, respectively and remained the same or slightly higher for study banks 31, 28, and 22 at 75%, 85%, and 60% (Figure 106). At study bank 20, the percentage increased by 15% from 69% to 84%, while remaining low for study bank 16 at 37%. While certainty decreases as the percentage of matching cells decreases, as with the previous period, visual inspection of the point clouds in CC reveal that the surfaces of both point clouds in areas where obvious erosion had been present resulting in them being included in the volume calculations. As with the previous period, areas where vegetation had been established were more likely to have experienced deposition leading to voids in the point clouds that likely resulted in an overestimation of deposition given the convex shape of the BVR riverbanks (Figure 104, p.225).

During this 4th period of erosion hotspot monitoring study banks 19, 28, 30 and 31 experienced moderate rates of net erosion ranging from 0.05 m^3 to 0.14 m^3 (Int. -0.017 m^3 to -0.015 m^3) (Figure 106, Appendix C). The remaining study banks experienced minor net erosion or deposition all lower than the overall uncertainty for each study bank, indicating little change during this period. Total erosion for this period for all study banks was approximately 278 m^3 (Int. 392 m^3), similar to the total erosion of the previous summer. During this period, the erosion on banks that did experience erosion was concentrated along the toe of the bank, as seen in study banks 20 and 30 (Figure 114).

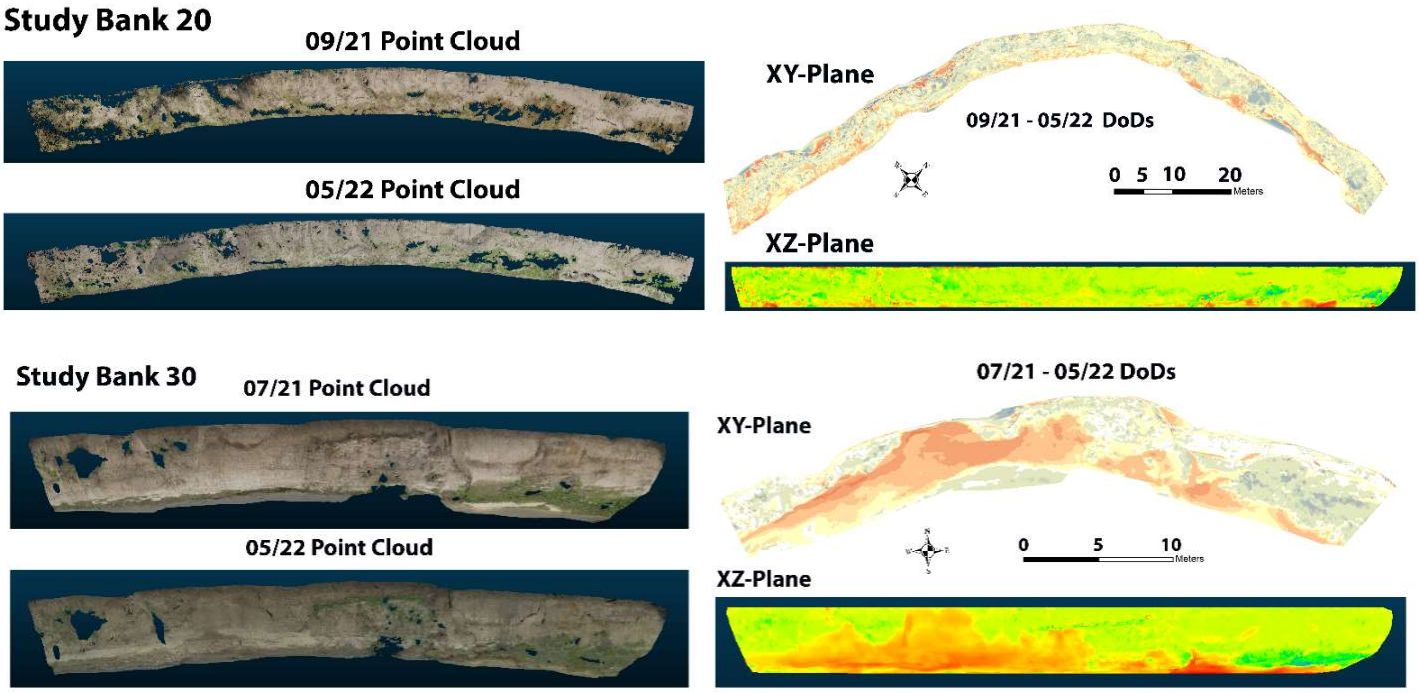


Figure 114: Two Examples of Erosion Concentrated at Toe of Bank in 4th Evaluation Period: SB20 and SB30

The final round of UAV surveys was conducted for seven of nine study banks between July 24th and July 26th of 2022, with study banks 28 and 22 not being resurveyed for reasons noted earlier. The final (5th) period of assessment was similar in time frame as the third period (summer 2021). However, in contrast to only one 0.25-bankfull flow during the previous summer, there were two high flows during the summer of 2022, one near bankfull flow in late-May and another 0.75-bankfull flow in mid-July as well as two additional, smaller 0.25-bankfull flows in late-May and mid-June (Figure 86, p.202).

For all except two study bank, between the early 2022 survey date and the July survey date, the percentage of matching cells decreased due to vegetation growth and therefore voids in the later point clouds. The percentage of matching cells remained the

highest with study banks 30, 19, and 9 at 89%, 87%, and 84%, respectively (Figure 106). For study bank 31, the percentage remained the same at 75%. Study bank 23 saw the highest decrease in percentage of matching cells due to a dramatic increase in vegetative cover throughout the bank compared to the previous summer (Figure 115). Study bank 20 also saw a substantial decrease in matching cells from 84% in the previous period to 60%. Study bank 16 saw an increase in the percentage of matching cells due to shallow scour along the toe of the riverbank that removed some of the herbaceous vegetation established the previous summer, which can be seen in the XZ-plane DoD as areas of red (erosion) at the toe of the bank (Figure 116).

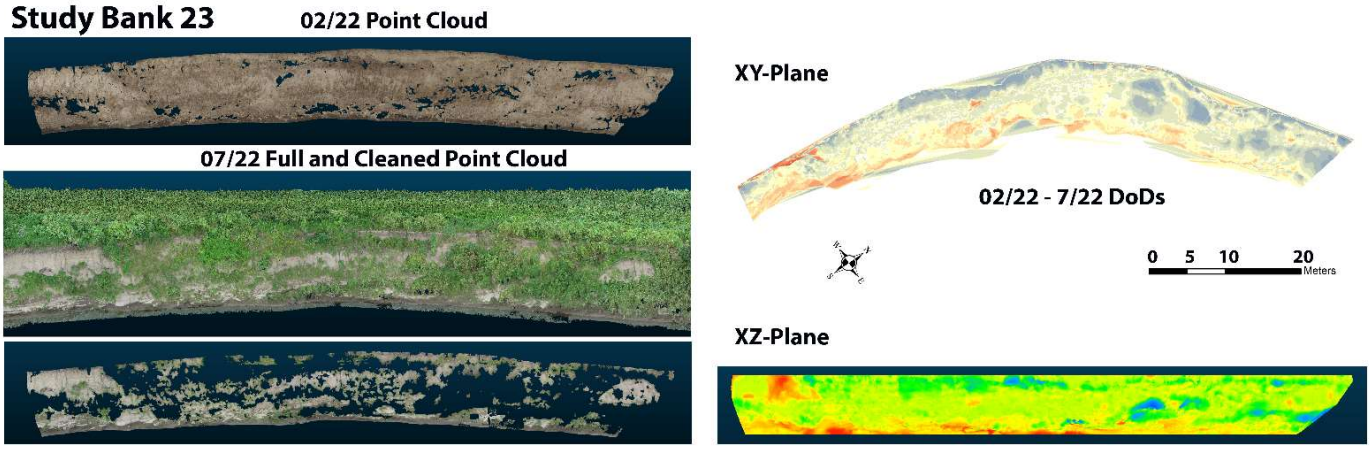


Figure 115: Increase in Bank Vegetation on Study Bank 23: Summer 2022

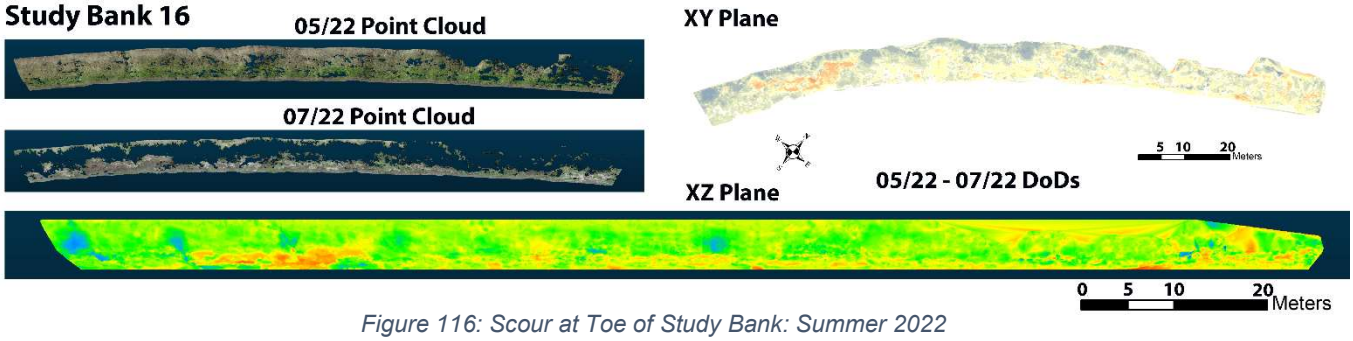


Figure 116: Scour at Toe of Study Bank: Summer 2022

The high flows noted above resulted in this last period having the highest overall total erosion of any period, 904 m^3 (Int. 1,083 m^3), even though two study banks were not included. Study banks 19, 31, and 30 experienced the highest rates of net erosion (-0.67 m^3, -0.43 m^3, and -.034 m^3 (Int. -0.77 m^3, -0.45 m^3, and -.035 m^3), respectively) as well as amounts of net erosion (-232 m^3, -94 m^3, and -371 m^3 (Int. - 269 m^3, -100 m^3, and -376 m^3), respectively) (Figure 106, Appendix C). Study banks 23, 20, and 9 saw more moderate to low rates of erosion at -0.05 m^3, -0.09 m^3, and -0.12 m^3 (Int. -0.02 m^3, -0.12 m^3, and -0.13 m^3), respectively. The minor amount of erosion at study bank 16 along the toe of the bank was below the overall uncertainty for the study bank.

Erosional Processes and River Flows

In addition to evaluating the use SfM to monitor erosion hotspots along the BVR riverbank, the DoDs and volume change calculations generated in this research were used to assess riverbank erosional processes and their relation to river flows at selected study banks. The three study banks that experienced the greatest amount of erosion (30, 31, and 19) and the relation of their erosional processes to river flows will be discussed. “Time-series: Current/Historical Observations” that reports discharge every 15 minutes was collected for the study period for the USGS gauge station (November 2020 through July 2022) (Figure 86, p.202). As noted, bankfull was determined as the 1.5-year return interval to be 5,016cfs (142 m^3/s) (Sass & Keane, 2012). In addition, 75%, 50% and 25% of bankfull were also calculated and are shown in Figure 86, p. 202. Figure 117 shows selected point clouds and DoD for Study Bank 30, and Figure 118 shows erosion and river flows for each time period (Table 28, p.210). The initial 12/20-01/21 DoD and point clouds illustrate a buildup of deposition resulting from winter freeze

thaw and dry ravel erosional processes over the winter. The winter's deposition is then removed most likely by the high flow in March of 2021 resulting in a high erosion rate during the second period of study bank 30 (Figure 117). In addition, the onset of an area of rotational slump (one of two types of erosional mass wasting common in the BVR system) can be seen near the middle of the study bank in the 01/21-04/21 DoDs indicated by an area of erosion near the top of the bank with deposition near the bank toe. This area of rotational slump becomes much more pronounced in the 04/21-07-21 (XZ-Plane) DoD with intensive erosion near the top of bank with a large area of deposition just below. This slumped material was then removed by the high flows of the summer of 2022 (Figure 118) as seen in the final, 05/22-07/22 DoDs (Figure 117).

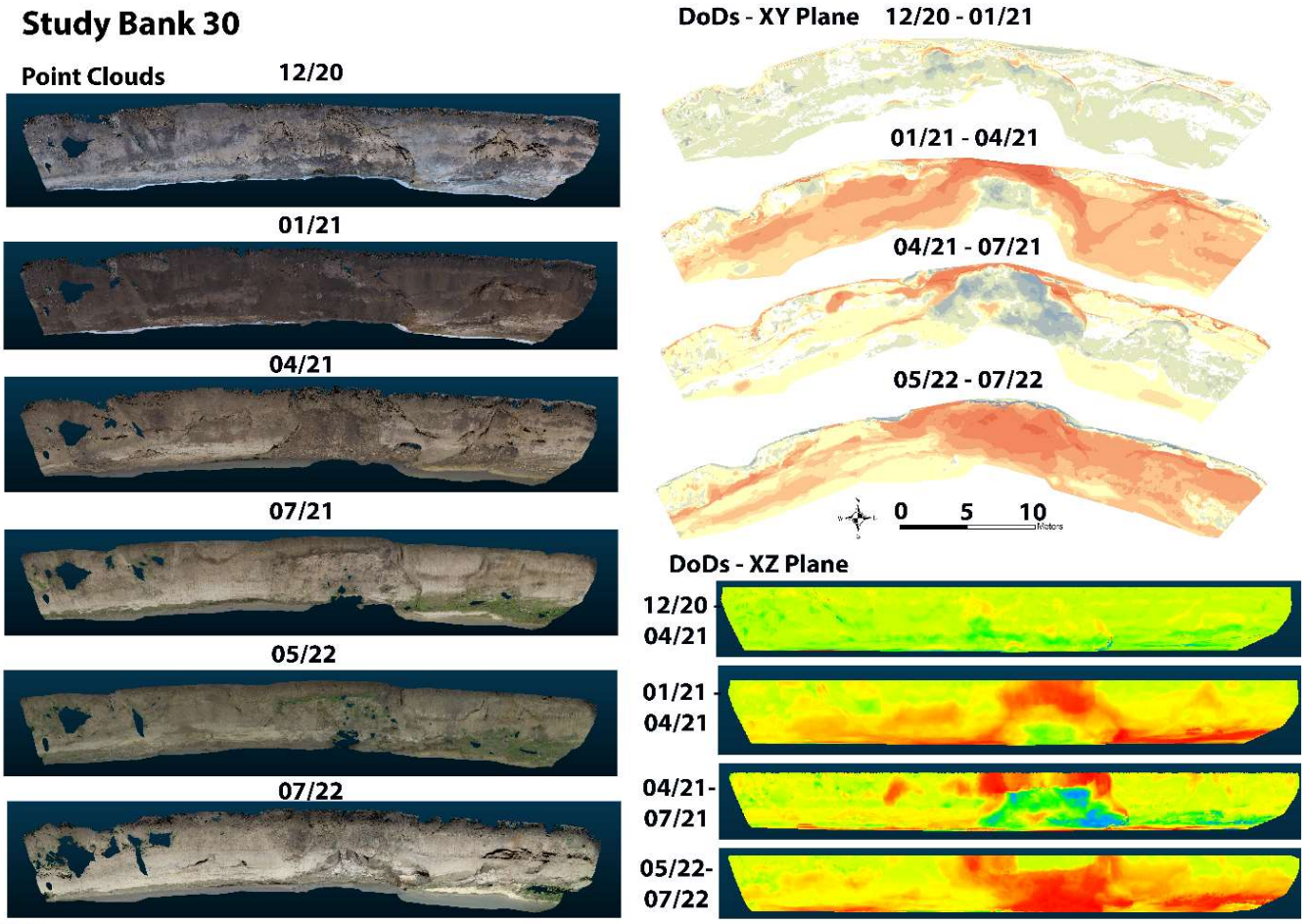


Figure 117: Selected Study Bank 30 Point Clouds and DoDs Illustrating Rotational Slump

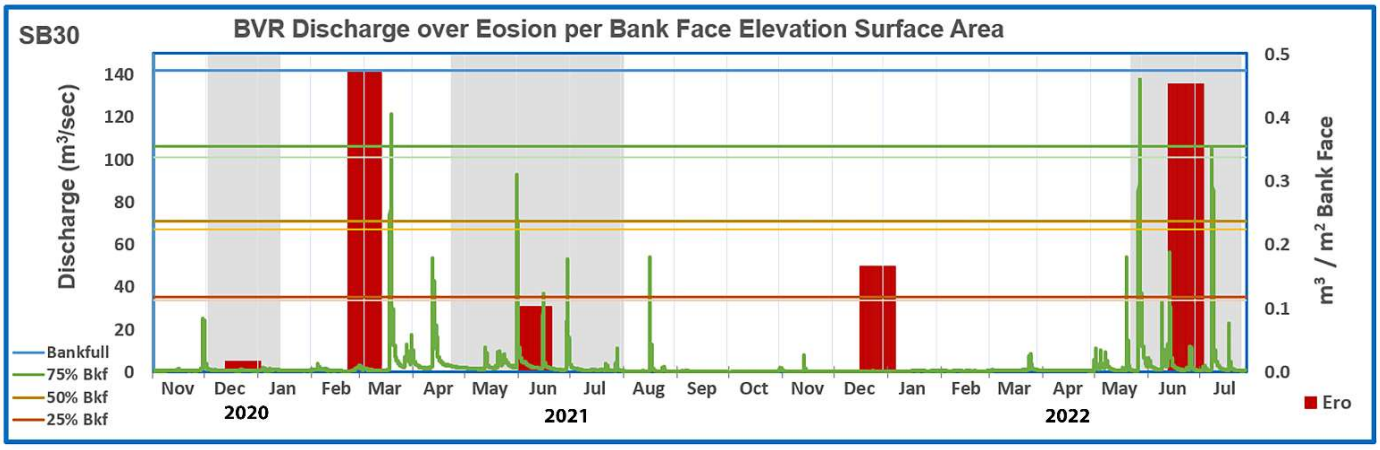


Figure 118: BVR Discharge Over Erosion per Period: Study Bank 30

In contrast to study bank 30, study bank 31 appears to illustrate the mass wasting erosional process of fall, the second type of mass failure common in BVR system. In the first three periods (Table 28, p.210), represented by DoDs 12/31-03/21, 03/21-05/21, and 05/21-07/21, moderate levels of riverbank erosion occur primarily along the toe of the south half of the bank (Figures 119 and 120). The north half of the study bank that did not see large areas of erosion, began to establish vegetation in the summer of 2021 which became more substantial in the summer of 2022. In the final period DoD (02/22-07/22) a large area of erosion can be seen primarily on the middle and upper bank of the south portion of the bank above the previous bank toe erosion (Figure 120). In addition, the amount of erosion in the last period is substantially larger compared to the earlier 4 periods, which is indicative of fall. The increase in the bank angle of the southern half of the study bank to near vertical between 03/21 and 07/22 (Figure 120 Nadir Views, and Table 29, p.217) are also common in erosional process of fall. However, given the final period assessed for study bank 31 was five months long, it is impossible to determine the exact timing of when the material was removed.

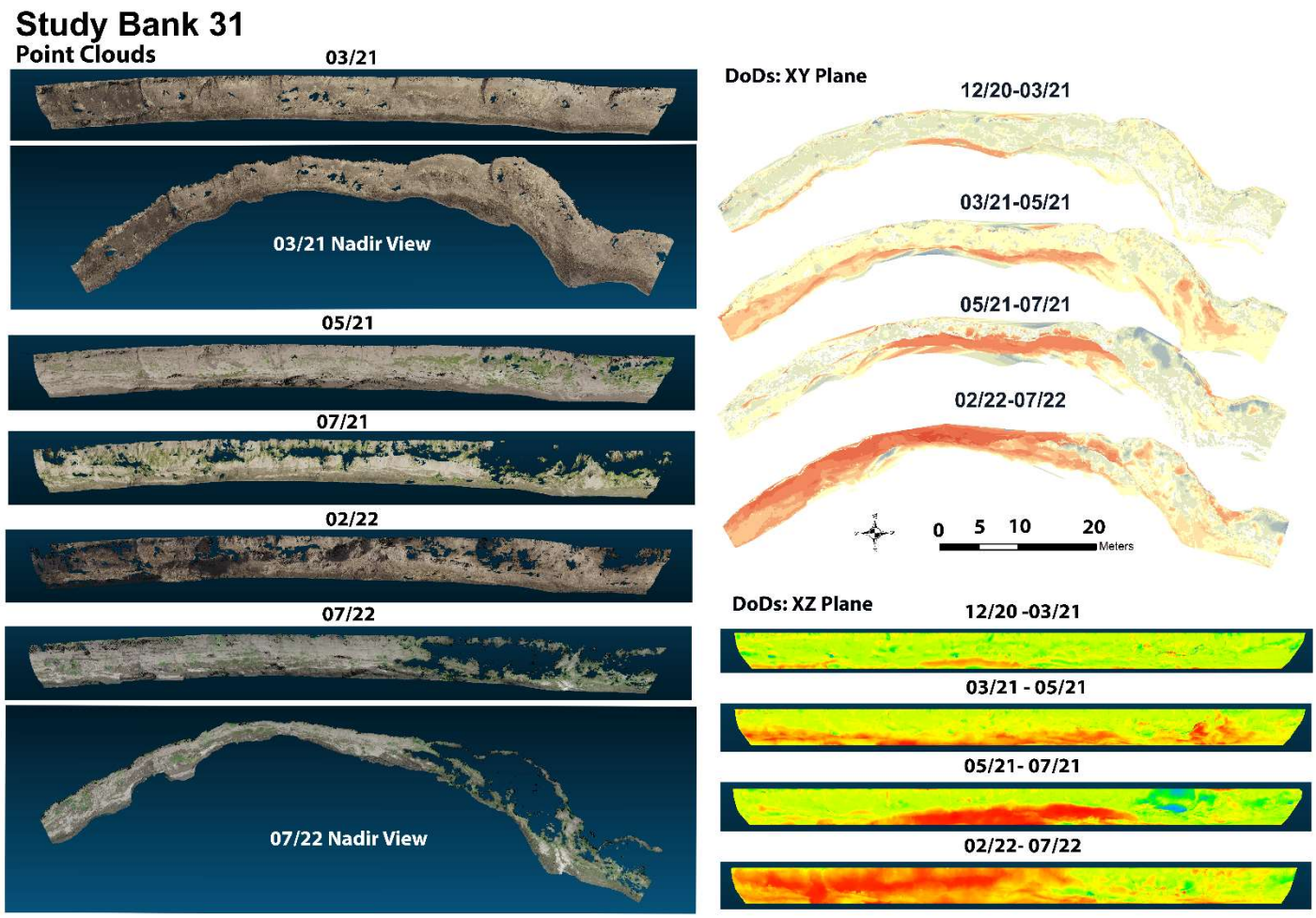


Figure 119: Selected Study Bank 31 Point Clouds and DoDs Illustrating Fall

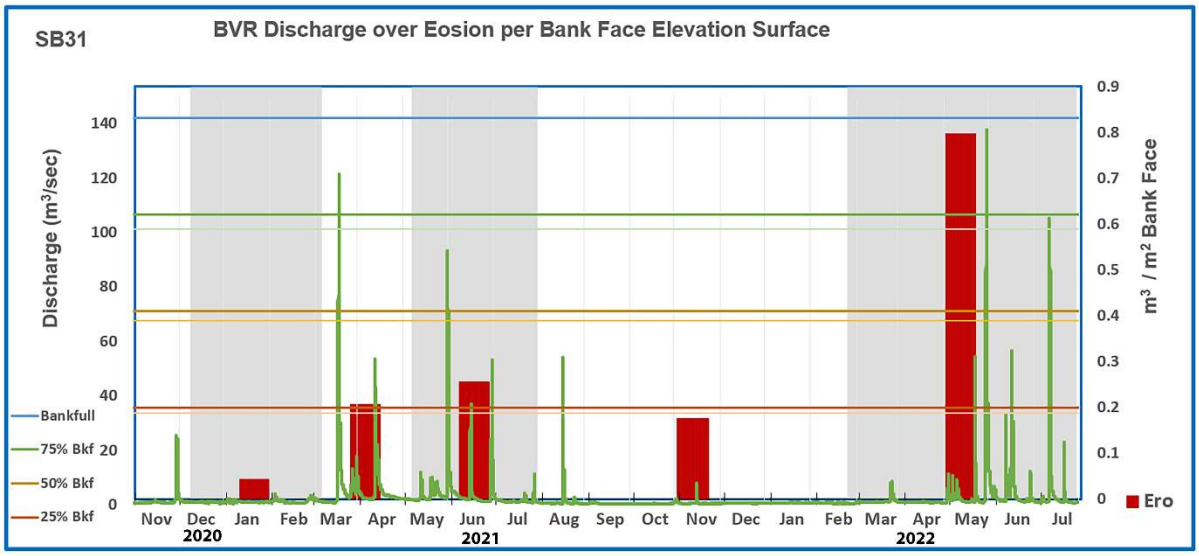


Figure 120: BVR Discharge over Erosion per Period for Study Bank 31

While study bank 19 experienced the largest amount of erosion of any study bank (726 m^3) over the entire study period, its large bank surface area resulted in it having the third largest rate of erosion per square meter of bank face (-.068 m^3) (Table 30, p.221). In contrast to study bank 31 that experienced more intense areas of erosion along the toe of the bank in the second period, study bank 19 experienced less intense erosion more evenly spread along most of the bank below what is assumed to be the high-water mark of the high-flow event of March 2021 (Figures 121, 122, and 111, p.234). The water line related to the March high flow, is clearly visible along Study Bank 19 as well as the XZ-plane DoD (Figure 122).

The pattern of evenly spread erosion was also seen in the DoD of the last period (05/22-07/22, Figure 122); however, there were patches of more intense erosion along the top of the bank likely due to fall of material resulting from the removal of material on the lower bank in the second period. Amounts of erosion for each period are also closely aligned with the highest flow of each period (Figure 121). This pattern of more even erosion closely aligned with flow data could be due to the soil at study bank 19 being one of two study banks with a soil clay content of 46.7% compared to 25-26% at all other study banks (Table 26, p.205).

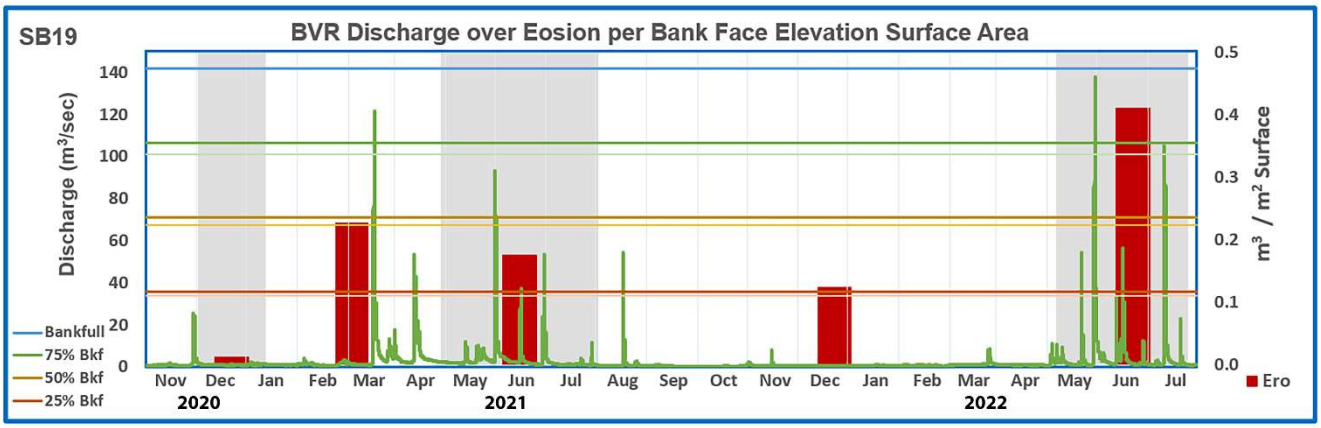


Figure 121: BVR Discharge Over Erosion per Period: Study Bank 19

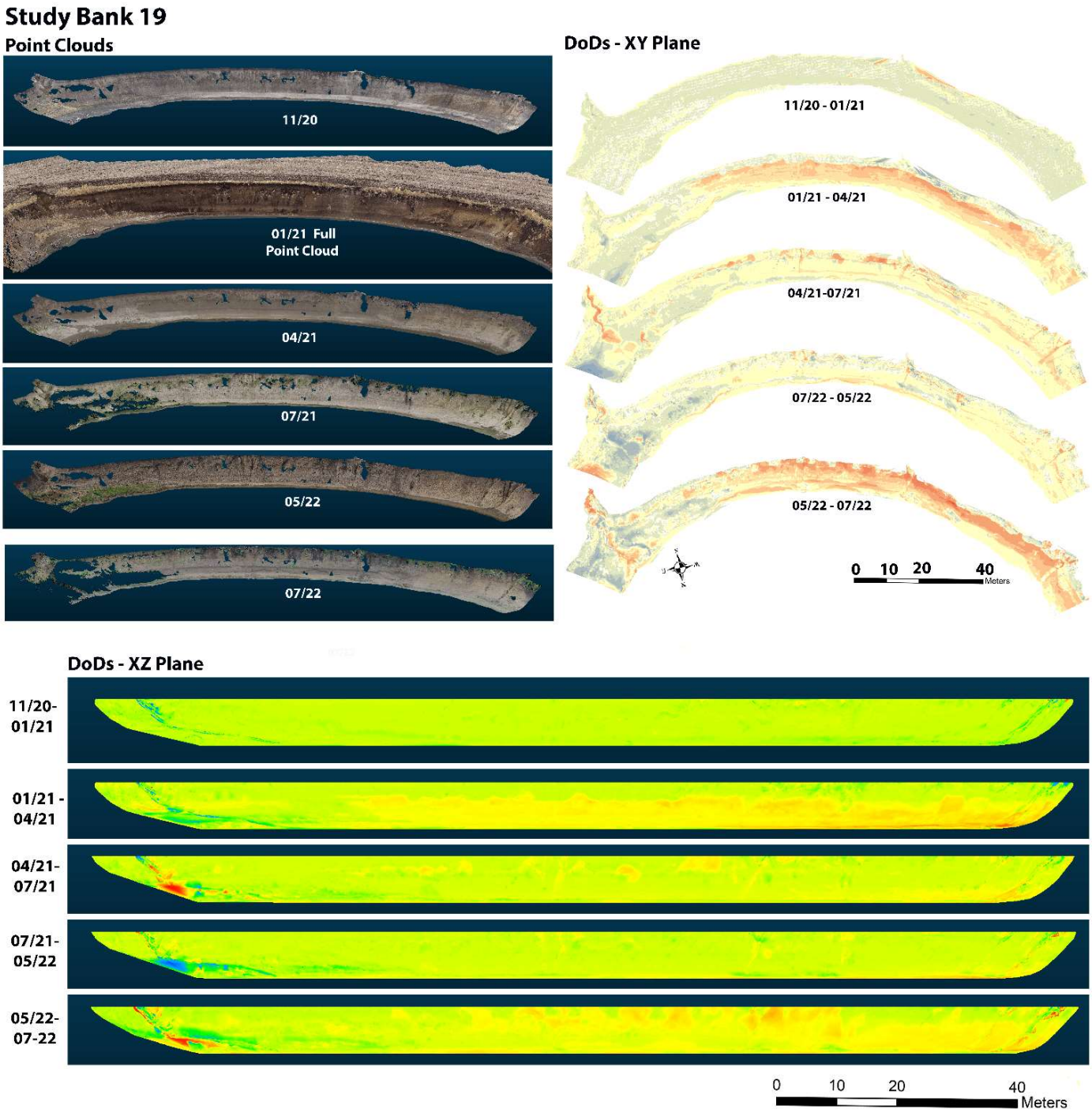


Figure 122: Selected Study Bank 19 Point louds and DoDs

Conclusion

Tuttle Creek Reservoir in northeast Kansas, originally constructed for flood control, is now being considered as a municipal water supply for the surrounding area including Manhattan, KS; however, the reservoir has lost almost fifty percent of its capacity since its construction in 1961 due to sediment being supplied by the Big Blue River and its tributaries (Rattanavong, 2019). The U.S. Army Corps of Engineers is planning a pilot project that utilizes injection dredging to agitate sediment at the bottom of the reservoir and flush it downstream; however, the ecological consequences of transferring such large amounts of sediment downstream are unknown (Llopis-Jepsen, 2022). Identifying and addressing sediment sources to prevent excessive sediment being delivered to the reservoir would be a better option. In 2017, the Kansas Water Office conducted an "assessment" of the Big Blue River and three of its tributaries aimed at identifying erosional "hotspots" between 2003 and 2015. However, moving forward, monitoring erosional hotspots at a fine temporal scale within the context of changing precipitation patterns due to climate change could better inform the prioritization of river restoration efforts aimed at reducing sediment.

A large number of erosional hotspots are good candidates for monitoring with the remote sensing technique of SfM. This study evaluated the use of SfM to monitor nine study banks throughout the BVR system that had experienced significant streambank erosion over the last two decades based on the KWO assessment and the 2010-12 to 2018 LiDAR analysis of Chapter IV. While 6 of 9 banks experienced significant amounts of erosion, the remaining three banks became heavily vegetated and most likely experienced little change; however, the change was not able to be measured. Moving

forward, the continued monitoring of the vegetated banks would be helpful in determining if these banks will continue to stabilize or again experience bank failure know to be episodic in nature within the BVR system. The results of this study suggest that SfM can accurately determine amounts of erosion along actively eroding banks at a fine spatial resolution as well as temporal scale. However, the establishment of vegetation on banks most likely experiencing little change or net deposition led to voids in the point cloud models making the estimation of deposition along these banks difficult and most likely inaccurate.

CHAPTER VI – Summary and Conclusions

Tuttle Creek Reservoir in Northeast Kansas is one of many reservoirs constructed in the mid-20th century to control flooding that is now being considered as a municipal water supply (KWO, 2017). However, since being completed in 1961, the reservoir has lost almost fifty percent of its storage capacity due to sediment being delivered from the Big Blue River and its tributaries (Rattanavong, 2019). A large source of sediment being delivered to the Tuttle Creek Reservoir is from channel adjustment (incision and widening) set in motion by the conversion of land use from native tallgrass prairie to agriculture and the practice of channelization. Sediment-reducing restoration efforts within the Tuttle Creek Reservoir watershed have been guided by a streambank erosion assessment (KWO, 2017) that focused on the Big Blue River and three of its tributaries, one of which was the Black Vermillion River; however, the assessment only included the lower portion of the BVR and missed a number of areas with very high rates of riverbank retreat.

With the aim of guiding BVR restoration efforts, the overall goal of this research was to determine how a variety of methods, such as traditional river surveying methods, LiDAR-derived DEMs, and SfM Photogrammetry compare when utilized to estimate amounts and patterns of streambank erosion and deposition over time at both the reach and system-wide scales. This goal was accomplished with three studies (Chapters III-V) utilizing three unique data sets, methodologies, and time periods over a total of 15 years.

Comparison of Data Set Spatial and Temporal Resolution

Data collected with traditional methods at seven study reaches between 2007 and 2021 provided detailed vector data of changes in dimension of both the BVR riverbed and banks at 14 specific cross sections. The cross sections were surveyed annually between 2007 and 2009 and again in 2021. While the cross sectional data may be helpful when evaluating channel succession over time, it is important to note that only two cross sections were measured within each study reach. Changes in dimension at a specific location may be sensitive to localized bank erosion or bed feature migration and, therefore, not be reflective of the entire study reach nor be appropriate for stream classification. In contrast to the spatial resolution of the cross-sectional data, the 2010, 2012, and 2018 publically-available LiDAR datasets provided continuous estimations of erosion and deposition along the entire BVR riverbank included in this study, but only above the waterline and at a coarse resolution (1-m raster). Temporally, the LiDAR data only reflects eight years of change in Marshall Co. (2010-18) and six year of change in Nemaha Co. (2012-18). Finally, the SfM data collected between 2020 and 2022 provides high spatial resolution volume change data (3 cm raster) for portions of the BVR riverbank ranging from approximately 30 m to 186 m in length; however, the SfM data is only above the waterline and sensitive to the establishment of bank vegetation between collection dates. At a fine temporal scale when compared to the cross sectional and LiDAR datasets, the SfM study banks were surveyed every two to four months over a 1.5-year period.

Chapter Summaries

The objective of Chapter III was to use traditional surveying methods at seven study reaches along with the LiDAR data sets to better understand how the BVR channel succession may be influencing sediment production. Little change in pattern or profile was observed at any of the seven study reaches; however, a number of changes in channel dimension were observed. Six of 7 riffle cross sections had an increase in width/depth ratio indicating a transition from a more narrow and deep channel to a wider and shallower channel. In addition, 12 of 14 cross sections experienced widening at the bankfull elevation, as evidenced by increases in bankfull width and cross sectional area. In contrast, North Fork (NF) 2 was the only reach that experienced deposition on both bed and banks of the riffle and no change in bankfull width or cross-sectional area at the pool, likely due to recent channelization.

These results suggest that within the “C”-“Gc”-“F”-“C” Rosgen successional scenario, the BVR ranges between a late “Gc” to an early “F” channel in the upper reaches, with some of the lower reaches being a later “F” stage channel and further along in the evolutionary process as speculated by Keane & Sass (2017). In addition, the BVR may be entering or in a phase of rapid widening, which is possible within the “Gc” to early “F” transition and would result in increased rates of streambank erosion and sediment production moving forward.

Throughout the Irish Creek (IC) and Main Stem (MS) subwatersheds, this pattern of widening was further supported by the comparison of the 2010 (12) and 2018 LiDAR-derived DEMs, with 59 of 62 1-km segments having greater erosion than deposition. Along the North Fork-Lower Main Stem (NF-LMS) channel, upstream of the North Fork

and Weyer Creek (WC) confluence, the pattern of channel change was similar to IC and Main Stem with 20 of 24 1-km segments having net erosion. In contrast, along the NF-LMS channel downstream of WC, a pattern of deposition outpacing erosion was observed within all but one of ten 1-km segments, which supports the cross-sectional data at NF2. The large amount of deposition downstream of WC initiated it being added to the study. Weyer Creek experienced the largest amount of erosion per 1-km segment (5,439 m^3), with erosion outpacing deposition in all but one of 16 1-km segments.

The objective for Chapter IV was to further utilize the LiDAR-derived DEMs and DoDs to estimate amounts of erosion and deposition along the entire BVR main channel and three tributaries over a period of 8 years (6 in Nemaha Co.) and to assess how the presence, amount, and density of woody vegetation affects riverbank erosion and deposition. The three BVR tributaries, Irish Creek, Main Stem (upstream of North Fork confluence), and Weyer Creek, as well as the portion of the NF-LMS upstream of the Weyer Creek confluence experienced net erosion (sediment production). Along the NF-LMS downstream of the WC confluence, two areas of excessive deposition were identified: 1) just downstream of the Weyer Creek confluence, and 2) just upstream of the BVR confluence with the Big Blue River, resulting net deposition.

Rates of erosion and deposition along banks void of woody vegetation was compared to rates along banks with little or ample woody riparian vegetation. Along banks void of woody vegetation, erosion was higher than when at least some woody vegetation was present in both Marshall and Nemaha Counties. In contrast, no correlation was found between LiDAR Normalized Relative Point Density (NRD) metrics

that estimate understory and overstory vegetation density and the amount of erosion along the BVR main channel or any of the three tributaries. The lack of correlation of erosion and NRD was due to numerous areas of high erosion in areas where the LiDAR point cloud NRD indicated dense over and understory vegetation, which may provide further evidence the BVR may be entering or in an evolutionary phase of rapid widening. In addition, no correlation between under or over story NRD and deposition was found except along the NF-LMS in Marshall Co., where a moderate correlation (R^2 0.035) was found with both over and understory vegetation density (NRD), which was not surprising given the dramatic increase of in-channel vegetation observed along much of the North Fork channel between 2007 and 2021.

The objective of Chapter V was to evaluate the use of SfM photogrammetry to monitor BVR riverbank erosion “hotspots”, which are typically void of woody vegetation, at both the annual and seasonal temporal scales over a 1.5-year study period. Portions of the BVR riverbank suited for monitoring with SfM were initially identified using Google Earth, with the final sites selected being dependent on landowners’ access permission. The comparison of each pair of sequential surveys was evaluated using checkpoint errors and the percentage of matching cells when using the CloudCompare volume calculation tool, which was an indication of voids resulting from the establishment of herbaceous vegetation during each period.

Chapter V results indicated several study banks experienced large amounts of erosion (up to 1.34 m^3 per square meter of bank face), while a few banks became vegetated and experienced little change. In addition, the average erosion per meter of the bank face of the three study banks in the upper watershed was greater than that of

the six in the lower watershed. It is believed that the use of SfM to monitor the study banks was effective in the calculation of erosion, as areas with significant bank erosion did not accumulate vegetation. SfM may not be as effective at estimating deposition, as deposition is usually accompanied with the establishment of vegetation that impedes the accuracy of SfM, primarily by overestimating deposition. Evaluation of the use of SfM to monitor banks was also based on the RMSE of the checkpoints of each pair of surveys, which remained low over the entire study period.

Future Research

Several questions arise from the results of Chapters III-V suggesting the continued monitoring of the upper BVR would be helpful in predicting future sediment production from bank erosion. Related to channel evolution: Will the widening experienced within the upper reaches of the watershed continue at the same rate or will the rate increase as the channel continues to transition from the G to the F stream type? Accelerated bank erosion due to rapid widening is possible as the width/depth ratio increases resulting in increased hydraulic, near bank stress (Rosgen, 1996). Questions related to in-channel deposition: Is the large amount of sediment downstream of Weyer Creek a pulse of sediment originating in the upper North Fork and Weyer Creek that will continue to be transported downstream? Similarly, will the sediment accumulating in the lower watershed near the confluence with the Big Blue River continue to accumulate? Will these areas of deposition continue to accumulate and decrease the ability of the channel to drain surrounding fields? If the drainage of fields is significantly impeded, it will likely result in new instances of channelization, leading to renewed channel adjustment. Finally, two questions related to the use of SfM to monitor erosion

hotspots: Will the banks experiencing erosion continue to do so at the same rate? Will the banks that did experience erosion between 2010 and 2018 yet experienced little or no erosion over this study period continue to stabilize?

Contributions

The most immediate and local contribution of this research is to the understanding of sediment being delivered to the Big Blue River and Tuttle Creek Reservoir. The three unique datasets and studies outlined in this research, provide methods for more accurately identifying and monitoring erosion and deposition along the BVR riverbanks. The cross sectional data, collected between 2007 and 2021, provides documentation of actual channel change at specific locations over the 14-year period contributing to the database of documented channel changes in the BVR and to the understanding of the BVR channel succession or evolution. Analysis of the LiDAR data provides a better method for identifying erosion “hotspots” between 2010 and 2018 in Marshall Co. and between 2012 and 2018 in Nemaha Co. The SfM data illustrates a low-cost accurate method for the monitoring of erosional “hotspots”, identified with the LiDAR analysis. If the aim of the KWO is to identify and prioritize area of high erosion, the methods outlined in this research could provide a more accurate method than those previously used using aerial photographs and roughly estimated average bank heights.

The larger contribution of this research is to the body of work using remote sensing techniques in conjunction with traditional river surveying methods for fluvial geomorphological research. It is difficult to capture the 3-D complexity of long reaches of riverbank using traditional cross sections and longitudinal profiles. The LiDAR data analysis in this research results in continuous volume change data along the entire BVR

riverbank. However, perhaps more importantly, the DoDs created for this research provide a record of geomorphic change over the entire earth surface within each study area (Marshall Co. and Nemaha Co.), which could be used in upland as well as fluvial geomorphological research. Specifically, this research builds on the work establishing methodology to identify and correct systematic errors in DEMs and DoDs. While Kessler et al. (2012) and Schaffrath et al. (2015) established methodology for correcting errors when using legacy LiDAR-derived DEMs and DoDs, this research contributed to the existing methodology by introducing a specific methodology for identifying areas of little change using slope analysis. Publically available repeat LiDAR datasets are a new phenomenon, and the latter, 2018 dataset used in this research just became available in 2022. The DoD LiDAR analysis outlined in this research was the first such analysis for this study area.

The Structure-from-Motion (SfM) methods utilized in this research contribute to the newly evolving body of work (Lazell et al., 2022) illustrating SfM as a viable method for 3-D monitoring of volume change along actively eroding riverbanks in eastern KS. Specifically, Chapter V presents a novel approach to automated flight planning for collection of oblique imagery and a novel approach for calculating riverbank volume change using the Y-projection in CloudCompare that may lead to more accurate volume change estimations. In addition, Chapter V presents methodology for the removal of bank vegetation in SfM point clouds. As technology progresses, these and other remote sensing techniques will be introduced and used in conjunction with traditional surveying methods to gain a more complete understanding of fluvial geomorphological processes.

References

Aber, J. S. (2007). *Geology, Geomorphology, and Geohydrology of the Flint Hills: East Central Kansas*. Emporia Kansas: Emporia State University.

Alho, P., Kukko, A., Hyyppä, H., Kaartinen, H., Hyyppä, J., & Jaakkola, A. (2009). Application of boat-based laser scanning for river survey. *Earth Surface Processes and Landforms, 34*(13), 1831-1838. doi:10.1002/esp.1879

Anderson, S., & Pitlick, J. (2014). Using repeat LiDAR to estimate sediment transport in a steep stream. *Journal of Geophysical Research. Earth Surface, 119*(3), 621-643. doi:10.1002/2013JF002933

Bartleby. (2023). XZ plane. Retrieved from https://www.bartleby.com/subject/math/geometry/concepts/xz-plane

Basche, A. D., & DeLonge, M. S. (2019). Comparing infiltration rates in soils managed with conventional and alternative farming methods: A meta-analysis. *PLoS ONE, 14*(9), e0215702. doi:10.1371/journal.pone.0215702

Bater, C. W., & Coops, N. C. (2009). Evaluating error associated with LiDAR-derived dem interpolation. *Computers & Geosciences, 35*(2), 289-300. doi:10.1016/j.cageo.2008.09.001

Beach, T. (1994). The fate of eroded soil: Sediment sinks and sediment budgets of agrarian landscapes in southern Minnesota, 1851-1988. *Annals of the Association of American Geographers, 84*(1), 5-28. doi:10.1111/j.1467-8306.1994.tb01726.x

Big Blue River. (N.D.). Big Blue River Compact. Retrieved from https://dnr.nebraska.gov/water-planning/big-blue-river-compact

Bird, S., Hogan, D., & Schwab, J. (2010). Photogrammetric monitoring of small streams under a riparian forest canopy. *Earth Surface Processes and Landforms, 35*(8), 952-970. doi:10.1002/esp.2001

Brasington, J., Rumsby, B. T., & McVey, R. A. (2000). Monitoring and modelling morphological change in a braided gravel-bed river using high resolution gps-based survey. *Earth Surface Processes and Landforms, 25*(9), 973-990. doi:10.1002/1096-9837(200008)25:93.0.CO;2-Y

Boggess, W., Miranowski, J., Alt, K., & Heady. (1980). Sediment damage and farm production costs: A multiple-objective analysis. North Central Journal of Agricultural Economics, 2(2), 107-112. doi:10.2307/1349173

Bretar, F., Pierrot-Deseilligny, M., & Roux, M. Solving the strip adjustment problem of 3D airborne LiDAR data. Paper presented at the *, 7* 4734-4737 vol.7. doi:10.1109/IGARSS.2004.1370216 Retrieved from https://ieeexplore.ieee.org/document/1370216

Briggs, M. B., Knapp, A. K., Blair, J. M., Heisler, J. L., Hoch, G. A., Lett, M. S., & McCarron, J. K. (2005). An ecosystem in transition: Causes and consequences of the conversion of mesic grassland to shrubland. *Bioscience, 55*(3), 243-254. doi:10.1641/0006-3568(2005)055[0243:AEITCA]2.0.CO;2

Brock, G. C. (1975). *Photogrammetric Guide: Albertz/Kreiling. Herbert Wichman, Karlsruhe, 1975, 2nd ed., 283 pp., DM 39.00, format 12 × 17 cm 2* Elsevier B.V. doi:10.1016/0031-8663(75)90005-8

Brogan, C. O. B. (2018). *A Dam Conundrum: The role of impoundments in stream flow alteration.* Virginia Tech.

Brookes, A. (1985). Traditional engineering methods, physical consequences, and alternative practices. *Progress in Physical Geography, 9*(1), 44-73. doi:10.1177/030913338500900103

Bull, L. J. (1997). Magnitude and variation in the contribution of bank erosion to the suspended sediment load of the River Severn, UK. *Earth Surface Processes and Landforms, 22*(12), 1109-1123. doi:10.1002/(SICI)1096-9837(199712)22:123.0.CO;2-O

Campbell, M. J., Dennison, P. E., Hudak, A. T., Parham, L. M., & Butler, B. W. (2018). Quantifying understory vegetation density using small-footprint airborne LiDAR. *Remote Sensing of Environment, 215*, 330-342. doi:10.1016/j.rse.2018.06.023

CC. (2015). CloudCompare 2.5D volume. Retrieved from https://www.cloudcompare.org/doc/wiki/index.php/2.5D_Volume

Chapman, S. S., Omernik, J. M., Freeouf, J. A., Huggins, D. G., & McCauley, J. R. (2001). *Ecoregions of Nebraska and Kansas (color poster with map, descriptive text, summary tables and photographs)* U.S. Geological Survey.

Chow, V. T., Maidment, D. R., & Mays, L. W. (1988). *Applied Hydrology*. New York [u.a.]: McGraw-Hill.

Civil Tracker. (2023). All About Ground Control Points (GCP). Retrieved from https://civiltracker.xyz/all-about-ground-control-points/#:~:text=What%20are%20Ground%20Control%20Points,drones%20into%20survey%20grade%20products.

Cluer, B., & Thorne, C. (2014). A stream evolution model integrating habitat and ecosystem benefits. *River Research and Applications, 30*(2), 135-154. doi:10.1002/rra.2631

Collinson, J. D. (1971). Some effects of ice on a river bed. *Journal of Sedimentary Petrology, 41*(2), 557-564. doi:10.1306/74D722CF-2B21-11D7-8648000102C1865D

Couper, P., Stott, T., & Maddock, I. (2002). Insights into river bank erosion processes derived from analysis of negative erosion-pin recordings: Observations from three recent UK studies. *Earth Surface Processes and Landforms, 27*(1), 59-79. doi:10.1002/esp.285

Darby, S., & Simon, A. (1999). *Incised River Channels : Processes, Forms, Engineering, and Management*. England: Retrieved from http://catalog.hathitrust.org/Record/004052632

Davis. (2007). Spatial patterns of geomorphic processes in channelized tributary streams. *Physical Geography, 28*(4), 301-310. doi:10.2747/0272-3646.28.4.301

Davis, W. M. (1902). Base level, grade and peneplain. *Journal Geology, 10*, 77-111.

DeLong, S. B., Hammer, M. N., Engle, Z. T., Richard, E. M., Breckenridge, A. J., Gran, K. B., . . . Jalobeanu, A. (2022). Regional-scale landscape response to an extreme precipitation event from repeat LiDAR and object-based image analysis. *Earth and Space Science (Hoboken, N.J.), 9*(12), n/a. doi:10.1029/2022EA002420

deNoyelles, F., & Jakubauskas, M. (2008). *Current State, Trend, and Spatial Variability of Sediment in Kansas Reservoirs*. Manh: Agricultural Experiment Station and Cooperative Extension Service. Retrieved from https://www.kcare.k-state.edu/pubs/water_quality_issues/Sedimentation%20in%20our%20Reservoirs%20pub.pdf

Dietrich, J. T. (2014). *Applications of Structure-From-Motion Photogrammetry to Fluvial Geomorphology* Available from ProQuest One Academic Eastern Edition. Retrieved from https://search.proquest.com/docview/1652557717

Dietrich, J. T. (2016). Riverscape mapping with helicopter-based structure-from-motion photogrammetry. *Geomorphology (Amsterdam, Netherlands), 252*, 144-157. doi:10.1016/j.geomorph.2015.05.008

Dunne, T., & Leopold, L. B. (1998). *Water in Environmental Planning* (15. printing ed.). New York: Freeman.

Duro, G., Crosato, A., Kleinhans, M. G., & Uijttewaal, W. S. J. (2018). Bank erosion processes measured with UAV-SfM along complex banklines of a straight mid-sized river reach. *Earth Surface Dynamics, 6*(4), 933-953. doi:10.5194/esurf-6-933-2018

Eltner, A., & Schneider, D. (2015). Analysis of different methods for 3d reconstruction of natural surfaces from parallel-axes UAV images. *Photogrammetric Record, 30*(151), 279-299. doi:10.1111/phor.12115

Esri. (N.D.). Tuttle Creek Lake: A story map. Retrieved from https://www.arcgis.com/apps/MapJournal/index.html?appid=2a313bd13d24489cad6a367e33ec0c07

Fonstad, M. A., Dietrich, J. T., Courville, B. C., Jensen, J. L., & Carbonneau, P. E. (2013). Topographic structure from motion: A new development in photogrammetric measurement. *Earth Surface Processes and Landforms, 38*(4), 421-430. doi:10.1002/esp.3366

Fox, G. A., Wilson, G. V., Simon, A., Langendoen, E. J., Akay, O., & Fuchs, J. W. (2007). Measuring streambank erosion due to ground water seepage: Correlation to bank pore water pressure, precipitation, and stream stage. *Earth Surface Processes and Landforms, 32*(10), 1558-1573. doi:10.1002/esp.1490

Gabet, E. J. (2003). Sediment transport by dry ravel. *Journal of Geophysical Research - Solid Earth, 108*(B1), 2049-n/a. doi:10.1029/2001JB001686

Genet, M., Stokes, A., Salin, F., Mickovski, S. B., Forced, T., Dumail, J-F., et al. (2005). The influence of cellulose content on tensile strength in tree roots. *Plant and Soil,* 278, 1-9.

Gilbert, G. K. (1877). *Report On The Geology of the Henry Mountains*. Washington: Govt. Printg. Office.

Goodwell, A. E., Zhu, Z., Dutta, D., Greenberg, J. A., Kumar, P., Garcia, M. H., . . . Jacobson, R. B. (2014). Assessment of floodplain vulnerability during extreme Mississippi River flood 2011. *Environmental Science & Technology, 48*(5), 2619-2625. doi:10.1021/es404760t

Gordon, N. D., Finlayson, B. L., & McMahon, T. A. (1992). *Stream Hydrology* (Reprint. ed.). Chichester, England: Wiley.

Gosh, S. K. (1979). *Analytical Photogrammetry*. New York: Pergamon Pr.

Gurnell, A. (1997). The hydrological and geomorphological significance of forested floodplains. Global Ecology and Biogeography Letters, 6, 219-229.

Guo, Q., Li, W., Yu, H., & Alvarez, O. (2010). Effects of topographic variability and LiDAR sampling density on several DEM interpolation methods. *Photogrammetric Engineering and Remote Sensing, 76*(6), 701-712. doi:10.14358/PERS.76.6.701

Haddock, M. J. (2005). *Wildflowers and Grasses of Kansas: A Field Guide*. Lawrence, Kansas: University Press of Kansas.

Hamshaw, S. D., Bryce, T., Rizzo, D. M., O'Neil-Dunne, J., Frolik, J., & Dewoolkar, M. M. (2017). Quantifying streambank movement and topography using unmanned aircraft system photogrammetry with comparison to terrestrial laser scanning. *River Research and Applications, 33*(8), 1354-1367. doi:10.1002/rra.3183

Hamshaw, S. D., Engel, T., Rizzo, D. M., O'Neil-Dunne, J., & Dewoolkar, M. M. (2019). Application of unmanned aircraft system (UAS) for monitoring bank erosion along river corridors. *Geomatics, Natural Hazards, and Risk, 10*(1), 1285-1305. doi:10.1080/19475705.2019.1571533

Hargrove, W. L. (2008). *Sedimentation in Our Reservoirs: Causes and Solutions*. Manhattan, Kan.: Kansas State University Agricultural Experiment Station and Cooperative Extension Service.

Hargrove, W. L., Johnson, D., Snethen, D., & Middendorf, J. (2010). From dust bowl to mud bowl: Sedimentation, conservation measures, and the future of reservoirs. *Journal of Soil and Water Conservation, 65*(1), 14-17A. doi:10.2489/jswc.65.1.14A

Harpstead, M. I., Sauer, T. J., Bennett, W. F., & Bratz, M. C. (2001). *Soil Science Simplified (4th ed.)*. Ames, Iowa: Wiley-Blackwell.

Harvey, M. D., & Watson, C. C. (1986). Fluvial process and morphological thresholds in incised channel restoration . *Journal of the American Water Resources Association, 22*(3), 359-368. doi:10.1111/j.1752-1688.1986.tb01890.x

Hawley, R. J., & Bledsoe, B. P., Stein, E.D., Haines, B. (2012). channel enlargement in semiarid suburbanizing watersheds: A southern California case study. *Journal of Hydrology, 496*, 17-30. doi:10.1016/j.jhydrol.2013.05.010

Hellmund, P. C., & Smith, D. S. (2006). *Designing Greenways*. Washington, DC [u.a.]: Island Press. Retrieved from http://www.loc.gov/catdir/toc/ecip063/2005031595.html

Hjulstrom, F. (1935). *Studies of the Morphological Activity of Rivers as Illustrated by The River Fyris*. Uppsala: Almqvist & Wiksell. Retrieved from http://www.econis.eu/PPNSET?PPN=065631978

Hjulstrom, F. (1939). Transportation of detritus by moving water. Paper presented at the *Recent Marine Sediments, a Symposium,* 5-31.

Hodgson, M. E., & Bresnahan, P. (2004). Accuracy of airborne LiDAR-derived elevation: Empirical assessment and error budget. *Photogrammetric Engineering and Remote Sensing, 70*(3), 331-339.

Hugenholtz, C. H., Whitehead, K., Brown, O. W., Barchyn, T. E., Moorman, B. J., LeClair, A., . . . Hamilton, T. (2013). Geomorphological mapping with a small, unmanned aircraft system: Feature detection and accuracy assessment of a photogrammetrically-derived digital terrain model. *Geomorphology (Amsterdam, Netherlands)*, 194, 16-24. doi:10.1016/j.geomorph.2013.03.023

Iverson, R. M., Reid, M. E., Iverson, N. R., LaHusen, R. G., Logan, M., Mann, J. E., & Brien, D. L. (2000). Acute sensitivity of landslide rates to initial soil porosity. *Science, 290*(5491), 513-516. doi:10.1126/science.290.5491.513

Jaebin Lee, Kiyun Yu, Yongil Kim, & Habib, A. F. (2007). Adjustment of discrepancies between LiDAR data strips using linear features. *IEEE Geoscience and Remote Sensing Letters, 4*(3), 475-479. doi:10.1109/LGRS.2007.898079

James, M. R., & Robson, S. (2014). Mitigating systematic error in topographic models derived from UAV and ground-based image networks. *Earth Surface Processes and Landforms, 39*(10), 1413-1420. doi:10.1002/esp.3609

Javernick, L., Brasington, J., & Caruso, B. (2014). Modeling the topography of shallow braided rivers using Structure-from-Motion photogrammetry. *Geomorphology (Amsterdam, Netherlands), 213*, 166-182. doi:10.1016/j.geomorph.2014.01.006

Jones, J. A. A. (1997). Pipeflow contributing areas and runoff response. Hydrological Processes. 11, 34-41.

Keane, T.D., 2004. Learning from Nature's Stability: Building a multi-purpose data base applicable to stream assessment, restoration, and education. Proceedings of the September 2004 ASAE Conference.

Keane, T. D., & Sass, C. K. (2017). Channel evolution models as predictors of sediment yield. *JAWRA Journal of the American Water Resources Association, 53*(6), 1513-1529. doi:10.1111/1752-1688.12598

Kessler, A. C., Gupta, S. C., Dolliver, H. A. S., & Thoma, D. P. (2012). LiDAR quantification of bank erosion in Blue Earth County, Minnesota. *Journal of Environmental Quality, 41*(2), 619. doi:10.2134/jeq2011.0181er

KGS. (2007). Physiographic map of Kansas. Retrieved from http://www.kgs.ku.edu/Physio/physio.html

Kinzel, P. J., Wright, C. W., Nelson, J. M., & Burman, A. R. (2007). Evaluation of an experimental LiDAR for surveying a shallow, braided, sand-bedded river. *Journal of Hydraulic Engineering (New York, N.Y.), 133*(7), 838-842. doi:10.1061/(ASCE)0733-9429(2007)133:7(838)

Knighton, D. (2014). *Fluvial Forms and Processes*. London: Taylor and Francis. doi:10.4324/9780203784662 Retrieved from https://www.taylorfrancis.com/books/9781134666614

Knox, J. C. (2001). Agricultural influence on landscape sensitivity in the upper Mississippi River valley. *Catena, 42*(2), 193-224. doi:10.1016/S0341-8162(00)00138-7

KSLS. (2005). *Public land survey system: Territory of Kansas Maps and Notes*. Wichita, KS: Kansas Society of Land Surveyors.

KWO. (2017). *Tuttle Creek Watershed Streambank Erosion Assessment.* (). Topeka, KS: Kansas Water Office.

Lane. (1954). *The Importance of Fluvial Morphology in Hydraulic Engineering.* (). Denver, CO: Department of the Interior.

Lane, Richards, K. S., & Chandler, J. H. (1993). Developments in photogrammetry; The geomorphological potential. *Progress in Physical Geography, 17*(3), 306-328. doi:10.1177/030913339301700302

Lane, Richards, K. S., & Chandler, J. H. (1994). Developments in monitoring and modelling small-scale river bed topography. *Earth Surface Processes and Landforms, 19*(4), 349-368. doi:10.1002/esp.3290190406

Langbein, W. B., & Leopold, L. B. (1966). *River meanders - theory of minimum variance*. Washington: Gov. Print. Office.

Langhammer, J., Lendzioch, T., Miřijovský, J., & Hartvich, F. (2017). UAV-based optical granulometry as tool for detecting changes in structure of flood depositions. *Remote Sensing (Basel, Switzerland), 9*(3), 240. doi:10.3390/rs9030240

Langhammer, J., & Vacková, T. (2018). Detection and mapping of the geomorphic effects of flooding using UAV photogrammetry. *Pure and Applied Geophysics, 175*(9), 3223-3245. doi:10.1007/s00024-018-1874-1

Lawler, D. M. (1986). River bank erosion and the influence of frost: A statistical examination. *Transactions - Institute of British Geographers (1965), 11*(2), 227-242. doi:10.2307/622008

Lawler, D. M. (1995). The impact of scale on the processes of channel-side sediment supply: A conceptual model. *Effects of Scale on Interpretation and Management of Sediment and Water Quality*. 226, 175-184.

Lawler, D. M., Grove, J. R., Couperthwaite, J. S., & Leeks, G. J. L. (1999). Downstream change in river bank erosion rates in the Swale-Ouse System, Northern England. *Hydrological Processes, 13*(7), 977-992. doi:10.1002/(SICI)1099-1085(199905)13:73.0.CO;2-5

Layzell, A. L., Peterson, A., Moore, T. L., & Bigham, K. A. (2022). UAS-based assessment of streambank stabilization effectiveness in an incised river system. *Geomorphology (Amsterdam, Netherlands), 408*, 108240. doi:10.1016/j.geomorph.2022.108240

Legends of Kansas. (2022). Marshall County, Kansas. Retrieved from https://legendsofkansas.com/marshall-county-kansas/

Leopold, L. B., & Maddock, T. (1963). *The Hydraulic Geometry of Stream Channels and Some Physiographic Implications*. Washington:

Leopold, L. B., Miller, J. P., & Wolman, M. G. (1964). *Fluvial Processes in Geomorphology*. San Francisco [u.a.]: Freeman.

Leopold, L. B. (1968). Hydrology for urban land planning: A guidebook on the hydrologic effects of urban land use. U.S. Geological Survey Circular, 554(18)

Leyland, J., Darby, S. E., Teruggi, L., Rinaldi, M., & Ostuni, D. (2015). A self-limiting bank erosion mechanism? Inferring temporal variations in bank form and skin drag from high resolution topographic data. *Earth Surface Processes and Landforms, 40*(12), 1600-1615. doi:10.1002/esp.3739

Leyland, J., Hackney, C. R., Darby, S. E., Parsons, D. R., Best, J. L., Nicholas, A. P., . . . Lague, D. (2017). extreme flood-driven fluvial bank erosion and sediment loads: Direct process measurements using integrated mobile laser scanning (MLS) and hydro-acoustic techniques. *Earth Surface Processes and Landforms, 42*(2), 334-346. doi:10.1002/esp.4078

Lindberg, E., & Hollaus, M. (2012). Comparison of methods for estimation of stem volume, stem number and basal area from airborne laser scanning data in a hemi-boreal forest. *Remote Sensing (Basel, Switzerland), 4*(4), 1004-1023. doi:10.3390/rs4041004

Llopis-Jepsen, C. (2022). *Kansas Scientists are Testing Jacuzzi-Like Water Jets to Save Reservoir (radio broadcast transcript)*. Manhattan, KS: NPR.

Lo, C.P. and Wong, F.Y. 1973, Microscale geomorphology features. *Photogrammetric Engineering and Remote Sensing* 39, 1289-96

Luttenegger, A. J. In situ shear strength of friable loess. Paper presented at the *, 9* 27-34.

Machado, R. E., Cardoso, T. O., & Mortene, M. H. (2022). Determination of runoff coefficient (C) in catchments based on analysis of precipitation and flow events. *International Soil and Water Conservation Research, 10*(2), 208-216. doi:10.1016/j.iswcr.2021.09.001

Mackin, J. H. (1948). Concept of the graded river. *GSA Bulletin, 59*(5), 463. doi:COTGR]2.0.CO;2

Marcus, W. A., & Fonstad, M. A. (2010). Remote sensing of rivers: The emergence of a subdiscipline in the river sciences. *Earth Surface Processes and Landforms, 35*(15), 1867-1872. doi:10.1002/esp.2094

Marteau, B., Vericat, D., Gibbins, C., Batalla, R. J., & green, D. R. (2017). Application of Structure-from-Motion Photogrammetry to River Restoration. *Earth Surface Processes and Landforms, 42*(3), 503-515. doi:10.1002/esp.4086

Meade, B. K. (2009). *Spatial Extent, Timing, and Causes of Channel Incision, Black Vermillion Watershed, Northeastern Kansas.* Retrieved from http://hdl.handle.net/2097/1451

Mei, X., Dai, Z., Darby, S. E., Gao, S., Wang, J., & Jiang, W. (2018). Modulation of extreme flood levels by impoundment significantly offset by floodplain loss downstream of the Three Gorges Dam. *Geophysical Research Letters, 45*(7), 3147-3155. doi:10.1002/2017GL076935

Meinen, B. U., & Robinson, D. T. (2020). Streambank topography: An accuracy assessment of UAV-based and traditional 3D reconstructions. *International Journal of Remote Sensing, 41*(1), 1-18. doi:10.1080/01431161.2019.1597294

Micheletti, N., Chandler, J. H., & Lane, S. N. (2015). Investigating the geomorphological potential of freely available and accessible Structure-from-Motion photogrammetry using a smartphone. *Earth Surface Processes and Landforms, 40*(4), 473-486. doi:10.1002/esp.3648

Miller, B. (2022). Email conversation with Bret miller, GIS specialist at DASC

Miřijovský, J., & Langhammer, J. (2015). Multitemporal monitoring of the morphodynamics of a mid-mountain stream using UAS photogrammetry. *Remote Sensing, 7*(7), 8586-8609. doi:10.3390/rs70708586

Mirijovsky, J., & Vavra, A. (2012). UAV Photogrammetry in Fluvial Geomorphology. *International Multidisciplinary Scientific GeoConference SGEM, 2*, 909. Retrieved from https://search.proquest.com/docview/1443480092

Moretto, J., Delai, F., Rigon, E., Picco, L., Mao, L., & Lenzi, M. (2012). Assessing short term erosion-deposition processes of the Brenta River using LiDAR surveys. *WIT Transactions on Engineering Sciences, 73*, 149. doi:10.2495/DEB120131

Naiman and, R. J., & Décamps, H. (1997). The ecology of interfaces: Riparian zones. *Annual Review of Ecology and Systematics, 28*(1), 621-658. doi:10.1146/annurev.ecolsys.28.1.621

National Park Service. (2020). Geology in The Flint Hills. Retrieved from https://www.nps.gov/tapr/learn/nature/geology-at-the-preserve.htm

NGS. (2022). Geoid Models. Retrieved from https://geodesy.noaa.gov/GEOID/

NOAA. (2022a). Climate Data Online. Retrieved from https://www.ncdc.noaa.gov/cdo-web/

NOAA. (2022b). What is a geoid? Retrieved from https://oceanservice.noaa.gov/facts/geoid.html#:~:text=The%20geoid%20is%20a%20model,result%20of%20the%20Rocky%20Mountains.

NRCS. (2008). Buffer Strips: Common Sense Conservation. Retrieved from http://www.nrcs.usda.gov/FEATURE/buffers/

NRCS. (2011). NRCS (Natural Resources Conservation Service). Web Soil Survey. Retrieved from http://websoilsurey.nrcs.usda.gov/.

Odum, E. P. (1971). *Fundamentals of Ecology (3rd ed.)*. Philadelphia, PA: W.B Saunders Company.

Omernik, J. M. (1987). Ecoregions of the conterminous United States. *Annals of the Association of American Geographers, 77*(1), 118-125. doi:10.1111/j.1467-8306.1987.tb00149.x

O'Neal, M. A., & Pizzuto, J. E. (2011). The rates and spatial patterns of annual riverbank erosion revealed through terrestrial laser-scanner surveys of the South River, Virginia. *Earth Surface Processes and Landforms*, 36(5), 695-701. doi:10.1002/esp.2098

Oznet. (2008). *Report of the Kansas State Board of Agriculture: Climate of Kansas.* (). Topeka, KS: Retrieved from http://www.oznet.ksu.edu/wdl/climate/cok/index.asp

Perkins, F. E., & Solo-Gabriele, H. M. (1997). Streamflow and suspended sediment transport in an urban environment. Journal of Hydraulic Engineering, 123(9), 807-811. doi:9(807)

Peterson, E. (1991). *Channelization and Land Use Changes Along The Black Vermillion River.* Unpublished manuscript.

Plowright, A. (n.d.). ForestTools: Tools for analyzing remotely sensed forest data. Retrieved from https://cran.r-project.org/web/packages/ForestTools/readme/README.html

Pollen, N. (2007). Temporal and spatial variability in root reinforcement of streambanks: Accounting for soil shear strength and moisture. *Catena*, 69, 197-205.

Popescu, S. C., & Wynne, R. H. (2004). Seeing the trees in the forest: Using LiDAR and multispectral data fusion with local filtering and variable window size for estimating tree height. *Photogrammetric Engineering and Remote Sensing, 70*(5), 589-604. doi:10.14358/PERS.70.5.589

Popotnik, G., & Giuliano, W. (2000). Response of birds to grazing of riparian zones. *The Journal of Wildlife Management, 64*(4), 976-982. doi:10.2307/3803207

Prosdocimi, M., Calligaro, S., Sofia, G., Dalla Fontana, G., & Tarolli, P. (2015). Bank erosion in agricultural drainage networks: New challenges from structure-from-motion photogrammetry for post-event analysis. *Earth Surface Processes and Landforms, 40*(14), 1891-1906. doi:10.1002/esp.3767

Qiao, L., Zou, C. B., Stebler, E., & Will, R. E. (2017). Woody plant encroachment reduces annual runoff and shifts runoff mechanisms in the tallgrass prairie, USA. *Water Resources Research, 53*(6), 4838-4849. doi:10.1002/2016WR019951

Rapp, A. 1960. Talus slopes and mountain walls at Templefjorden, Spitsbergen. *Norsk Geologisk Tidsschrift* 119, 1-96.

Rattanavong, S. (2019). With sediment filling Tuttle creek lake, officials look for methods to reduce rate. *The Murcury* Retrieved from https://themercury.com/news/area/with-sediment-filling-tuttle-creek-lake-officials-look-for-methods-to-reduce-rate/article_a1509929-61dd-5c78-a428-3f002dc679b3.html#:~:text=The%20Kansas%20Water%20Office%20estimated,since%20it%20opened%20in%201962.&text=Tuttle%20Creek%20Lake%20reservoir%20has,in%201962%2C%20according%20to%20estimates.

Reichman, O. J. (1987). *Konza Prairie: A Tallgrass Natural History*. Lawrence, Kan: Univ. Press of Kansas. Retrieved from http://bvbr.bib-bvb.de:8991/F?func=service&doc_library=BVB01&local_base=BVB01&doc_numbe

r=018388195&sequence=000002&line_number=0001&func_code=DB_RECORDS&service_type=MEDIA

Resop, J. P., & Hession, W. C. (2010). Terrestrial laser scanning for monitoring streambank retreat: Comparison with traditional surveying techniques. *Journal of Hydraulic Engineering, 136*(10), 794-798. doi:10.1061/(ASCE)HY.1943-7900.0000233

Rice, R. M. (1982). Sedimentation in the Chaparral: How do you handle unusual events? [erosion, Hyperschedasticity, San Gabriel and San Bernardino Mountains, southern California]. *USDA Forest Service General Technical Report PNW United States, Pacific Northwest Forest, and Range Experiment Station,* Retrieved from https://agris.fao.org/agris-search/search.do?recordID=US19830919634

Riley, A. L. (1998). *Restoring Streams in Cities*. Washington, DC [u.a.]: Island Press.

Rinaldi, M., & Darby, S. E. (2008). *Modelling River-Bank-Erosion Processes and Mass Failure Mechanisms: Progress Towards Fully Coupled Simulations.* Elsevier.

Rinaldi, M., Casagli, N., Dapporto, S., & Gargini, A. (2004). Monitoring and modelling of pore water pressure changes and riverbank stability during flow events. *Earth Surface Processes and Landforms, 29*(2), 237-254. doi:10.1002/esp.1042

Ringler, N. H., & Hall, J. D. (1975). Effects of logging on water temperature, and dissolved oxygen in spawning beds. *Transactions of the American Fisheries Society (1900), 104*(1), 111-121. doi:10.1577/1548-8659(1975)1042.0.CO;2

Rittenburg, R. A., Squires, A. L., Boll, J., Brooks, E. S., Easton, Z. M., & Steenhuis, T. S. (2015). Agricultural BMP effectiveness and dominant hydrological flow paths: Concepts and a review. *Journal of the American Water Resources Association, 51*(2), 305-329. doi:10.1111/1752-1688.12293

Rosgen. (1994). A classification of Natural Rivers. *Catena, 22*(3), 169-199. doi:10.1016/0341-8162(94)90001-9

Rosgen. (1996). *Applied River Morphology* (2. ed.). Pagosa Springs, Colo: Wildland Hydrology.

Rosgen. (2008). Discussion, " Critical Evaluation of how the Rosgen Classification and Associated 'Natural Channel Design' Methods Fail to Integrate and Quantify Fluvial Processes and Channel Responses" by A. Simon. et al. *Journal of the American*

Water Resources Association, (44(3)), 782-792. doi:10.1111/j.1752-1688.2008.00169.x

Rosgen, D. (2006). *Watershed Assessment for River Stability and Sediment Supply, WARSSS*. Ft. Collins, CO: Wildland Hydrology Books.

Rossi, P., Mancini, F., Dubbini, M., Mazzone, F., & Capra, A. (2017). Combining nadir and oblique uav imagery to reconstruct quarry topography: Methodology and feasibility analysis. *European Journal of Remote Sensing, 50*(1), 211-221. doi:10.1080/22797254.2017.1313097

Rousseau, D., Antoine, P., Kunesch, S., Hatté, C., Rossignol, J., Packman, S., . . . Gauthier, C. (2007). Evidence of cyclic dust deposition in the us great plains during the last deglaciation from the high-resolution analysis of the peoria loess in the eustis sequence (Nebraska, USA). *Earth and Planetary Science Letters, 262*(1), 159-174. doi:10.1016/j.epsl.2007.07.016

Sass, C. K. (2011). *Evaluation and Development of Predictive Streambank Erosion Curves for Northeast Kansas Using Rosgen's "BANCS" Methodology* Available from Dissertations & Theses Europe Full Text: Science & Technology. Retrieved from https://search.proquest.com/docview/875539207

Sass, C. K., & Keane, T. D. (2012). Application of Rosgen's BANCS Model for NE Kansas and the development of predictive streambank erosion curves. *Journal of the American Water Resources Association, 48*, 774. doi:10.1111/j.1752-1688.2012.00644.x

Sass, C. K., & Keane, T. D. (2016). Riparian corridor change in a northeastern Kansas Watershed. *Landscape Journal: Design, Planning, and Management of the Land, 35*(1), 57-77. doi:10.3368/lj.35.1.57

Schaffrath, K. R., Belmont, P., & Wheaton, J. M. (2015). landscape-scale geomorphic change detection: Quantifying spatially variable uncertainty and circumventing legacy data issues. *Geomorphology (Amsterdam, Netherlands), 250*, 334-348. doi:10.1016/j.geomorph.2015.09.020

Sekely, A.C., Mulla, D.J. & Bauer, D.W. (2002). Streambank slumping and its contribution to the phosphorus and suspended sediment loads of the Blue Earth River, Minnesota. *Journal of Soil and Water Conservation, 57*(5), 243-250. Retrieved from http://www.jswconline.org/content/57/5/243.abstract

Schultz, R. C., Colletti, T. M., & Isenhart, C. O. (2000). Riparian forest buffer practices. In Garrett, Rietveld & Fisher (Eds.), *North American agroforestry: An integrated science and practices* (). Madison, WI: American Society of Agronomy.

Schumm, S. A. (1973). geomorphic thresholds and complex response of drainage systems. *Fluvial Geomorphology*, In: M. Morisawa (Editor). Binghamton, New York. 299-309.

Schumm, S. (1977). *The Fluvial System*. United States: Retrieved from http://catalog.hathitrust.org/Record/000684907

Schumm, S., Harvey, M., & Watson, C. (1984). *Incised Channels : Morphology, Dynamics, and Control*. United States: Retrieved from http://catalog.hathitrust.org/Record/000576887

Shields, N. D. (1936). Anwendung der Ahnlickeit Mechanki und der Turbulenzforschung auf die Geschiebelerwegung. *Mitt Preoss Versuchanstalt Fur Wasserbau Und Schiffbau,*

Silva, C. A., Hudak, A. T., Vierling, L. A., Valbuena, R., Cardil, A., Mohan, M., . . . Klauberg, C. (2022). Treetop: A shiny-based application and r package for extracting forest information from LiDAR data for ecologists and conservationists. *Methods in Ecology and Evolution, 13*(6), 1164-1176. doi:10.1111/2041-210X.13830

Simon, A., & Hupp, C. (1986). Channel evolution in modified alluvial streams. *Transportation Research Record,* (1151), 16-24.

Simon, A., & Rinaldi, M. (2006). Disturbance, stream incision, and channel evolution: The roles of excess transport capacity and boundary materials in controlling channel response. *Geomorphology, 79*(3), 361-383. doi:10.1016/j.geomorph.2006.06.037

Simon, A., & Collison, A. J. C. (2001). Pore-water pressure effects on the detachment of cohesive streambeds: Seepage forces and matric suction. *Earth Surface Processes and Landforms, 26*(13), 1421-1442. doi:10.1002/esp.287

Simon, A., & Rinaldi, M. (2000). Channel instability in the loess area of the midwestern United States. *JAWRA Journal of the American Water Resources Association, 36*(1), 133-150. doi:10.1111/j.1752-1688.2000.tb04255.x

Slama, C. C. (1980). *Manual of Photogrammetry* (4. ed. ed.). Falls Church, Va: American Soc. of Photogrammetry.

Smith, D. G., & Pearce, C. M. (2002). Ice jam-caused fluvial gullies and scour holes on Northern River flood plains. *Geomorphology (Amsterdam, Netherlands), 42*(1), 85-95. doi:10.1016/S0169-555X(01)00076-9

Smith, R. L., & Smith, T. M. (2000). *Elements of Ecology (4th ed.)*. San Francisco:

Steiner, J., Steiner, J., Briske, D., Briske, D., Brown, D., Brown, D., . . . Rottler, C. (2018). Vulnerability of southern plains agriculture to climate change. *Climatic Change, 146*(1), 201-218. doi:10.1007/s10584-017-1965-5

Stott, T. (1997). A Comparison of stream bank erosion processes on forested and moorland streams in the Balquhidder catchments, central Scotland. *Earth Surface Processes and Landforms, 22*(4), 383-399. doi:10.1002/(SICI)1096-9837(199704)22:43.0.CO;2-4

Szafarczyk, A., & Toś, C. (2022). The use of green laser in LiDAR bathymetry: State of the art and recent advancements. *Sensors (Basel, Switzerland), 23*(1), 292. doi:10.3390/s23010292

Tamminga, A., Hugenholtz, C., Eaton, B., & Lapointe, M. (2015). Hyperspatial remote sensing of channel reach morphology and hydraulic fish habitat using an unmanned aerial vehicle (UAV): A first assessment in the context of river research and management. *River Research and Applications, 31*(3), 379-391. doi:10.1002/rra.2743

Tamminga, A. D., Eaton, B. C., & Hugenholtz, C. H. (2015). UAS-Based Remote Sensing of Fluvial Change Following an Extreme Flood Event. *Earth Surface Processes and Landforms, 40*(11), 1464-1476. doi:10.1002/esp.3728

Thorne. (1999). Bank Processes and channel evolution in the incised rives of north-central Mississippi. In S. E. Darby (Ed.), *Incised river channels* (). Chichester [u.a.]: Wiley. Retrieved from http://bvbr.bib-bvb.de:8991/F?func=service&doc_library=BVB01&local_base=BVB01&doc_number=008571733&sequence=000001&line_number=0001&func_code=DB_RECORDS&service_type=MEDIA

Thorne, C. R. (2006). *Applied Fluvial Geomorphology for River Engineering and Management* (Reprint. ed.). Chichester [u.a.]: Wiley.

Trimble, S. W. (1999). Decreased rates of alluvial sediment storage in the Coon Creek Basin, Wisconsin, 1975-93. *Science, 285*(5431), 1244-1246. doi:10.1126/science.285.5431.1244

US-COE. (1998). *Black Vermillion Watershed Study Kansas.* ().U.S. Army Corps of Engineers.

US-COE. (2011). Tuttle Creek Lake Information Website. Retrieved from https://www.nwk.usace.army.mil/Locations/District-Lakes/Tuttle-Creek-Lake/Daily-Lake-Info-2/

USDA. (2021). First Order LiDAR Metrics. Retrieved from chrome-extension://efaidnbmnnnibpcajpcglclefindmkaj/https://fsapps.nwcg.gov/gtac/CourseDownloads/Reimbursables/FY21/LiDAR_Material/LiDARMetrics_Descriptions_2021.pdf

USDA -SCS. (1966). *Watershed Work Plan: Upper Black Vermillion Watershed Marshall and Nemaha Counties, Kansas.* (). Kansas:

USDA-SCS_KES. (1951). *Physical Land Conditions Affecting Use, Conservation, and Management of Land Resources, Marshall county, Kansas*. Kansas: U.S. Department of Agriculture, Soil Conservation Service, and the Kansas Agricultural Experiment Station.

US-EPA, Tetra Tech, KS State Conservation Commission. (2005). Assessment, geomorphic definition, and documentation of Kansas stream corridor reference reaches. Tetra Tech. Kansas

US-EPA. (2018). Ecoregions. Retrieved from https://www.epa.gov/eco-research/ecoregions

USGCRP. (2018). *Fourth National Climate Assessment Volume II*. Washington, DC: U.S. Government. Retrieved from https://nca2018.globalchange.gov/chapter/front-matter-about/

USGS. (2021). What is a digital elevation model (DEM)? Retrieved from https://www.usgs.gov/faqs/what-digital-elevation-model-dem

Walters, K. L. (1954). Geology and ground-water resources of Marshall county, Kansas. Retrieved from http://www.kgs.ku.edu/General/Geology/Marshall/index.html

Wasko, C., & Sharma, A. (2017). Global assessment of flood and storm extremes with increased temperatures. *Scientific Reports, 7*(1), 7945-8. doi:10.1038/s41598-017-08481-1

Whitney, G. G. (1994). *From Coastal Wilderness to Fruited Plain* (1. publ. ed.). Cambridge [u.a.]: Cambridge Univ. Press. Retrieved from http://www.loc.gov/catdir/toc/cam026/93029701.html

Wilkin, D. C., & Hebel, S. J. (1982). Erosion, redeposition, and delivery of sediment to midwestern streams. *Water Resources Research, 18*(4), 1278-1282. doi:10.1029/WR018i004p01278

Williams, G. P. (1986). River meanders and channel size. *Journal of Hydrology (Amsterdam), 88*(1), 147-164. doi:10.1016/0022-1694(86)90202-7

Williams, J., & Smith, C. (2008). Economic issues of watershed protection and reservoir rehabilitation. *Sedimentation in our Reservoirs: Causes and Solutions* (). Manhattan, KS: Kansas Water Office, Kansas Water Resources Institute, Kansas Center for Agricultural Resource and the Environment, Kansas State University Agricultural Experiment Station, and Cooperative Extension Service.

Williams, R. (2012). DEMs of Difference. Retrieved from http://eprints.gla.ac.uk/114527

Wilson, G. V., Periketi, R. K., Fox, G. A., Dabney, S. M., Shields, F. D., and Cullum, R. F. (2007). Soil properties controlling seepage erosion contributions to streambank failure. Earth Surface Processes and Landforms. 32, 447-459. DOI: 10.1002/esp.1405.

Wolman, M. G. (1954). A method of sampling coarse river-bed material. *Eos, Transactions American Geophysical Union, 35*(6), 951-956. doi:10.1029/TR035i006p00951

Wolman, M. G. (1959). Factors influencing erosion of a cohesive river bank. *American Journal of Science (1880), 257*(3), 204-216. doi:10.2475/ajs.257.3.204

Wolman, M. G. (1967). A cycle of sedimentation and erosion in urban river channels. *Geografiska Annaler. Series A, Physical Geography*, 49(2/4), 385-395. doi:10.1080/04353676.1967.11879766

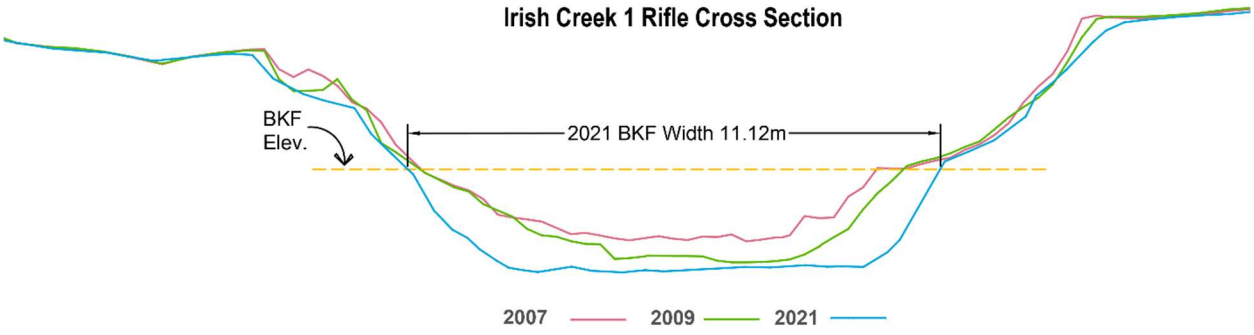
Wolman, M. G., & Leopold, L. B. (1957). *River flood plains; some observations on their formation* (Reprint ed.). Washington: Gov. Pr. Off.

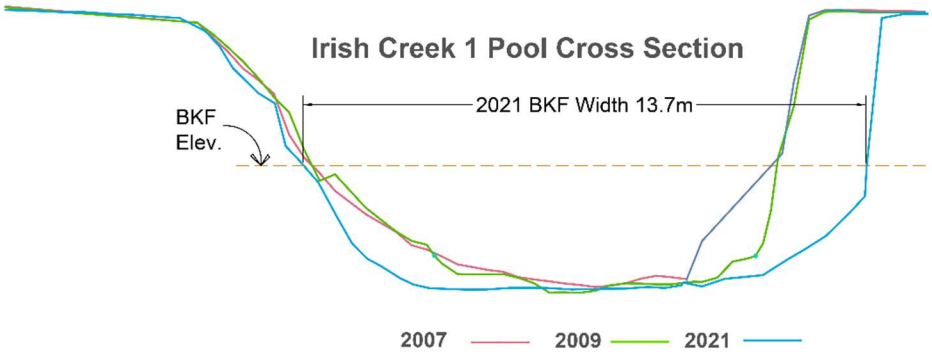
Wynn, T., & Mostaghimi, S. (2006). Effects of vegetation and soil type on streambank erosion, southwestern Virginia, USA. *Journal of the American Water Resources Association, 42*(1), 69-82. doi:10.1111/j.1752-1688.2006.tb03824.x

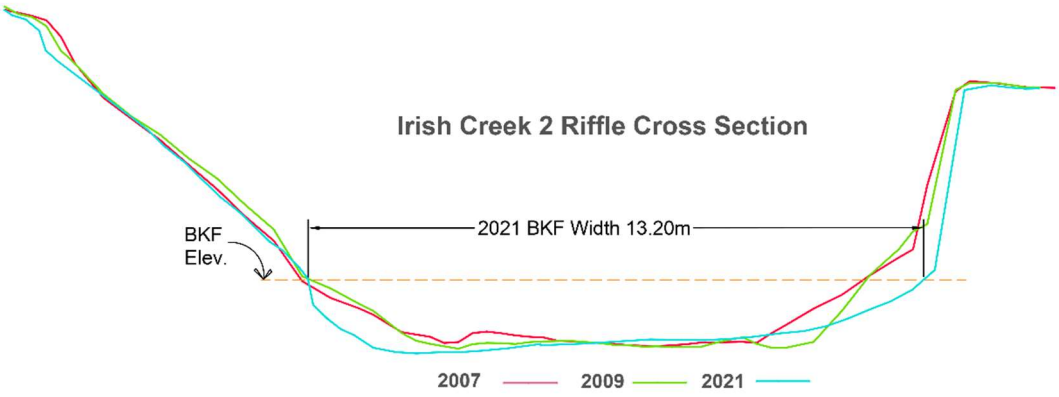
Zaimes, G. N., Schultz, R. C., & Isenhart, T. M. (2006). Riparian land uses and precipitation influences on stream bank erosion in central Iowa. *Journal of the American Water Resources Association, 42*(1), 83-97. doi:10.1111/j.1752-1688.2006.tb03825.x

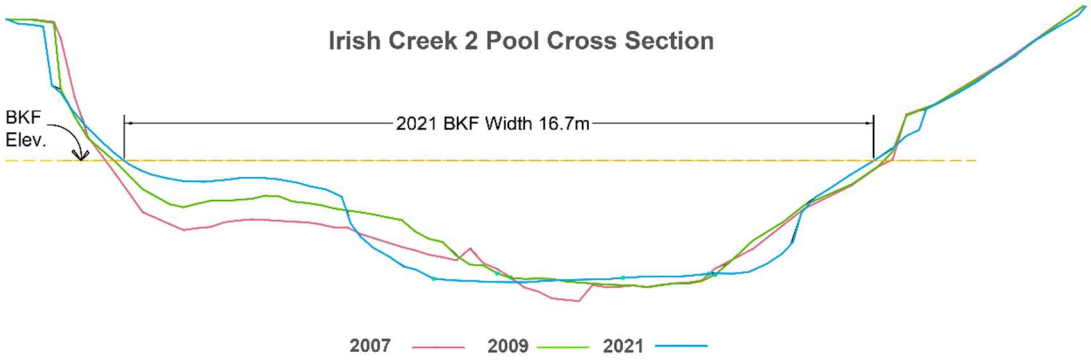
Appendix A: Study Reach Cross Sections

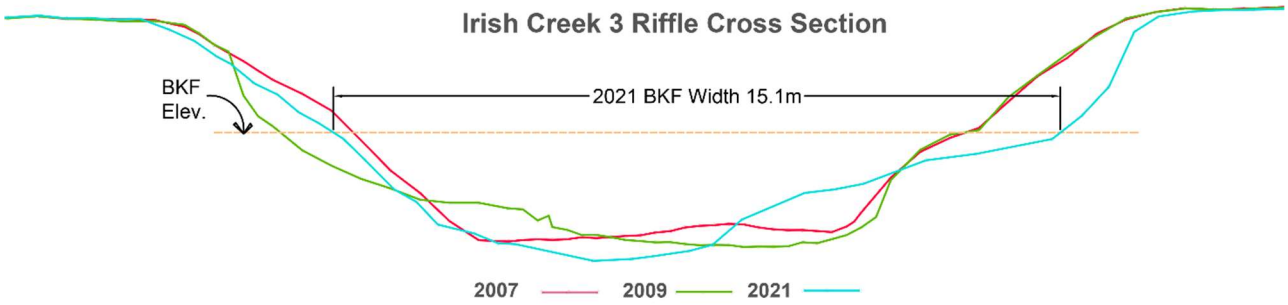
Irish Creek

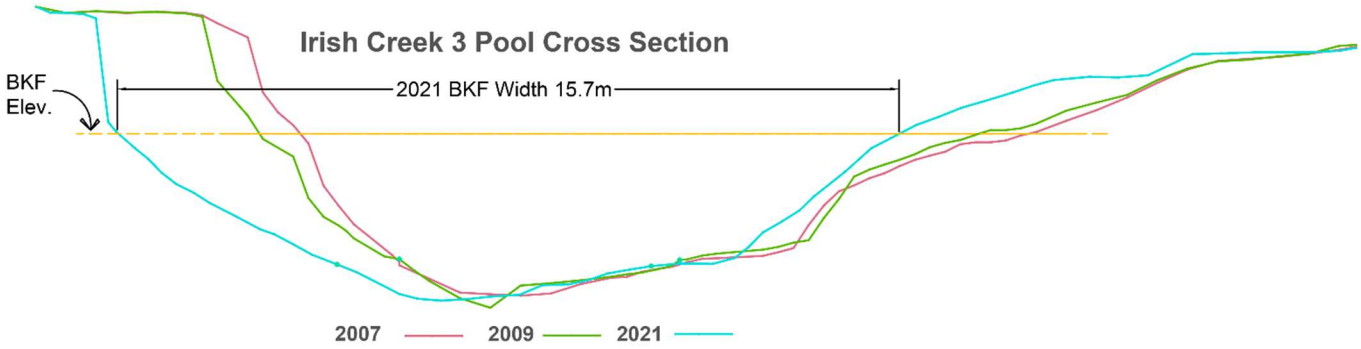




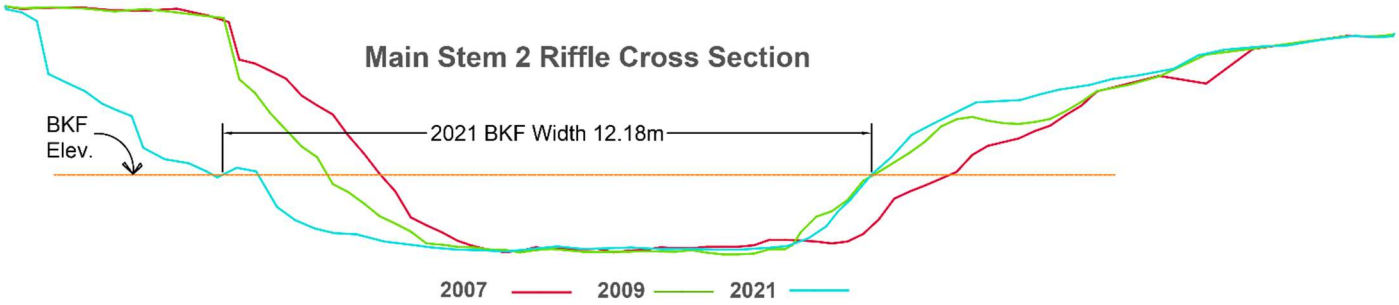


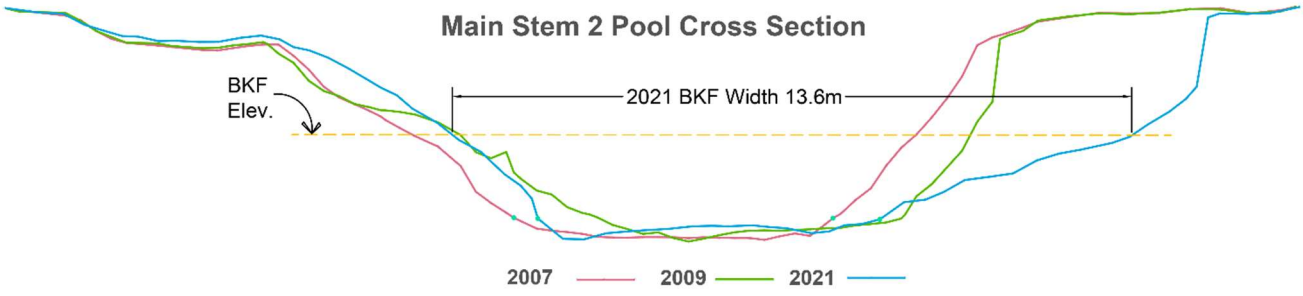


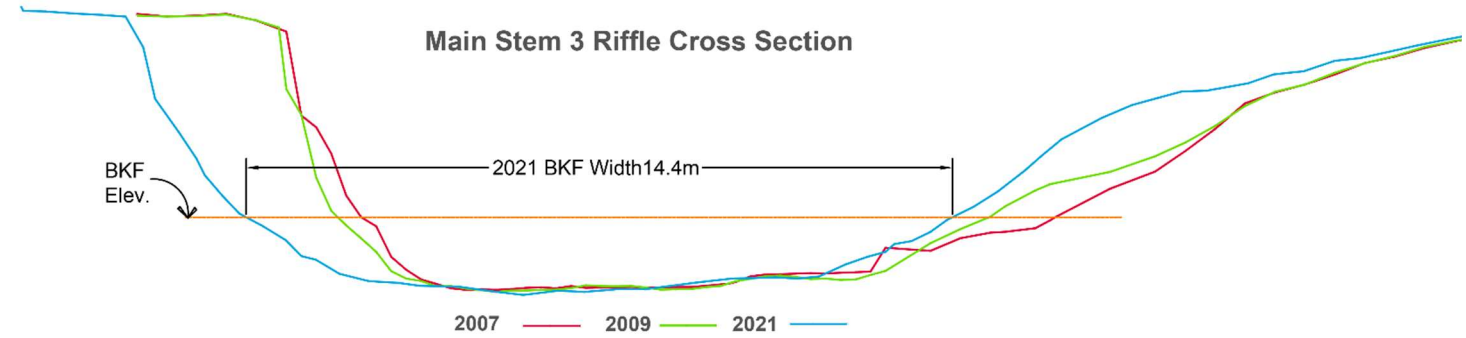


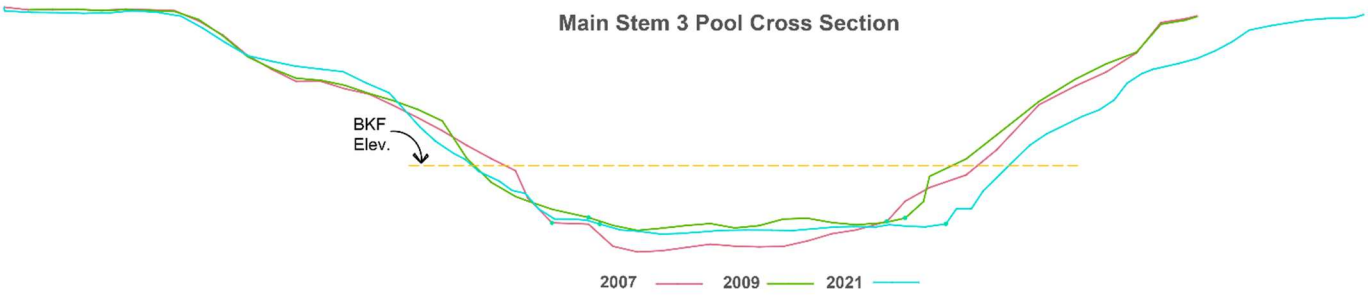


BVR Main Stem

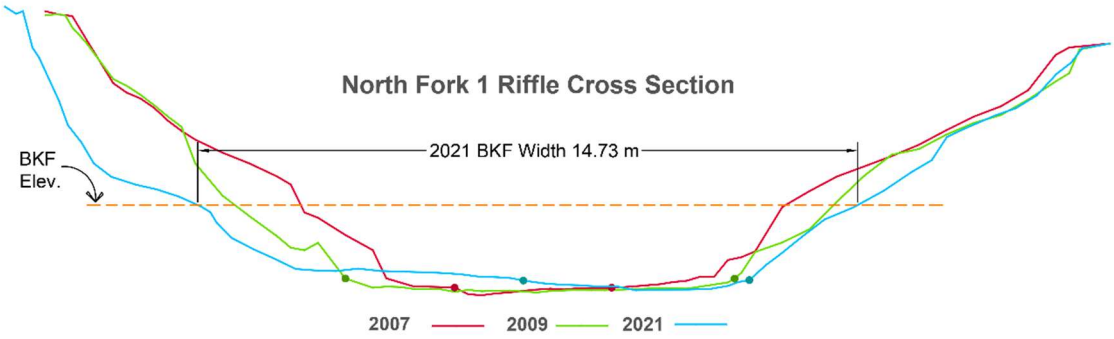


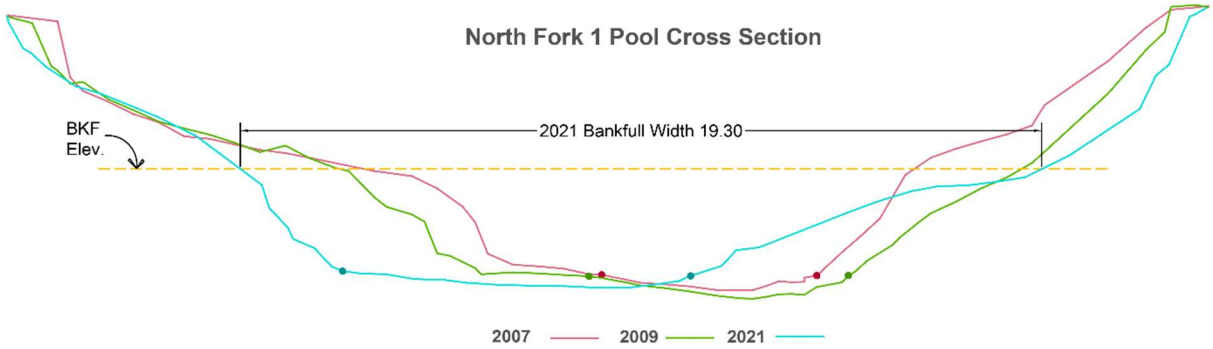


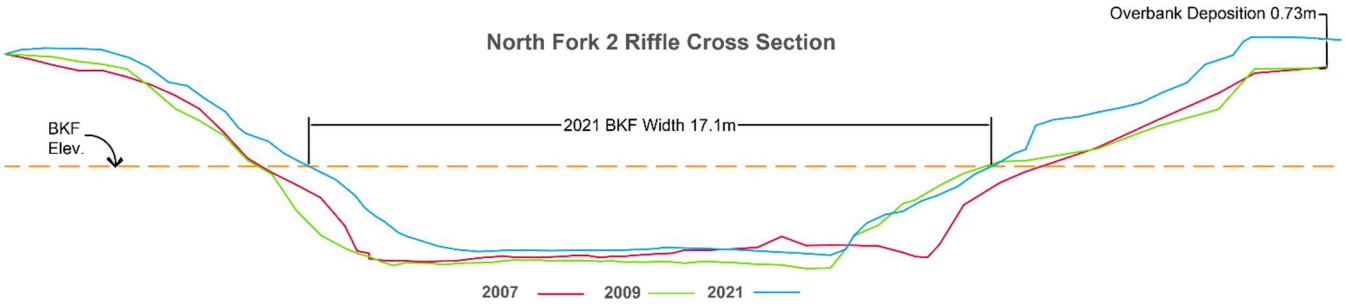

Main Stem 3 Riffle Cross Section
BKF
Elev.
2021 BKF Width14.4m
2007
2009
2021

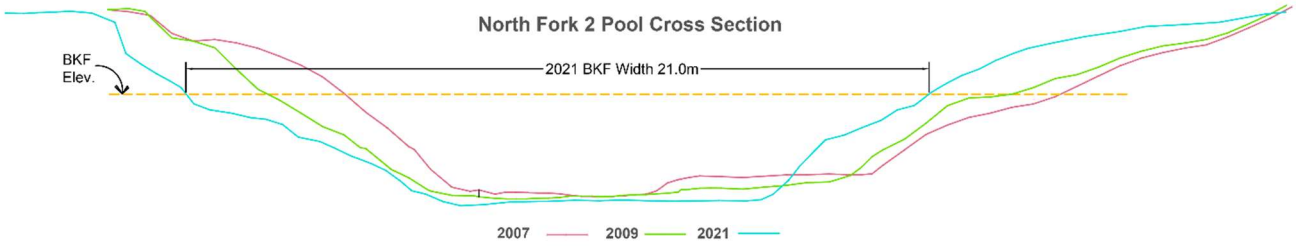

Main Stem 3 Pool Cross Section
BKF
Elev.
2007
2009
2021

North Fork


North Fork 1 Riffle Cross Section
BKF
Elev.
2021 BKF Width 14.73 m
2007
2009
2021

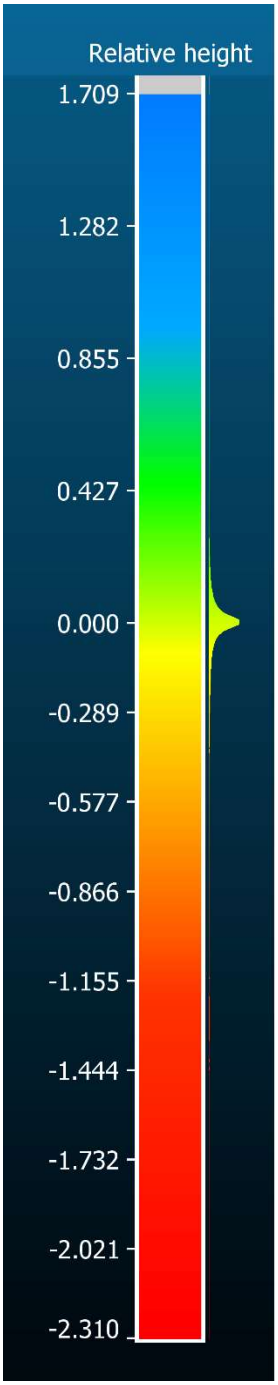

North Fork 1 Pool Cross Section
BKF
Elev.
2021 Bankfull Width 19.30
2007
2009
2021

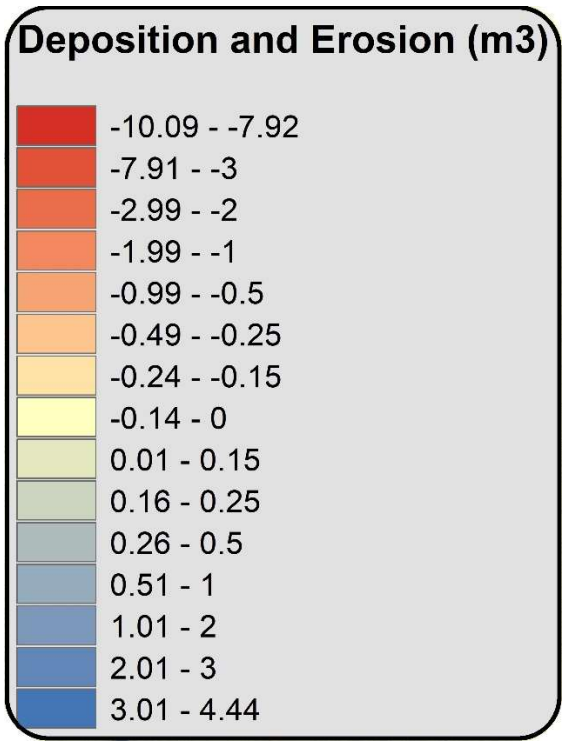

North Fork 2 Riffle Cross Section
Overbank Deposition 0.73m
2021 BKF Width 17.1m
BKF
Elev.
2007
2009
2021


North Fork 2 Pool Cross Section
2021 BKF Width 21.0m
BKF
Elev.
2007
2009
2021

Appendix B: Study Bank Point Clouds and DoDs

The following are the point clouds from each collection data and the digital elevation models of difference (DoDs) from both the XY-plane ArcGIS analysis and the XZ-plane CloudCompare analysis. Figures _ and _ below are the legends for each type of DoD.

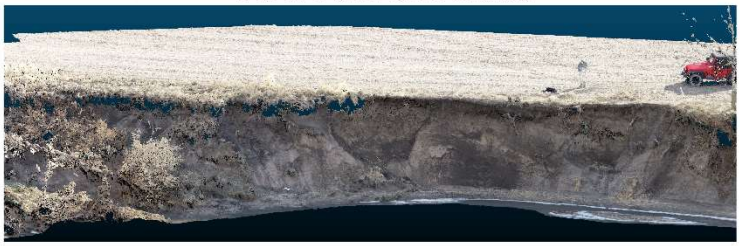




SB09 Point Clouds and DoDs

Point Clouds

12/20 Full Point Cloud









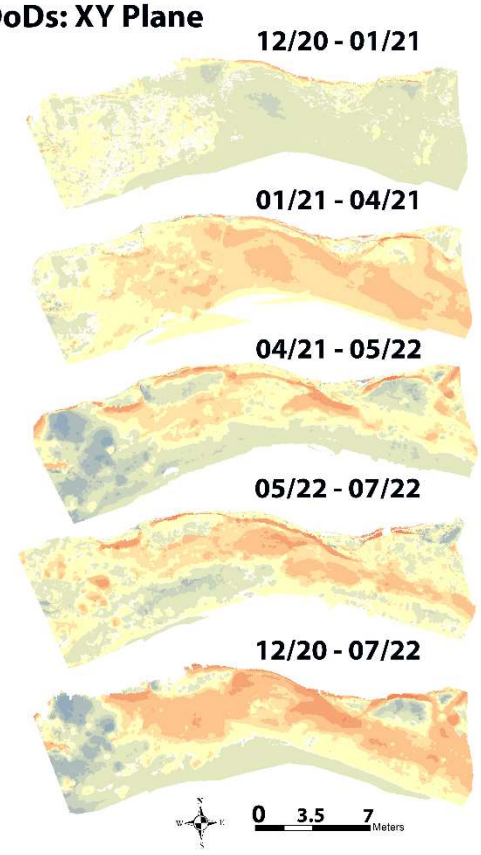
05/22 Full Point Cloud



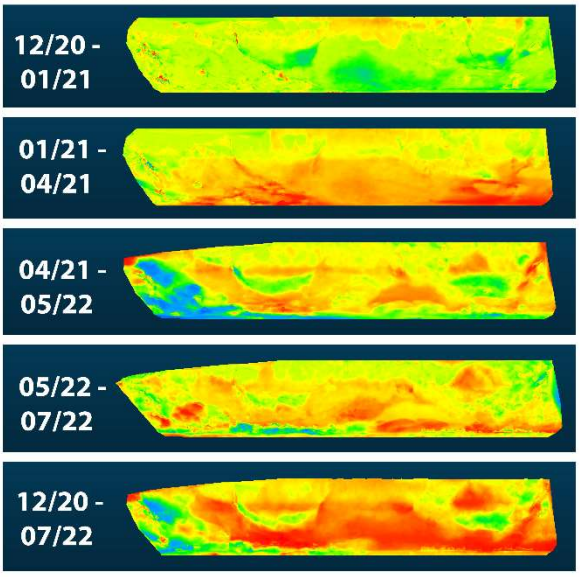




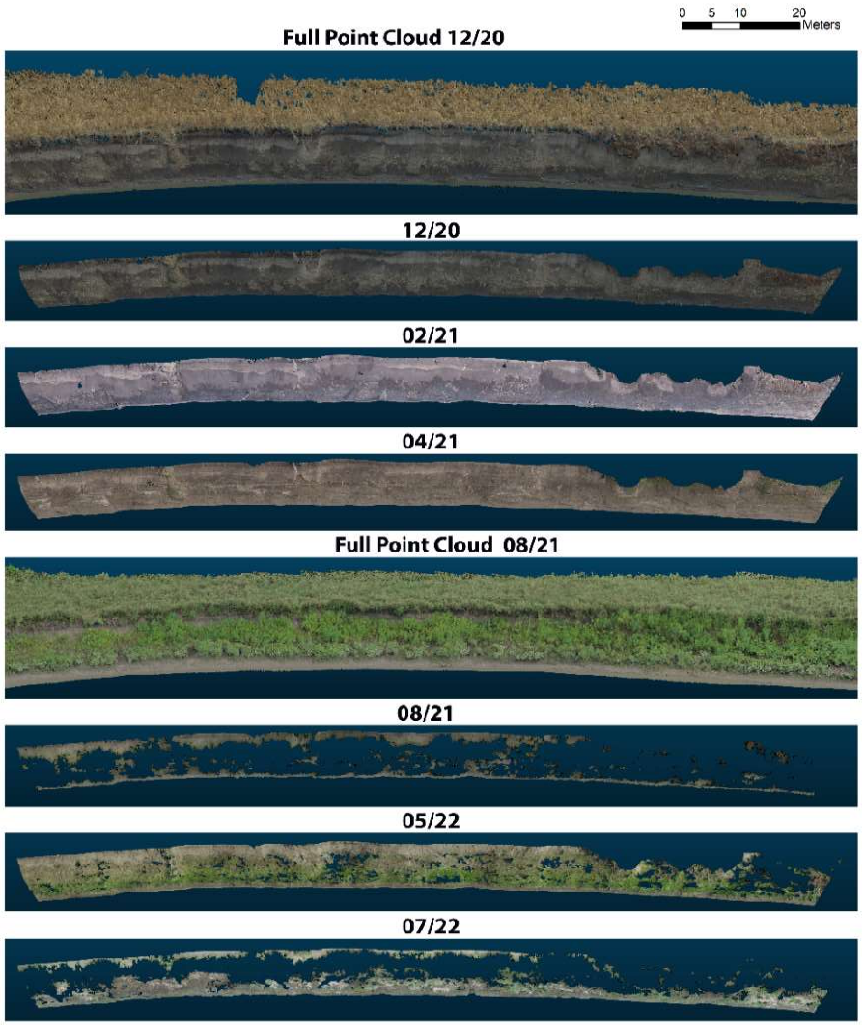
DoDs: XY Plane

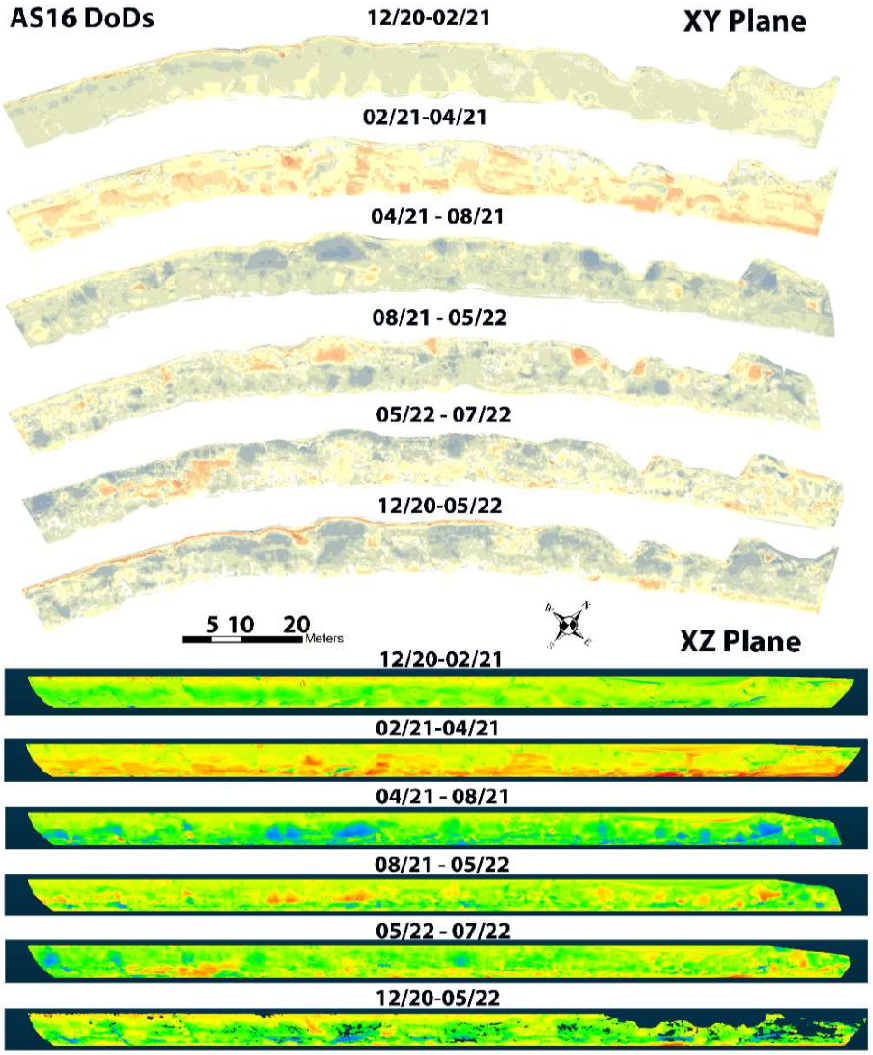


DoDs - XZ Plane



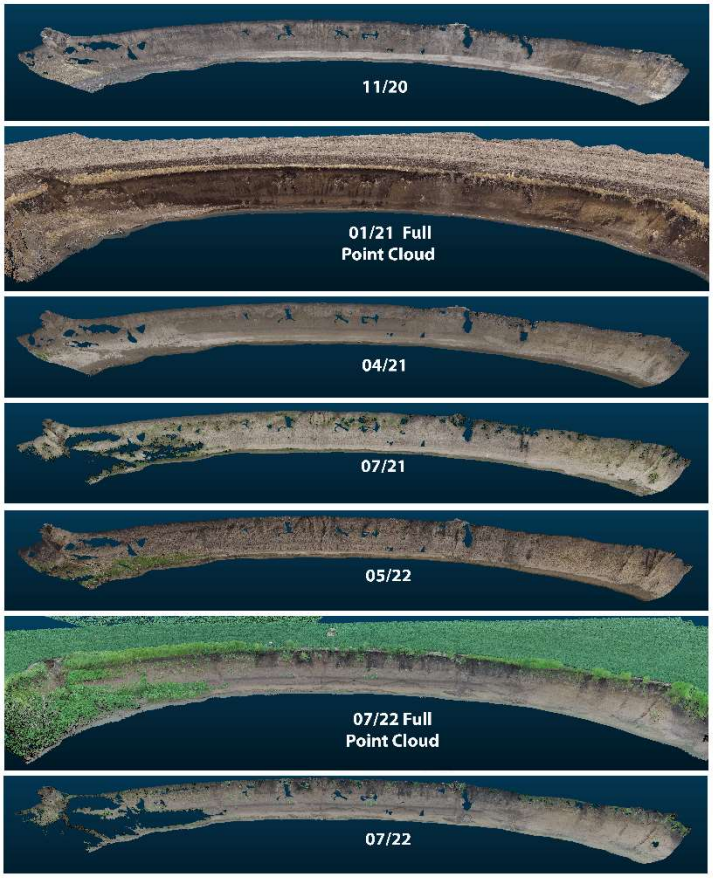
SB16 Point Clouds and DoDs



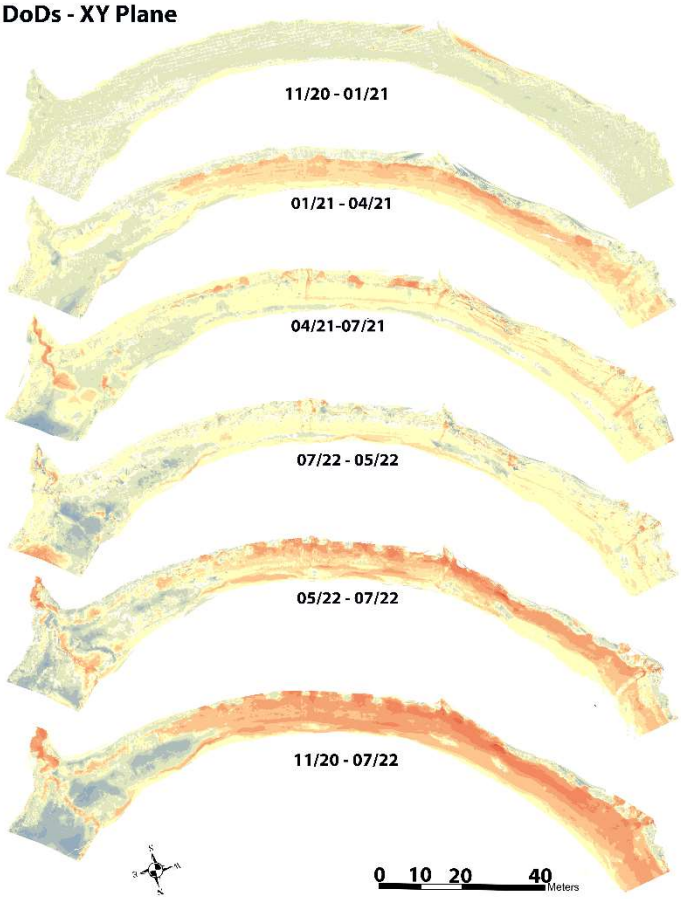


SB 19 Point Clouds and DoDs

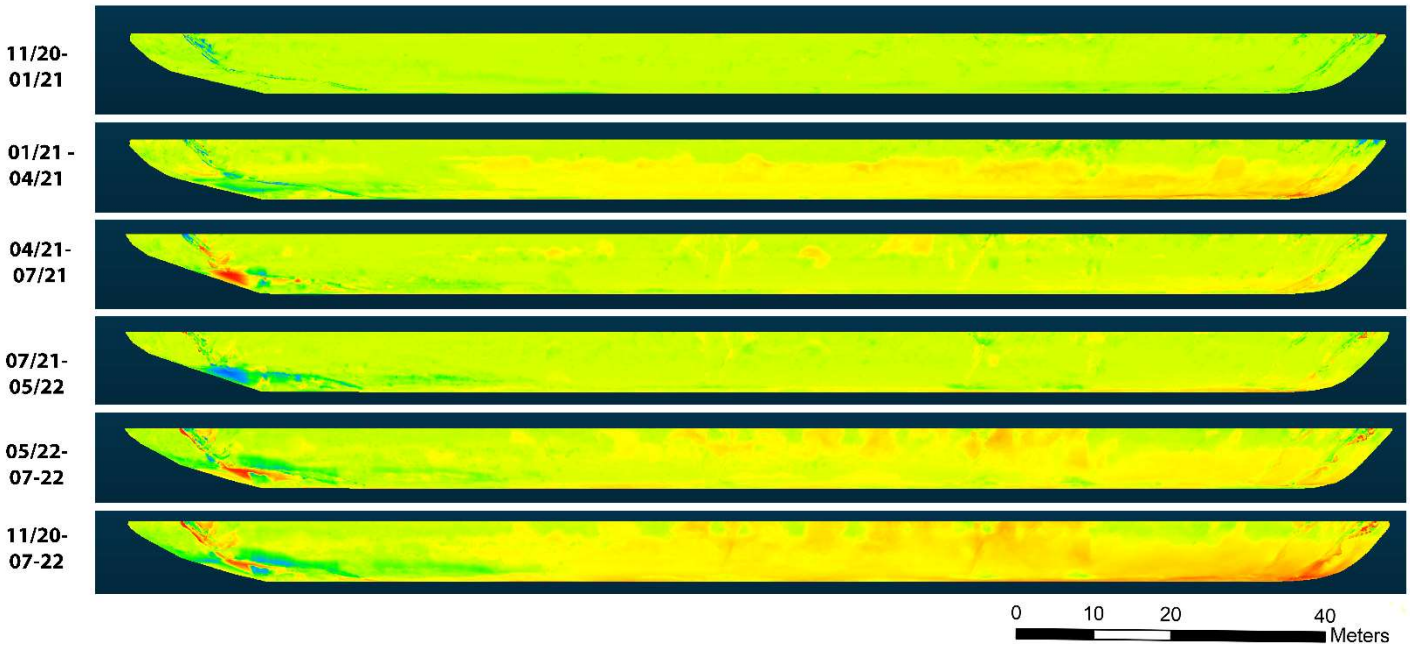
Point Clouds - Looking South



DoDs - XY Plane

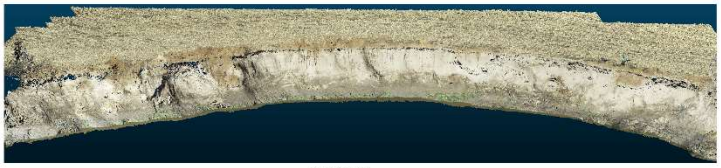


DoDs - XZ Plane - Looking South



SB20 Point Clouds and DoDs

11/20 Full Point Cloud



11/20



02/21



06/21



09/21



05/22



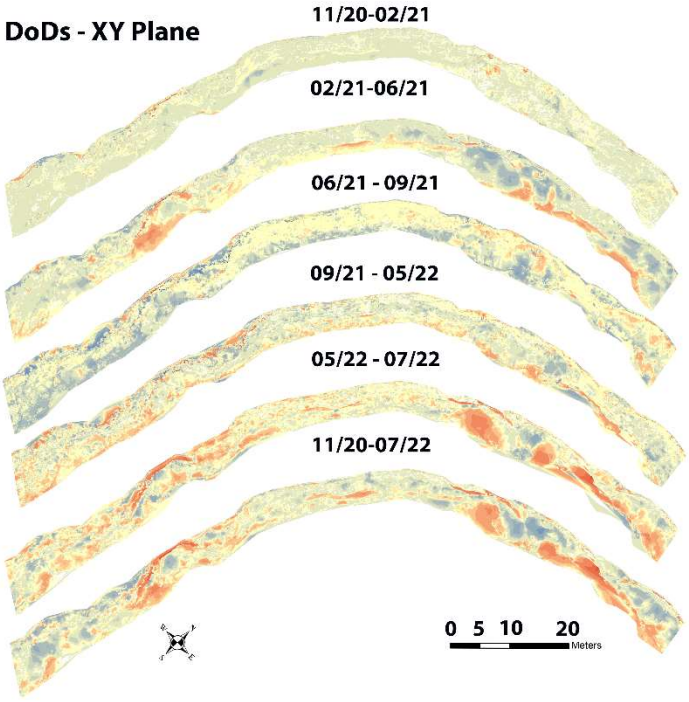
07/22 Full Point Cloud



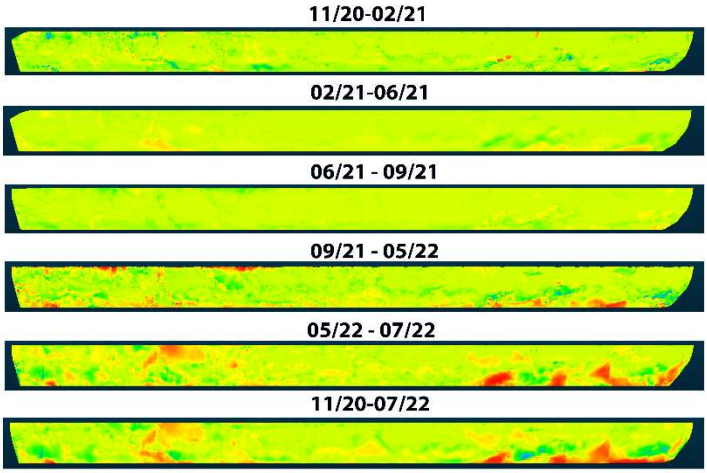
07/22



DoDs - XY Plane



DoDs - XZ Plane Looking South



SB22 Point Clouds and DoDs

10/20 Full Point Cloud



10/20



01/21



04/21



07/21



05/22 Full Point Cloud



05/22



DoDs: XY Plane

10/20 - 01/21



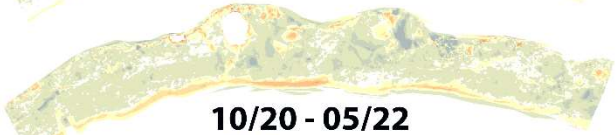
01/21 - 04/21



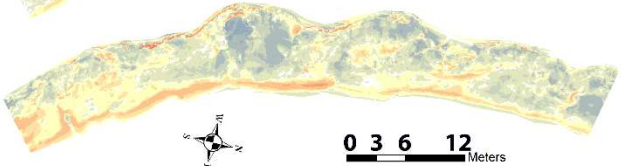
04/21 - 07/21



07/21 - 05/22

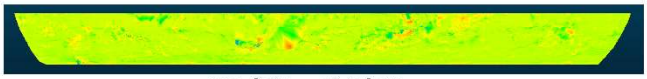


10/20 - 05/22

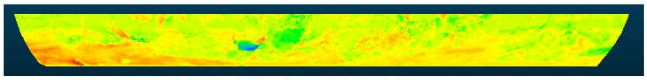


DoDs: XZ Plane

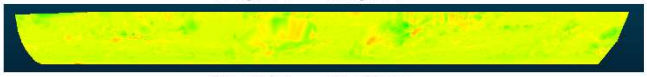
10/20 - 01/21



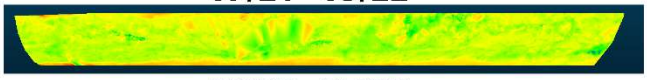
01/21 - 04/21



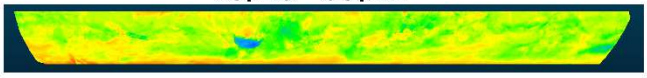
04/21 - 07/21



07/21 - 05/22



10/20 - 05/22

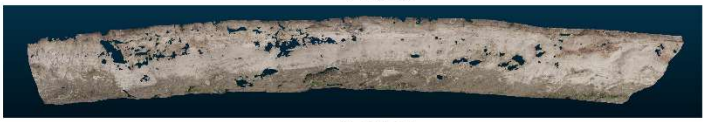


SB23 Point Clouds and DoDs

11/20 Full Point Cloud



11/20



01/21



04/21



07/21



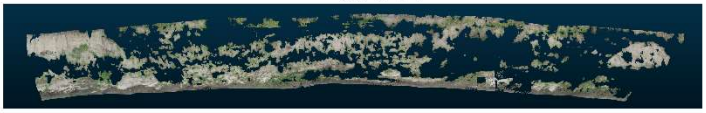
02/22



07/22 Full Point Cloud



07/22



DoDs: XY Plane

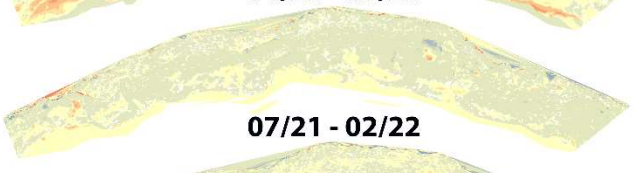
11/20 - 01/21



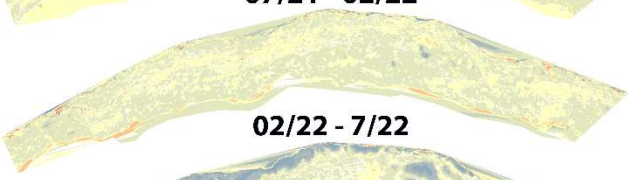
01/21 - 04/21



04/21 - 07/21



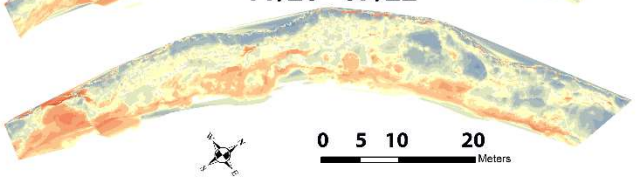
07/21 - 02/22



02/22 - 7/22

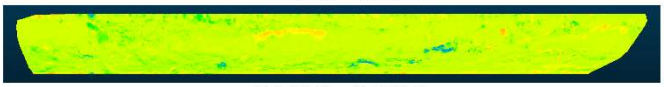


11/20 - 07/22

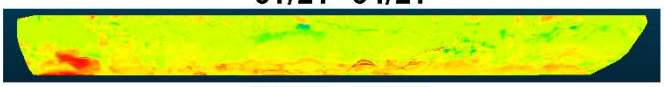


DoDs: XZ Plane

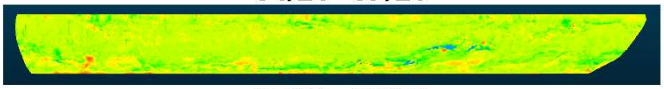
11/20 - 01/21



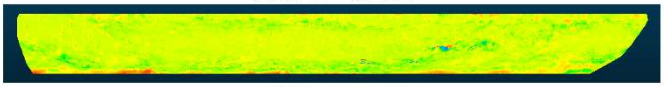
01/21 - 04/21



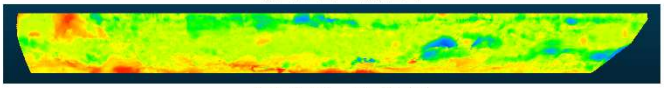
04/21 - 07/21



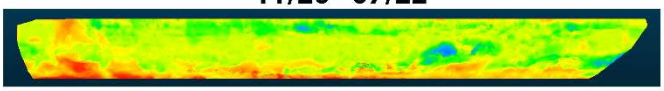
07/21 - 02/22



02/22 - 7/22



11/20 - 07/22



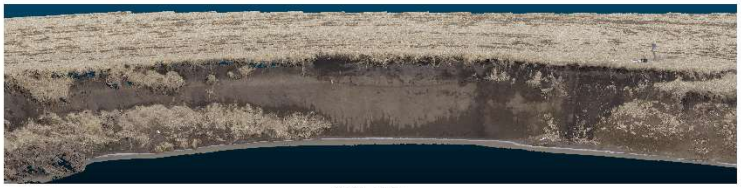
AS28 Point Clouds and DoDs

Point Clouds Looking South

12/20



02/21 Full Point Cloud



02/21



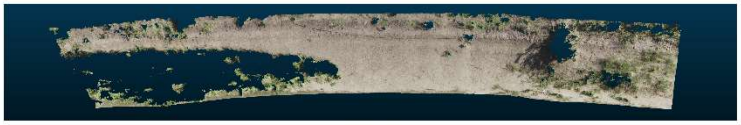
05/21



07/21 Full Point Cloud



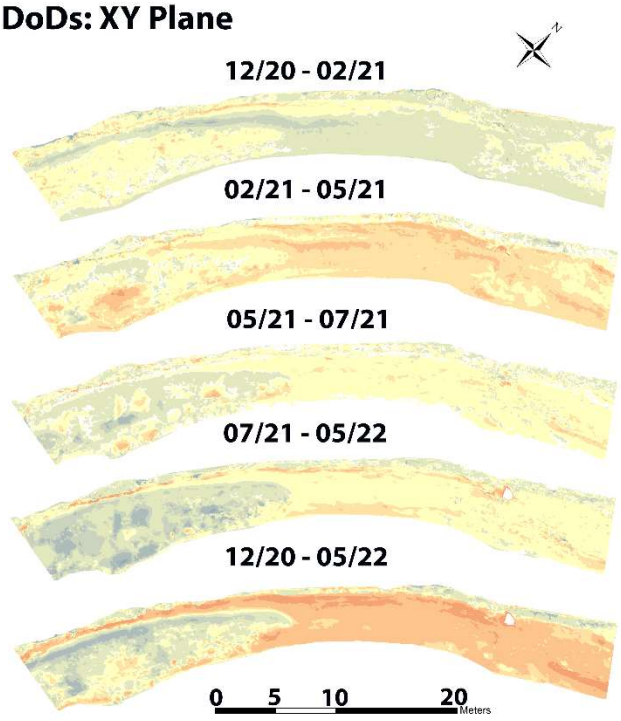
07/21



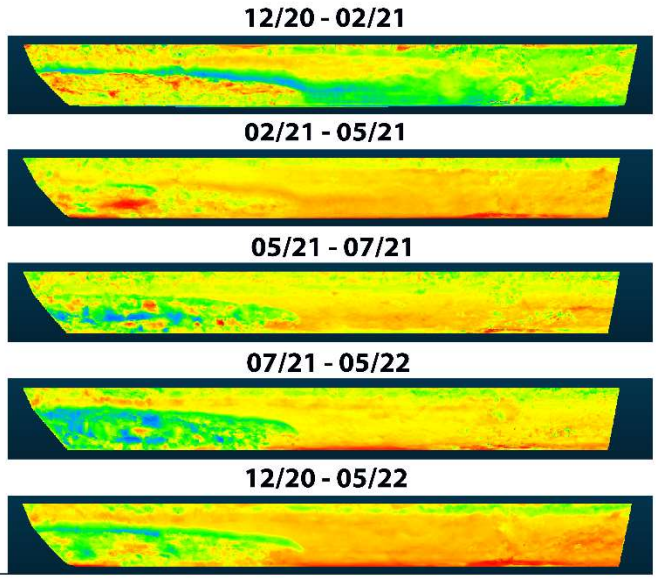
05/22



DoDs: XY Plane



DoDs: XZ Plane



SB30 Point Clouds and DoDs

Point Clouds

12/20



01/21 Full Point Cloud



01/21



04/21



07/21



05/22



07/22 Full Point Cloud



07/22



DoDs - XY Plane

12/20 - 01/21



01/21 - 04/21



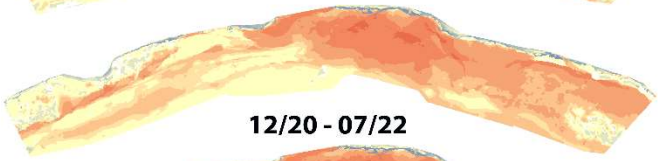
04/21 - 07/21



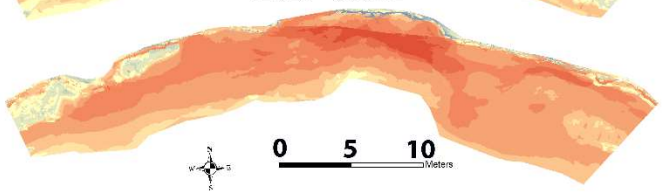
07/21 - 05/22



05/22 - 07/22



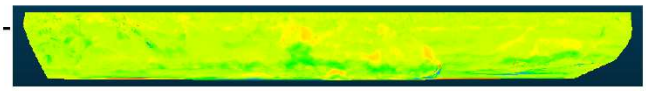
12/20 - 07/22



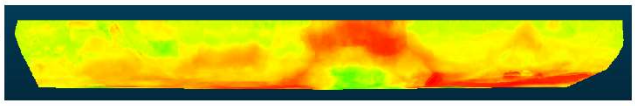
0 5 10 Meters

DoDs - XZ Plane

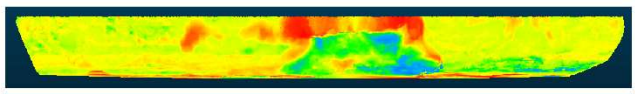
12/20 - 04/21



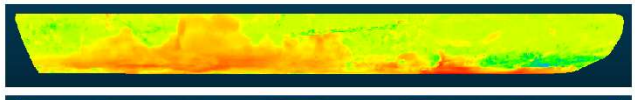
01/21 - 04/21



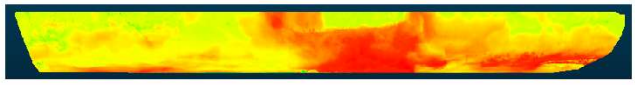
04/21- 07/21



07/21- 05/22



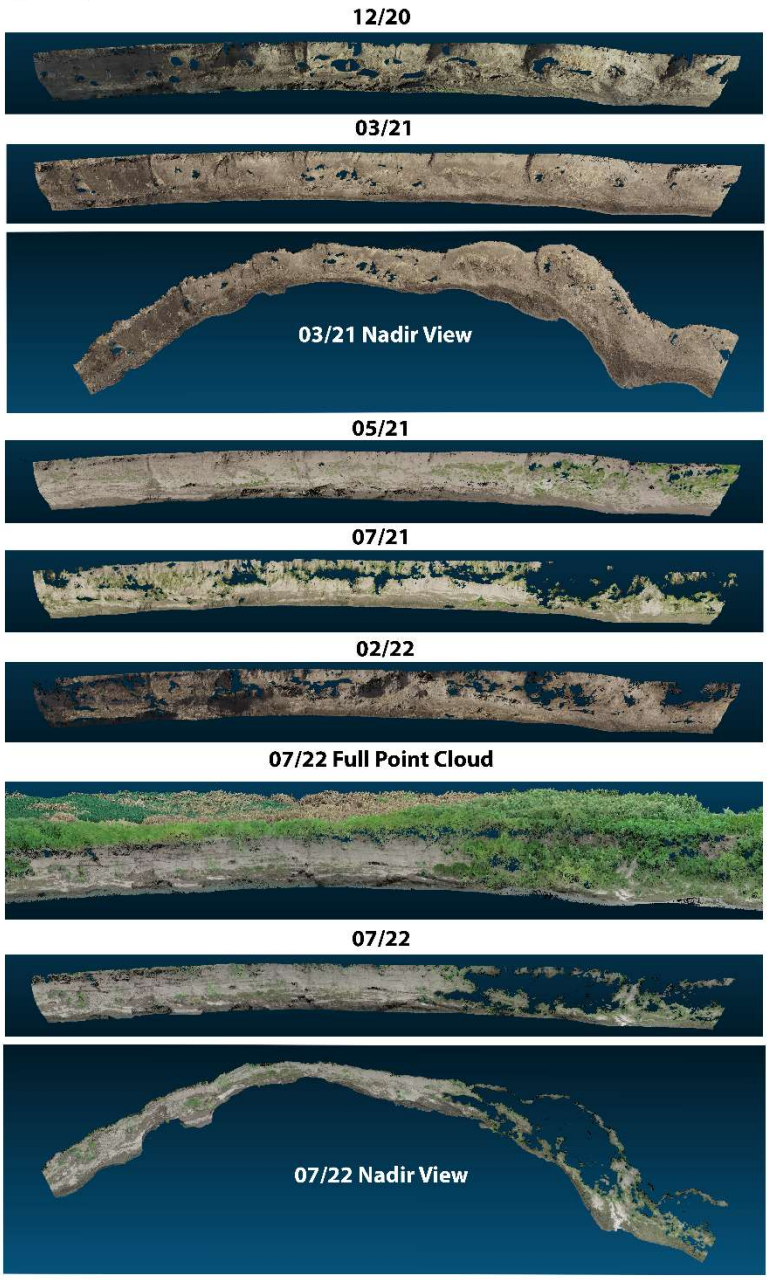
05/22- 07/22

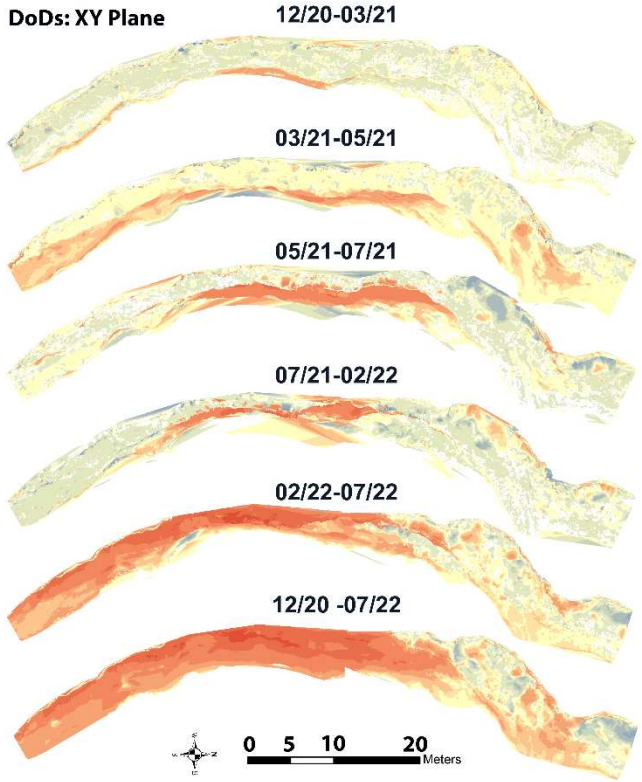


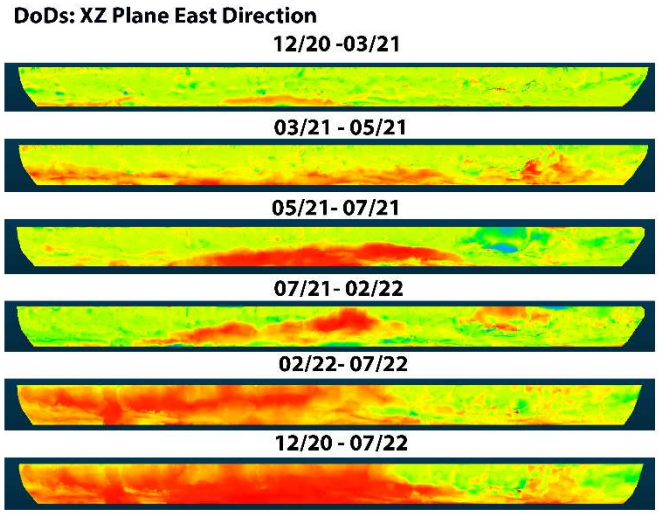
12/20 - 07/22



SB31 Point Clouds and DoDs







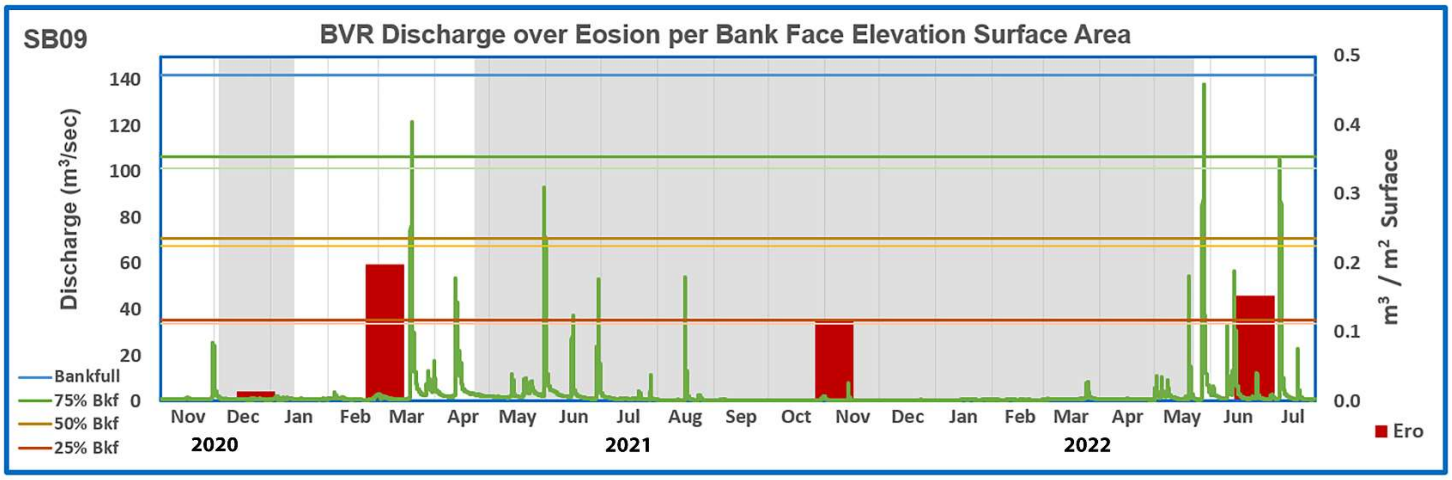
Appendix C: CC Volume Change for All Periods

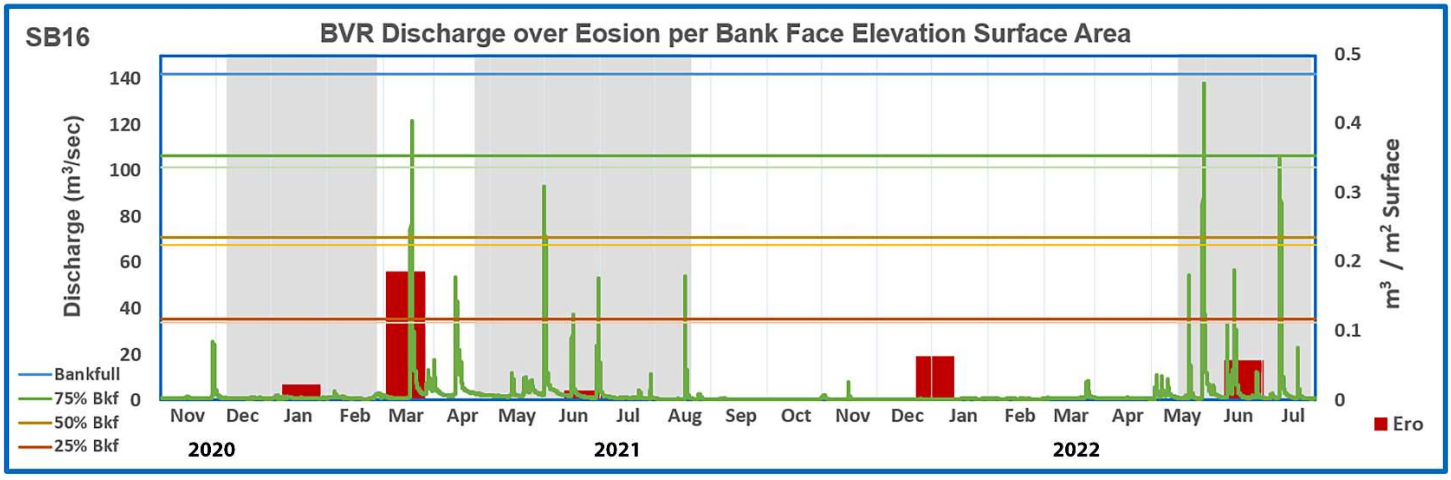
CloudCompare Volume Change with Empty Voids													
					Total Volume Change (m^3)				Vol. Change / M^2 Bk Face (m^3)			
Study Bank	Period	Begin Date	End Date	Bank Face Area (m^2)	Erosion (m^3)	Dep ($m^{3)}$	Net Ero-Dep (m^3)	+ - (m^3)	Ero/m^2 (m^3)	Dep/m^2 (m^3)	Net Ero-Dep/m^2 (m^3)	+ - (m^3)
31	1	12/20	03/21	347	13.71	8.85	-4.86	6.72	0.040	0.026	-0.014	0.019
	2	03/21	05/21	347	70.14	2.47	-67.66	7.48	0.202	0.007	-0.195	0.022
	3	05/21	07/21	347	83.97	3.39	-80.59	5.87	0.242	0.010	-0.232	0.017
	4	07/21	02/22	347	41.13	11.11	-30.02	6.14	0.119	0.032	-0.087	0.018
	5	02/22	07/22	347	232.31	0.08	-232.23	7.11	0.670	0.000	-0.670	0.021
30	1	12/20	01/21	221	2.36	9.66	7.30	2.26	0.011	0.044	0.033	0.010
	2	01/21	04/21	221	99.80	1.49	-98.31	1.97	0.451	0.007	-0.445	0.009
	3	04/21	07/21	221	21.60	10.67	-10.93	2.09	0.098	0.048	-0.049	0.009
	4	07/21	05/22	221	34.84	4.38	-30.46	1.75	0.158	0.020	-0.138	0.008
	5	05/22	07/22	221	94.55	0.30	-94.25	2.55	0.428	0.001	-0.426	0.012
28	1	11/20	02/21	242	6.23	10.30	4.07	3.48	0.026	0.042	0.017	0.014
	2	02/21	05/21	242	40.99	0.93	-40.06	4.32	0.169	0.004	-0.165	0.018
	3	05/21	07/21	242	12.39	1.34	-11.05	4.21	0.051	0.006	-0.046	0.017
	4	07/21	05/22	242	16.15	3.39	-12.76	4.31	0.067	0.014	-0.053	0.018
23	1	10/20	01/21	579	4.14	10.84	6.69	4.52	0.007	0.019	0.012	0.008
	2	01/21	04/21	579	56.59	5.10	-51.50	7.47	0.098	0.009	-0.089	0.013
	3	04/21	07/21	579	7.89	14.09	6.21	7.26	0.014	0.024	0.011	0.013
	4	07/21	02/22	579	13.92	7.23	-6.69	8.11	0.024	0.012	-0.012	0.014
	5	02/22	07/22	579	37.47	7.02	-30.45	9.73	0.065	0.012	-0.053	0.017
22	1	10/20	01/21	323	2.86	7.89	5.03	3.62	0.009	0.024	0.016	0.011
	2	01/21	04/21	323	30.58	5.00	-25.57	4.95	0.095	0.015	-0.079	0.015
	3	04/21	07/21	323	2.55	4.76	2.21	7.81	0.008	0.015	0.007	0.024
	4	07/21	05/22	323	7.56	9.04	1.48	8.47	0.023	0.028	0.005	0.026
20	1	11/20	02/21	769	8.97	21.13	12.17	19.82	0.012	0.027	0.016	0.026
	2	02/21	06/21	769	51.46	10.35	-41.11	14.45	0.067	0.013	-0.053	0.019
	3	06/21	09/21	769	30.10	17.02	-13.08	17.52	0.039	0.022	-0.017	0.023
	4	09/21	05/22	769	43.53	22.61	-20.93	17.54	0.057	0.029	-0.027	0.023
	5	05/22	07/22	769	80.12	10.00	-70.12	15.65	0.104	0.013	-0.091	0.020
19	1	12/20	01/21	1086	9.86	41.68	31.82	28.24	0.009	0.038	0.029	0.026
	2	01/21	04/21	1086	231.82	28.96	-202.86	23.76	0.213	0.027	-0.187	0.022
	3	04/21	07/21	1086	142.01	18.25	-123.76	18.05	0.131	0.017	-0.114	0.017
	4	07/21	05/22	1086	113.02	36.91	-76.11	18.59	0.104	0.034	-0.070	0.017
	5	05/22	07/22	1086	393.59	22.81	-370.77	20.87	0.362	0.021	-0.341	0.019
16	1	12/20	02/21	735	14.43	41.10	26.68	11.42	0.020	0.056	0.036	0.016
	2	02/21	04/21	735	125.37	4.09	-121.28	13.98	0.171	0.006	-0.165	0.019
	3	04/21	08/21	735	2.52	26.29	23.76	13.83	0.003	0.036	0.032	0.019
	4	08/21	05/22	735	7.77	11.16	3.39	12.65	0.011	0.015	0.005	0.017
	5	05/22	07/22	735	26.44	20.08	-6.36	13.78	0.036	0.027	-0.009	0.019
9	1	12/20	01/21	124	1.66	4.64	2.98	2.91	0.013	0.037	0.024	0.023
	2	01/21	04/21	124	24.16	0.48	-23.68	2.51	0.195	0.004	-0.191	0.020
	3	04/21	05/22	124	14.05	9.83	-4.22	1.62	0.113	0.079	-0.034	0.013
	4	05/22	07/22	124	15.92	1.51	-14.41	1.56	0.128	0.012	-0.116	0.013

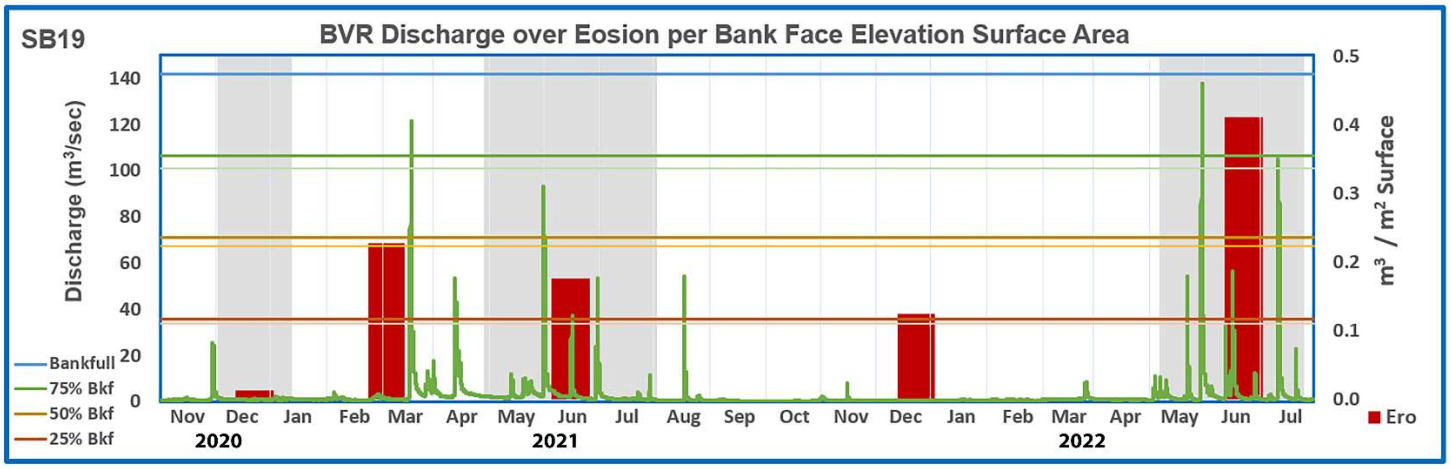
CloudCompare Volume Change with Interpolated Voids

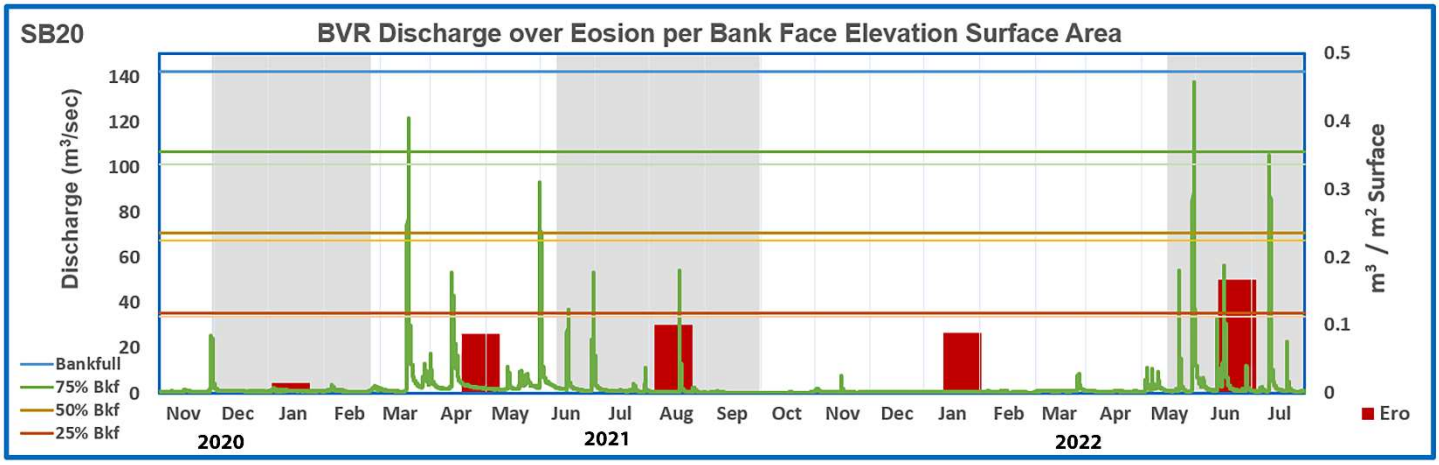
					Total Volume Change (m^3)				Vol. Change / M^2 Bk Face (m^3)			
Study Bank	Period	Begin Date	End Date	Bank Face Area (m^2)	Erosion (m^3)	Dep ($m^{3)}$	Net Ero-Dep (m^3)	+ - (m^3)	Ero/m^2 (m^3)	Dep/m^2 (m^3)	Net Ero-Dep/m^2 (m^3)	+ - (m^3)
31	1	12/20	03/21	347	14.68	10.22	-4.46	6.72	0.042	0.029	-0.013	0.019
	2	03/21	05/21	347	71.34	3.37	-67.98	7.48	0.206	0.010	-0.196	0.022
	3	05/21	07/21	347	88.56	19.19	-69.38	5.87	0.255	0.055	-0.200	0.017
	4	07/21	02/22	347	60.89	18.63	-42.26	6.14	0.176	0.054	-0.122	0.018
	5	02/22	07/22	347	276.29	6.64	-269.65	7.11	0.797	0.019	-0.777	0.021
30	1	12/20	01/21	221	3.63	14.50	10.87	2.26	0.016	0.066	0.049	0.010
	2	01/21	04/21	221	105.34	1.90	-103.44	1.97	0.476	0.009	-0.468	0.009
	3	04/21	07/21	221	22.73	11.16	-11.57	2.09	0.103	0.050	-0.052	0.009
	4	07/21	05/22	221	36.85	4.76	-32.08	1.75	0.167	0.022	-0.145	0.008
	5	05/22	07/22	221	100.32	0.36	-99.96	2.55	0.454	0.002	-0.452	0.012
28	1	11/20	02/21	242	7.37	10.91	3.54	3.48	0.030	0.045	0.015	0.014
	2	02/21	05/21	242	43.27	1.09	-42.18	4.32	0.178	0.004	-0.174	0.018
	3	05/21	07/21	242	13.84	5.67	-8.17	4.21	0.057	0.023	-0.034	0.017
	4	07/21	05/22	242	17.19	12.97	-4.22	4.31	0.071	0.053	-0.017	0.018
23	1	10/20	01/21	579	6.41	15.05	8.64	4.52	0.011	0.026	0.015	0.008
	2	01/21	04/21	579	61.56	7.37	-54.19	7.47	0.106	0.013	-0.094	0.013
	3	04/21	07/21	579	9.49	19.19	9.70	7.26	0.016	0.033	0.017	0.013
	4	07/21	02/22	579	16.72	10.95	-5.77	8.11	0.029	0.019	-0.010	0.014
	5	02/22	07/22	579	43.38	54.85	11.46	9.73	0.075	0.095	0.020	0.017
22	1	10/20	01/21	323	4.51	12.89	8.38	3.62	0.014	0.040	0.026	0.011
	2	01/21	04/21	323	34.21	9.30	-24.91	4.95	0.106	0.029	-0.077	0.015
	3	04/21	07/21	323	7.16	17.04	9.89	7.81	0.022	0.053	0.031	0.024
	4	07/21	05/22	323	11.77	28.68	16.91	8.47	0.036	0.089	0.052	0.026
20	1	11/20	02/21	769	11.16	26.28	15.13	19.82	0.015	0.034	0.020	0.026
	2	02/21	06/21	769	66.76	68.47	1.71	14.45	0.087	0.089	0.002	0.019
	3	06/21	09/21	769	76.66	85.95	9.29	17.52	0.100	0.112	0.012	0.023
	4	09/21	05/22	769	67.72	38.65	-29.07	17.54	0.088	0.050	-0.038	0.023
	5	05/22	07/22	769	157.64	34.66	-122.98	15.65	0.205	0.045	-0.160	0.020
19	1	12/20	01/21	1086	13.84	48.15	34.31	28.24	0.013	0.044	0.032	0.026
	2	01/21	04/21	1086	247.41	34.41	-213.01	23.76	0.228	0.032	-0.196	0.022
	3	04/21	07/21	1086	190.89	33.18	-157.71	18.05	0.176	0.031	-0.145	0.017
	4	07/21	05/22	1086	135.11	82.16	-52.95	18.59	0.124	0.076	-0.049	0.017
	5	05/22	07/22	1086	446.18	69.65	-376.53	20.87	0.411	0.064	-0.347	0.019
16	1	12/20	02/21	735	16.93	45.60	28.68	11.42	0.023	0.062	0.039	0.016
	2	02/21	04/21	735	136.50	4.51	-131.99	13.98	0.186	0.006	-0.180	0.019
	3	04/21	08/21	735	9.63	155.00	145.37	13.83	0.013	0.211	0.198	0.019
	4	08/21	05/22	735	46.61	69.82	23.20	12.65	0.063	0.095	0.032	0.017
	5	05/22	07/22	735	41.59	89.07	47.48	13.78	0.057	0.121	0.065	0.019
9	1	12/20	01/21	124	1.77	4.82	3.05	2.91	0.014	0.039	0.025	0.023
	2	01/21	04/21	124	24.47	0.60	-23.87	2.51	0.197	0.005	-0.193	0.020
	3	04/21	05/22	124	14.71	9.99	-4.72	1.62	0.119	0.081	-0.038	0.013
	5	05/22	07/22	124	18.95	2.95	-16.00	1.56	0.153	0.024	-0.129	0.013

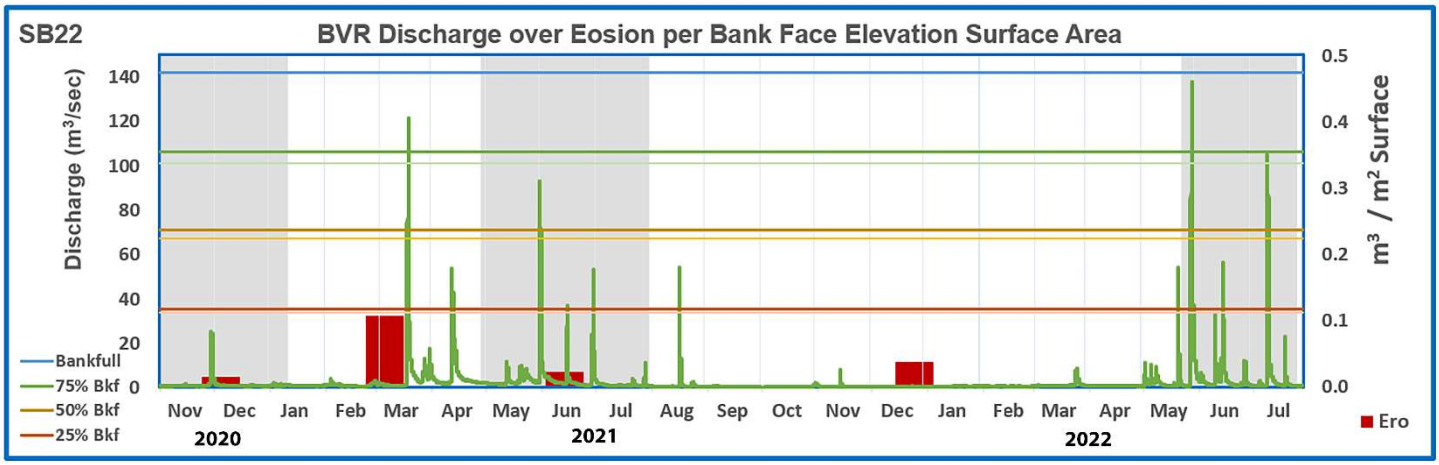
Appendix D: SfM Study Banks: BVR Discharge Overlain with Erosion

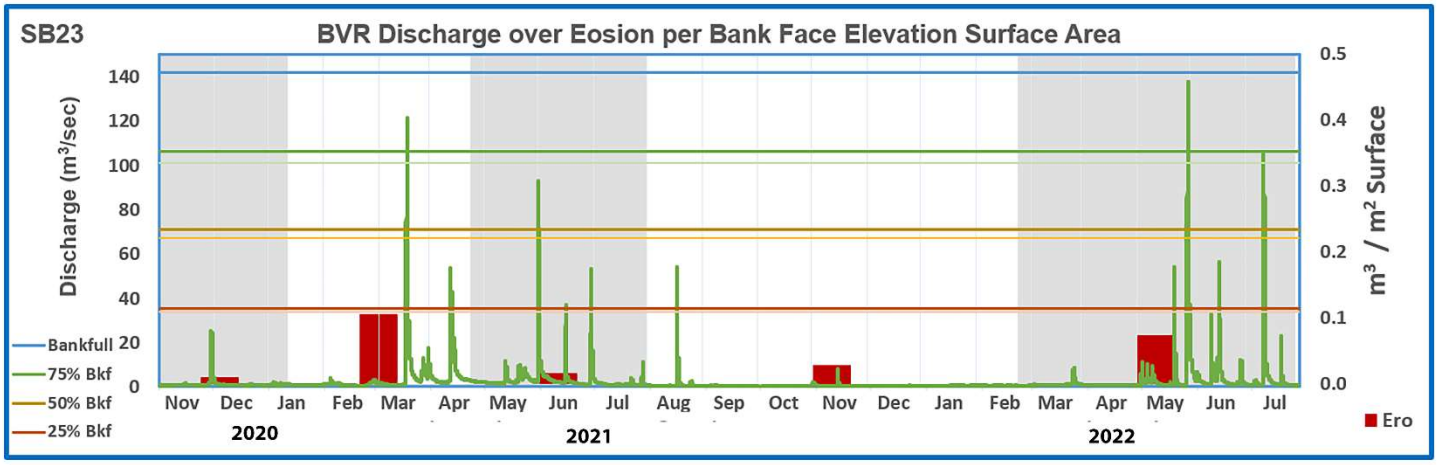


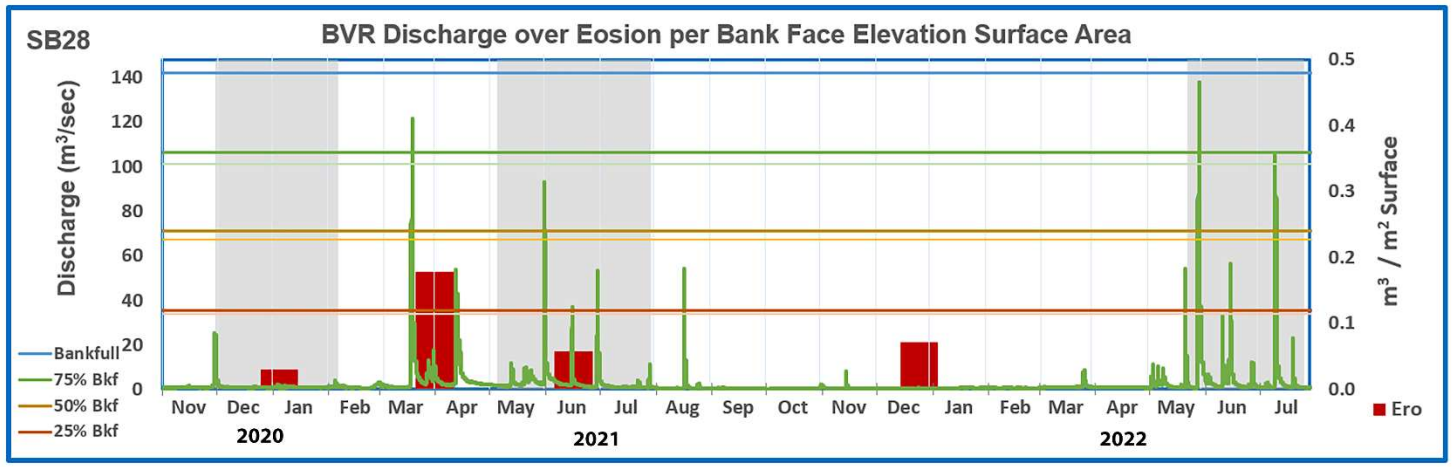


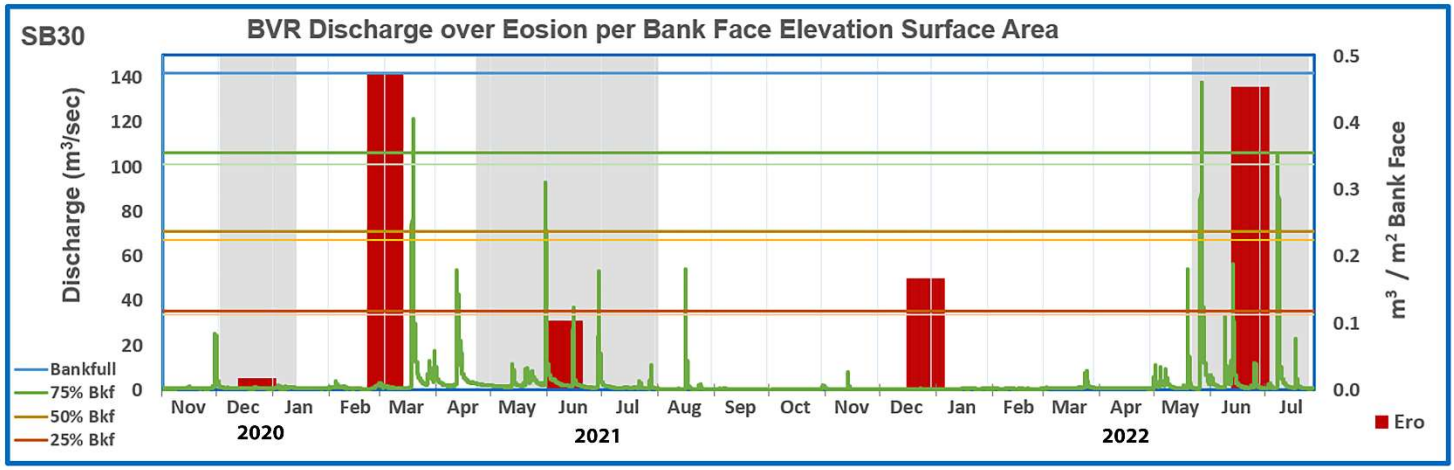


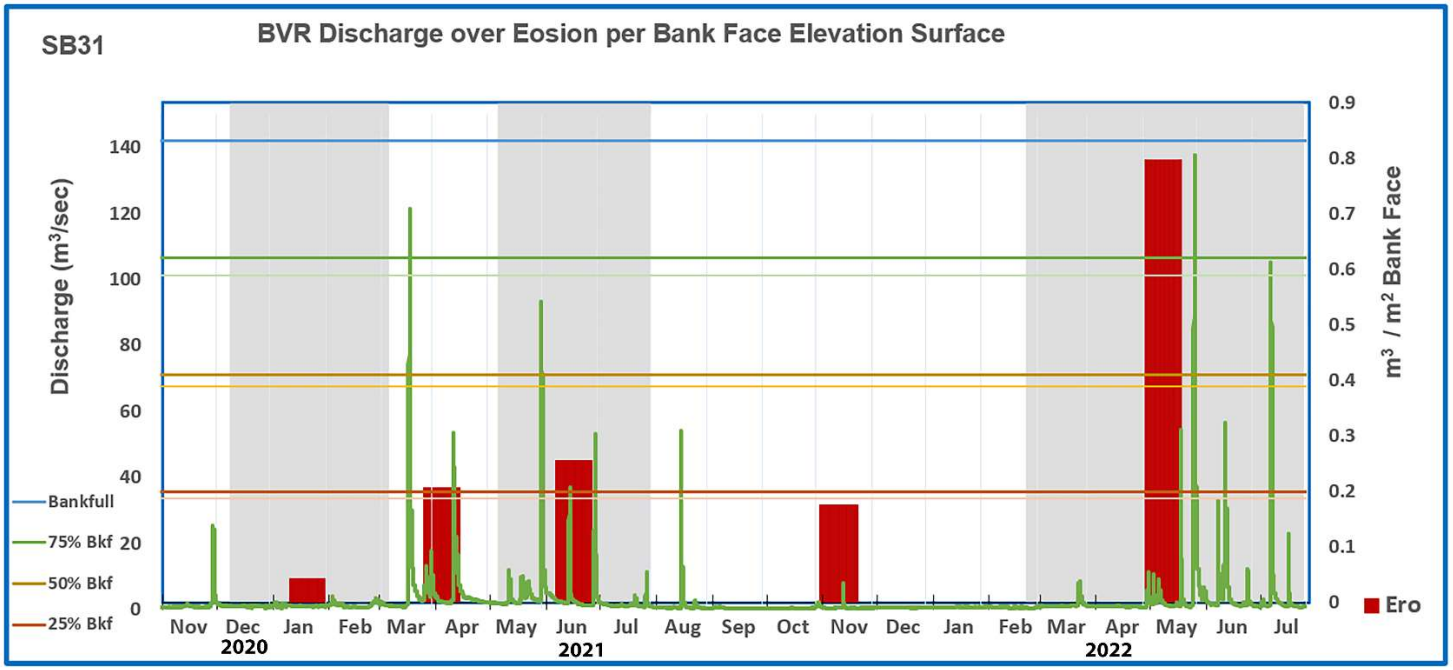

SB20
BVR Discharge over Eosion per Bank Face Elevation Surface Area
Discharge (m³/sec)
m³ / m² Surface
Bankfull
75% Bkf
50% Bkf
25% Bkf
Ero
Nov Dec Jan Feb Mar Apr May Jun Jul Aug Sep Oct Nov Dec Jan Feb Mar Apr May Jun Jul
2020
2021
2022


SB22
BVR Discharge over Eosion per Bank Face Elevation Surface Area
Discharge (m³/sec)
m³ / m² Surface
Bankfull
75% Bkf
50% Bkf
25% Bkf
Ero
Nov Dec Jan Feb Mar Apr May Jun Jul Aug Sep Oct Nov Dec Jan Feb Mar Apr May Jun Jul
2020
2021
2022


SB23
BVR Discharge over Eosion per Bank Face Elevation Surface Area
Discharge (m³/sec)
m³ / m² Surface
Bankfull
75% Bkf
50% Bkf
25% Bkf
Ero
Nov Dec Jan Feb Mar Apr May Jun Jul Aug Sep Oct Nov Dec Jan Feb Mar Apr May Jun Jul
2020
2021
2022


SB28
BVR Discharge over Eosion per Bank Face Elevation Surface Area
Discharge (m³/sec)
m³ / m² Surface
Bankfull
75% Bkf
50% Bkf
25% Bkf
Ero
Nov Dec Jan Feb Mar Apr May Jun Jul Aug Sep Oct Nov Dec Jan Feb Mar Apr May Jun Jul
2020
2021
2022


SB30
BVR Discharge over Eosion per Bank Face Elevation Surface Area
Discharge (m³/sec)
m³ / m² Bank Face
Bankfull
75% Bkf
50% Bkf
25% Bkf
Ero
Nov Dec Jan Feb Mar Apr May Jun Jul Aug Sep Oct Nov Dec Jan Feb Mar Apr May Jun Jul
2020
2021
2022


SB31
BVR Discharge over Eosion per Bank Face Elevation Surface
Discharge (m³/sec)
m³ / m² Bank Face
Bankfull
75% Bkf
50% Bkf
25% Bkf
Ero
Nov Dec Jan Feb Mar Apr May Jun Jul Aug Sep Oct Nov Dec Jan Feb Mar Apr May Jun Jul
2020
2021
2022

References

Bartleby. (2023). XZ plane. Retrieved from https://www.bartleby.com/subject/math/geometry/concepts/xz-plane

Chapman, S. S., Omernik, J. M., Freeouf, J. A., Huggins, D. G., & McCauley, J. R. (2001). *Ecoregions of nebraska and kansas (color poster with map, descriptive text, summary tables and photographs)* U.S. Geological Survey.

Chow, V. T., Maidment, D. R., & Mays, L. W. (1988). *Applied hydrology*. New York [u.a.]: McGraw-Hill.

Civil Tracker. (2023). All about ground control points (GCP). Retrieved from https://civiltracker.xyz/all-about-ground-control-points/#:~:text=What%20are%20Ground%20Control%20Points,drones%20into%20survey%20grade%20products.

Gabet, E. J. (2003). Sediment transport by dry ravel. *Journal of Geophysical Research - Solid Earth, 108*(B1), 2049-n/a. doi:10.1029/2001JB001686

Knighton, D. (2014). *Fluvial forms and processes*. London: Taylor and Francis. doi:10.4324/9780203784662 Retrieved from https://www.taylorfrancis.com/books/9781134666614

Langbein, W. B., & Leopold, L. B. (1966). *River meanders - theory of minimum variance*. Washington: Gov. Print. Office.

Layzell, A. L., Peterson, A., Moore, T. L., & Bigham, K. A. (2022). UAS-based assessment of streambank stabilization effectiveness in an incised river system. *Geomorphology (Amsterdam, Netherlands), 408*, 108240. doi:10.1016/j.geomorph.2022.108240

NOAA. (2022). Climate data online. Retrieved from https://www.ncdc.noaa.gov/cdo-web/

Sass, C. K., & Keane, T. D. (2012). Application of rosgen's BANCS model for NE kansas and the development of predictive streambank erosion Curves1. *Journal of the American Water Resources Association, 48*, 774. doi:10.1111/j.1752-1688.2012.00644.x

Williams, G. P. (1986). River meanders and channel size. *Journal of Hydrology (Amsterdam), 88*(1), 147-164. doi:10.1016/0022-1694(86)90202-7